Stellar Formation and Evolution

恆星形成與演化

Wen Ping Chen

http://www.astro.ncu.edu.tw/~wchen/Courses/Stars/Default.htm

Table of Contents

- ✓What is a "star"?
- ✓How hot is the surface of the Sun? How is this known? The Sun is gaseous, so how come it has a "surface"?
- ✓How hot is the center of the Sun? How is this known?
- ✓How long can the Sun remain as a shining body? How is this known?
- ✓Describe the radial structure of the Sun. How is this know?

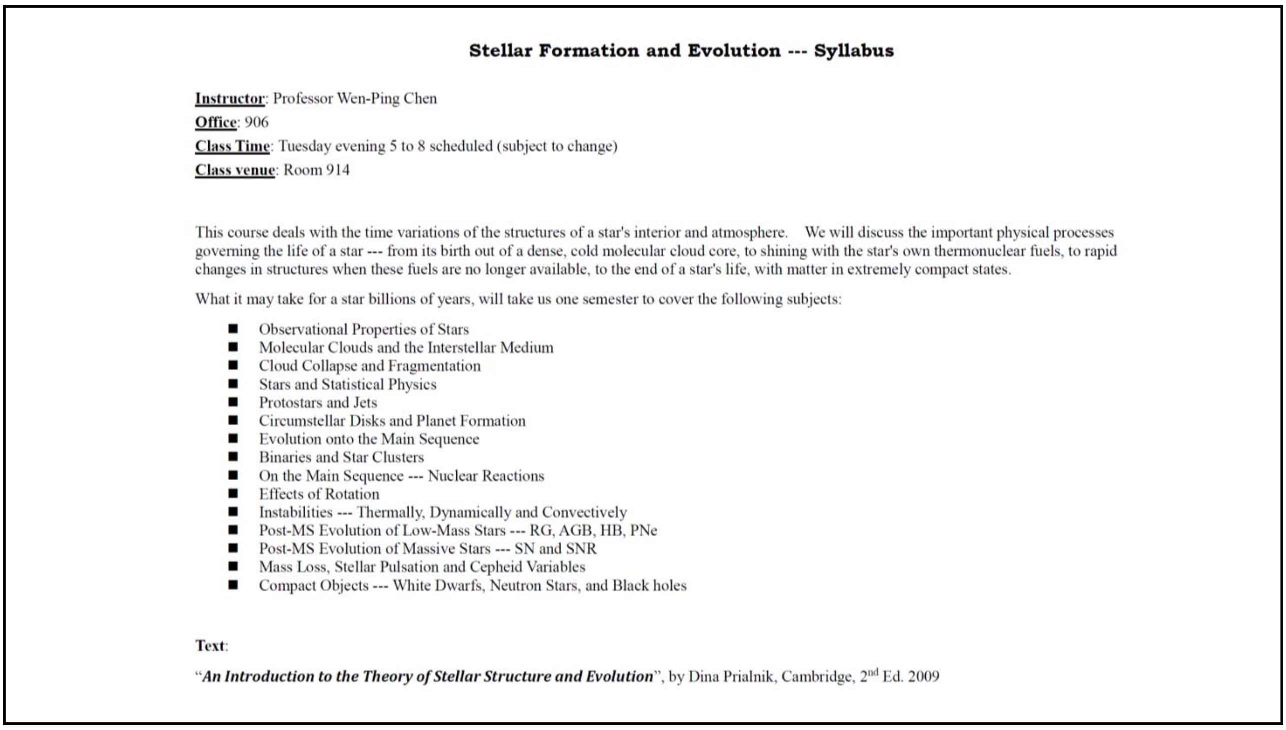

Stellar Formation and Evolution --- Syllabus

Instructor: Professor Wen-Ping Chen
Office: 906
Class Time: Tuesday evening 5 to 8 scheduled (subject to change)
Class venue: Room 914

This course deals with the time variations of the structures of a star's interior and atmosphere. We will discuss the important physical processes governing the life of a star --- from its birth out of a dense, cold molecular cloud core, to shining with the star's own thermonuclear fuels, to rapid changes in structures when these fuels are no longer available, to the end of a star's life, with matter in extremely compact states.

What it may take for a star billions of years, will take us one semester to cover the following subjects:

- Observational Properties of Stars
- Molecular Clouds and the Interstellar Medium
- Cloud Collapse and Fragmentation
- Stars and Statistical Physics
- Protostars and Jets
- Circumstellar Disks and Planet Formation
- Evolution onto the Main Sequence
- Binaries and Star Clusters
- On the Main Sequence --- Nuclear Reactions
- Effects of Rotation
- Instabilities --- Thermally, Dynamically and Convectively
- Post-MS Evolution of Low-Mass Stars --- RG, AGB, HB, PNe
- Post-MS Evolution of Massive Stars --- SN and SNR
- Mass Loss, Stellar Pulsation and Cepheid Variables
- Compact Objects --- White Dwarfs, Neutron Stars, and Black holes

Text:
"***An Introduction to the Theory of Stellar Structure and Evolution***", by Dina Prialnik, Cambridge, 2nd Ed. 2009

References

All the references you have found useful for the course ***Stellar Atmosphere and Structure*** will be also of use in this course. The following are the ones I have been using or were published in recent years.

- ✓ ***Physics of Stellar Evolution and Cosmology***, by H. Goldberg & Michael Scadron, 1982, Gordon and Breach
- ✓ ***Stellar Structure and Evolution***, by R. Kippenhahn & W. Weigert, 1990, Springer-Verlag
- ✓ ***Introduction to Stellar Astrophysics***, Vol 3 --- Stellar Structure and Evolution, by Erika Bohm-Vitense, 1992, Cambridge
- ✓ ***Stellar Structure and Evolution***, by Huang, R.Q. 黃潤乾, Guoshin, 1990
  This book, originally in Chinese, has an English version, and has recently been revised. The Chinese version（恆星物理）has also been revised
- ✓ ***The Physics of Stars***, by A.C. Phillips, 1994, John Wiley & Sons
- ✓ ***Stellar Evolution***, by Amos Harpaz, A K Peters, 1994
- ✓ ***The Stars*** --- Their Structure and Evolution, R. J. Tayler, 1994, Cambridge
- ✓ ***Theoretical Astrophysics, Vol II*: Stars and Stellar Systems** by Padmanabhan, T., a hefty, mathematical 3 volume set; comprehensive coverage of basic astrophysical processes in vol. 1, stars in vol. 2, and galaxies and cosmology in vol. 3, 2001, Cambridge
- ✓ ***Evolution of Stars and Stellar Populations***, by Maurizio Salaris and Santi, Cassisi, 2005, Wiley
- ✓ ***The Formation of Stars***, by Steven W. Stahler & Francesco Palla, 2004, Wiley
- ✓ ***From Dust to Stars***, by Norbert S. Schulz, 2005, Spinger
- ✓ ***Stellar Physics, 2: Stellar Evolution and Stability,*** by Bisnovatyi-Kogan, 2nd Ed., 2010, Springer (translated from Russian)

For star formation, the book "***Molecular Clouds and Star Formation***", edited by Chi Yuan（袁旂）& Junhan You（尤峻漢）and published by World Scientific in 1993, should be a good reference. Unfortunately this book is currently out of print, but Prof Yuan kindly donated his editor copy.

In addition to written midterm (30% grade) and final (30%) exams, there will be homework assignments, plus in-class exercises or projects (35%).

For an extensive listing of books on "stars" … http://www.ericweisstein.com/encyclopedias/books/Stars.html

Course Goals

- To know the properties of various phases of the interstellar matter;
- To understand how stars form out of molecular clouds; under what conditions;
- To understand the physical properties of stars, and to know how these properties change with time as a star evolves;
- To understand the basic physics underlying complex stellar evolution models;
- To know how to interpret observational parameters of stars;
- To understand how stars of different masses evolve and what the end products of their evolution are.

Stellar structure: balance of forces

Stellar evolution: (con)sequence of thermonuclear reactions in different parts of a star

Often used fundamental constants

Physical

a	radiation density constant	7.55×10^{-16} J m^{-3} K^{-4}
c	velocity of light	3.00×10^{8} m s^{-1}
G	gravitational constant	6.67×10^{-11} N m^{2} kg^{-2}
h	Planck's constant	6.62×10^{-34} J s
k	Boltzmann's constant	1.38×10^{-23} J K^{-1}
m_e	mass of electron	9.11×10^{-31} kg
m_H	mass of hydrogen atom	1.67×10^{-27} kg
N_A	Avogardo's number	6.02×10^{23} mol^{-1}
σ	Stefan Boltzmann constant	5.67×10^{-8} W m^{-2} K^{-4} (= ac/4)
R	gas constant (k/m_H)	8.26×10^{3} J K^{-1} kg^{-1}
e	charge of electron	1.60×10^{-19} C

Check out http://pdg.lbl.gov/2006/reviews/astrorpp.pdf

Astronomical

$L_\odot$	Solar luminosity	3.86×10^{26} W
$M_\odot$	Solar mass	1.99×10^{30} kg
$T_{eff\odot}$	Solar effective temperature	5780 K
$T_{c\odot}$	Solar Central temperature	1.6×10^{7} K (theoretical)
$R_\odot$	Solar radius	6.96×10^{8} m
$m_\odot$	apparent mag of Sun	−26.7 mag (V)
$M_\odot$	absolute mag of Sun	+4.8 mag (V)
θ	apparent size of Sun	32’
$<\rho>$	mean density of Sun	1.4 g cm^{-3}
$(B-V)_\odot$	Color of the Sun	0.6 mag
Parsec	*(unit of distance)*	3.09×10^{16} m

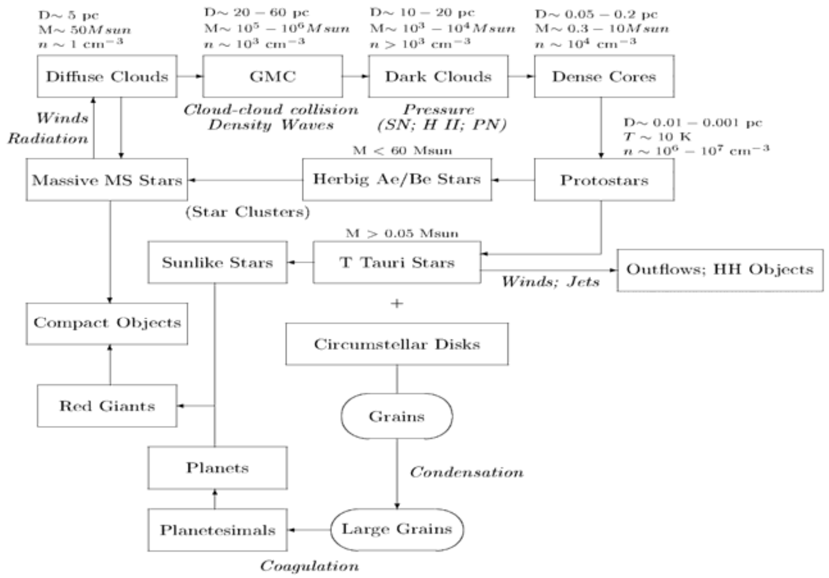

Galactic Ecology

Properties of Stars

Vocabulary

- **Luminosity** [erg s^{-1}] L = bolometric luminosity = power
- **Spectral luminosity** [erg s^{-1}µm^{-1}] L_λ $d\lambda = -(c/\nu^2)\, d\nu$
- **flux** [erg s^{-1} cm^{-2}] f
- **flux density** [erg s^{-1} cm^{-2} µm^{-1}] f_λ *or* f_ν 1 Jansky (Jy) = 10^{-23} [erg s^{-1}cm^{-2}Hz^{-1}]
  $f(\nu=0)$=3640 Jy
- **Brightness/intensity** [erg s^{-1} cm^{-2} sr^{-1}] B
- **Specific intensity** [erg s^{-1} cm^{-2} sr^{-1} Hz^{-1}] I_ν
- **Energy density** [erg cm^{-3}] u = (4 π/c) J
  J=mean intensity = (1/4π) ∫ I d Ω
- **Magnitude** … apparent, absolute, bolometric, AB

$$S_\nu\ [\mu\text{Jy}] = 10^{(23.9-\text{AB})/2.5}$$

$$m_{\text{AB}} = -2.5 \log_{10}\left(\frac{f_\nu}{3631\ \text{Jy}}\right)$$

Our Sun ---- the best studied star

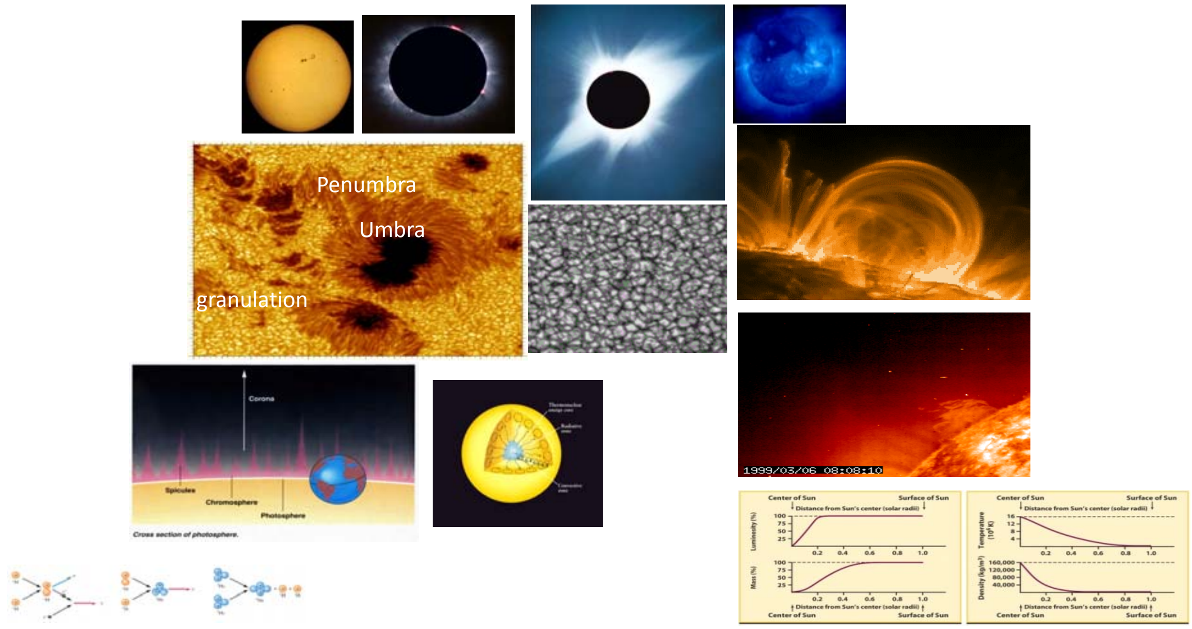

Observable properties of stars

Basic parameters to compare between theories and observations

- Mass (M)
- Luminosity (L)
- Radius (R)
- Effective temperature (T_e) $L = 4\pi R^2 \sigma T_e^4$
- Distance → measured flux $F = L / 4\pi d^2$

M, R, L and T_e not independent

- L and T_{eff} Hertzsprung-Russell (HR) diagram or color-magnitude diagram (CMD)
- L and M mass-luminosity relation

http://www.astrohandbook.com/links.html

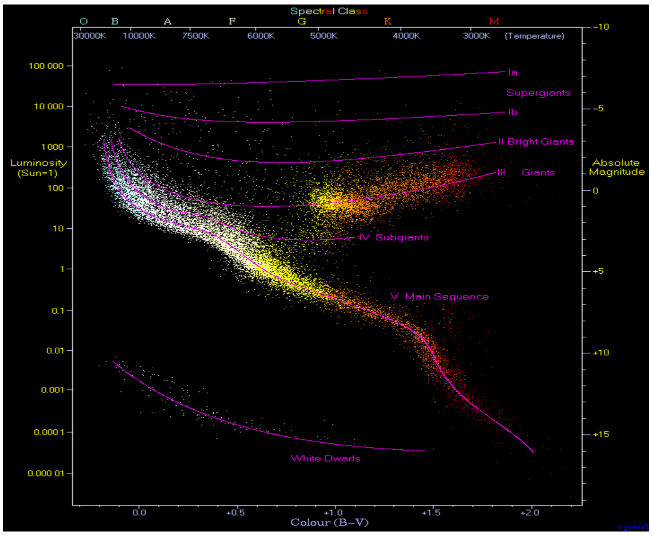

From wikipedia by Richard Powell based on *Hipparcos* data and Gliese catalog

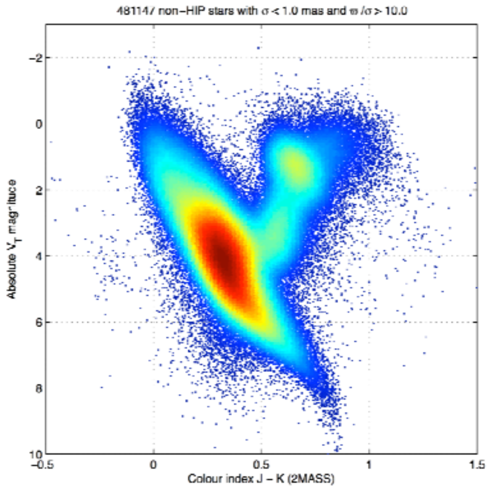

https://www.cosmos.esa.int/web/gaia/news_20150807

For (nearby) star databases http://www.projectrho.com/public_html/starmaps/catalogues.php

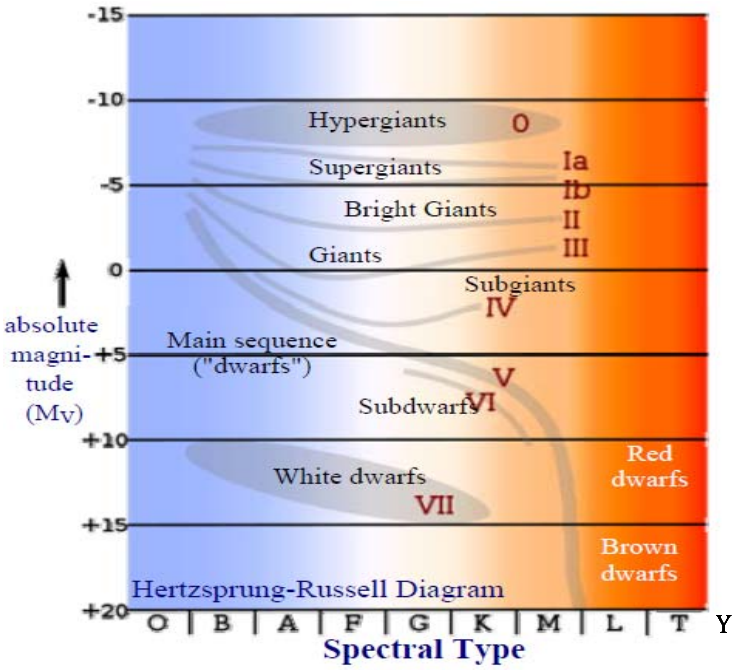

$\mathcal{M}_{\text{Jupiter}} \sim 0.001\ \mathcal{M}_{\odot}$

Stars:

$M > 0.08\ \mathcal{M}_{\odot}$

Brown Dwarfs:

$0.08\ \mathcal{M}_{\odot} > M > 13\ \mathcal{M}_{J}$

Planet-mass Objects:

$M < 13\ \mathcal{M}_{J}$

To measure the stellar distance

- Nearest stars $d > 1$pc → $p < 1''$
- For a star at d=100 pc, p= 0.01”
- Ground-based observations angular resolution ~1“; *HST* has 0.05”
- *Hipparcos* measured the parallaxes of 10^5 bright stars with p~0.001“ → reliable distance determinations for stars up to d=100 pc

→ ~100 stars with good parallax distances

Preliminary Version of the Third Catalogue of Nearby Stars
Gliese & Jahreiss (1991)

CDS catalog number: V/10A
2964/3803 complete entries

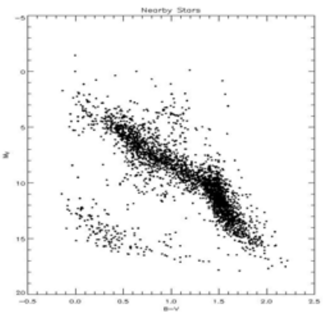

GAIA will measure 10^9 stars!

In most cases, the distance is estimated

- Stars with the same spectra are assumed to have identical set of physical parameters (spectroscopic parallax). For example, a G2V star should have the same absolute magnitude as the Sun.
- By comparison of the apparent brightness of an object with the <u>known</u> brightness of that particular kind of objects

  $$m_\lambda - M_\lambda = 5 \log d - 5 + A_\lambda$$

  A_λ is usually unknown; it depends on the intervening dust grains that scatter and absorb the star light, and also depends on the distance to the object
- Main-sequence fitting; moving-cluster method; Cepheid variables
- Other methods for Galactic molecular clouds, galaxies, etc.

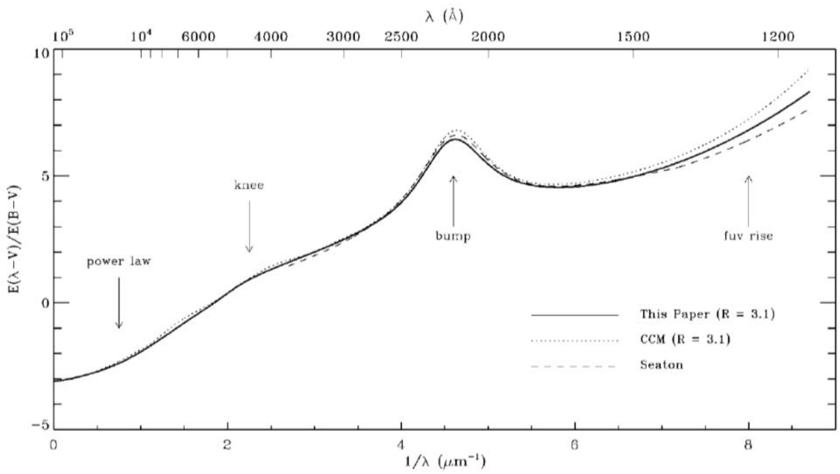

FIG. 1.—Normalized interstellar extinction curves from the far-IR through the UV. Several general features of the curves are noted. The solid and dotted curves are estimates for the case $R \equiv A(V)/E(B-V) = 3.1$ derived in the Appendix of this paper and by Cardelli et al. (1989), respectively. The dashed curve shows the average Galactic UV extinction curve from Seaton (1979).

To measure the stellar size

- Angular diameter of sun at 10 pc
  $= 2R_{\odot}/10\text{pc} = 5 \times 10^{-9}$ radians
  $= 10^{-3}$ arcsec
- Even the *HST* (0.05") barely capable of measuring directly the sizes of stars, except for the nearest supergiants
- Radii of ~600 stars measured with techniques such as interferometry, (lunar) occultation or for eclipsing binaries

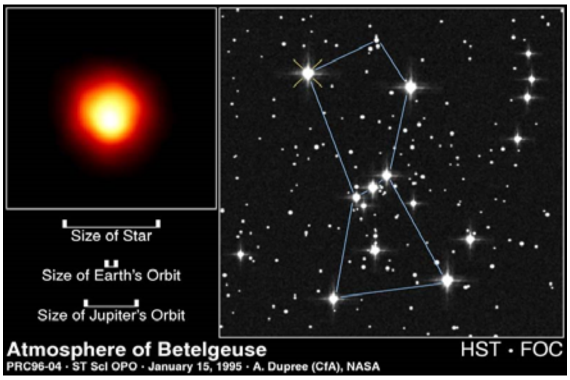

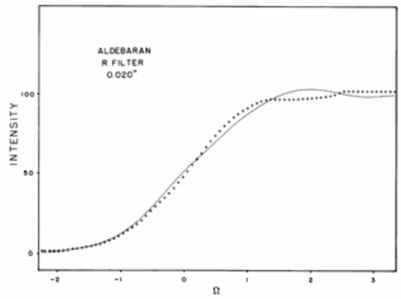

Fig. 1.—A comparison of the (*crosses*) observed points and the (*line*) theoretical pattern for the Aldebaran $\lambda = 7460$ Å record with $\theta = 0''.020$.

Lunar occultation

Beaver & Eitter (1979)

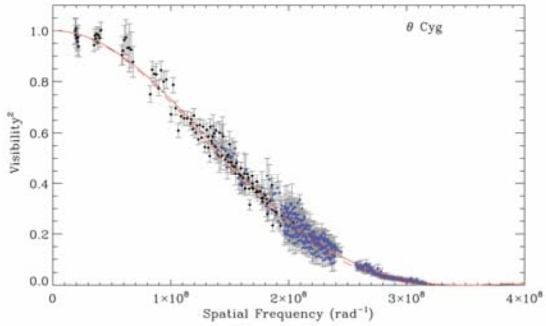

Figure 1. Squared visibility versus spatial frequency for θ Cyg for PAVO (blue circles) and MIRC (black diamonds) data. The red lines show the fitted limb-darkened model to the combined data. The solid line is for $\mu = 0.47 \pm 0.04$ (PAVO) while the dashed line is for $\mu = 0.21 \pm 0.03$ (MIRC).

Optical interferometery CHARA

White et al (2013)

To measure the stellar temperature

- What is $T_{\rm eff}$? What is the "surface" of a star?
- What is T anyway? Temperature is often defined by other physical quantities through an equation ("law") (by radiation or by particles)
  blackbody, radiation, color, excitation,
  ionization, kinetic, electron, conductive ...
- Only in thermal equilibrium are all these temperatures the same.
- Photometry (spectral energy distribution) gives a **rough** estimate of T, e.g., fluxes/magnitudes measured at different wavelengths, such as the "standard" Johnson system *UBVRI*

Band	U	B	V	R	I
λ/nm	365	445	551	658	806
Δλ/nm	66	94	88	138	149

- There are many photometric systems, using broad bands, intermediate bands, special bands, at optical or infrared wavelengths, etc.

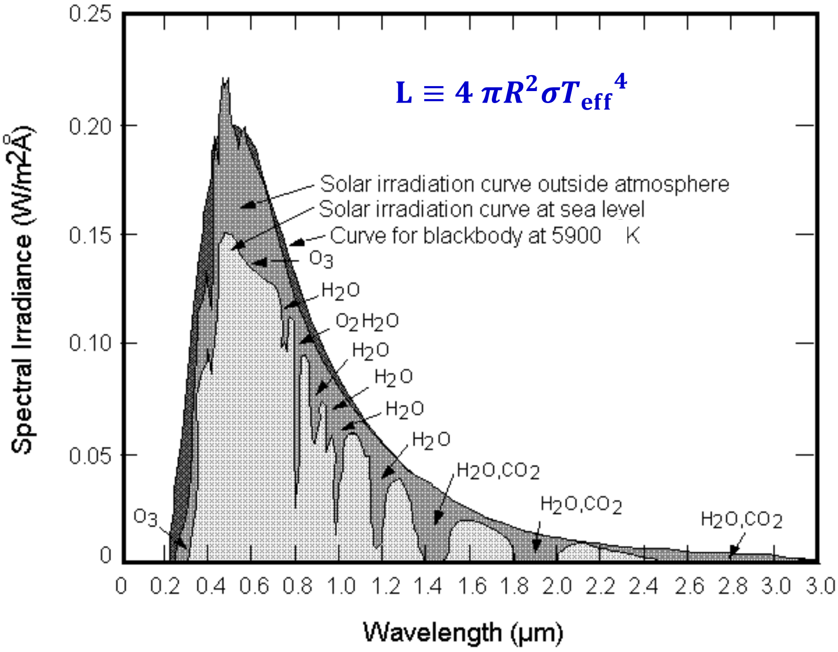

$L \equiv 4\pi R^2 \sigma T_{eff}^4$
Solar irradiation curve outside atmosphere
Solar irradiation curve at sea level
Curve for blackbody at 5900 K
O_3
H_2O
$O_2 H_2O$
H_2O
H_2O
H_2O
H_2O
H_2O, CO_2
H_2O, CO_2
H_2O, CO_2
O_3
Spectral Irradiance (W/m2Å)
0.25
0.20
0.15
0.10
0.05
0
0 0.2 0.4 0.6 0.8 1.0 1.2 1.4 1.6 1.8 2.0 2.2 2.4 2.6 2.8 3.0 3.0
Wavelength (μm)

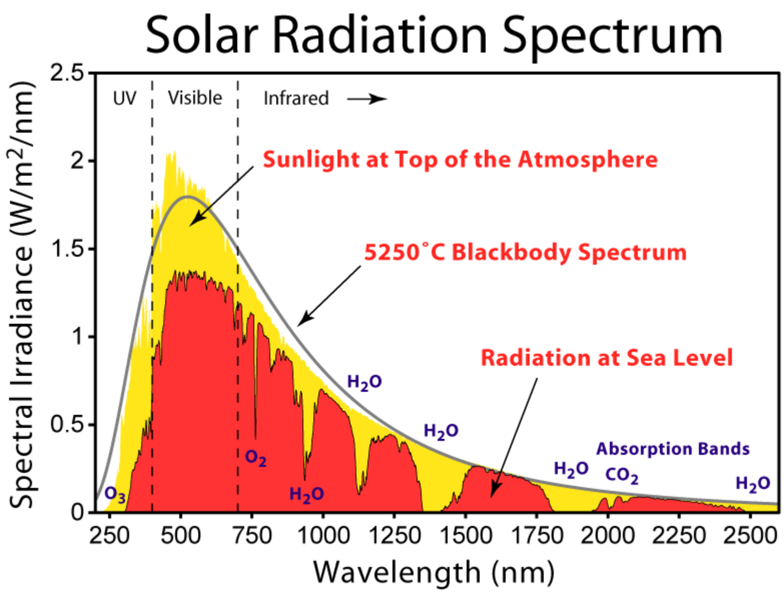

Solar Radiation Spectrum
UV
Visible
Infrared
Sunlight at Top of the Atmosphere
5250˚C Blackbody Spectrum
Radiation at Sea Level
H_2O
H_2O
Absorption Bands
H_2O
CO_2
H_2O
O_2
H_2O
O_3
Spectral Irradiance (W/m^2/nm)
2.5
2
1.5
1
0.5
0
250 500 750 1000 1250 1500 1750 2000 2250 2500
Wavelength (nm)

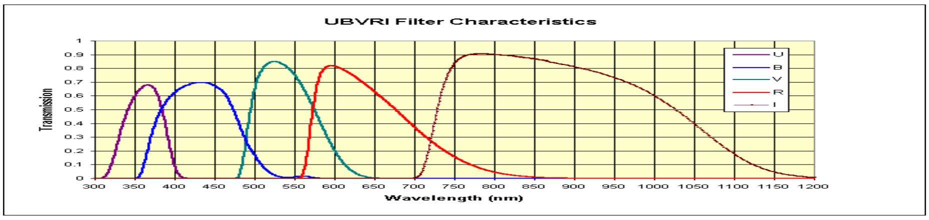

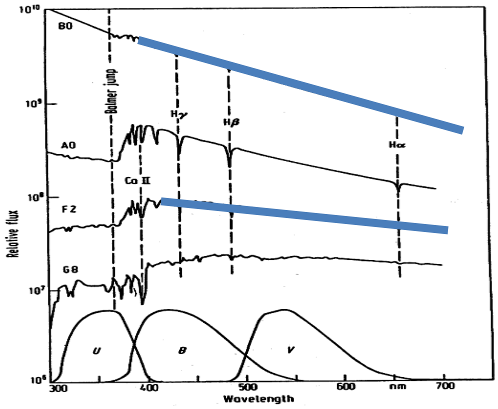

Running (slope) between B and V bands, i.e., the $(B - V)$ **color (index)** → photospheric temperature

The larger the value of $(B - V)$, the redder (cooler) the star.

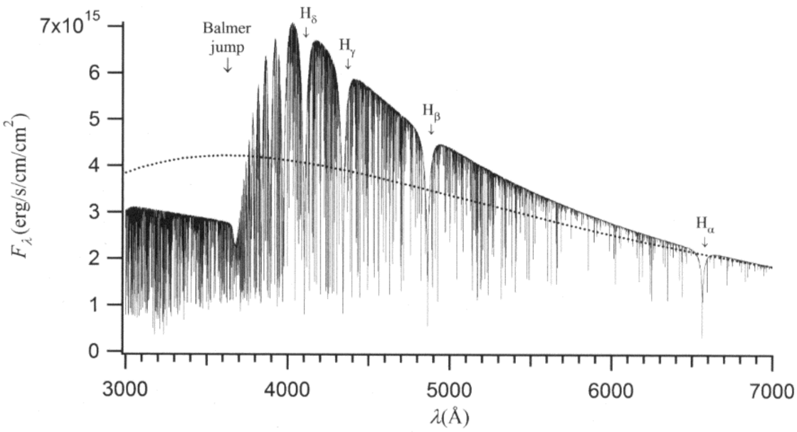

Figure 1.8 Theoretical monochromatic flux emerging form an A type star with $T_{\rm eff} = 8000\,{\rm K}$. The first four Balmer absorption lines, as well as the Balmer jump, are identified in this figure. Thousands of other absorption atomic lines can also be seen. This theoretical flux was obtained with the Phoenix stellar atmosphere code (Hauschildt, P.H., Allard, F. and Baron, E., *The Astrophysical Journal*, 512, 377 (1999)) while using the elemental abundances found in the Sun. The flux at the surface of a blackbody with $T = 8000\,{\rm K}$ (dotted curve) is also shown.

LeBlanc

◆ Calibration for $B - V = f(T_e)$

◆ The observed $(B - V)$ must be corrected for interstellar extinction in order to derive the stellar intrinsic $(B - V)0$

◆ More accurate determination of T by spectra and stellar atmosphere models, e.g., the Kurucz's model

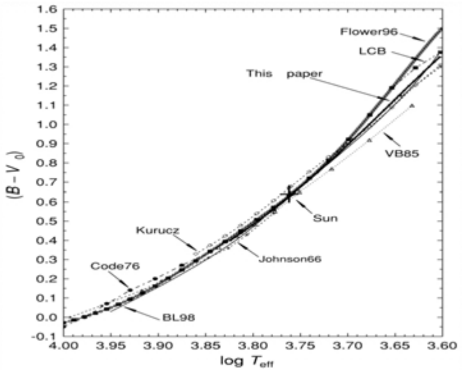

Color Excess

$$E_{B-V} = (B - V)_{\text{obs}} - (B - V)_{\text{int}}$$

$$(B - V)_\odot = 0.656 \pm 0.005$$

A special (line) filter

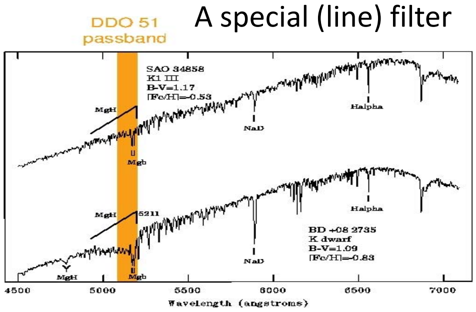

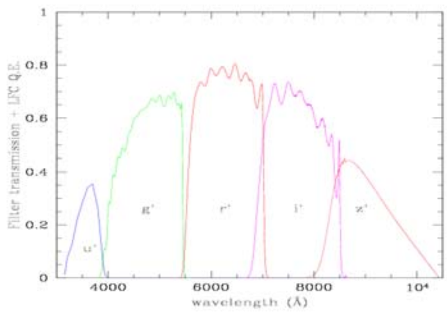

Sloan Digital Sky Survey

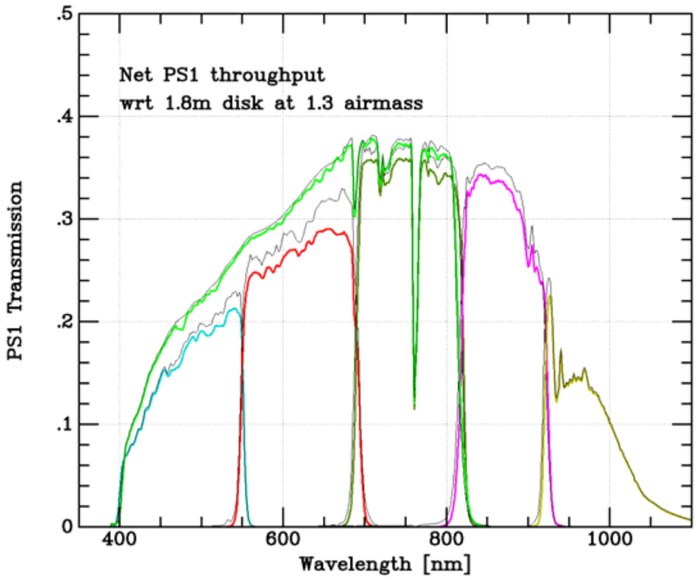

Different temperature, elements (at different excitation and ionization levels) → different set of spectral lines

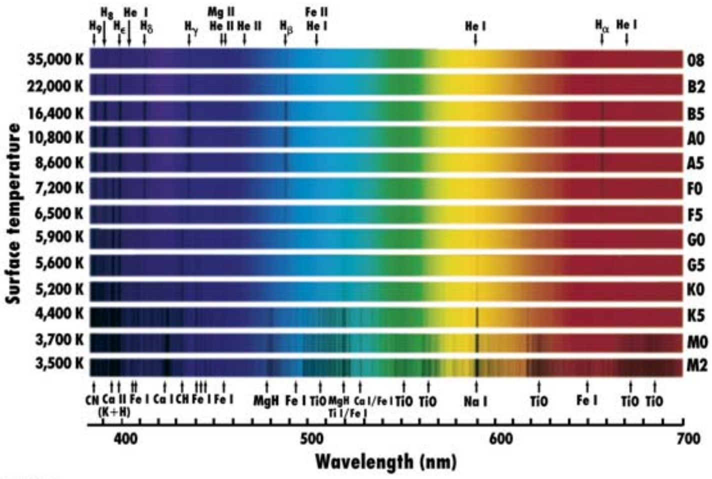

Figure 11-5
Discovering the Universe, Seventh Edition

Line ratios → Temperature

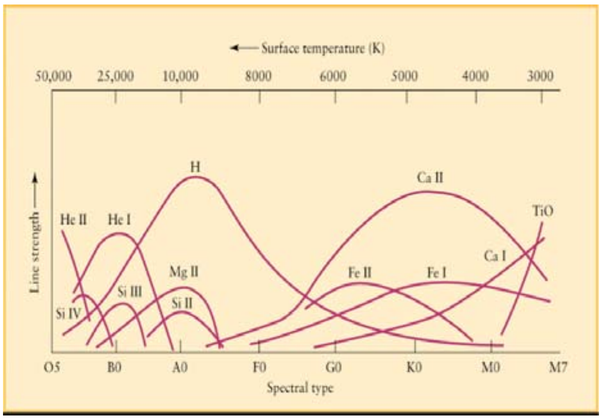

I --- neutral atoms; II --- ionized once; III --- ionized twice; …

e.g., H I = H^0 … H II = H^+ … He III = He^{+2} … Fe XXVI = Fe^{+25}

Hot stars --- peaked at short wavelengths (UV); mainly He lines, some H lines

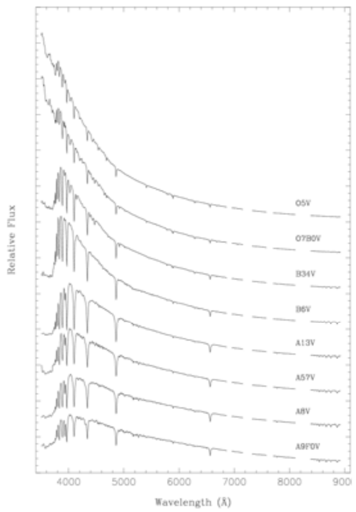

Warm stars --- peaked in the visible wavelengths; H lines prominent

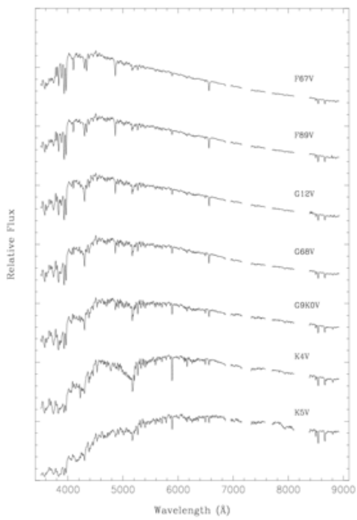

Cool stars --- peaked at long wavelengths (IR); molecular lines/bands

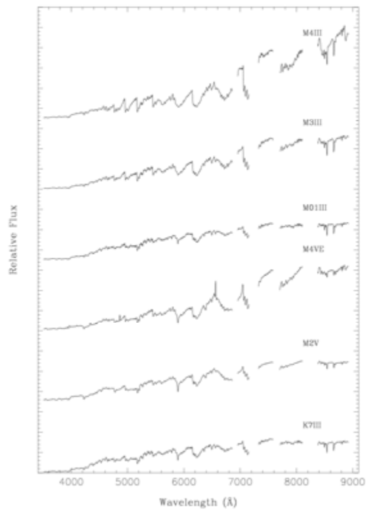

Brown dwarfs and Planetary Objects

L, T and Y types

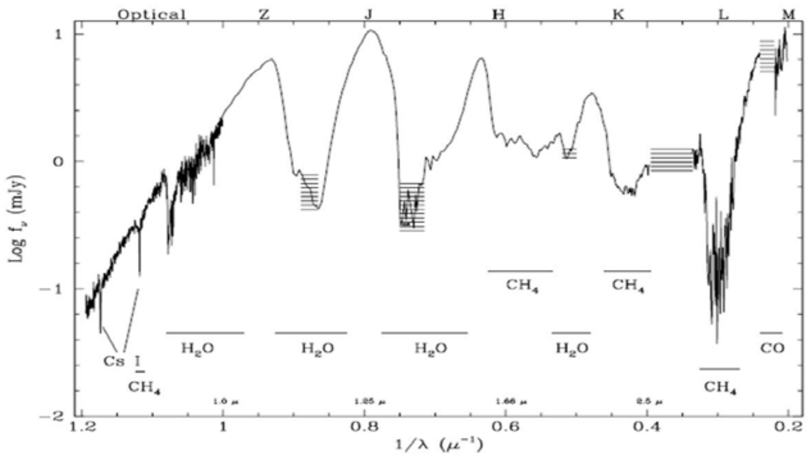

Oppenheimer et al. 1998

Brown dwarfs and Planetary Objects

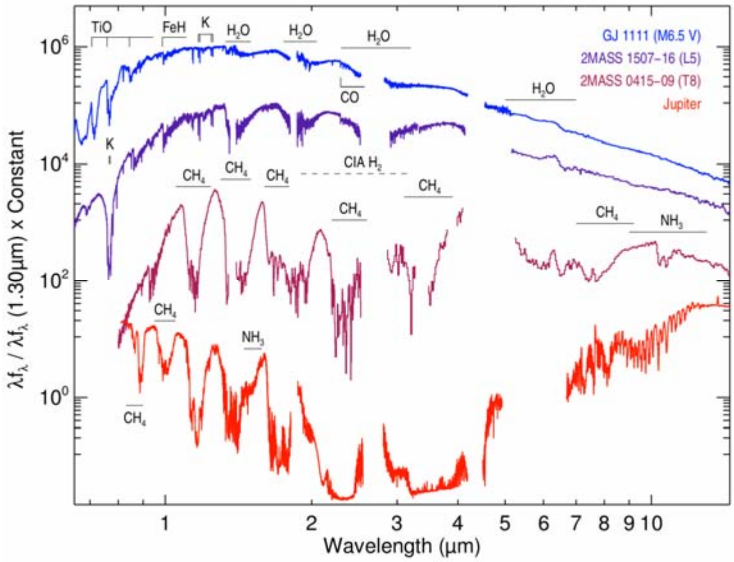

http://www.exoclimes.com/paper-outlines/exoplanets-and-brown-dwarfs-ii/

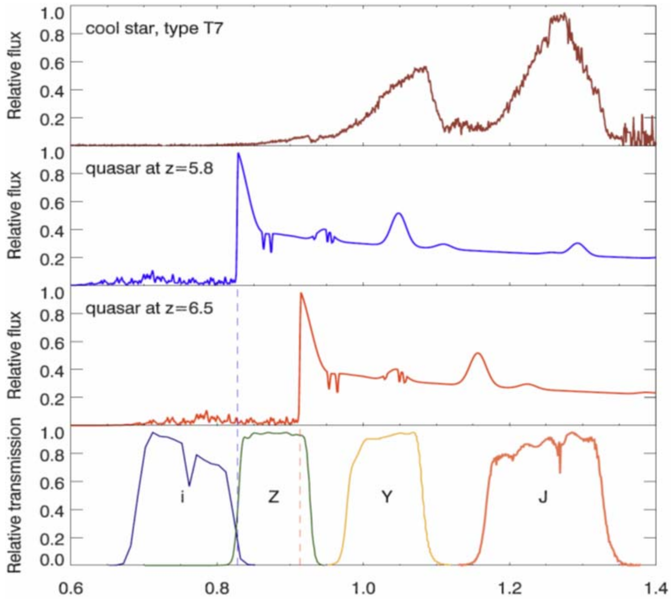

Using imaging photometry (time saving) to trace spectral features

One of the SDSS color-color diagrams

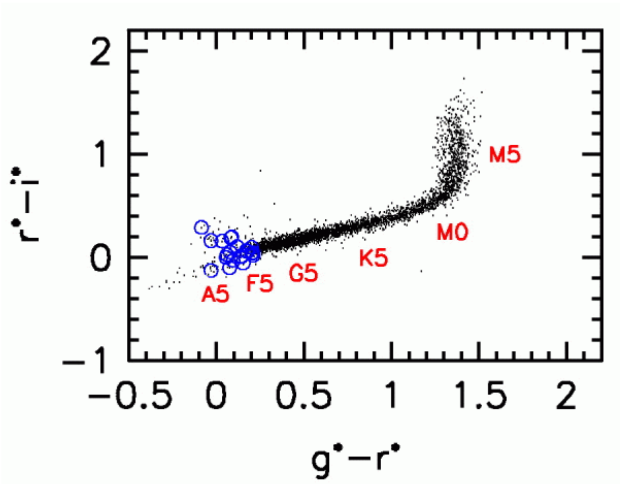

http://spiff.rit.edu/classes/phys440/lectures/color/sdss_color_color_b.gif

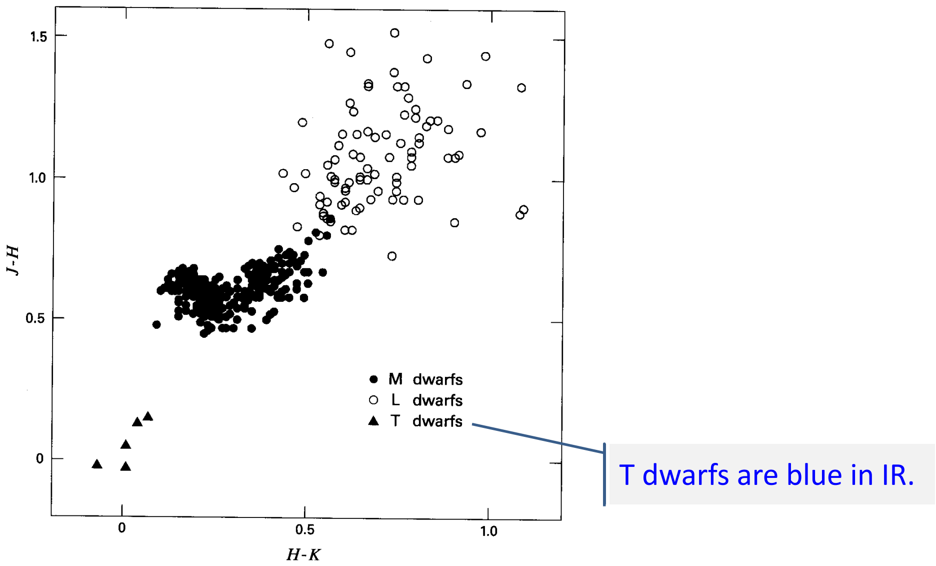

Figure 16.15 Near-infrared color-color plot of M dwarfs (*filled circles*), L dwarfs (*open circles*), and T dwarfs (*filled triangles*). The objects are from a variety of regions. Note that the typical measurement errors for the L- and T-dwarfs are quite large, about 0.13 mag.

Stahler & Palla

To measure the stellar luminosity

- **Absolute Magnitude** M defined as apparent magnitude of a star if it were placed at a distance of 10 pc

  $m_\lambda - M_\lambda = 5\log(d_{pc}) - 5$

  But there is extinction … $m_\lambda - M_\lambda = 5\log(d_{pc}) - 5 + A_\lambda$

- **Bolometric magnitude** – the absolute magnitude integrated over all wavelengths. We define the bolometric correction

  $M_{bol}^{\odot} = +4.74$

- **Bolometric Correction** $BC = M_{bol} - M_v$

  is a function of the spectral type (*min at the F type, why?*) and luminosity of a star.

  That is, we can apply BC (always negative, why?) to a star to estimate its luminosity (from the photosphere).

Apparent Magnitude $m = -2.5\ \log\ (\mathrm{Flux}) + \mathrm{ZeroPoint}$

- The Vega system: 0.0 mag (latest ~0.3 mag) at every Johnson band
- Gunn system: no Vega; use of F subdwarfs as standards (metal poor so smooth spectra), e.g., BD + 17 4708
- The AB system: $\mathrm{AB}_\nu = -2.5\ \log_{10} f_\nu - 48.60$
- STMAG system: used for HST photometry

$$\mathrm{STMAG}_\lambda = -2.5\ \log_{10} f_\lambda - 21.1$$

Table 15.7. *Calibration of MK spectral types.*

Sp	*M(V)*	*B − V*	*U − B*	*V − R*	*R − I*	T_{eff}	BC
MAIN SEQUENCE, V							
O5	−5.7	−0.33	−1.19	−0.15	−0.32	42 000	−4.40
O9	−4.5	−0.31	−1.12	−0.15	−0.32	34 000	−3.33
B0	−4.0	−0.30	−1.08	−0.13	−0.29	30 000	−3.16
B2	−2.45	−0.24	−0.84	−0.10	−0.22	20 900	−2.35
B5	−1.2	−0.17	−0.58	−0.06	−0.16	15 200	−1.46
B8	−0.25	−0.11	−0.34	−0.02	−0.10	11 400	−0.80
A0	+0.65	−0.02	−0.02	0.02	−0.02	9 790	−0.30
A2	+1.3	+0.05	+0.05	0.08	0.01	9 000	−0.20
A5	+1.95	+0.15	+0.10	0.16	0.06	8 180	−0.15
F0	+2.7	+0.30	+0.03	0.30	0.17	7 300	−0.09
F2	+3.6	+0.35	0.00	0.35	0.20	7 000	−0.11
F5	+3.5	+0.44	−0.02	0.40	0.24	6 650	−0.14
F8	+4.0	+0.52	+0.02	0.47	0.29	6 250	−0.16
G0	+4.4	+0.58	+0.06	0.50	0.31	5 940	−0.18
G2	+4.7	+0.63	+0.12	0.53	0.33	5 790	−0.20
G5	+5.1	+0.68	+0.20	0.54	0.35	5 560	−0.21
G8	+5.5	+0.74	+0.30	0.58	0.38	5 310	−0.40
K0	+5.9	+0.81	+0.45	0.64	0.42	5 150	−0.31
K2	+6.4	+0.91	+0.64	0.74	0.48	4 830	−0.42
K5	+7.35	+1.15	+1.08	0.99	0.63	4 410	−0.72
M0	+8.8	+1.40	+1.22	1.28	0.91	3 840	−1.38
M2	+9.9	+1.49	+1.18	1.50	1.19	3 520	−1.89
M5	+12.3	+1.64	+1.24	1.80	1.67	3 170	−2.73
GIANTS, III							
G5	+0.9	+0.86	+0.56	0.69	0.48	5 050	−0.34
G8	+0.8	+0.94	+0.70	0.70	0.48	4 800	−0.42
K0	+0.7	+1.00	+0.84	0.77	0.53	4 660	−0.50
K2	+0.5	+1.16	+1.16	0.84	0.58	4 390	−0.61
K5	−0.2	+1.50	+1.81	1.20	0.90	4 050	−1.02
M0	−0.4	+1.56	+1.87	1.23	0.94	3 690	−1.25
M2	−0.6	+1.60	+1.89	1.34	1.10	3 540	−1.62
M5	−0.3	+1.63	+1.58	2.18	1.96	3 380	−2.48

Table 15.7. *(Continued.)*

Sp	*M(V)*	*B − V*	*U − B*	*V − R*	*R − I*	T_{eff}	BC
SUPERGIANTS, I							
O9	−6.5	−0.27	−1.13	−0.15	−0.32	32 000	−3.18
B2	−6.4	−0.17	−0.93	−0.05	−0.15	17 600	−1.58
B5	−6.2	−0.10	−0.72	0.02	−0.07	13 600	−0.95
B8	−6.2	−0.03	−0.55	0.02	0.00	11 100	−0.66
A0	−6.3	−0.01	−0.38	0.03	0.05	9 980	−0.41
A2	−6.5	+0.03	−0.25	0.07	0.07	9 380	−0.28
A5	−6.6	+0.09	−0.08	0.12	0.13	8 610	−0.13
F0	−6.6	+0.17	+0.15	0.21	0.20	7 460	−0.01
F2	−6.6	+0.23	+0.18	0.26	0.21	7 030	−0.00
F5	−6.6	+0.32	+0.27	0.35	0.23	6 370	−0.03
F8	−6.5	+0.56	+0.41	0.45	0.27	5 750	−0.09
G0	−6.4	+0.76	+0.52	0.51	0.33	5 370	−0.15
G2	−6.3	+0.87	+0.63	0.58	0.40	5 190	−0.21
G5	−6.2	+1.02	+0.83	0.67	0.44	4 930	−0.33
G8	−6.1	+1.14	+1.07	0.69	0.46	4 700	−0.42
K0	−6.0	+1.25	+1.17	0.76	0.48	4 550	−0.50
K2	−5.9	+1.36	+1.32	0.85	0.55	4 310	−0.61
K5	−5.8	+1.60	+1.80	1.20	0.90	3 990	−1.01
M0	−5.6	+1.67	+1.90	1.23	0.94	3 620	−1.29
M2	−5.6	+1.71	+1.95	1.34	1.10	3 370	−1.62
M5	−5.6	+1.80	+1.60:	2.18	1.96	2 880	−3.47

Allen's *Astrophysical Quantities* (4th edition)

Table 15.8. *Calibration of MK spectral types.*[a]

Sp	$\mathcal{M}/\mathcal{M}_\odot$	$R/R_\odot$	$\log(g/g_\odot)$	$\log(\bar\rho/\bar\rho_\odot)$	v_{rot} (km s^{-1})
MAIN SEQUENCE, V					
O3	120	15	−0.3	−1.5	
O5	60	12	−0.4	−1.5	
O6	37	10	−0.45	−1.45	
O8	23	8.5	−0.5	−1.4	200
B0	17.5	7.4	−0.5	−1.4	170
B3	7.6	4.8	−0.5	−1.15	190
B5	5.9	3.9	−0.4	−1.00	240
B8	3.8	3.0	−0.4	−0.85	220
A0	2.9	2.4	−0.3	−0.7	180
A5	2.0	1.7	−0.15	−0.4	170
F0	1.6	1.5	−0.1	−0.3	100
F5	1.4	1.3	−0.1	−0.2	30
G0	1.05	1.1	−0.05	−0.1	10
G5	0.92	0.92	+0.05	−0.1	< 10
K0	0.79	0.85	+0.05	+0.1	< 10
K5	0.67	0.72	+0.1	+0.25	< 10
M0	0.51	0.60	+0.15	+0.35	
M2	0.40	0.50	+0.2	+0.8	
M5	0.21	0.27	+0.5	+1.0	
M8	0.06	0.10	+0.5	+1.2	

Table 15.8. *(Continued.)*

Sp	$\mathcal{M}/\mathcal{M}_\odot$	$R/R_\odot$	$\log(g/g_\odot)$	$\log(\bar\rho/\bar\rho_\odot)$	v_{rot} (km s^{-1})
GIANTS, III					
B0	20	15	−1.1	−2.2	120
B5	7	8	−0.95	−1.8	130
A0	4	5		−1.5	100
G0	1.0	6	−1.5	−2.4	30
G5	1.1	10	−1.9	−3.0	< 20
K0	1.1	15	−2.3	−3.5	< 20
K5	1.2	25	−2.7	−4.1	< 20
M0	1.2	40	−3.1	−4.7	
SUPERGIANTS, I					
O5	70	30:	−1.1	−2.6	
O6	40	25:	−1.2	−2.6	
O8	28	20	−1.2	−2.5	125
B0	25	30	−1.6	−3.0	102
B5	20	50	−2.0	−3.8	40
A0	16	60	−2.3	−4.1	40
A5	13	60	−2.4	−4.2	38
F0	12	80	−2.7	−4.6	30
F5	10	100	−3.0	−5.0	< 25
G0	10	120	−3.1	−5.2	< 25
G5	12	150	−3.3	−5.3	< 25
K0	13	200	−3.5	−5.8	< 25
K5	13	400	−4.1	−6.7	< 25
M0	13	500	−4.3	−7.0	
M2	19	800	−4.5	−7.4	

Note

[a] A colon indicates an uncertain value.

Allen's *Astrophysical Quantities* (4th edition)

Table 15.9. *Zero-age main sequence.*

$(B-V)_0$	$(U-B)_0$	M_v	$(B-V)_0$	$(U-B)_0$	M_v
$-0^m_.33$	$-1^m_.20$	$-5^m_.2$	+0.40	−0.01	+ 3.4
−0.305	−1.10	−3.6	+0.50	0.00	+ 4.1
−0.30	−1.08	−3.25	+0.60	+0.08	+ 4.7
−0.28	−1.00	−2.6	+0.70	+0.23	+ 5.2
−0.25	−0.90	−2.1	+0.80	+0.42	+ 5.8
−0.22	−0.80	−1.5	+0.90	+0.63	+ 6.3
−0.20	−0.69	−1.1	+1.00	+0.86	+ 6.7
−0.15	−0.50	−0.2	+1.10	+1.03	+ 7.1
−0.10	−0.30	+0.6	+1.20	+1.13	+ 7.5
−0.05	−0.10	+1.1	+1.30	+1.20	+ 8.0
0.00	+0.01	+1.5	+1.40	+1.22	+ 8.8
+0.05	+0.05	+1.7	+1.50	+1.17	+10.3
+0.10	+0.08	+1.9	+1.60	+1.20	+12.0

$(B-V)_0$	$(U-B)_0$	M_v	$(B-V)_0$	$(U-B)_0$	M_v
+0.15	+0.09	+2.1	+1.70	+1.32	+13.2
+0.20	+0.10	+2.4	+1.80	+1.43	+14.2
+0.25	+0.07	+2.55	+1.90	+1.53	+15.5
+0.30	+0.03	+2.8	+2.00	+1.64	+16.7
+0.35	0.00	+3.1			

Allen's *Astrophysical Quantities* (4th edition)

Main-Sequence Stars (Luminosity Class V)

Sp. Type	T_e (K)	$L/L_\odot$	$R/R_\odot$	$M/M_\odot$	M_{bol}	BC	M_V	$U-B$	$B-V$
O5	42000	499000	13.4	60	−9.51	−4.40	−5.1	−1.19	−0.33
O6	39500	324000	12.2	37	−9.04	−3.93	−5.1	−1.17	−0.33
O7	37500	216000	11.0	—	−8.60	−3.68	−4.9	−1.15	−0.32
O8	35800	147000	10.0	23	−8.18	−3.54	−4.6	−1.14	−0.32
B0	30000	32500	6.7	17.5	−6.54	−3.16	−3.4	−1.08	−0.30
B1	25400	9950	5.2	—	−5.26	−2.70	−2.6	−0.95	−0.26
B2	20900	2920	4.1	—	−3.92	−2.35	−1.6	−0.84	−0.24
B3	18800	1580	3.8	7.6	−3.26	−1.94	−1.3	−0.71	−0.20
B5	15200	480	3.2	5.9	−1.96	−1.46	−0.5	−0.58	−0.17
B6	13700	272	2.9	—	−1.35	−1.21	−0.1	−0.50	−0.15
B7	12500	160	2.7	—	−0.77	−1.02	+0.3	−0.43	−0.13
B8	11400	96.7	2.5	3.8	−0.22	−0.80	+0.6	−0.34	−0.11
B9	10500	60.7	2.3	—	+0.28	−0.51	+0.8	−0.20	−0.07
A0	9800	39.4	2.2	2.9	+0.75	−0.30	+1.1	−0.02	−0.02
A1	9400	30.3	2.1	—	+1.04	−0.23	+1.3	+0.02	+0.01
A2	9020	23.6	2.0	—	+1.31	−0.20	+1.5	+0.05	+0.05
A5	8190	12.3	1.8	2.0	+2.02	−0.15	+2.2	+0.10	+0.15
A8	7600	7.13	1.5	—	+2.61	−0.10	+2.7	+0.09	+0.25
F0	7300	5.21	1.4	1.6	+2.95	−0.09	+3.0	+0.03	+0.30
F2	7050	3.89	1.3	—	+3.27	−0.11	+3.4	+0.00	+0.35
F5	6650	2.56	1.2	1.4	+3.72	−0.14	+3.9	−0.02	+0.44
F8	6250	1.68	1.1	—	+4.18	−0.16	+4.3	+0.02	+0.52

Carroll & Ostelie

Main-Sequence Stars (Luminosity Class V)

Sp. Type	T_e (K)	$L/L_\odot$	$R/R_\odot$	$M/M_\odot$	M_{bol}	BC	M_V	$U-B$	$B-V$
G0	5940	1.25	1.06	1.05	+4.50	−0.18	+4.7	+0.06	+0.58
G2	5790	1.07	1.03	—	+4.66	−0.20	+4.9	+0.12	+0.63
Sun[a]	5777	1.00	1.00	1.00	+4.74	−0.08	+4.82	+0.195	+0.650
G8	5310	0.656	0.96	—	+5.20	−0.40	+5.6	+0.30	+0.74
K0	5150	0.552	0.93	0.79	+5.39	−0.31	+5.7	+0.45	+0.81
K1	4990	0.461	0.91	—	+5.58	−0.37	+6.0	+0.54	+0.86
K3	4690	0.318	0.86	—	+5.98	−0.50	+6.5	+0.80	+0.96
K4	4540	0.263	0.83	—	+6.19	−0.55	+6.7	—	+1.05
K5	4410	0.216	0.80	0.67	+6.40	−0.72	+7.1	+0.98	+1.15
K7	4150	0.145	0.74	—	+6.84	−1.01	+7.8	+1.21	+1.33
M0	3840	0.077	0.63	0.51	+7.52	−1.38	+8.9	+1.22	+1.40
M1	3660	0.050	0.56	—	+7.99	−1.62	+9.6	+1.21	+1.46
M2	3520	0.032	0.48	0.40	+8.47	−1.89	+10.4	+1.18	+1.49
M3	3400	0.020	0.41	—	+8.97	−2.15	+11.1	+1.16	+1.51
M4	3290	0.013	0.35	—	+9.49	−2.38	+11.9	+1.15	+1.54
M5	3170	0.0076	0.29	0.21	+10.1	−2.73	+12.8	+1.24	+1.64
M6	3030	0.0044	0.24	—	+10.6	−3.21	+13.8	+1.32	+1.73
M7	2860	0.0025	0.20	—	+11.3	−3.46	+14.7	+1.40	+1.80

Carroll & Ostelie

Giant Stars (Luminosity Class III)

Sp. Type	T_e (K)	$L/L_\odot$	$R/R_\odot$	$M/M_\odot$	M_{bol}	BC	M_V	$U-B$	$B-V$
O5	39400	741000	18.5	—	−9.94	−4.05	−5.9	−1.18	−0.32
O6	37800	519000	16.8	—	−9.55	−3.80	−5.7	−1.17	−0.32
O7	36500	375000	15.4	—	−9.20	−3.58	−5.6	−1.14	−0.32
O8	35000	277000	14.3	—	−8.87	−3.39	−5.5	−1.13	−0.31
B0	29200	84700	11.4	20	−7.58	−2.88	−4.7	−1.08	−0.29
B1	24500	32200	10.0	—	−6.53	−2.43	−4.1	−0.97	−0.26
B2	20200	11100	8.6	—	−5.38	−2.02	−3.4	−0.91	−0.24
B3	18300	6400	8.0	—	−4.78	−1.60	−3.2	−0.74	−0.20
B5	15100	2080	6.7	7	−3.56	−1.30	−2.3	−0.58	−0.17
B6	13800	1200	6.1	—	−2.96	−1.13	−1.8	−0.51	−0.15
B7	12700	710	5.5	—	−2.38	−0.97	−1.4	−0.44	−0.13
B8	11700	425	5.0	—	−1.83	−0.82	−1.0	−0.37	−0.11
B9	10900	263	4.5	—	−1.31	−0.71	−0.6	−0.20	−0.07
A0	10200	169	4.1	4	−0.83	−0.42	−0.4	−0.07	−0.03
A1	9820	129	3.9	—	−0.53	−0.29	−0.2	+0.07	+0.01
A2	9460	100	3.7	—	−0.26	−0.20	−0.1	+0.06	+0.05
A5	8550	52	3.3	—	+0.44	−0.14	+0.6	+0.11	+0.15
A8	7830	33	3.1	—	+0.95	−0.10	+1.0	+0.10	+0.25

Carroll & Ostelie

F0	7400	27	3.2	—	+1.17	−0.11	+1.3	+0.08	+0.30
F2	7000	24	3.3	—	+1.31	−0.11	+1.4	+0.08	+0.35
F5	6410	22	3.8	—	+1.37	−0.14	+1.5	+0.09	+0.43
G0	5470	29	6.0	1.0	+1.10	−0.20	+1.3	+0.21	+0.65
G2	5300	31	6.7	—	+1.00	−0.27	+1.3	+0.39	+0.77
G8	4800	44	9.6	—	+0.63	−0.42	+1.0	+0.70	+0.94
K0	4660	50	10.9	1.1	+0.48	−0.50	+1.0	+0.84	+1.00
K1	4510	58	12.5	—	+0.32	−0.55	+0.9	+1.01	+1.07
K3	4260	79	16.4	—	−0.01	−0.76	+0.8	+1.39	+1.27
K4	4150	93	18.7	—	−0.18	−0.94	+0.8	—	+1.38
K5	4050	110	21.4	1.2	−0.36	−1.02	+0.7	+1.81	+1.50
K7	3870	154	27.6	—	−0.73	−1.17	+0.4	+1.83	+1.53
M0	3690	256	39.3	1.2	−1.28	−1.25	+0.0	+1.87	+1.56
M1	3600	355	48.6	—	−1.64	−1.44	−0.2	+1.88	+1.58
M2	3540	483	58.5	1.3	−1.97	−1.62	−0.4	+1.89	+1.60
M3	3480	643	69.7	—	−2.28	−1.87	−0.4	+1.88	+1.61
M4	3440	841	82.0	—	−2.57	−2.22	−0.4	+1.73	+1.62
M5	3380	1100	96.7	—	−2.86	−2.48	−0.4	+1.58	+1.63
M6	3330	1470	116	—	−3.18	−2.73	−0.4	+1.16	+1.52

Carroll & Ostelie

Supergiant Stars (Luminosity Class Approximately Iab)

Sp. Type	T_e (K)	$L/L_\odot$	$R/R_\odot$	$M/M_\odot$	M_{bol}	BC	M_V	$U-B$	$B-V$
O5	40900	1140000	21.2	70	−10.40	−3.87	−6.5	−1.17	−0.31
O6	38500	998000	22.4	40	−10.26	−3.74	−6.5	−1.16	−0.31
O7	36200	877000	23.8	—	−10.12	−3.48	−6.6	−1.14	−0.31
O8	34000	769000	25.3	28	−9.98	−3.35	−6.6	−1.13	−0.29
B0	26200	429000	31.7	25	−9.34	−2.49	−6.9	−1.06	−0.23
B1	21400	261000	37.3	—	−8.80	−1.87	−6.9	−1.00	−0.19
B2	17600	157000	42.8	—	−8.25	−1.58	−6.7	−0.94	−0.17
B3	16000	123000	45.8	—	−7.99	−1.26	−6.7	−0.83	−0.13
B5	13600	79100	51.1	20	−7.51	−0.95	−6.6	−0.72	−0.10
B6	12600	65200	53.8	—	−7.30	−0.88	−6.4	−0.69	−0.08
B7	11800	54800	56.4	—	−7.11	−0.78	−6.3	−0.64	−0.05
B8	11100	47200	58.9	—	−6.95	−0.66	−6.3	−0.56	−0.03
B9	10500	41600	61.8	—	−6.81	−0.52	−6.3	−0.50	−0.02
A0	9980	37500	64.9	16	−6.70	−0.41	−6.3	−0.38	−0.01
A1	9660	35400	67.3	—	−6.63	−0.32	−6.3	−0.29	+0.02
A2	9380	33700	69.7	—	−6.58	−0.28	−6.3	−0.25	+0.03
A5	8610	30500	78.6	13	−6.47	−0.13	−6.3	−0.07	+0.09
A8	7910	29100	91.1	—	−6.42	−0.03	−6.4	+0.11	+0.14

Carroll & Ostelie

F0	7460	28800	102	12	−6.41	−0.01	−6.4	+0.15	+0.17
F2	7030	28700	114	—	−6.41	0.00	−6.4	+0.18	+0.23
F5	6370	29100	140	10	−6.42	−0.03	−6.4	+0.27	+0.32
F8	5750	29700	174	—	−6.44	−0.09	−6.4	+0.41	+0.56
G0	5370	30300	202	10	−6.47	−0.15	−6.3	+0.52	+0.76
G2	5190	30800	218	—	−6.48	−0.21	−6.3	+0.63	+0.87
G8	4700	32400	272	—	−6.54	−0.42	−6.1	+1.07	+1.15
K0	4550	33100	293	13	−6.56	−0.50	−6.1	+1.17	+1.24
K1	4430	34000	314	—	−6.59	−0.56	−6.0	+1.28	+1.30
K3	4190	36100	362	—	−6.66	−0.75	−5.9	+1.60	+1.46
K4	4090	37500	386	—	−6.70	−0.90	−5.8	—	+1.53
K5	3990	39200	415	13	−6.74	−1.01	−5.7	+1.80	+1.60
K7	3830	43200	473	—	−6.85	−1.20	−5.6	+1.84	+1.63
M0	3620	51900	579	13	−7.05	−1.29	−5.8	+1.90	+1.67
M1	3490	60300	672	—	−7.21	−1.38	−5.8	+1.90	+1.69
M2	3370	72100	791	19	−7.41	−1.62	−5.8	+1.95	+1.71
M3	3210	89500	967	—	−7.64	−2.13	−5.5	+1.95	+1.69
M4	3060	117000	1220	—	−7.93	−2.75	−5.2	+2.00	+1.76
M5	2880	165000	1640	24	−8.31	−3.47	−4.8	+1.60	+1.80
M6	2710	264000	2340	—	−8.82	−3.90	−4.9	—	—

Carroll & Ostelie

TABLE II

Adopted calibration of MK spectral types in absolute magnitudes M_V

Sp	ZAMS	V	IV	III	II	Ib	Iab	Ia
O5	−4.6	−5.6	−5.8	−6.0	−6.3	−6.6	−6.9	−7.2
O6	−4.0	−5.4	−5.7	−5.9	−6.3	−6.6	−6.9	−7.2
O7	−3.9	−5.2	−5.5	−5.8	−6.2	−6.5	−6.8	−7.2
O8	−3.7	−4.9	−5.2	−5.6	−6.1	−6.4	−6.7	−7.2
O9	−3.5	−4.5	−4.9	−5.3	−5.9	−6.3	−6.6	−7.2
B0	−3.1	−4.0	−4.4	−4.9	−5.6	−6.1	−6.5	−7.2
B1	−2.3	−3.3	−3.9	−4.5	−5.2	−5.9	−6.4	−7.2
B2	−1.6	−2.5	−3.1	−3.7	−5.0	−5.9	−6.4	−7.2
B3	−1.0	−1.7	−2.3	−3.0	−4.8	−5.9	−6.4	−7.2
B5	−0.1	−0.8	−1.2	−1.7	−4.6	−5.9	−6.4	−7.2
B6	0.3	−0.5	−0.9	−1.3	−4.4	−5.8	−6.4	−7.2
B7	0.6	−0.2	−0.6	−1.0	−4.2	−5.8	−6.4	−7.2
B8	1.0	0.1	−0.3	−0.7	−3.9	−5.8	−6.4	−7.2
B9	1.4	0.5	0.1	−0.4	−3.6	−5.7	−6.4	−7.2
A0	1.6	0.8	0.4	−0.1	−3.4	−5.5	−6.4	−7.2
A1	1.7	1.1	0.7	0.2	−3.2	−5.3	−6.4	−7.2
A2	1.8	1.3	0.9	0.4	−3.1	−5.2	−6.4	−7.3
A3	1.9	1.5	1.0	0.5	−3.0	−5.1	−6.4	−7.3
A5	2.3	1.9	1.4	0.8	−2.9	−5.0	−6.5	−7.5
A7	2.6	2.3	1.7	1.1	−2.8	−5.0	−6.7	−7.7
F0	3.0	2.8	2.2	1.5	−2.7	−5.0	−6.9	−7.9
F2	3.2	3.1	2.4	1.8	−2.6	−4.9	−7.0	−8.0
F5	3.7	3.6	2.6	2.0	−2.6	−4.8	−7.1	−8.0
F8	4.2	4.1	2.8		−2.5	−4.7	−7.2	−8.1
G0	4.5	4.4	2.9		−2.4	−4.6	−7.2	−8.2
G2		4.7	3.0	1.1:	−2.4	−4.5	−7.2	−8.2
G5		5.1	3.1	1.0	−2.4	−4.4	−7.2	−8.2
G8		5.6	3.2	0.9	−2.5	−4.3	−7.0	−8.1
K0		6.0	3.2	0.8	−2.5	−4.3	−6.8	−7.9
K1		6.2	3.2	0.8	−2.5	−4.3	−6.7	−7.7
K2		6.5		0.7	−2.5	−4.3	−6.6	−7.6
K3		6.7		0.6	−2.5	−4.3	−6.5	−7.5
K4		7.0		0.5	−2.6	−4.4	−6.4	−7.4
K5		7.3		0.3	−2.6	−4.4	−6.2	−7.2
K7		8.1		0.0	−2.7	−4.5	−6.0	−7.0
M0		8.9		−0.6	−2.8	−4.6	−5.8	−6.9
M1		9.4		−0.8	−2.9	−4.6	−5.8	−6.8
M2		10.0		−0.9	−3.0	−4.7	−5.8	−6.7
M3		10.5		−1.0	−3.0	−4.7	−5.8	−6.7
M4		11.5		−0.6	−3.1	−4.7	−5.8	−6.7
M5		13.5		−0.1	−3.1	−4.7	−5.8	−6.7

TABLE III

Adopted temperatures and bolometric corrections for MK spectral types

	log T_{eff}			Bol. Correction		
Sp	V	III	I–II	V	III	I–II
O5	4.626		4.618	−4.15		−3.80
O6	4.593		4.585	−3.90		−3.55
O7	4.568		4.556	−3.65		−3.30
O8	4.550		4.535	−3.40		−3.15
O9	4.525		4.512	−3.15		−2.95
B0	4.498		4.431	−2.95		−2.50
B1	4.423		4.371	−2.60		−2.15
B2	4.362		4.307	−2.20		−1.75
B3	4.286		4.243	−1.85		−1.40
B5	4.188		4.137	−1.30		−0.90
B6	4.152		4.100	−1.05		−0.75
B7	4.107		4.068	−0.80		−0.60
B8	4.061		4.041	−0.55		−0.45
B9	4.017		4.013	−0.35		−0.35
A0	3.982		3.991	−0.25		−0.25
A1	3.973		3.978	−0.16		−0.16
A2	3.961		3.964	−0.10		−0.10
A3	3.949		3.949	−0.03		−0.03
A5	3.924		3.919	0.02		0.05
A7	3.903		3.897	0.02		0.09
F0	3.863		3.869	0.02		0.13
F2	3.845		3.851	0.01		0.11
F5	3.813		3.813	−0.02		0.08
F8	3.789	3.782	3.778	−0.03		0.03
G0	3.774	3.763	3.756	−0.05		0.00
G2	3.763	3.740	3.732	−0.07		−0.05
G5	3.740	3.712	3.699	−0.09	−0.22	−0.13
G8	3.720	3.695	3.663	−0.13	−0.28	−0.22
K0	3.703	3.681	3.643	−0.19	−0.37	−0.29
K1	3.695	3.663	3.633		−0.43	−0.35
K2	3.686	3.648	3.623	−0.30	−0.49	−0.42
K3	3.672	3.628	3.613		−0.66	−0.57
K4	3.663	3.613			−0.86	−0.75
K5	3.643	3.602	3.585	−0.62	−1.15	−1.17
K7	3.602			−0.89		
M0	3.591	3.591	3.568	−1.17	−1.25	−1.25
M1	3.574	3.580	3.556	−1.45	−1.45	−1.40
M2	3.550	3.574	3.544	−1.71	−1.65	−1.60
M3	3.531	3.562	3.518	−1.92	−1.95	−2.0
M4	3.512	3.550	3.491	−2.24	−2.4	−2.6
M5	3.491	3.531	3.470	−2.55	−3.1	−3.3
M6		3.512		−4.4	−4.0	

Straižys & Kuriliene (1981)

TABLE IV

Bolometric absolute magnitudes M_{bol} for MK spectral types

Sp	ZAMS	V	IV	III	II	Ib	Iab	Ia
O5	−8.7	−9.8	−10.0	−10.2	−10.3	−10.4	−10.7	−11.0
O6	−8.0	−9.3	−9.6	−9.8	−9.9	−10.2	−10.4	−10.8
O7	−7.5	−8.8	−9.1	−9.3	−9.5	−9.8	−10.1	−10.5
O8	−7.2	−8.3	−8.6	−8.9	−9.2	−9.6	−9.8	−10.4
O9	−6.7	−7.6	−8.1	−8.4	−8.9	−9.3	−9.6	−10.2
B0	−6.2	−7.0	−7.4	−7.9	−8.1	−8.6	−9.0	−9.7
B1	−4.9	−5.8	−6.3	−6.8	−7.4	−8.0	−8.6	−9.4
B2	−4.0	−4.7	−5.3	−5.9	−6.8	−7.6	−8.2	−9.0
B3	−2.8	−3.6	−4.1	−4.7	−6.2	−7.3	−7.8	−8.6
B5	−1.4	−2.1	−2.5	−3.0	−5.4	−6.8	−7.3	−8.1
B6	−0.9	−1.6	−2.0	−2.4	−5.2	−6.6	−7.2	−7.9
B7	−0.2	−1.0	−1.4	−1.8	−4.8	−6.4	−7.0	−7.8
B8	0.4	−0.4	−0.8	−1.2	−4.4	−6.2	−6.9	−7.6
B9	1.0	0.1	−0.2	−0.8	−4.0	−6.0	−6.8	−7.5
A0	1.4	0.7	0.2	−0.3	−3.6	−5.7	−6.6	−7.4
A1	1.6	0.9	0.5	−0.1	−3.3	−5.5	−6.6	−7.4
A2	1.7	1.2	0.7	0.1	−3.1	−5.3	−6.5	−7.4
A3	1.9	1.5	1.0	0.4	−3.0	−5.2	−6.4	−7.4
A5	2.3	1.9	1.4	0.8	−2.8	−5.0	−6.4	−7.4
A7	2.6	2.3	1.8	1.1	−2.7	−4.9	−6.5	−7.6
F0	3.0	2.9	2.2	1.6	−2.6	−4.8	−6.7	−7.8
F2	3.2	3.1	2.4	1.8	−2.5	−4.8	−6.8	−7.9
F5	3.7	3.6	2.6	2.0	−2.5	−4.7	−7.0	−7.9
F8	4.2	4.1	2.8		−2.4	−4.6	−7.1	−8.0
G0	4.4	4.4	2.9		−2.4	−4.6	−7.2	−8.1
G2	4.6	4.6	2.9	1.0	−2.4	−4.6	−7.2	−8.2
G5		5.1	3.0	0.8	−2.5	−4.5	−7.3	−8.3
G8		5.5	3.1	0.6	−2.7	−4.5	−7.2	−8.3
K0		5.8	3.0	0.5	−2.8	−4.6	−7.1	−8.2
K1		5.9	3.0	0.4	−2.9	−4.6	−7.1	−8.1
K2		6.0		0.2	−3.0	−4.7	−7.0	−8.0
K3		6.2		−0.1	−3.1	−4.9	−7.0	−8.0
K4		6.4		−0.4				
K5		6.7		−0.9	−3.7	−5.4	−7.0	−8.0
K7		7.3						
M0		7.5		−1.8	−4.0	−5.8	−7.0	−8.1
M1		7.9		−2.4	−4.3	−6.0	−7.2	−8.2
M2		8.3		−2.6	−4.5	−6.2	−7.4	−8.3
M3		8.8		−2.9	−5.1	−6.7	−7.8	−8.7
M4		9.3		−3.1	−5.7	−7.3	−8.4	−9.3
M5		11.0		−3.2	−6.3	−8.0	−9.1	−10.0
M6				−3.6				

TABLE VI

Stellar masses log $\mathfrak{M}/\mathfrak{M}_\odot$ for different MK spectral types derived from the evolutionary tracks

Sp	ZAMS	V	IV	III	II	Ib	Iab	Ia
O5	1.60	1.81	1.85	1.89	1.90	1.92	1.99	
O6	1.48	1.70	1.76	1.80	1.80	1.87	1.91	2.00
O7	1.40	1.59	1.65	1.68	1.71	1.76	1.83	1.92
O8	1.34	1.48	1.54	1.60	1.65	1.72	1.76	1.90
O9	1.28	1.38	1.45	1.49	1.58	1.66	1.72	1.83
B0	1.20	1.30	1.34	1.40	1.40	1.48	1.56	1.70
B1	1.04	1.11	1.18	1.23	1.28	1.38	1.46	1.64
B2	0.92	0.99	1.04	1.08	1.18	1.30	1.38	1.54
B3	0.78	0.84	0.88	0.94	1.11	1.23	1.32	1.45
B5	0.62	0.68	0.72	0.75	1.00	1.18	1.26	1.40
B6	0.56	0.61	0.64	0.68	0.94	1.15	1.26	1.38
B7	0.49	0.53	0.57	0.60	0.91	1.11	1.23	1.36
B8	0.43	0.48	0.49	0.52	0.88	1.08	1.20	1.34
B9	0.36	0.41	0.45	0.49	0.85	1.04	1.20	1.32
A0	0.32	0.35	0.39	0.43	0.81	1.04	1.18	1.30
A1	0.31	0.34	0.36	0.41	0.78	1.00	1.18	1.30
A2	0.29	0.32	0.34	0.39	0.75	0.98	1.15	1.30
A3	0.27	0.30	0.32	0.36	0.75	0.97	1.11	1.30
A5	0.23	0.26	0.29	0.33	0.74	0.95	1.11	1.30
A7	0.20	0.22	0.26	0.30	0.73	0.94	1.15	1.32
F0	0.16	0.16	0.20	0.23	0.72	0.93	1.20	1.38
F2	0.13	0.13	0.16	0.20	0.72	0.93	1.20	1.40
F5	0.08	0.08	0.13	0.18	0.72	0.93	1.26	1.40
F8	0.04	0.04	0.11		0.72	0.93	1.28	1.41
G0	0.02	0.02	0.10		0.72	0.93	1.30	1.43
G2	0.00	0.00	0.10	0.33	0.72	0.93	1.30	1.45
G5		−0.02	0.08	0.39	0.73	0.94	1.32	1.46
G8		−0.04	0.08	0.42	0.76	0.94	1.32	1.46
K0		−0.07	0.11	0.46	0.78	0.96	1.30	1.45
K1		−0.10	0.13	0.46	0.78	0.96	1.30	1.45
K2		−0.10		0.45	0.79	0.98	1.28	1.43
K3		−0.12		0.38	0.80	1.00	1.30	1.43
K4		−0.15		0.36				
K5		−0.19		0.37	0.83	1.08	1.30	1.45
K7		−0.22						
M0		−0.26		0.48	0.83	1.15	1.32	1.46
M1		−0.30		0.54	0.83	1.18	1.34	1.48
M2		−0.35		0.54	0.81	1.18	1.36	1.50
M3		−0.40		0.52	0.84	1.20	1.38	1.56
M4		−0.52		0.51				
M5		(−0.82)		(0.41)				
M6				(0.40)				

Straižys & Kuriliene (1981)

TABLE VII

Calibration of MK spectral types in surface gravities (log g)

Sp	ZAMS	V	IV	III	II	Ib	Iab	Ia
O5	4.13	3.90	3.86	3.82	3.76	3.74	3.69	
O6	4.16	3.86	3.80	3.76	3.69	3.64	3.60	3.53
O7	4.18	3.85	3.80	3.74	3.64	3.57	3.52	3.45
O8	4.17	3.87	3.81	3.75	3.62	3.53	3.49	3.39
O9	4.21	3.95	3.82	3.74	3.58	3.50	3.44	3.31
B0	4.22	4.00	3.88	3.74	3.39	3.27	3.19	3.05
B1	4.28	4.00	3.86	3.71	3.31	3.17	3.01	2.87
B2	4.28	4.06	3.88	3.68	3.19	3.00	2.84	2.68
B3	4.31	4.06	3.89	3.71	3.12	2.79	2.68	2.49
B5	4.32	4.10	3.98	3.81	2.90	2.52	2.40	2.22
B6	4.32	4.09	3.96	3.84	2.77	2.42	2.29	2.13
B7	4.35	4.07	3.95	3.82	2.77	2.33	2.21	2.02
B8	4.34	4.07	3.92	3.79	2.79	2.27	2.11	1.97
B9	4.34	4.03	3.94	3.75	2.81	2.20	2.04	1.88
A0	4.32	4.07	3.91	3.75	2.85	2.23	2.01	1.81
A1	4.35	4.10	3.96	3.78	2.88	2.22	1.96	1.76
A2	4.32	4.16	3.98	3.78	2.87	2.23	1.92	1.71
A3	4.34	4.20	4.03	3.83	2.85	2.20	1.86	1.65
A5	4.36	4.22	4.06	3.86	2.81	2.14	1.74	1.53
A7	4.36	4.26	4.10	3.86	2.75	2.08	1.65	1.38
F0	4.32	4.28	4.05	3.83	2.67	2.00	1.51	1.25
F2	4.30	4.26	4.01	3.81	2.63	1.92	1.39	1.15
F5	4.32	4.28	3.93	3.74	2.48	1.81	1.22	1.00
F8	4.39	4.35	3.89		2.38	1.71	1.06	0.83
G0	4.39	4.39	3.84		2.29	1.62	0.95	0.72
G2	4.40	4.40	3.77	3.20	2.20	1.53	0.86	0.61
G5		4.49	3.71	3.07	2.04	1.45	0.71	0.45
G8		4.55	3.64	2.95	1.84	1.30	0.60	0.30
K0		4.57	3.57	2.89	1.74	1.20	0.54	0.25
K1		4.55	3.55	2.78	1.66	1.16	0.54	0.25
K2		4.55		2.63	1.59	1.10	0.48	0.23
K3		4.56		2.36	1.52	1.00	0.46	0.19
K4		4.57		2.16				
K5		4.57		1.93	1.20	0.77	0.35	0.10
K7		4.62						
M0		4.61		1.63	1.01	0.61	0.30	0.00
M1		4.67		1.41	0.84	0.51	0.19	−0.07
M2		4.69		1.31	0.70	0.39	0.09	−0.13
M3		4.71		1.12	0.38	0.10	−0.16	−0.34
M4		4.77		0.98				
M5		5.06		(0.76)				
M6				(0.52)				

TABLE VIII

Stellar radii log $R/R_\odot$ for different MK spectral types

Sp	ZAMS	V	IV	III	II	Ib	Iab	Ia
O5	0.95	1.17	1.21	1.25	1.28	1.30	1.36	
O6	0.87	1.13	1.19	1.23	1.27	1.33	1.37	1.45
O7	0.82	1.08	1.14	1.18	1.25	1.31	1.37	1.45
O8	0.80	1.02	1.08	1.14	1.23	1.31	1.35	1.47
O9	0.75	0.93	1.03	1.09	1.22	1.30	1.36	1.48
B0	0.70	0.86	0.94	1.04	1.20	1.32	1.40	1.54
B1	0.59	0.77	0.87	0.97	1.20	1.32	1.44	1.60
B2	0.54	0.68	0.80	0.92	1.21	1.37	1.49	1.65
B3	0.45	0.61	0.71	0.83	1.21	1.43	1.53	1.69
B5	0.36	0.50	0.58	0.68	1.27	1.55	1.65	1.81
B6	0.34	0.48	0.56	0.64	1.30	1.58	1.70	1.84
B7	0.29	0.45	0.53	0.61	1.28	1.60	1.72	1.88
B8	0.26	0.42	0.50	0.58	1.26	1.62	1.76	1.90
B9	0.23	0.41	0.47	0.59	1.23	1.63	1.79	1.93
A0	0.22	0.36	0.46	0.56	1.20	1.62	1.80	1.96
A1	0.19	0.33	0.41	0.53	1.16	1.60	1.82	1.98
A2	0.20	0.30	0.40	0.52	1.15	1.59	1.83	2.01
A3	0.18	0.26	0.36	0.48	1.16	1.60	1.84	2.04
A5	0.15	0.23	0.33	0.45	1.18	1.62	1.90	2.10
A7	0.13	0.19	0.29	0.43	1.21	1.65	1.97	2.19
F0	0.13	0.15	0.29	0.41	1.24	1.68	2.06	2.28
F2	0.13	0.15	0.29	0.41	1.26	1.72	2.12	2.34
F5	0.09	0.11	0.31	0.43	1.30	1.77	2.23	2.41
F8	0.04	0.06	0.33		1.38	1.82	2.32	2.50
G0	0.03	0.03	0.34		1.43	1.87	2.39	2.57
G2	0.01	0.01	0.38	0.78	1.48	1.92	2.44	2.64
G5		−0.04	0.41	0.88	1.56	1.96	2.52	2.72
G8		−0.08	0.43	0.95	1.67	2.03	2.57	2.79
K0		−0.11	0.48	1.00	1.73	2.09	2.59	2.81
K1		−0.11	0.50	1.05	1.77	2.11	2.61	2.81
K2		−0.11		1.12	1.81	2.15	2.61	2.81
K3		−0.12		1.22	1.85	2.21	2.63	2.83
K4		−0.15		1.31				
K5		−0.17		1.44	2.03	2.37	2.69	2.89
K7		−0.20						
M0		−0.22		1.64	2.12	2.48	2.72	2.92
M1		−0.27		1.78	2.21	2.55	2.78	2.99
M2		−0.30		1.83	2.27	2.61	2.85	3.03
M3		−0.36		1.92	2.44	2.76	2.98	3.16
M4		−0.42		1.98				
M5		−0.72		(2.04)				
M6				(2.16)				

Straižys & Kuriliene (1981)

Table 7.5. *Filter wavelengths, bandwidths, and flux densities for Vega.*[a]

Filter name	λ_{iso}[b] (μm)	$\Delta\lambda$[c] (μm)	F_λ (W m^{-2} μm^{-1})	F_ν (Jy)	N_ϕ (photons s^{-1} m^{-2} μm^{-1})
V	0.5556[d]	. . .	3.44×10^{-8}	3 540	9.60×10^{10}
J	1.215	0.26	3.31×10^{-9}	1 630	2.02×10^{10}
H	1.654	0.29	1.15×10^{-9}	1 050	9.56×10^{9}
K_s	2.157	0.32	4.30×10^{-10}	667	4.66×10^{9}
K	2.179	0.41	4.14×10^{-10}	655	4.53×10^{9}
L	3.547	0.57	6.59×10^{-11}	276	1.17×10^{9}
L'	3.761	0.65	5.26×10^{-11}	248	9.94×10^{8}
M	4.769	0.45	2.11×10^{-11}	160	5.06×10^{8}
8.7	8.756	1.2	1.96×10^{-12}	50.0	8.62×10^{7}
N	10.472	5.19	9.63×10^{-13}	35.2	5.07×10^{7}
11.7	11.653	1.2	6.31×10^{-13}	28.6	3.69×10^{7}
Q	20.130	7.8	7.18×10^{-14}	9.70	7.26×10^{6}

$$1\ \text{Jansky} = 10^{-23}\ \text{erg s}^{-1}\ \text{cm}^{-2}\ \text{Hz}^{-1}$$
$$= 1.51 \times 10^{7}\ \text{photons s}^{-1}\ \text{m}^{-2}\ (\Delta\lambda/\lambda)^{-1}$$

Allen's *Astrophysical Quantities* (4th edition)

Band	λ_0	$d\lambda/\lambda$	f_ν (m=0)	Reference
	μm		Jy	
U	0.36	0.15	1810	Bessel (1979)
B	0.44	0.22	4260	Bessel (1979)
V	0.55	0.16	3640	Bessel (1979)
R	0.64	0.23	3080	Bessel (1979)
I	0.79	0.19	2550	Bessel (1979)
J	1.26	0.16	1600	Campins, Reike, & Lebovsky (1985)
H	1.60	0.23	1080	Campins, Reike, & Lebovsky (1985)
K	2.22	0.23	670	Campins, Reike, & Lebovsky (1985)
g	0.52	0.14	3730	Schneider, Gunn, & Hoessel (1983)
r	0.67	0.14	4490	Schneider, Gunn, & Hoessel (1983)
i	0.79	0.16	4760	Schneider, Gunn, & Hoessel (1983)
z	0.91	0.13	4810	Schneider, Gunn, & Hoessel (1983)

https://www.astro.umd.edu/~ssm/ASTR620/mags.html

Notes

[a]Cohen et al. [1] recommend the use of Sirius rather than Vega as the photometric standard for $\lambda > 20$ μm because of the infrared excess of Vega at these wavelengths. The magnitude of Vega depends on the photometric system used, and it is either assumed to be 0.0 mag or assumed to be 0.02 or 0.03 mag for consistency with the visual magnitude.

[b]The infrared isophotal wavelengths and flux densities (except for K_s) are taken from Table 1 of [1], and they are based on the UKIRT filter set and the atmospheric absorption at Mauna Kea. See Table 2 of [1] for the case of the atmospheric absorption at Kitt Peak. The isophotal wavelength is defined by $F(\lambda_{\rm iso}) = \int F(\lambda)S(\lambda)\,d\lambda / \int S(\lambda)\,d\lambda$, where $F(\lambda)$ is the flux density of Vega and $S(\lambda)$ is the (detector quantum efficiency) × (filter transmission) × (optical efficiency) × (atmospheric transmission) [2]. $\lambda_{\rm iso}$ depends on the spectral shape of the source and a correction must be applied for broadband photometry of sources that deviate from the spectral shape of the standard star [3]. The flux density and $\lambda_{\rm iso}$ for K_s were calculated here. For another filter, K', at 2.11 μm, see [4].

[c]The filter full width at half maximum.

[d]The wavelength at V is a monochromatic wavelength; see [5].

References

1. Cohen, M. et al. 1992, *AJ*, **104**, 1650
2. Golay, M. 1974, *Introduction to Astronomical Photometry* (Reidel, Dordrecht), p. 40
3. Hanner, M.S., et al. 1984, *AJ*, **89**, 162
4. Wainscoat, R.J., & Cowie, L.L. 1992, *AJ*, **103**, 332
5. Hayes, D.S. 1985, in *Calibration of Fundamental Stellar Quantities*, edited by D.S. Hayes, et al., Proc. IAU Symp. No. 111 (Reidel, Dordrecht), p. 225

Allen's *Astrophysical Quantities* (4th edition)

Exercise

Sirius, the brightest star in the night sky, has been measured $m_B = -1.47,\ m_V = -1.47.$ The star has an annual parallax of $0.379''/\text{yr}$.

1. What is its distance in parsec?
2. What is its absolute V-band magnitude?
3. From the absolute magnitude, what spectral type can be inferred for Sirius?
4. From the observed (B-V) color, what spectral type can be inferred?
5. What kinds of uncertainties/assumptions are associated with the above estimations?

SIMBAD Astronomical Database


2015/4/21 sirius

Portal Simbad VizieR Aladin X-Match Other Help

sirius

other query modes : Identifier query Coordinate query Criteria query Reference query Basic query Script submission Output options Help

Query : sirius

Available data : Basic data • Identifiers • Plot & images • Bibliography • Measurements • External archives • Notes • Ann

Basic data :

* **alf CMa** -- Double or multiple star

Other object types:	* (* ,BD,GC,HD,HIC,HIP,HR,SAO,UBV) , IR (AKARI ,IRAS,IRC,2MASS,RAFGL) , ** (** ,WDS) , PM* (LHS) , V* (NSV) , UV (TD1)
ICRS coord. *(ep=J2000) :*	06 45 08.91728 -16 42 58.0171 (Optical) [11.70 10.90 90] A 2007A&A...474..653V
FK5 coord. *(ep=J2000 eq=2000) :*	06 45 08.917 -16 42 58.02 [11.70 10.90 90]
FK4 coord. *(ep=B1950 eq=1950) :*	06 42 56.72 -16 38 45.4 [67.39 63.09 0]
Gal coord. *(ep=J2000) :*	227.2303 -08.8903 [11.70 10.90 90]
Proper motions *mas/yr* :	-546.01 -1223.07 [1.33 1.24 0] A 2007A&A...474..653V
Radial velocity / Redshift / cz :	V(km/s) -5.50 [0.4] / z(~) -0.000018 [0.000001] / cz -5.50 [0.40] (~) A 2006AstL...32..759G
Parallaxes *mas*:	379.21 [1.58] A 2007A&A...474..653V
Spectral type:	A1V+DA C 2013yCat....1.2023S
Fluxes (8) :	U -1.51 [~] C 2002yCat.2237....0D
	B -1.46 [~] C 2002yCat.2237....0D
	V -1.46 [~] C 2002yCat.2237....0D
	R -1.46 [~] C 2002yCat.2237....0D
	I -1.43 [~] C 2002yCat.2237....0D
	J -1.36 [~] C 2002yCat.2237....0D
	H -1.33 [~] C 2002yCat.2237....0D
	K -1.35 [~] C 2002yCat.2237....0D

http://simbad.u-strasbg.fr/simbad/

To measure the stellar mass

- Stellar mass difficult to measure, direct measurements, except the Sun, only by binary systems
  (but uncertain even for these, why?)
- Then one gets the m*ass-luminosity relation* $L \propto M^{\alpha}$ where the slope α=3 to 5, <u>depending on the mass range</u>
- The main-sequence (MS) is a sequence of stellar mass under hydrostatic equilibrium
- Why are lower mass stars cooler on the surface and fainter in luminosity?

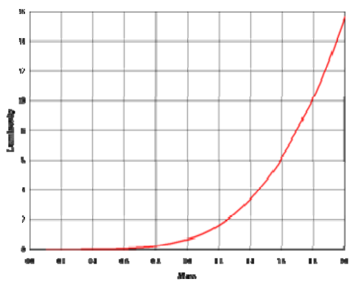

$M_{\max} \sim 120\ M_{\odot}$
$M_{\min} \sim 0.008\ M_{\odot}$
$L_{\max} \sim 10^{+6}\ L_{\odot}$
$L_{\min} \sim 10^{-4}\ L_{\odot}$

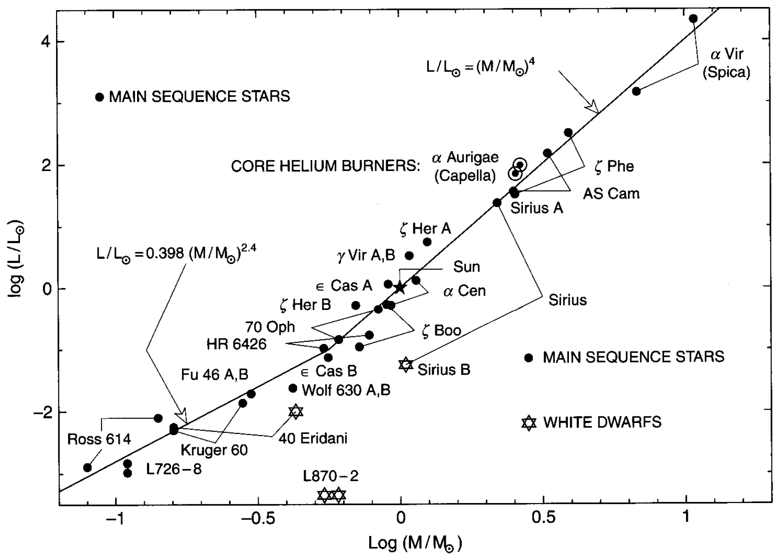

Luminosity versus mass for a selection of stars in binaries

Iben (2013)

Luminosity class and surface gravity

$\log g = \log GM/R^2$

- Betelgeuse ... (M2 I) $\log g \approx -0.6$ [cgs]
- Jupiter ... $\log g = 3.4$
- Sun (G2 V) ... $\log g = 4.44$
- Gℓ229B ... (T6.5) $\log g \approx 5$
- Sirius B... (WD) $\log g \approx 8$

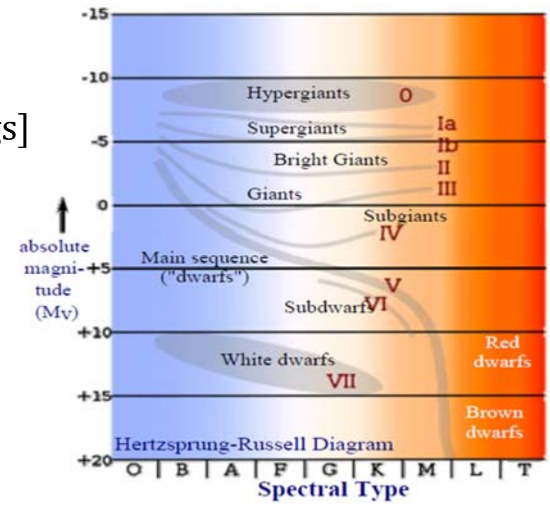

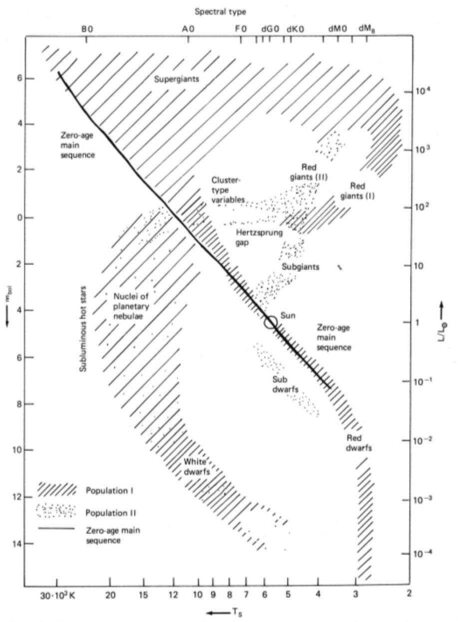

Composite Hertzsprung-Russell Diagram. Stars of different absolute luminosity, L - right axis, or bolometric absolute magnitude, M_{bol} - left axis, are plotted as a function of surface temperature, T_s - bottom axis, or spectral type - top axis. (Adapted from L. Goldberg and E.R. Dyer, Science in Space, eds. L.V. Berkner and H. Odishaw (1961).)

Lang "Data"

Exercise

1. What is the spectral type of Alpha Scorpii?
2. What is its apparent magnitude? Expected absolute magnitude? Bolometric luminosity?
3. What is its distance estimated from its apparent magnitude? Measured directly by parallax? Why do these differ?
4. What is the expected diameter of the star in km, in $R_\odot$ and in AU? What is then the expected angular diameter seen from Earth? Can it be resolved by the *HST*?

(Always show your work clearly, and cite the references.)

To measure the stellar abundance

- By spectroscopy
- Stellar composition *X,Y, Z* = mass fraction of H, He and all other elements ("metals") *Z*: *metallicity* $X+Y+Z=1$
- Solar abundance: $X_\odot = 0.747$; $Y_\odot = 0.236$; $Z_\odot = 0.017$
- One often compares the iron abundance of a star to that of the sun. Iron is not the most abundant (only 0.001), but easy to measure in spectra. *Why?*

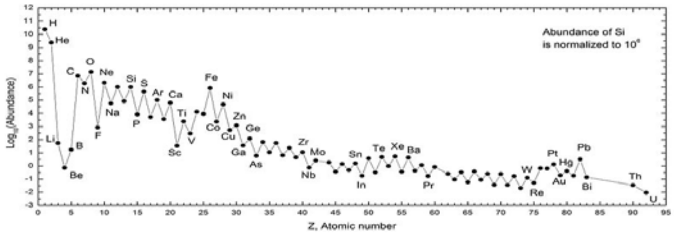

Data from: Katharina Lodders (2003) ApJ, 591, 1220

$$[\mathrm{Fe/H}] = \log_{10}\left(\frac{\mathrm{N_{Fe}}}{\mathrm{N_H}}\right)_{\mathrm{star}} - \log_{10}\left(\frac{\mathrm{N_{Fe}}}{\mathrm{N_H}}\right)_\odot$$

$$\log\left(\frac{N_{Fe}}{N_H}\right)_\odot = -4.33$$

i.e., 1 iron atom for 20,000 H atoms

$$[M/H] \approx \log(Z/Z_\odot)$$

Younger stars tend to be more metal-rich. Stars older than 10 Gyr almost all have [Fe/H] $\lesssim -0.5$; stars younger than 5 Gyr have [Fe/H] $\gtrsim -0.5$.

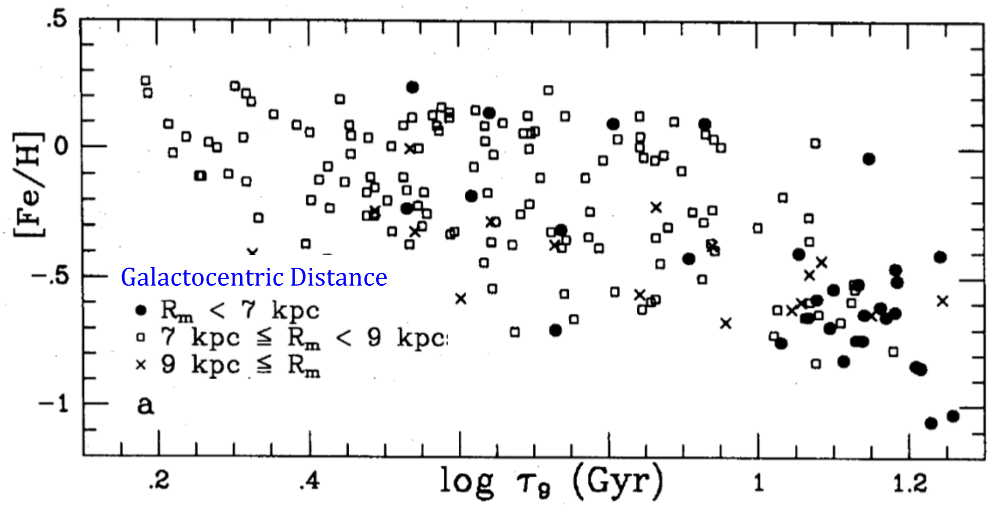

Edvardsson et al. (1993)

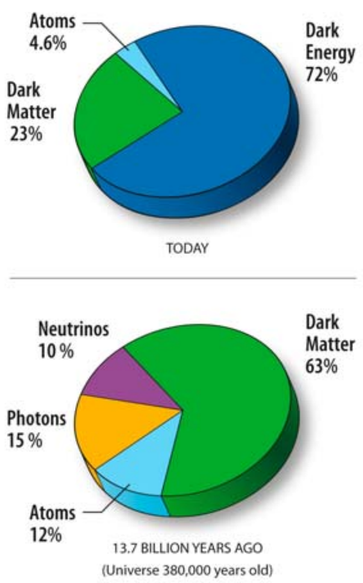

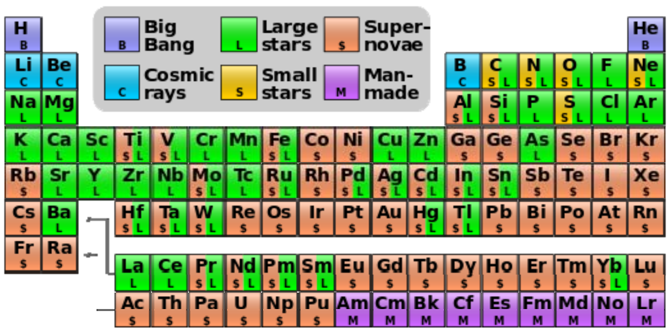

Cosmic element factories --- the Big Bang, stellar nucleosynthesis, supernova explosions, and compact mergers

http://en.wikipedia.org/wiki/Abundance_of_the_chemical_elements

To measure the stellar age

- Very tricky. Often one relies on measurements of M_V, T_{eff}, [Fe/H], and then uses some kind of theoretically computed isochrones to interpolate the age (and mass)
- Crude diagnostics include
  - ✓ Lithium absorption line, e.g., 6707A
  - ✓ Chromospheric activities, e.g., X-ray or Ca II emission
  - ✓ Evolving off the main sequence
- ... hence subject to large uncertainties

References:

Edvardsson et al., 1993, A&A, 275, 101
Nordström et al., 2004, A&A, 418, 989

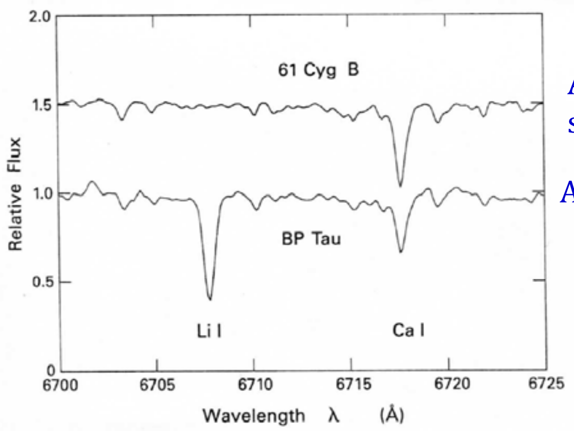

An MS star of the same spectral type

A PMS (young) star

Figure 16.9 Lithium absorption in a pre-main-sequence star. Shown is a portion of the optical spectrum of BP Tau, a T Tauri star of spectral type K7, corresponding to an effective temperature of 4000 K. Also shown, for comparison, is a main-sequence star of the same spectral type, 61 Cyg B. Only in the first star do we see the Li I absorption line at 6708 Å. Both objects also have a strong line due to neutral calcium.

Stahler

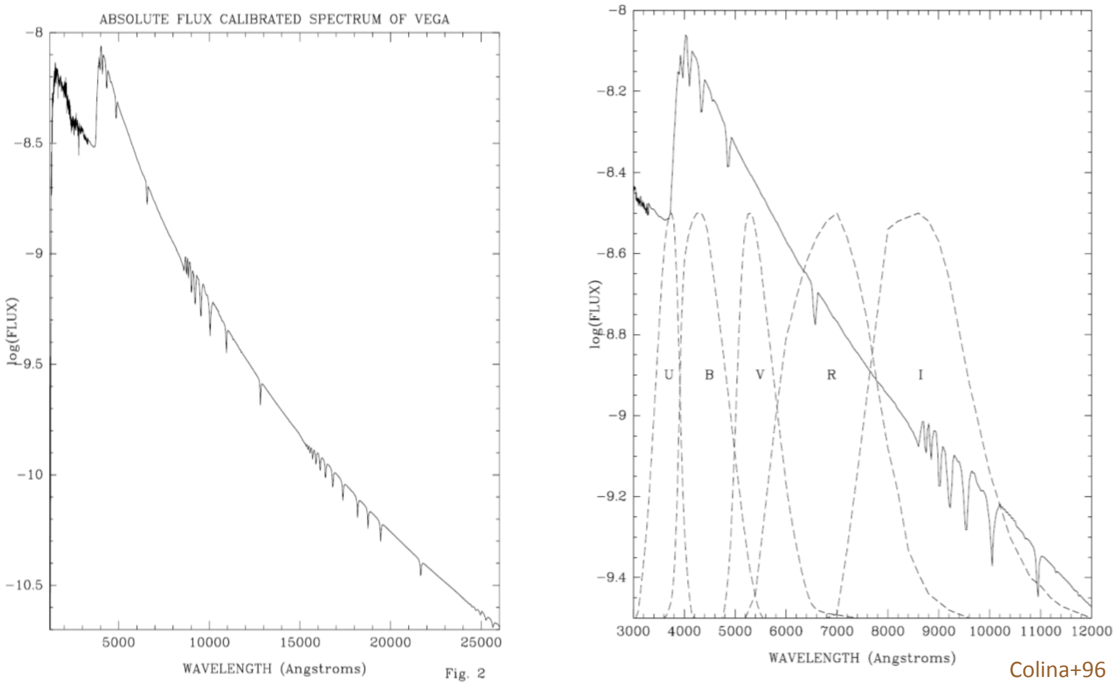

Fig. 2

Colina+96

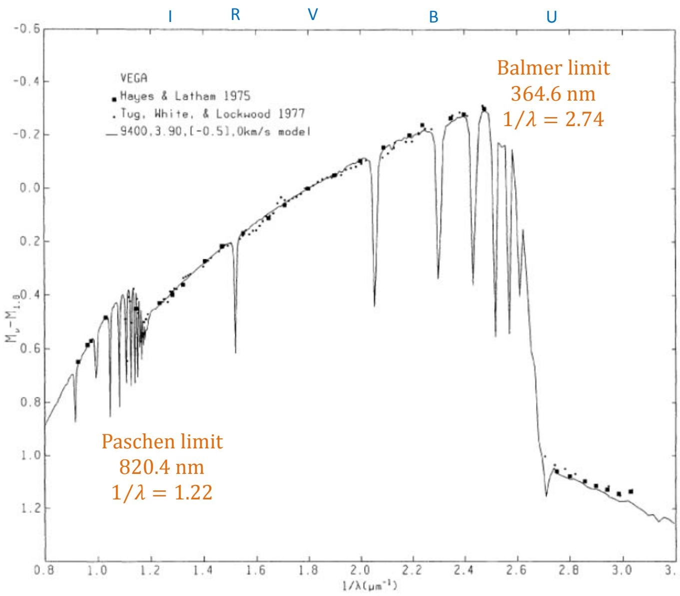

FIG. 1. Kurucz's (1991a) new model for Vega compared with a series of independent UV optical measurements, specifically those by Hayes & Latham (1985) and by Tug *et al.* (1977).

Cohen+92

Check out Aumann+84 for discovery of debris materials by IRAS.

Pre-main sequence evolutionary models (tracks)

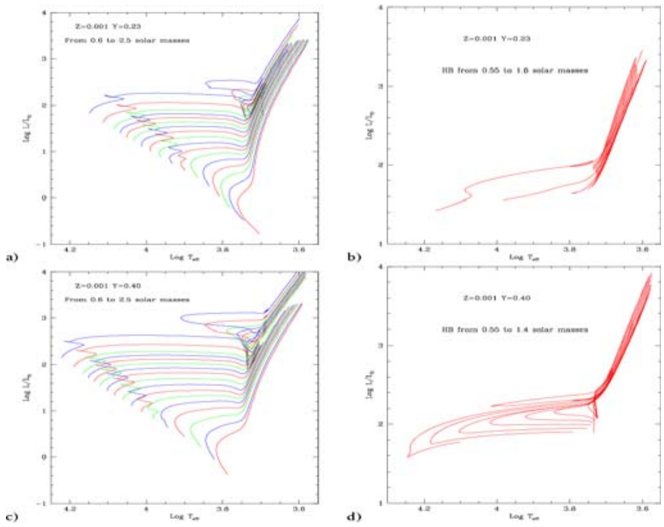

http://stev.oapd.inaf.it/

Bertelli et al, 2008, A&A, 484, 815

Stellar populations

- Population I ……. Stars in the Galactic disk; like the Sun;
  metal rich
- Population II ….. Stars like those in the globular clusters;
  metal poor
- Population III …. Stars formed in the early universe; perhaps very
  hot and luminous; *metal free*

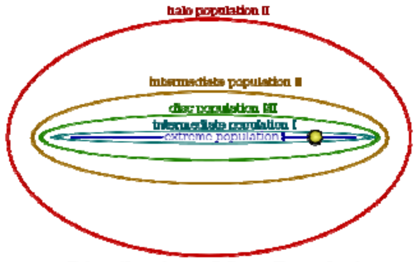

Distribution of Star Populations in Milky Way

http://en.wikipedia.org/wiki/Metallicity

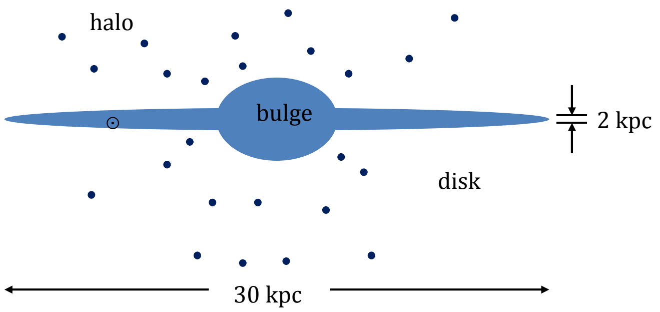

Typical properties of Stellar Populations in the Milky Way

	Population I		Population II	
	very young	young	old	very old
Scale height [kpc]	60	100	500	2000
Σ_w [km s^{-1}]	8	10	25	75
Z	> 0.02	0.01	0.005	<0.002
Age (rel. to the Universe)	<0.05	0.25	0.75	1
Distribution	generally in aggregates		spherical	

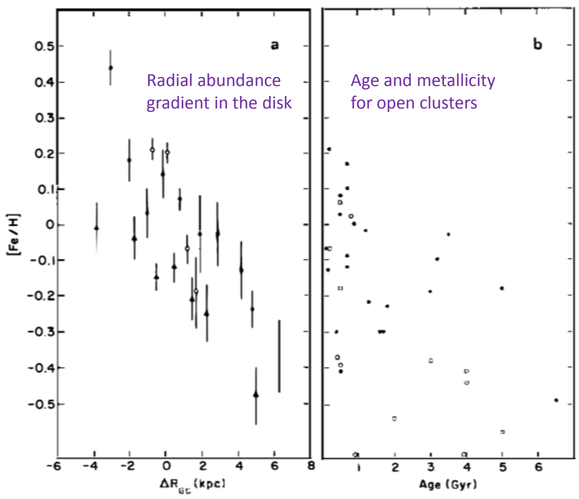

Figure 2 (*a*) The radial abundance gradient in the galactic disk. Mean metallicities from DDO and *UBV* photometry from Janes (1979) (*triangles*) are plotted versus galactocentric distance relative to the Sun. Also shown are results from Washington photometry of classical Cepheids by Harris (1981) (*solid circles*) and high-dispersion abundance analysis of G to M supergiants by Luck & Bond (1980) (*open circles*); (*b*) The relation between age and metallicity for the open cluster samples of Janes (1979, Table 8). Ages are taken from McClure & Twarog (1978), Jennens & Helfer (1975), Cannon (1970), and sources quoted by Janes. (Reliable ages were not found for six clusters.) Open circles distinguish clusters with galactocentric radius larger than the solar value by more than 1 kpc. No correction has been made for any vertical abundance gradient.

Mould 1982 ARA&A, 20, 91

Star clusters are good laboratories to study stellar evolution, because member stars in a star cluster

- are (almost) of the same age;
- are (almost) at the same distance;
- evolve in the same Galactic environments;
- have the same chemical composition;
- are dynamical bound.

Two distinct classes:

- ✓**globular clusters** (100+ in the MW)
- ✓**open clusters** (a few 10^3 known in the MW)

How do these two classes differ in terms of shape, size, spatial distribution, number of member stars, and stellar population?

Open Clusters

10^2 to 10^3 member stars; ~10 pc across; loosely bound; open shape;
young population I;
located mainly in spiral arms;
>1000 open clusters known in the MW

Globular Clusters

10^5 to 10^6 member stars; up to 100 pc across; tightly bound;
centrally concentrated;
spherical shape; old population II;
located in the Galactic halo;
200 globular clusters known in the MW

Stars in M80 are mostly old, metal poor members of Population II.

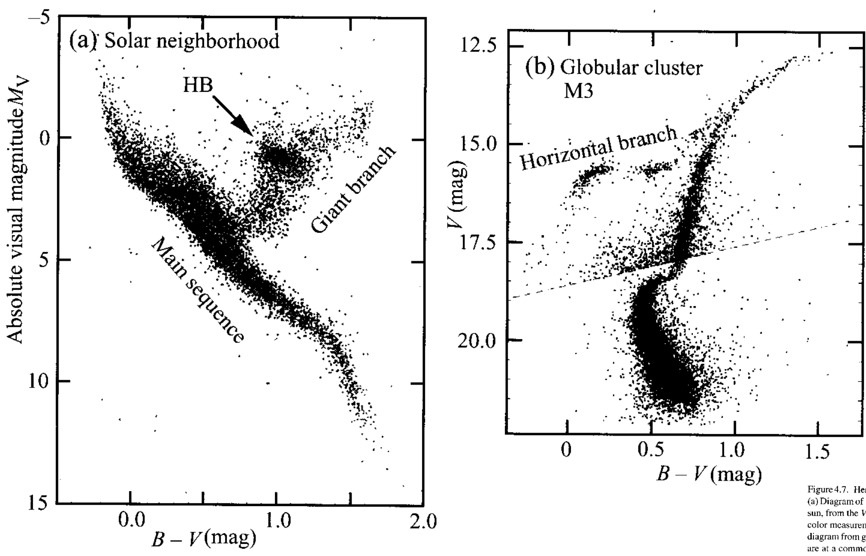

Figure 4.7. Hertzsprung–Russell color-magnitude diagrams for two very different samples of stars. (a) Diagram of 16 631 stars of various ages and various distances that are within about 330 LY of the sun, from the V-band and parallax distance measures by the Hipparcos satellite and ground-based color measurements. Horizontal-branch (HB) stars overlie the giant branch. (b) Color-magnitude diagram from ground-based studies of ~12 200 stars in globular cluster M3. The stars in the cluster are at a common distance of ~32 000 LY, and thus apparent magnitudes suffice for the ordinate of this H-R diagram. The stars are mostly of the common age of ~12 Gyr. The data come in two distinct samples. A deep photographic sample yields most of the stars in the diagram both above and below the diagonal line. Short exposures with a charge-coupled device (CCD) camera provide fluxes for the rarer brighter stars plotted only above the dashed line representing $B = 18.6$. The scatter just above the diagonal line is mostly due to increased uncertainty at the fainter end of the CCD sample. The distance modulus of M3 is 14.93. Thus, $M_V = 0$ in (a) corresponds to $V = 14.93$ in (b). Note the absence of bright main-sequence stars in M3 and also the well-defined horizontal branch. [(a) ESA SP-1200, Hipparcos catalog (1997) in J. Kovalevsky, *ARAA* **36**, 121 (1998); (b) F. Ferraro *et al.*, *A&A* **320**, 757 (1997); photographic data from R. Buonanno *et al.*, *A&A* **290**, 69 (1994)]

Bradt "Astrophysics Processes"

OB associations in the solar neighborhood

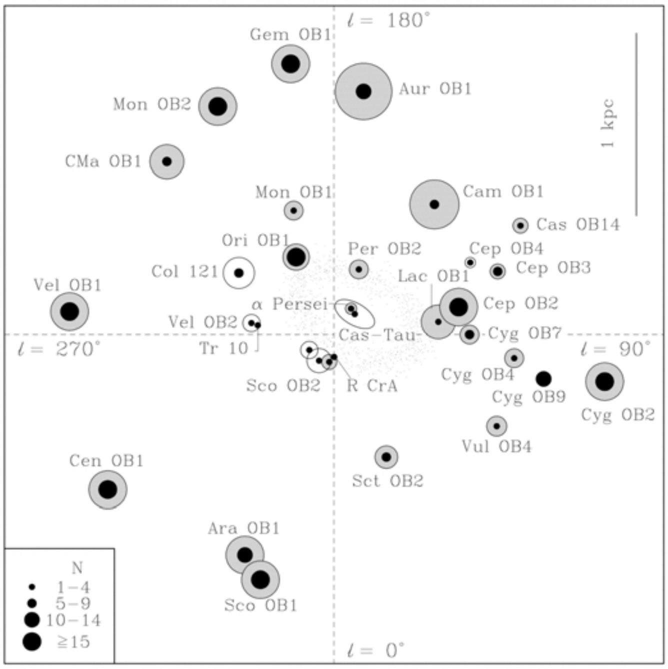

De Zeeuw +1999

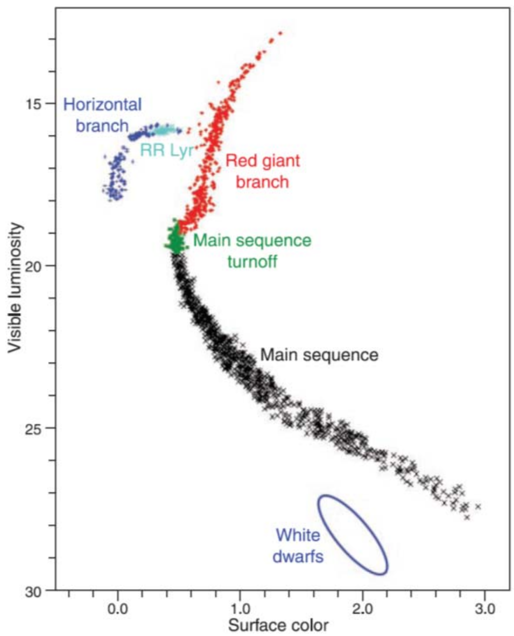

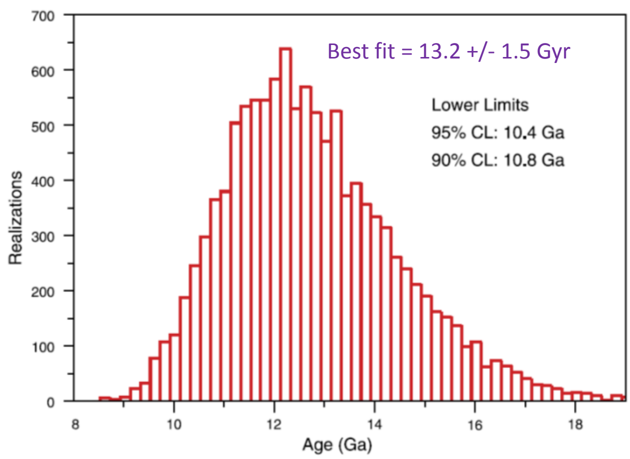

Range of possible GC ages (Chaboyer & Krauss 2003)

http://www.astro.caltech.edu/~george/ay127/readings/KraussChaboyer2003.pdf

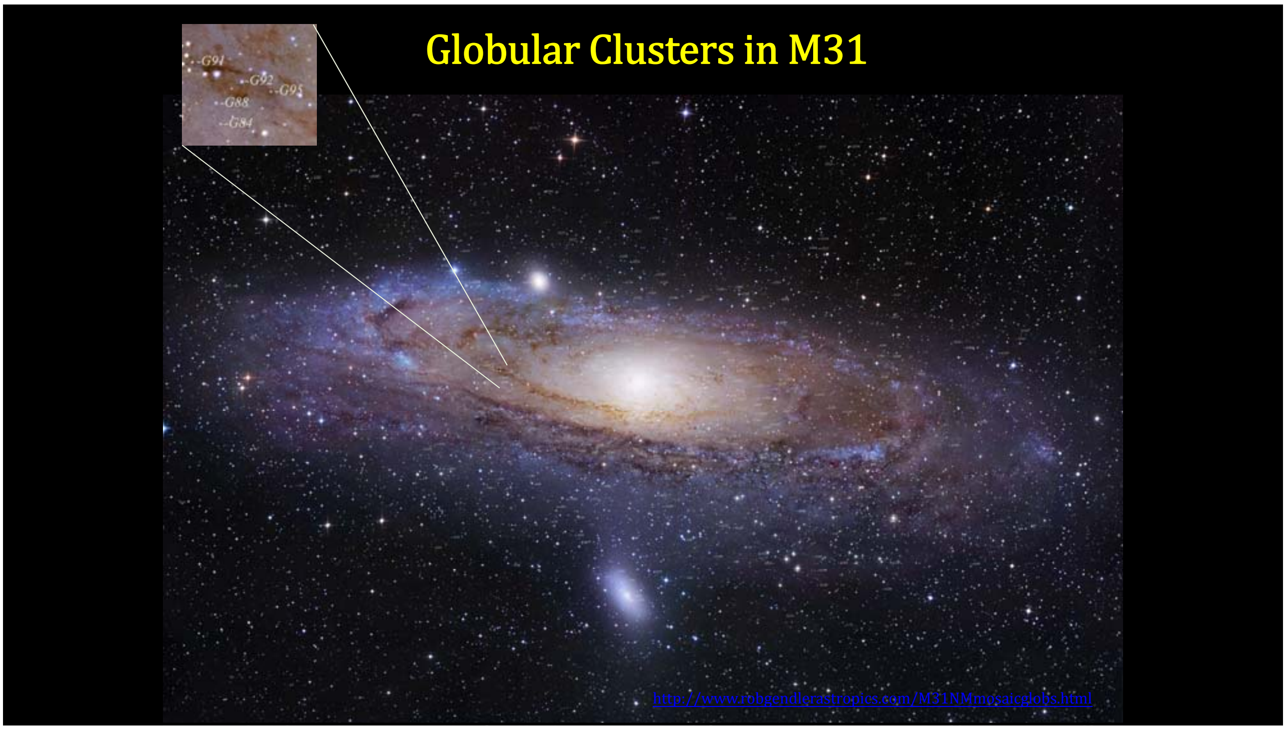
Globular Clusters in M31
G91
G92
G95
G88
G84
http://www.robgendlerastropics.com/M31NMmosaicglobs.html

Molecular Clouds
and
Star Formation

Stars are formed in molecular cloud cores,
whereas planets are formed,
contemporaneously, in young circumstellar disks.

http://www.astro.ncu.edu.tw/~wchen/Courses/Stars/Lada1995summerschool.pdf

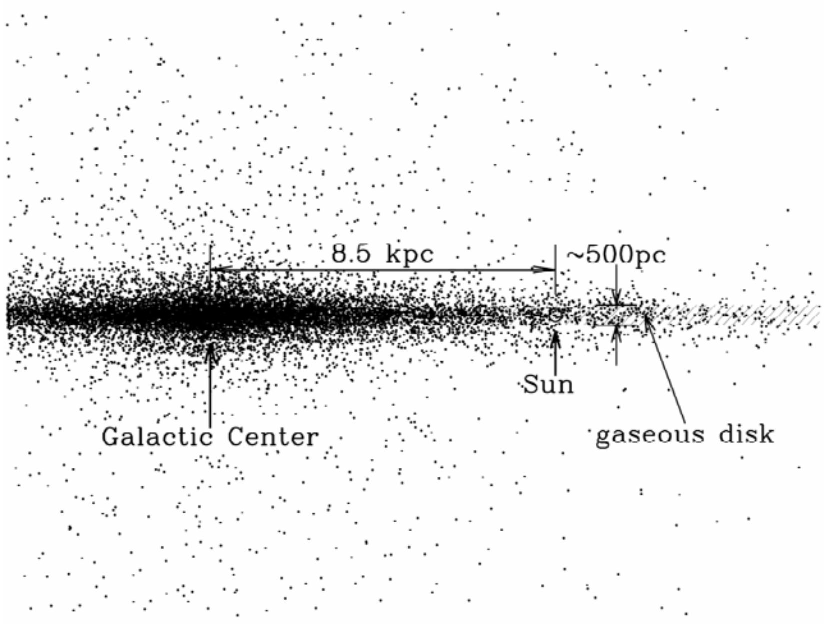

2

THE ASTROPHYSICAL JOURNAL, **218**: 148–169, 1977 November 15

A THEORY OF THE INTERSTELLAR MEDIUM: THREE COMPONENTS REGULATED BY SUPERNOVA EXPLOSIONS IN AN INHOMOGENEOUS SUBSTRATE

CHRISTOPHER F. MCKEE
Departments of Physics and Astronomy, University of California, Berkeley
AND
JEREMIAH P. OSTRIKER
Princeton University Observatory
Received 1977 February 3; accepted 1977 May 2

ABSTRACT

Supernova explosions in a cloudy interstellar medium produce a three-component medium in which a large fraction of the volume is filled with hot, tenuous gas. In the disk of the galaxy the evolution of supernova remnants is altered by evaporation of cool clouds embedded in the hot medium. Radiative losses are enhanced by the resulting increase in density and by radiation from the conductive interfaces between clouds and hot gas. Mass balance (cloud evaporation rate = dense shell formation rate) and energy balance (supernova shock input = radiation loss) determine the density and temperature of the hot medium with $(n, T) = (10^{-2.5}, 10^{5.7})$ being representative values. Very small clouds will be rapidly evaporated or swept up. The outer edges of "standard" clouds ionized by the diffuse UV and soft X-ray backgrounds provide the warm ($\sim 10^4$ K) ionized and neutral components. A self-consistent model of the interstellar medium developed herein accounts for the observed pressure of interstellar clouds, the galactic soft X-ray background, the O VI absorption line observations, the ionization and heating of much of the interstellar medium, and the motions of the clouds. In the halo of the galaxy, where the clouds are relatively unimportant, we estimate $(n, T) = (10^{-3.3}, 10^{6.0})$ below one pressure scale height. Energy input from halo supernovae is probably adequate to drive a galactic wind.

3

Interstellar Medium (ISM)

- Gas, dust + radiation, magnetic fields, cosmic rays (i.e., charged particles)
- Very sparse ---

  [star-star distance] / [stellar diameter] ~ 1 pc/10^{11} cm ~ 3 x 10^7 :1
  or ~1: 10^{22} in terms of volume (space)
- Mass: 99% mass in gas, 1% in dust ~ 15% of total MW visible matter
- Of the gas, 90%, H; 10% He
- Hydrogen: mainly H I (atomic), H II (ionized), and H_2 (molecular)
- Studies of ISM ---
  - Beginning of evolution of baryonic matter "recombination"
  - Stars form out of ISM
  - Important ingredient of a galaxy

4

Material Constituents of the ISM

Component	T (K)	n (cm^{-3})	Properties
Hot, intercloud and coronal gas	10^6	10^{-4}	
Warm intercloud gas	10^4	0.1	
Diffuse cloud (H I)	10^2	0.1	Mostly H I; $n_e/n_0=10^{-4}$
H II regions	10^4	>10	
Dark Molecular Clouds	10	> 10^3	Mostly H_2 mol. and dust
Supernova Remnants	10^4~10^7	>1	
Planetary Nebulae			

5

Energy Density in the Local ISM

Component	u (eV/cm^{-3})	Properties
Cosmic microwave background	0.265	
FIR radiation from dust	0.31	
Starlight	0.54	
Thermal kinetic energy	0.49	
Turbulent kinetic energy	0.22	
Magnetic field	0.89	
Cosmic rays	1.39	

There seems to be equi-partition between these energies. Why?
Read Draine's book, page 10

6

A "standard" HI cloud

$D \sim 5$ pc
$M \sim 50\ M_{\odot}$;
$d_{\text{intercloud}} \sim 100$ pc
$v_{\text{cloud}} \sim 10\ \text{kms}^{-1}$

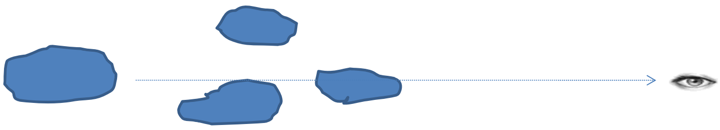

Clouds are patchy ➔ extinction depends greatly on the sightline

Extinction = absorption + scattering

Extinction *versus* *reddening* Av=30 toward the Galactic center

In the Galactic plane, **Av ~ 0.7-1 mag kpc^{-1}**

Extinction ←→ amounts of dust grains along the line of sight

Reddening ←→ grain properties (size, shape, composition, structure)

7

Different clouds along the line of sight …

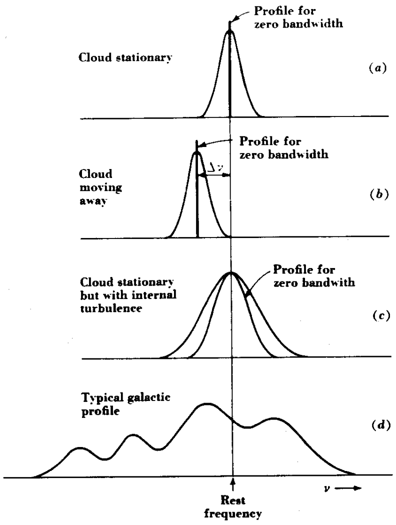

Fig. 8-59. Idealized hydrogen-line profiles.

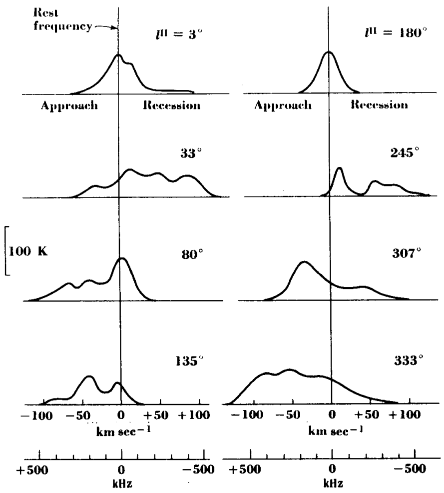

Fig. 8-60. Hydrogen-line profiles at different longitudes in the plane of our galaxy. (*After Kerr and Westerhout*, 1964).

John Kraus "Radio Astronomy"

8

The ‘normalized’ extinction (extinction law)

$$F(\lambda) = \frac{A_\lambda - A_V}{A_B - A_V} = \frac{E_{\lambda-V}}{E_{B-V}}$$

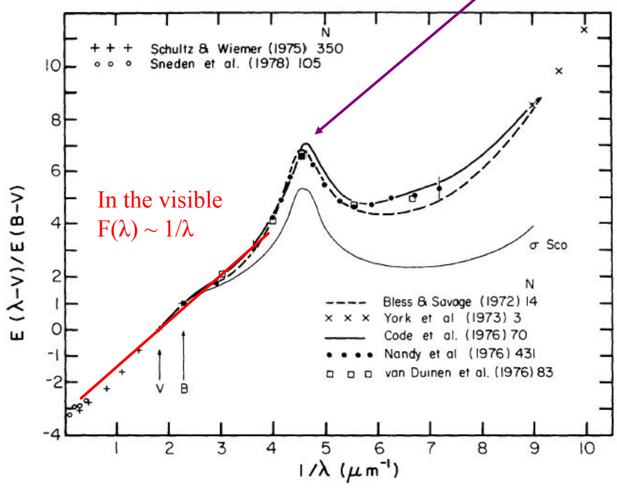

F(V) = 0

F(B) = +1

Find

A_B/A_V=?

9

The ‘normalized’ extinction (extinction law)

$$F(\lambda) = \frac{A_\lambda - A_V}{A_B - A_V} = \frac{E_{\lambda-V}}{E_{B-V}}$$

F(V) = 0

F(B) = +1

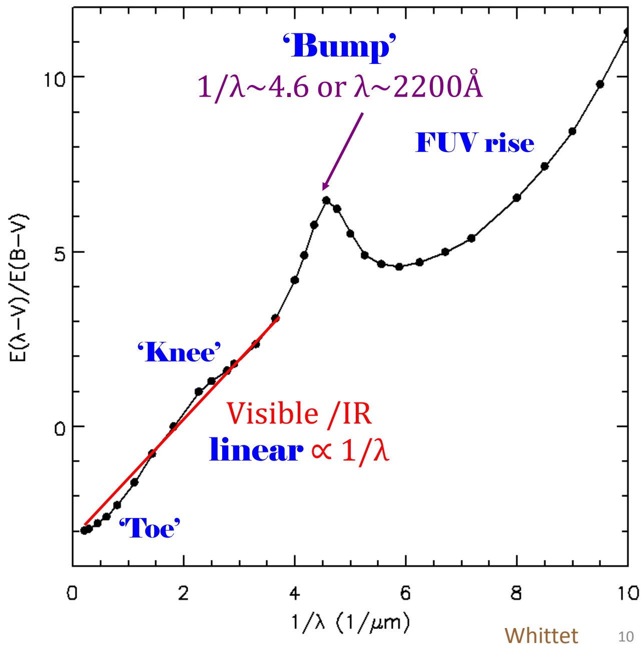

Whittet

10

$$A_\lambda = -2.5\log(e^{-\tau_\lambda}) \equiv 1.086\tau_\lambda \equiv 1.086 N_d\,\sigma_\lambda\,Q_{ext}$$

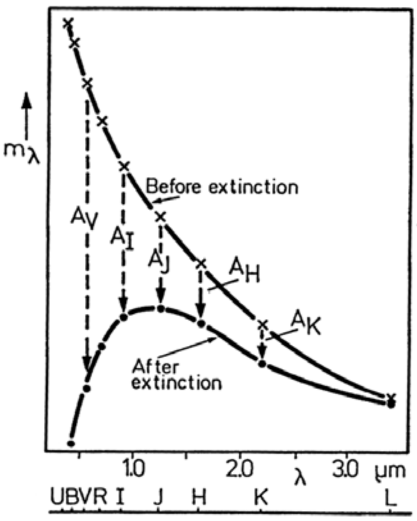

Filter	A_λ/A_V
U	1.531
B	1.324
V	1.000
R	0.748
I	0.482
J	0.282
H	0.175
K	0.112
L	0.058
M	0.028
N	0.052

$A_K \approx 0.1\ A_V$

Rieke & Lebofsky (1985)

11

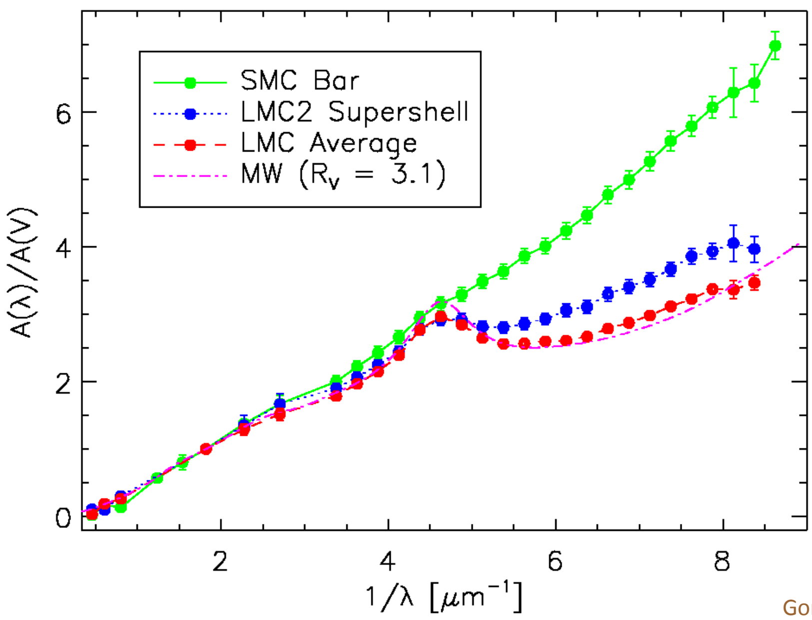

Gordon et al (2003)

12

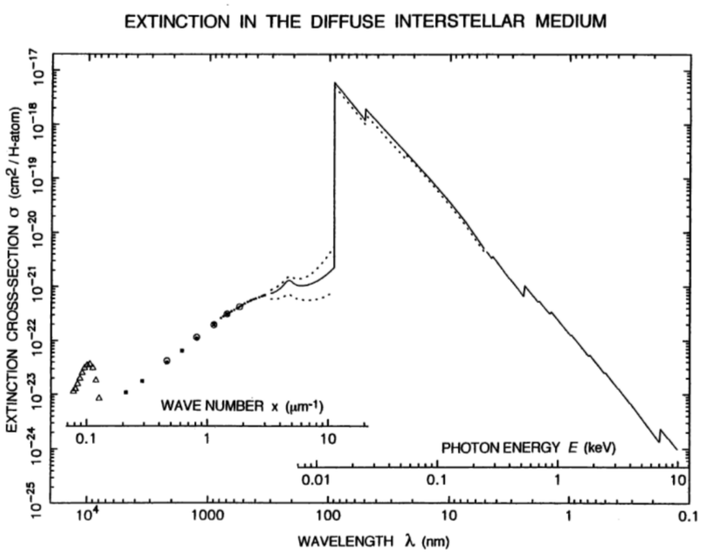

Figure 1. Solid line: The extinction cross-section normalized per H-atom of the diffuse neutral (95% HI, 5% HII, 10% HeI) interstellar medium from the far-infrared to the X-rays. Dotted lines: The UV extinction on the lines of sight in two extreme cases, HD 204827 (upper curve) and HD 37023 (θ_1-Orionis D, lower curve). Shortward of the Lyman limit, the dotted line corresponds to the ionization state of the solar neighbourhood (80% HI, 20% HII, 5% HeI, 5% HeII). The sources of the data are given in the text.

Ryter (1996)

13

Gas and dust coexist.

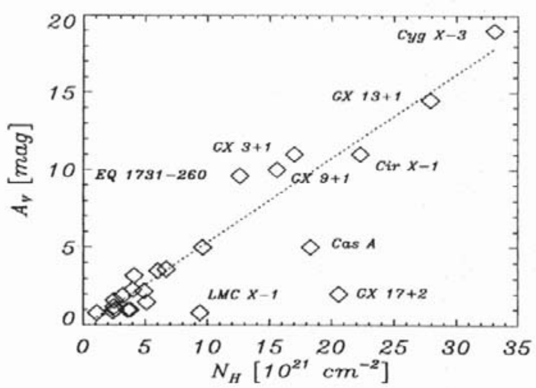

Fig. 3. Visual extinction vs. equivalent hydrogen column density. The fit (dotted line) does not contain GX 17+2 and LMC X-1. It yields $N_H = 1.79 \pm 0.03\ A_V[mag] \times 10^{21} [cm^{-2}]$

A gas-to-dust ratio ~100 (by mass) seems universal.

$$\frac{N_H}{A_V} \approx 1.8 \times 10^{21} \text{atoms cm}^{-2}\ \text{mag}^{-1}$$

Predehl & Schmitt (1995)

14

Exercise

1. The star Vega is used to define the zeroth magnitude in all the classical (Vega) photometric systems, e.g., Johnson.
2. Plot its spectral energy distribution (SED) from UV to IR.
3. What is the spectral type of Vega? What is its effective temperature?
4. Compare this in a plot with a blackbody curve of the temperature.
5. It was surprising hence when *IRAS* data revealed IR excess of Vega. What are the flux densities observed by *IRAS*? Given the age of Vega, why is this discovery significant?

15

http://www.astro.utoronto.ca/~patton/astro/mags.html#conversions

Band	lambda_c	dlambda/lambda	Flux at m=0	Reference
	um		Jy	
U	0.36	0.15	1810	Bessel (1979)
B	0.44	0.22	4260	Bessel (1979)
V	0.55	0.16	3640	Bessel (1979)
R	0.64	0.23	3080	Bessel (1979)
I	0.79	0.19	2550	Bessel (1979)
J	1.26	0.16	1600	Campins, Reike, & Lebovsky (1985)
H	1.60	0.23	1080	Campins, Reike, & Lebovsky (1985)
K	2.22	0.23	670	Campins, Reike, & Lebovsky (1985)

Astronomical Magnitude Systems.pdf

16

Stars are formed <u>in groups</u> → seen as star clusters if gravitationally bound

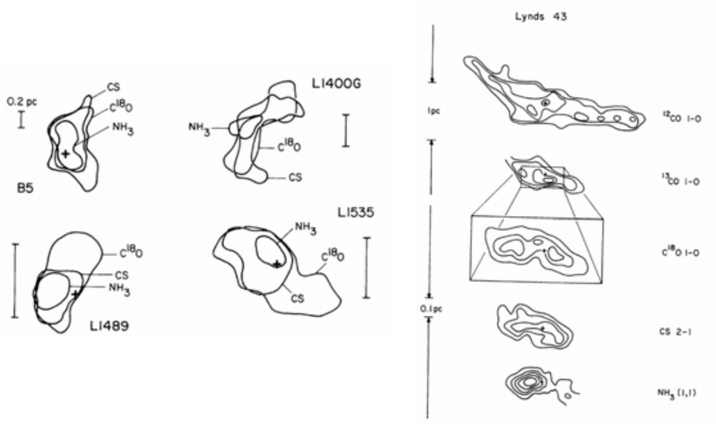

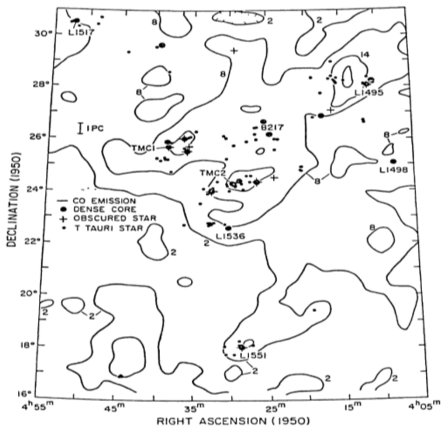

Figure 2 CO contour map of the Taurus molecular cloud with positions of dense NH_3 cores, embedded infrared sources, and visible T Tauri stars (from Myers 1986).

Molecular clouds observed by different tracers …

Taurus molecular cloud

17

Filamentary Molecular Clouds

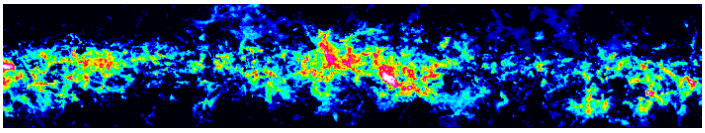

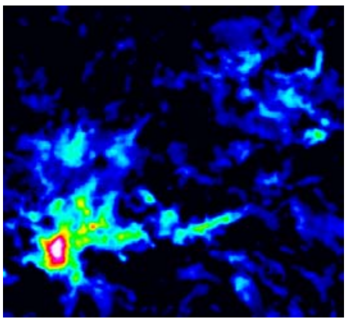

Molecular clumps/ clouds/condensations

$n \sim 10^3$ cm^{-3}, $D \sim 5$ pc,
$M \sim 10^3$ $M_\odot$

Dense molecular cores

$n \geq 10^4$ cm^{-3}, $D \sim 0.1$ pc,
$M \sim$ 1-2 $M_\odot$

Giant Molecular Clouds

D=20~100 pc
$\mathcal{M} = 10^5 \sim 10^6\ \mathcal{M}_\odot$
$\rho \approx 10 \sim 300$ cm^{-3}
$T \approx 10 \sim 30$ K
$\Delta v \approx 5 \sim 15$ km^{-1}

http://www.bu.edu/galacticring/outgoing/PressRelease/

18

Nearby Examples

Massive Star-Forming Region

- *Per OB2* (350 pc)
- *Orion OB Association* (350-400 pc) … rich

Low-Mass Star-Forming Regions

- *Taurus Molecular Cloud (TMC-1)* (140 pc)
- *Rho Ophiuchi cloud* (130 pc)
- *Lupus* (140 pc)
- *Chamaeleon* (160 pc)
- *Corona Australis* (130 pc)

4/5 in the southern sky … why?

19

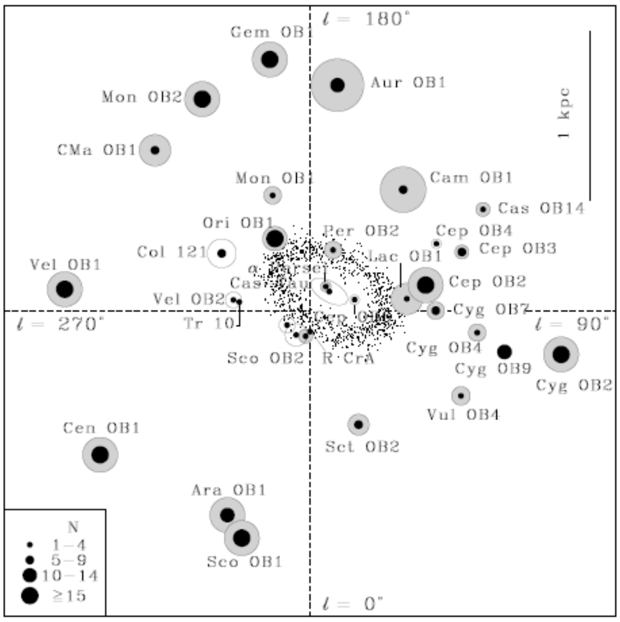

http://hera.ph1.uni-koeln.de/~heintzma/All/OB_stars.htm

20

The Gould Belt, a (partial) ring in the sky, ~1 kpc across, centered on a point 100 pc from the Sun and tilted about 20 deg to the Galactic plane, containing star-forming molecular clouds and OB stars
= local spiral arm

Origin unknown (dark matter induced star formation?)

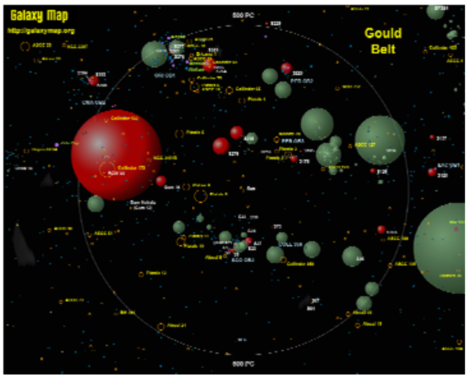

http://galaxymap.org/detail_maps/download_maps/gould.png

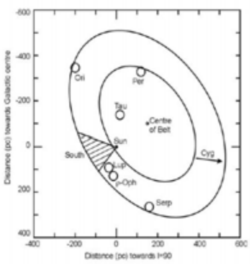

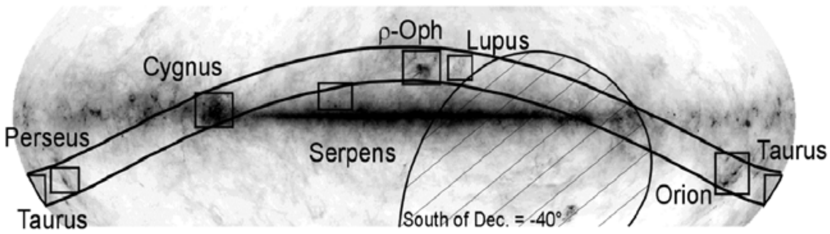

http://www.jach.hawaii.edu/JCMT/surveys/gb/ *Gould's Belt superimposed on to an IRAS 100 micron emission map*

The Local Bubble, a cavity of sparse, hot gas, ~100 pc across, in the interstellar medium, with H density of 0.05 cm^{-3}, an order less than typical in the Milky Way.

Likely caused by a (or multiple) supernova explosion (10-30 Myr ago).

Where is the supernova (remnant)?
Check out the Orion-Eridanus Superbubble

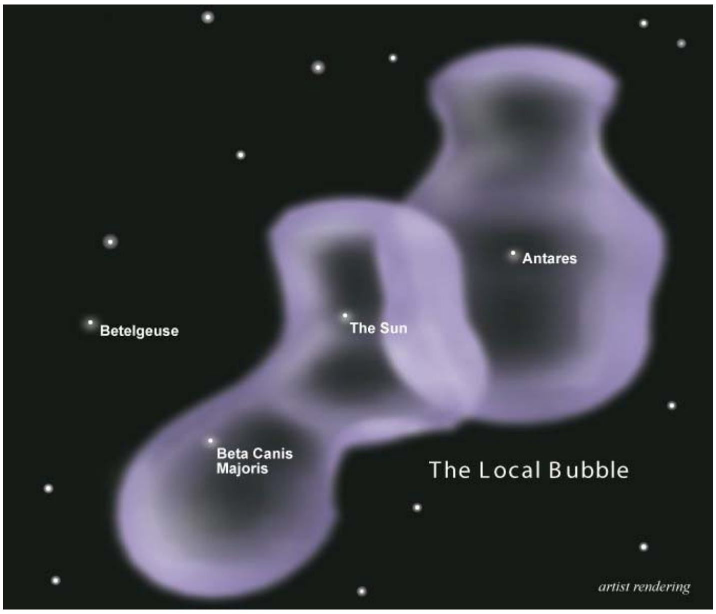

https://en.wikipedia.org/wiki/Local_Bubble

22

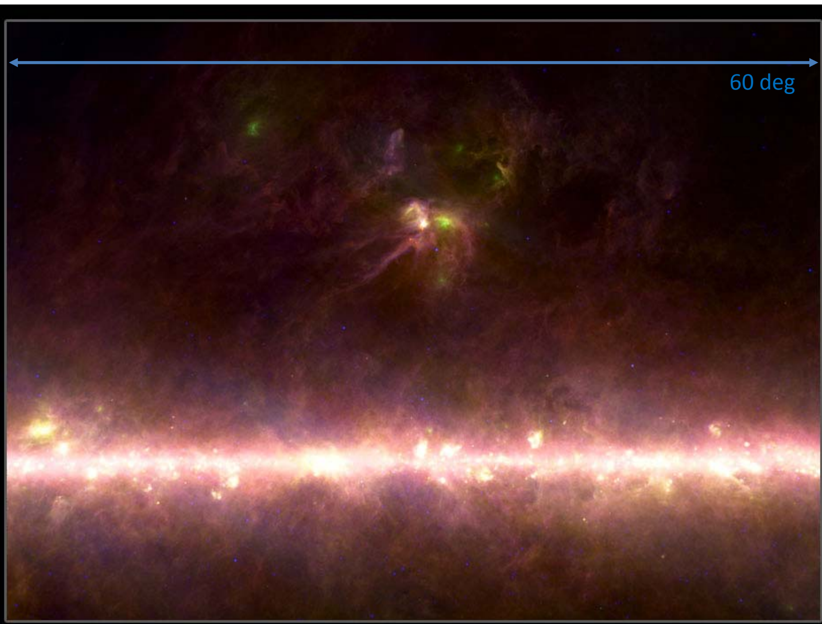

Rho Oph & The Galactic Center
IRAS

InfraRed Legacy

Blue , green and red = 12, 60, and 100 micron

23

Barnard 72 in Ophiuchus

http://www.robgendlerastropics.com/B72JMM.jpg

24

Massive Star-Forming Regions ---- OB associations

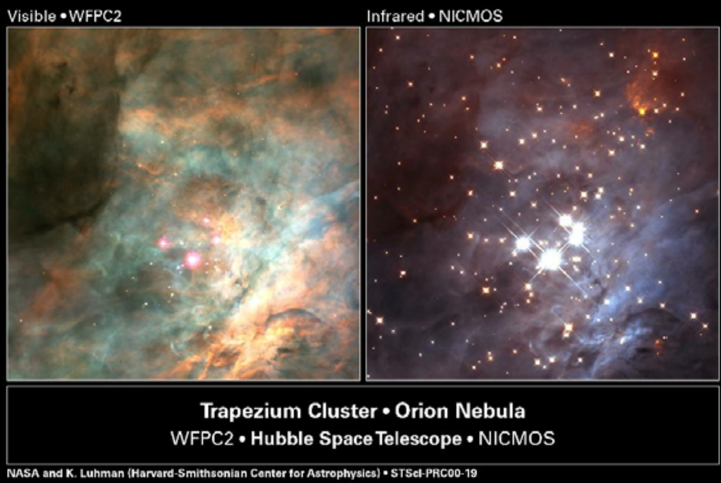

25

(Bok) Globules silhouetted against emission nebulosity

A dark cloud core seen against a star field

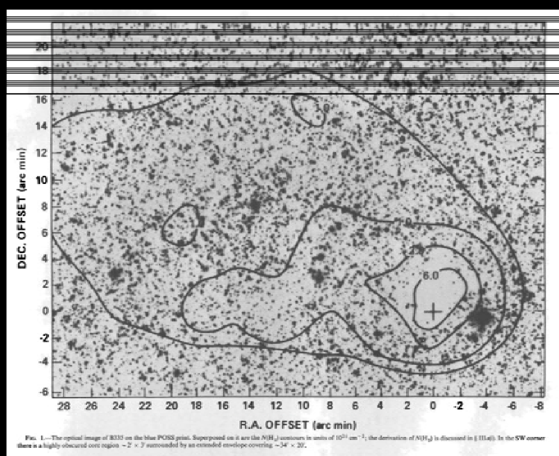

Frerking et al. (1987)

Molecules in space

H_2 molecules

- the main constituent of cold clouds, but lacking a permanent electric dipole moment, so is very difficult to detect. A rotationally excited molecule would radiate through a relatively slow electric quadrupole transition.
- Only in a hot medium, where stellar radiation or stellar wind excites vibrational and electronic states which then decay relatively quickly.

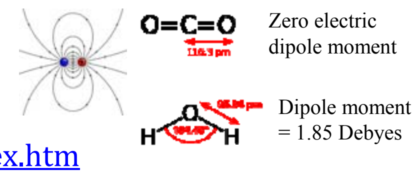

Refer to the slides for WPC's ISM course
http://www.astro.ncu.edu.tw/~wchen/Courses/ISM/index.htm

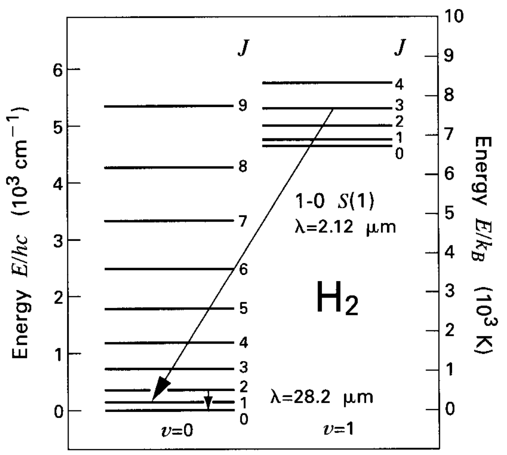

Figure 5.4 Rotational levels of H_2 for the first two vibrational states. Within the $v = 0$ state, the $J = 2 \rightarrow 0$ transition at 28.2 μm is displayed. Also shown is the transition giving the 1-0 S(1) rovibrational line at 2.12 μm. Note that two different energy scales are used.

Stahler & Palla

28

CO molecules

- simple and abundant. Strong binding energy E=11.1 eV self-shielding against UV field
- with a permanent electric dipole moment; radiating strongly at radio frequencies.
- $^{12}C^{16}O$ easiest to detect; isotopes $^{13}C^{16}O$, $^{12}C^{18}O$, $^{12}C^{17}O$, $^{13}C^{18}O$ also useful
- Excitation of CO to the J=1 level mainly through collisions with ambient H_2 $X_{CO} = 2 \times 10^{20}$ cm^{-2} [K km/s]$^{-1}$ (Bolatto et al. 2013, ARAA)
- At low densities, each excitation is followed by emission of a photon. At high densities, the excited CO transfers the energy by collision to another H_2 molecule; $n_{\rm crit} \approx 3 \times 10^3$ cm^{-3}. Low critical density → CO to study large-scale distribution of clouds, as a tracer of H_2
- $^{12}C^{16}O$ almost always optical thick; same line from other rare isotopes usually not. $N_H = 10^6\, N_{^{13}CO}$

29

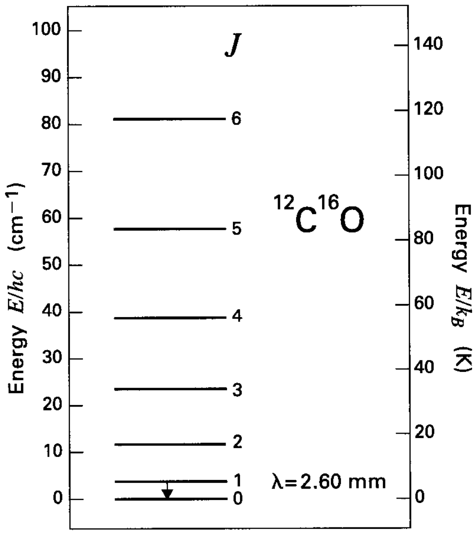

2.6 mm = 115 GHz

Only 5 K above the ground level ... can be excited by collisions with ambient molecules or CMB photons

Figure 5.6 Rotational levels of $^{12}C^{16}O$ within the ground ($v = 0$) vibrational state. The astrophysically important $J = 1 \rightarrow 0$ transition at 2.60 mm is shown.

Stahler & Palla

30

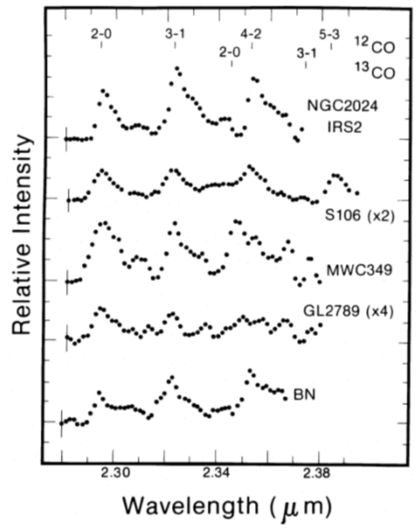

FIG. 2.—Spectra of those sources in which CO band head emission was detected. Linear baselines have been subtracted from each spectrum. The positions of the band heads are indicated at the top of the figure. Vertical scale marks are separated by 2×10^{-17} W cm^{-2} μm^{-1}. Noise levels are indicated on the short wavelength data points.

Gaballe & Persson (1987)

CO band heads in the Becklin-Neugebauer (BN) object --- an infrared-emitting, embedded, massive protostar

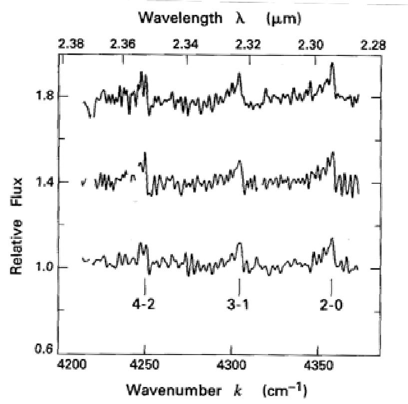

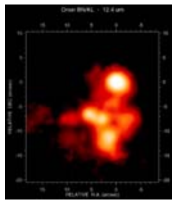

Figure 5.8 Near-infrared spectrum of the BN object in Orion, shown at three different observing times. The relative flux is plotted against the wave number k, defined here as $1/\lambda$.

Stahler & Palla

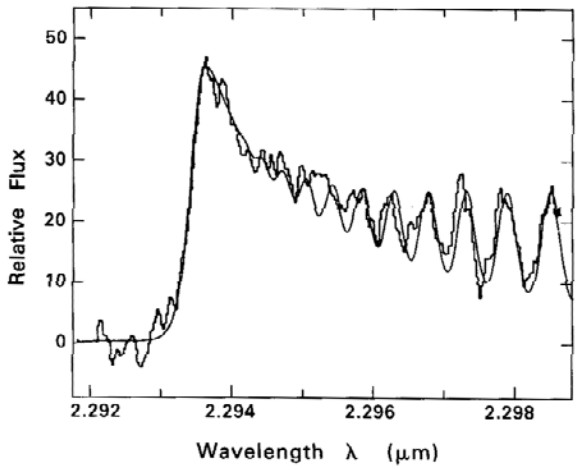

Figure 5.9 High-resolution near-infrared spectrum of the embedded stellar source SSV 13. The structure of the $v = 2 \rightarrow 0$ band head in $^{12}C^{16}O$ is evident. The smooth curve is from a theoretical model that employs an isothermal slab at 3500 K. Note that the spectrum here represents only a portion of the R-branch.

Stahler & Palla

32

Each species has a different set of excitation conditions (density, temperature; cf. Boltzmann equation)

➔ Different molecules/isotopes serve as <u>tracers</u> of these conditions, e.g., C18O traces denser parts of a cloud than 12CO does; NH3 maps the dense cores where protostars are located.

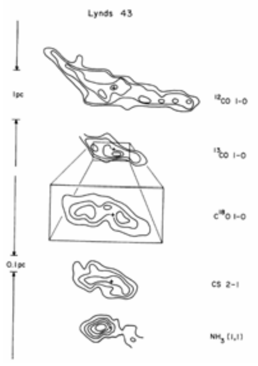

Myers et al. 1991

^{12}CO

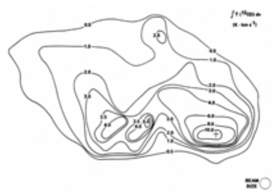

^{13}CO

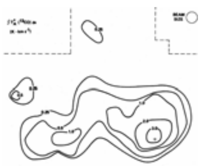

C^{18}O

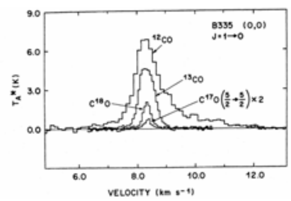

Frerking et al. (1987)

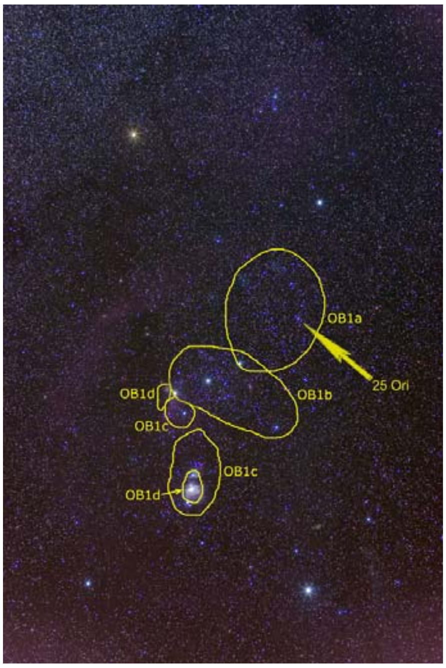

http://en.wikipedia.org/wiki/File:Orion_OB1_%26_25_Ori_Group.png

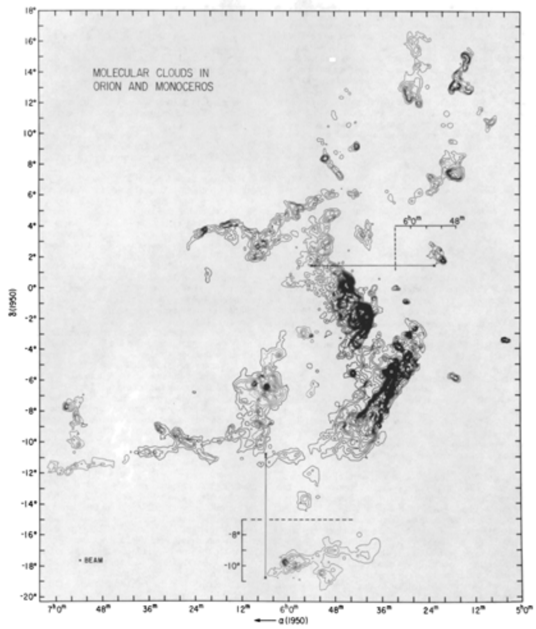

FIG. 2.—Contour map of integrated intensity of CO emission (W_{CO}) in the velocity range of −10 to 20 km s^{-1}. (Along the Galactic plane, CO emission was found at higher velocities, presumably from unrelated clouds more distant than the Orion clouds. These clouds are discussed elsewhere.) The lowest contour level is at 1.28 K km s^{-1} with subsequent levels at 3, 5, 7, ... times this value. The peaks of emission from the Orion Nebula and from NGC 2023 and 2024 (see Fig. 3) are designated by crosses. Two clouds, shown here in insets (see § III and also Figs. 3–5), that overlap other clouds in the survey lie at the positions indicated by arrows.

Maddalena+86

HCN (hydrogen cyanide) the poisonous gas? HCO^+?
What is going on?

Layers of circumstellar envelope of IRC+10216 (Leão+06)

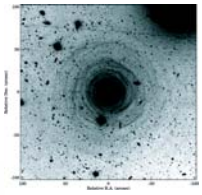

Kleinmann-Low (KL) object

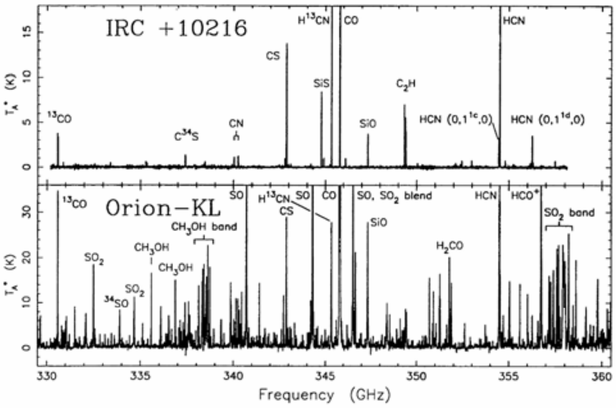

FIG. 4.—Comparison of the CSO spectral line surveys of IRC +10216 and Orion-KL. The data have been corrected by the main beam (0.6) and extended efficiencies (0.76) for IRC +10216 and Orion-KL, respectively. Note the difference in vertical scale between the two panels.

= CW Leo, a carbon (i.e., evolved) star, puffing off its dusty atmosphere

A protostar in Orion

Groesbeck+94 35

Star formation is not an isolated event.

Massive stars in particular may trigger the birth of next-generation stars → **triggered star formation**

... also possible by stellar jets, Galactic density waves, cloud-cloud collisions ...

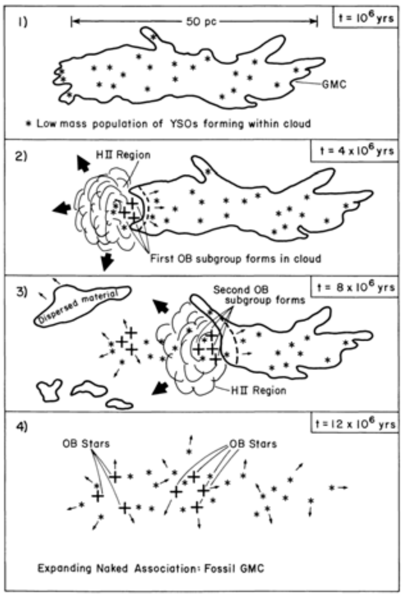

Figure 1. Probable stages in the formation of an expanding OB association from a giant molecular cloud. Low star formation efficiency in conjunction with efficient dispersal of residual, unprocessed molecular gas by OB stars result in a stellar system with positive total energy.

Lada 1987

Luminous stars → photoionization of a nearby cloud
→ Radiative driven implosion

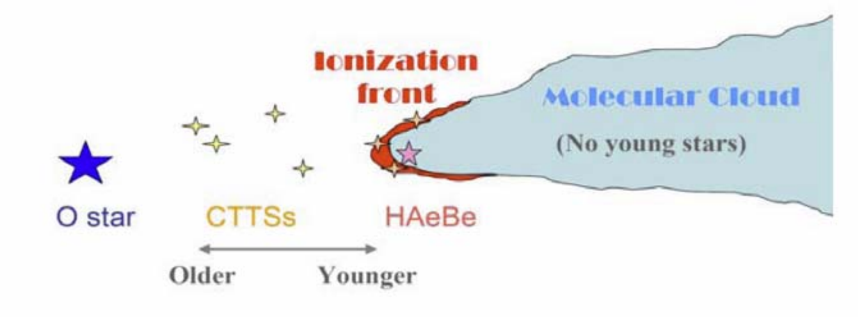

Figure 2. An illustration of a massive star to trigger star formation in a nearby molecular cloud.

Chen+06

37

Luminous stars → photoionization/winds on a surrounding cloud
→ Collect and collapse

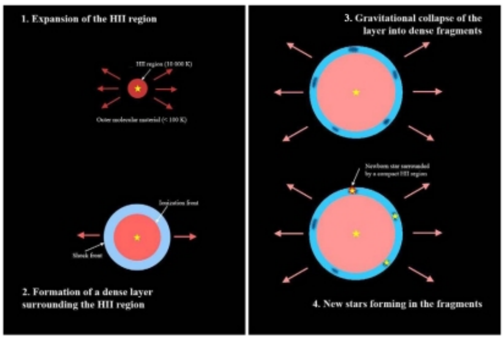

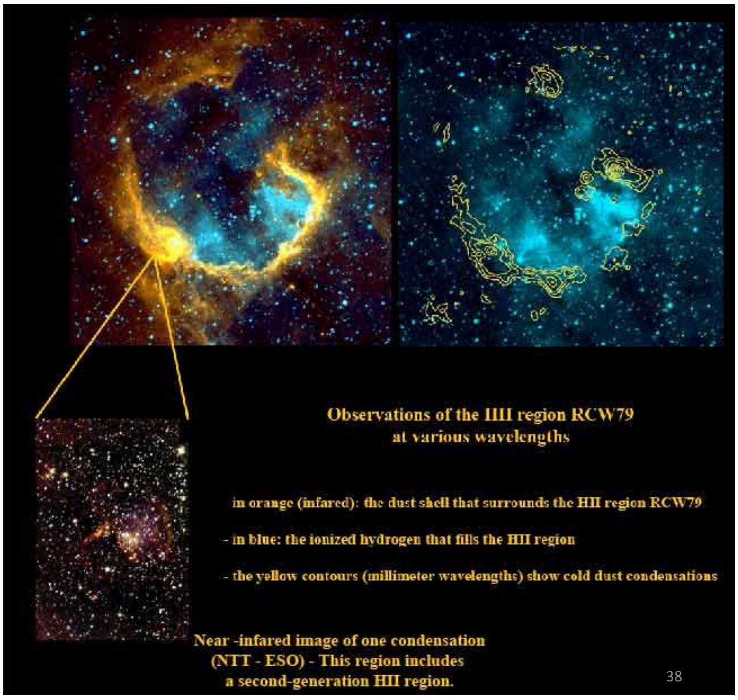

38

Size Scales for Star Formation.

Object	log size scale [cm]
Galactic spiral arm	22
Giant molecular cloud	20
Molecular dense core	17
Protostellar accretion disk	15
Protostar	11

Myers in You & Yuan (1995), p. 47

39

Mass Inventory in a Star-Forming Galaxy

Component	log M [$M_\odot$]
Molecular clouds	9
H_2	9
He	8
CO	7
Young stars	5

Myers in You & Yuan (1995), p. 47

40

Properties of Giant Molecular Clouds

Diameter [pc]	Mass [$M_\odot$]	Density [cm^{-3}]	T [K]	Velocity Width [km/s]
20-100	$10^5 - 10^6$	10-300	10-30	5-15

Myers in You & Yuan (1995), p. 47

41

Exercise

1. What is the BN object (why is it called an "object")? What is its brightness, distance, luminosity, and mass (how are these known)?
2. Answer the same for the KL object. What is the relation between the two?
3. There is a class of objects called the "Herbig-Haro objects". What are they?
4. "Quasi-Stellar Objects (QSOs)

42

43

Cloud Stability --- The Virial Theorem

Moment of Inertia $I = \int r^2 dm = \sum_i m_i r_i^2$

$$\frac{d^2 I}{dt^2} = \frac{d^2}{dt^2}(mr^2) \cdots (\text{if } \dot{m} = 0) \cdots$$
$$= 2m\frac{d}{dt}(r\dot{r}) = 2m(\dot{r}^2 + r\ddot{r})$$

$$\frac{1}{2}\frac{d^2 I}{dt^2} = 2E_K + E_P$$

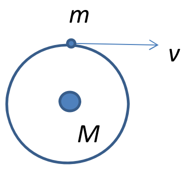

$$\frac{GmM}{r^2} = m\frac{v^2}{r}$$

To be stable, LHS = 0

$$2E_K + E_P = 0$$

$$2\left(1/2\right) mv^2 = GM/r$$

44

Virial Mass

MASS, LUMINOSITY, AND LINE WIDTH RELATIONS OF GALACTIC MOLECULAR CLOUDS

P. M. SOLOMON, A. R. RIVOLO, J. BARRETT, AND A. YAHIL
Astronomy Program, State University of New York–Stony Brook

THE ASTROPHYSICAL JOURNAL, 319:730–741, 1987 August 15
Received 1986 October 2; accepted 1987 February 2

ABSTRACT

We present measurements of the velocity line width, size, virial mass, and CO luminosity for 273 molecular clouds in the Galactic disk between longitudes of 8° and 90°. These are obtained from three-dimensional data in the Massachusetts–Stony Brook CO Galactic Plane Survey. From an analysis of these measurements we show that the molecular clouds are in or near virial equilibrium and are not confined by pressure equilibrium with a warm or hot phase of interstellar matter. The velocity line width is shown to be proportional to the 0.5 power of the size, $\sigma_v \propto S^{0.5}$. Combined with virial equilibrium, this shows that the clouds are characterized by a constant mean surface density of 170 $M_\odot$ pc^{-2} and have a mass $M \propto \sigma_v^4$. A tight relationship, over four orders of magnitude, is found between the cloud dynamical mass, as measured by the virial theorem, and the CO luminosity $M \propto (L_{CO})^{0.81}$. This relationship establishes a calibration for measuring the total molecular cloud mass from CO luminosity for individual clouds and for the Galactic disk. The cloud CO luminosity is $L_{CO} \propto \sigma_v^5$, which is the molecular cloud analog of the Tully-Fisher or Faber-Jackson law for galaxies.

The mass-luminosity law is accounted for by a cloud model consisting of a large number of optically thick clumps in virial equilibrium, each with a thermal internal velocity dispersion, but with the clouds effectively optically thin at a fixed velocity along the line of sight. The typical clump mass is of order a stellar mass and approximately equal to the Jeans mass at the clump density and thermal velocity dispersion.

TABLE 1

GALACTIC FIRST QUADRANT MOLECULAR CLOUD CATALOG

(1) No.	(2) T_{min}–I (K)	(3) ℓ_p (Deg.)	(4) b_p (Deg.)	(5) v_p (km·s^{-1})	(6) T_p (K)	(7) R (kpc)	(8) D (kpc)	(9) z (pc)	(10) σ_ℓ (Deg.)	(11) σ_b (Deg.)	(12) σ_v (km·s^{-1})	(13) $L_{CO}/10^4$ (K·km·s^{-1}·pc^2)	(14) $M_{VT}/10^4$ ($M_\odot$)	(15) Flag
1	4–3	8.00	−0.50	128.	5.7	1.4	10.1	−89.	0.06	0.07	4.4	7.27	44.4	T
2	5–3	8.20	0.20	20.	10.2	6.2	15.9	56.	0.17	0.21	4.1	140.2	176.3	F,V
3	4–4	8.30	0.00	3.	5.7	4.0	6.2	0.	0.40	0.11	3.8	22.6	65.4	X
4	4–5	8.30	−0.10	48.	8.2	3.6	13.2	−23.	0.05	0.05	2.2	5.02	11.1	F,U
5	5–6	8.40	−0.30	37.	17.0	4.4	5.7	−30.	0.32	0.15	3.9	23.3	66.5	N,H

45

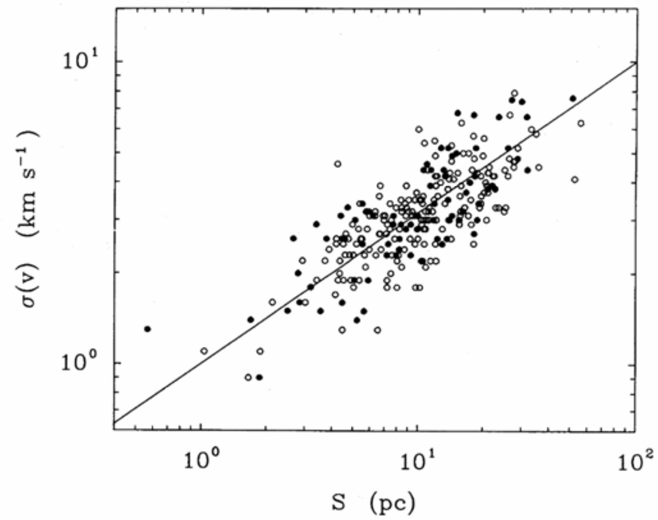

FIG. 1.—Molecular cloud velocity dispersion $\sigma(v)$ as a function of size S (defined in text) for 273 clouds in the Galaxy. The solid circles are calibrator clouds with known distances and the open circles are for clouds with the near-far distance ambiguity resolved by the method discussed in the text. The fitted line is $\sigma(v) = S^{0.5}$ km s^{-1}. For virial equilibrium the 0.5 power law requires clouds of constant average surface density.

46

LHS = 0 → stable

LHS < 0 → collapsing

LHS > 0 → expanding

E_K
- Kinetic energy of molecules
- Bulk motion of clouds
- Rotation
- …

E_P
- Gravitation
- Magnetic field
- Electrical field
- …

$E_{total} = E_K + E_P$

$E_{total} = E_K + \Omega$ (mostly)

47

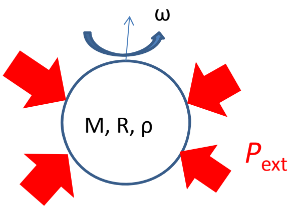

Cloud of mass M, radius R, rotating at ω

$$E_{rot} = \frac{1}{2} I \omega^2 \qquad I = \frac{2}{5} M R^2 \qquad \Omega = -\frac{3}{5}\frac{GM^2}{R}$$

Generalized virial theorem

$$\frac{1}{2}\frac{d^2 I}{dt^2} = 2 < E_K > + \int \vec{r} \cdot \vec{F} dm + 3 \int P dV - \oint P \vec{r} \cdot d\vec{s}$$

If ω = 0, and $P_{ext} = 0$
$$2 \cdot \frac{3}{2} \frac{M}{\mu m_H} kT - \frac{3}{5}\frac{GM^2}{R} = 0$$

$$R_J = \frac{1}{5}\frac{GM\mu m_H}{kT}$$

This is the Jeans length.

$\mu \approx 2.37$ for solar abundance with H_2

Jeans length = critical spatial wavelength

If perturbation length scale is longer
→ Medium is decoupled from self-gravity ➔ stable

$$M_J = \frac{4}{3}\pi R_J^3\,\rho$$

$$R_J = \left(\frac{15}{4\pi}\frac{kT}{\mu m_H G\rho}\right)^{1/2} \sim \sqrt{\frac{T}{\rho}}$$

$$M_J = \left(\frac{\pi kT}{4\mu m_H G}\right)^{3/2}\sqrt{\frac{1}{\rho}} \sim \frac{T^{3/2}}{\rho^{1/2}}$$

This is the Jeans mass ... the **critical** mass for onset of gravitational collapse

If cloud mass M > M_{Jeans} ➔ cloud collapse
Note the above does not consider external pressure, or other internal supporting mechanisms.

49

A non-magnetic, isothermal cloud in equilibrium with external pressure
→ a Bonnor-Ebert sphere (Bonnor 1956, Ebert 1955)

$$2E_K + E_P - 3P_{\text{ext}}V = 0$$

The potential term can include, other than the gravitational force, also rotation, magnetic field, etc.

At first, the cloud is optically **thin**.

Contraction → density ↑ → collisions more frequent
→ molecules excited and radiated → radiation escapes
→ cooling → less resistance to the contraction
➔ collapse (free fall)

$R_J \approx c_s\, \tau_{\text{ff}}$ = [isothermal sound speed] * [free fall time]

A spherical symmetric gas cloud with temperature T and external pressure P

For one particle, $F_i = m_i \ddot{r}_i \leftarrow \frac{\partial}{\partial r}$

$$m_i r_i \cdot \ddot{r}_i = m_i \frac{d}{dt}(\dot{r}_i \cdot r_i) - m_i \dot{r}_i \cdot \dot{r}_i$$
$$= \frac{1}{2} m_i \frac{d^2}{dt^2}(r_i^2) - m \dot{r}_i{}^2$$

Summing over all particles

$$\frac{1}{2}\frac{d^2}{dt^2}\left[\sum_i m_i r_i^2\right] - 2\sum_i \frac{1}{2} m_i \dot{r}_i^2 = \sum_i r_i F_i$$

Moment of inertial　　Kinetic energy

51

To maintain $2E_K + E_P = 0$, the total energy $E_t = E_K + E_P$ must change. The gravitational energy

$$\Omega \sim -\frac{GM^2}{r} \rightarrow d\Omega \sim \frac{dr}{r^2}$$

For contraction, $\mathrm{d}r < 0$, so $\mathrm{d}\Omega < 0$ → Then $\mathrm{d}E_t = \mathrm{d}E_K + \mathrm{d}\Omega = ½\,\Omega = L\,\Delta t$

This means to maintain quasistatic contraction, <u>half</u> of the gravitation energy from the contraction is radiated away.

Eventually the cloud becomes dense enough (i.e., optically <u>thick</u>) and contraction leads to temperature increase.

The cloud's temperature increases while energy is taken away
→ negative heat capacity

52

- <u>H I clouds</u>

  $R_J \approx 25$ pc; $M_J \approx 120\ M_\odot > M_{obs}$
  So H I clouds are not collapsing.

- <u>Dark molecular clouds</u>

  $M_{obs} \approx$ 100-1000 $M_\odot > M_J \approx 10\ M_\odot$
  So H_2 clouds should be collapsing. But observations show that most are not.
  → There is additional support other than the thermal pressure, e.g., rotation, magnetic field, turbulence, etc.

53

Roughly, the requirement for a cloud to be gravitational stable is

$$|E_{grav}| > E_{th} + E_{rot} + E_{turb} + E_{mag} + \ \ldots$$

For a spherical cloud, $E_{grav} = -C_{grav}\, {GM^2}/{R}$, where C_{grav} is a constant depending on the mass distribution (=3/5 for uniform density).

The thermal energy, $E_{th} = \frac{3}{2}\frac{m}{\mu m_H}\, k_B T$, where μ is the mean molecular weight of the gas in atomic mass units.

54

The rotational energy $E_{\text{rot}} = C_{\text{rot}}\ M\ R^2\omega^2$, where C_{rot} depends on the mass distribution and is 1/5 for uniform density; ω is the (assumed) uniform angular velocity.

The turbulent kinetic energy $E_{\text{turb}} = \frac{1}{2}\ M\sigma^2$, where σ is the mean turbulent velocity.

The magnetic energy $E_{\text{mag}} = \frac{1}{8}\int B^2\ \text{d}V \approx \frac{1}{6}B^2R^3$, where B is the uniform magnetic field.

55

For rotational support to be important,

$$\frac{3}{5}\frac{GM}{R} = \frac{1}{2}I\omega^2 = \frac{1}{2}\left(\frac{2}{5}MR^2\right)\left(\frac{v_{\text{crit}}}{R}\right)^2 = \frac{1}{5}Mv_{\text{crit}}^2$$

So $v_{\text{crit}} = (3GM/R)^{1/2}$, where v_{crit} is the critical rotation velocity at the equator.

Numerically, $v_{\text{crit}} = 0.11\ \left[\frac{M}{M_\odot}\frac{\text{pc}}{R}\right]^{1/2}$ [km/s]

For HI clouds, $v_{\text{crit}} = 0.11\ [\frac{50}{2.5}]^{1/2} \approx 0.5$ [km/s]

Typically, $\omega \approx 10^{-16}\ \text{s}^{-1}$, so $v \approx 0.01$ to 0.1 [km/s]

➔ Clouds are generally not rotationally supported.

56

Measuring the ISM Magnetic Fields

Method	Medium	Info
Polarization of starlight	Dust	$B_\perp$
Zeeman effect	Neutral hydrogen; a few mol. lines	$B_\parallel$
Synchrotron radiation	Relativistic electrons	$B_\perp$
Faraday rotation	Thermal electrons	$B_\parallel$

The Zeeman effect is the only technique for **direct** measurements of magnetic field strengths.

Unsöld, Crutcher (2012) ARAA

57

Polarization of Starlight

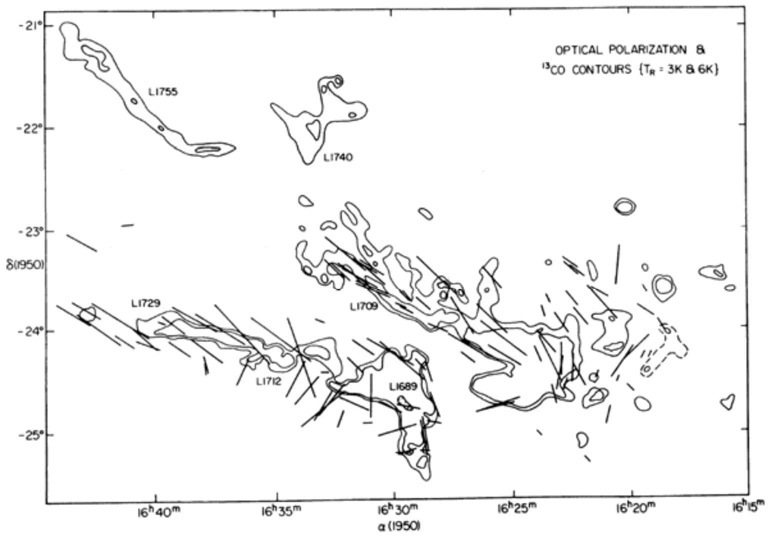

FIG. 7.—Orientation and relative magnitude of optical polarization vectors toward field stars at the cloud edges (Vrba, Strom, and Strom 1976). Solid contours of $T_R^*(^{13}CO)$ are at 3 and 6 K, with a dotted 1 K contour added around R5–R6 and R8–R9.

Loren (1989)

58

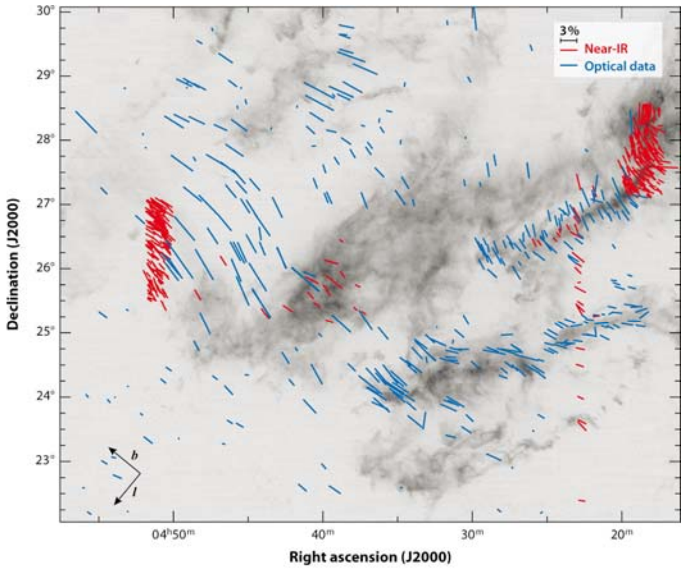

Crutcher RM. 2012.
Annu. Rev. Astron. Astrophys. 50:29–63

Organized magnetic field morphology in the Taurus dark-cloud complex superposed on a ^{13}CO map (Chapman et al. 2011). Blue lines show polarization measured at optical wavelengths and red lines show near-IR (H-band and I-band) polarization.

Dichroic extinction by dust (optical and near-IR) $\vec{P} \parallel \vec{B}$

59

Interstellar Polarization

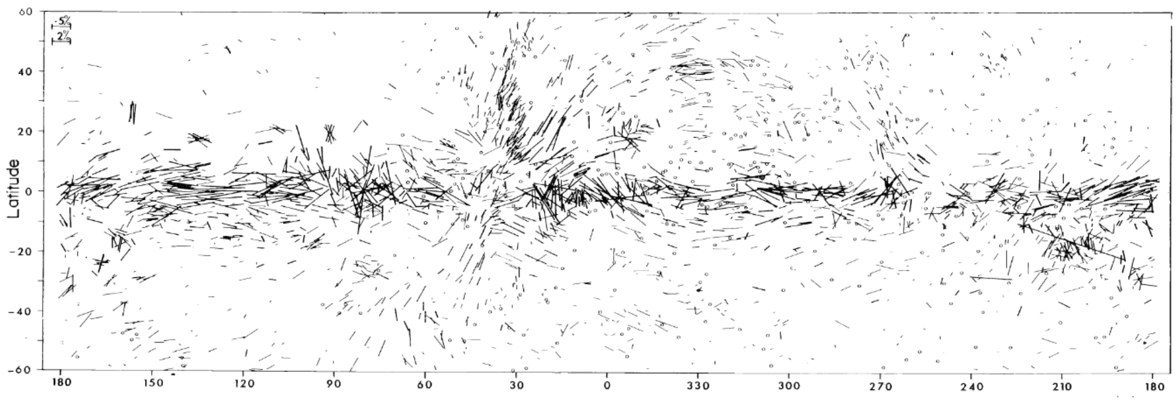

Mathewson & Ford (1970)

60

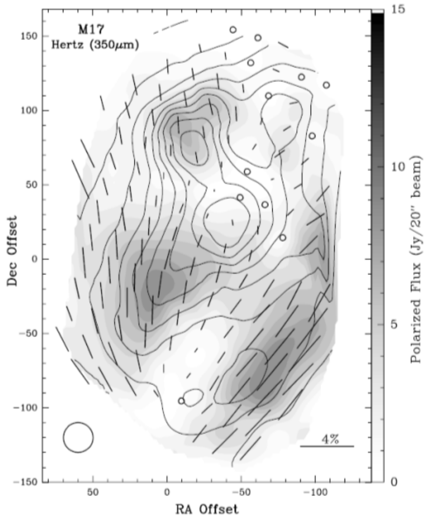

Fig. 6.—HERTZ polarization map of M17 at 350 μm. All of the polarization vectors shown have a polarization level and error such that $P > 3\sigma_P$. Circles indicate cases where $P + 2\sigma_P < 1\%$. The contours delineate the total continuum flux (from 10% to 90% with a maximum flux of ≈700 Jy), whereas the underlying gray scale gives the polarized flux according to the scale on the right. The beam width (≃20″) is shown in the lower left corner and the origin of the map is at R.A. = $18^h17^m31^s.4$, decl. = −16°14′25″.0 (B1950.0).

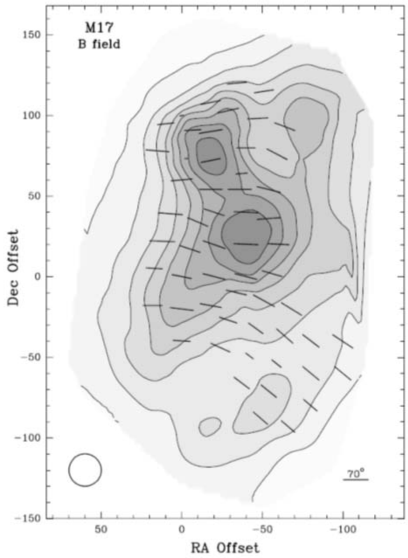

Fig. 11.—Orientation of the magnetic field in M17. The orientation of the projection of the magnetic field in the plane of the sky is shown by the vectors and the viewing angle is given by the length of the vectors (using the scale shown in the bottom right corner). The contours and the gray scale delineate the total continuum flux. The beam width (≃20″) is shown in the lower left corner, and the origin of the map is at R.A. = $18^h17^m31^s.4$, decl. = −16°14′25″.0 (B1950.0).

Thermal emission by dust (far-IR, and smm) $\vec{P} \perp \vec{B}$

Houde et al. (2002)

61

Zeeman effect

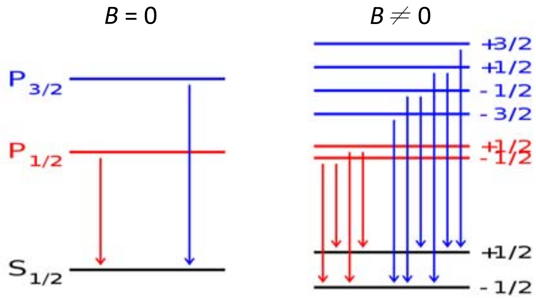

$\Delta \nu_B$ [Hz] = 1.40 x 10^{10} g B[T]

$\Delta \lambda_B$ [nm] = 4.67 x 10^{-8} g (λ_0 [nm])^2 B[T]

g: Landé or g factor (L, S, J) ~ 1

Ex: B = 0.1 T (1 kG) for a typical sunspot, at 500 nm, g=1

→ wavelength shift 0.001 nm ≈ natural line width

→ difficult to measure

62

Astron. Astrophys. 125, L 23–L 26 (1983)

Letter to the Editor

The magnetic field of the NGC 2024 molecular cloud: detection of OH line Zeeman splitting

Richard M. Crutcher[1,2] and Ilya Kazès[1]

[1] Department de Radioastronomie, Observatoire de Paris-Meudon, F-92195 Meudon, France
[2] Department of Astronomy, University of Illinois, Urbana, IL 61801, USA

Summary

Zeeman splitting of the main lines of OH in absorption has been detected for the first time. The derived magnetic field for a clump in the NGC 2024 molecular cloud is -38 ± 1 microgauss.

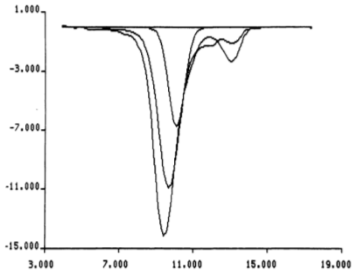

Fig. 1. Spectra of the 1667 (strongest) and 1665 lines observed for 13^h 18^m toward NGC 2024 (RA/DEC [1950.0] 05^h 39^m $14^s.3$ / -01° 55' 57"). The weakest line is the assumed gaussian component used for Zeeman analysis.

The abscissa scale in all figures is the same and is given in km s^{-1} relative to the LSR. The ordinate scale in °K antenna temperature is correct except that displacements of zero have been made in most figures.

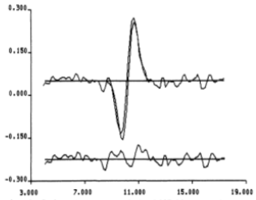

Fig. 4. Stokes V spectrum of the 1667 line together with a fit derived from the gaussian of figure 1. At the bottom the fitted minus the observed residuals are shown.

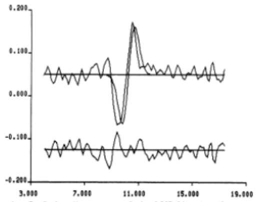

Fig. 5. Stokes V spectrum of the 1665 line together with a fit derived from the gaussian of figure 1. At the bottom the observed minus the fitted residuals are shown.

63

Faraday Rotation --- rotation of the plane of polarization when light passes through a magnetic field

Circularly polarized light → $\boldsymbol{E}$ field rotates → force on the charged particles to make circular motion → creating its own $\boldsymbol{B}$ field, either parallel or in opposite direction to the external field → phase difference
➔ Change of position angle of the linear polarization

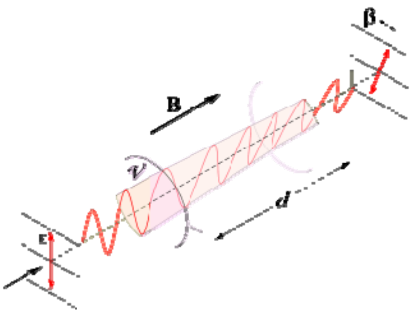

Faraday rotation angle $\beta = RM\ \lambda^2$
where the rotation measure (RM) is

$$\mathrm{RM} = \frac{e^3}{2\pi m^2 c^4} \int_0^d n_e(s) B_{\parallel}(s)\, \mathrm{d}s$$

64

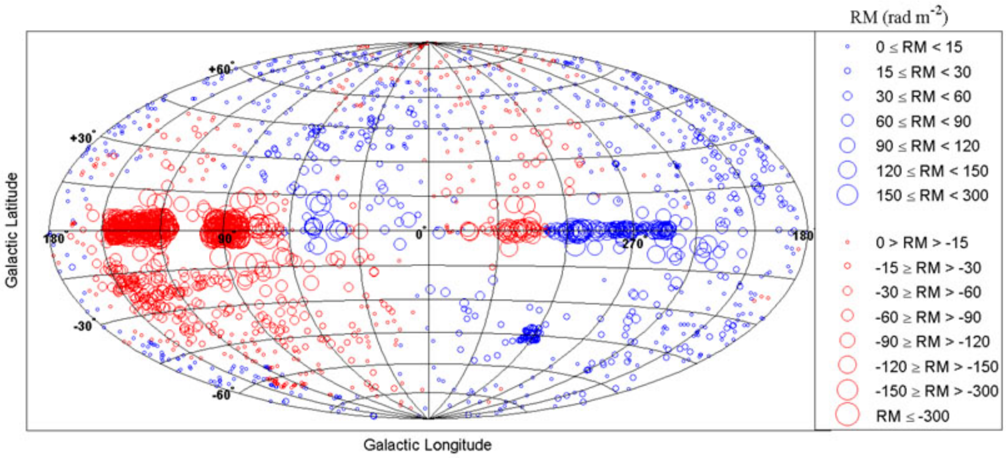

Figure 3. A smoothed representation of 2257 **Faraday rotation** measures in Galactic coordinates with the Galactic center at (0,0). (Kronberg & Newton-McGee, [3]). Blue and red circles represent positive and negative RM's respectively, and the circle size is proportional to RM strength.

http://ned.ipac.caltech.edu/level5/Sept10/Kronberg/Figures/figure3.jpg

65

For **magnetic support** to be important,

$$\frac{3}{5}\frac{GM^2}{R} = \frac{B^2}{8\pi}\left(\frac{4}{3}\pi R^3\right) = \frac{1}{6}B^2R^3$$

So, $M \propto BR^2$, and since $M \propto \rho R^3$, we get $R \propto \frac{B}{\rho}$

The magnetic Jeans mass becomes

$$M^B_{\text{Jeans}} \propto BR^2 \propto {B^3}/{\rho^2}$$

Numerically, $M^B_{\text{Jeans}} \approx 2.4 \times 10^4\, B^3_{\mu\text{G}}\, n_H^{-2}\ [M_\odot]$

and $B_{\text{crit}} = 0.1\ \frac{M}{M_\odot}\ (\frac{\text{pc}}{R})^2\ [\mu\text{G}]$

66

If the magnetic flux is conserved, $\boldsymbol{B} \propto \frac{1}{R^2}$

Because $M \propto R^3 \rho =$ constant, the **frozen-in** (i.e., flux conservation) condition would have led to $\boldsymbol{B} \propto R^{-2} \sim \rho^{2/3}$

If flux is conserved, $\boldsymbol{B}_0$ (ISM) $\sim 10^{-6}$ [G]

$R_0 \approx 0.1$ [pc] $\rightarrow R = R_\odot$ ➔ $\boldsymbol{B} \approx 10^7$ [G]

But what has been actually observed is

$$\boldsymbol{B} \propto \rho^{1/3} \text{ to } \rho^{1/2},$$

Implying magnetic flux loss.

67

THE ASTROPHYSICAL JOURNAL, **301**: 339–345, 1986 February 1

INTERSTELLAR MAGNETIC FIELD STRENGTHS AND GAS DENSITIES: OBSERVATIONAL AND THEORETICAL PERSPECTIVES

T. H. TROLAND
Physics and Astronomy Department, University of Kentucky
AND
CARL HEILES
Astronomy Department, University of California, Berkeley
Received 1985 January 31, accepted 1985 July 16

ABSTRACT

We present an updated compilation of observational data concerning the relationship between the interstellar magnetic field strength and the gas density. Pulsar and Zeeman-effect data provide the only reliable information about the (B, n) relationship, and they now span nearly six orders of magnitude in gas density. Field strengths show no evidence of increase over the density range 0.1–$\sim$100 cm^{-3}. At higher densities, a modest increase in field strength is observed in some regions, in line with theoretical expectations for self-gravitating clouds. In two regions of the interstellar medium, the magnetic field is unusually high; however, these are not locales where self-gravitation is important. Despite the consistency between observations and theory, questions still exist about how the magnetic field strength remains constant for densities up to $\sim$100 cm^{-3}. Further Zeeman effect studies and a better theoretical understanding of the formation of interstellar clouds and complexes will be necessary to answer these questions.

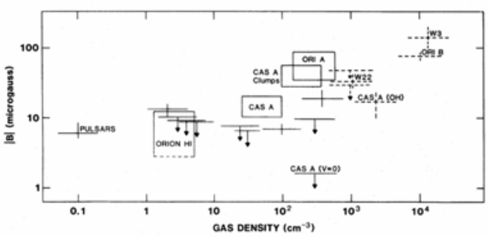

FIG. 1.—Observed magnetic field strengths as a function of estimated volume density. All results come from measurements of the H I (*solid lines*) and OH (*dashed lines*) Zeeman effect, except for the point labeled "pulsars." This point is derived from pulsar rotation and dispersion measures. Rectangular boxes represent ranges of field strengths encountered in Zeeman effect maps made either with a single-dish or with aperture synthesis instruments. See § II for further details.

68

A&A 484, 773-781 (2008)
DOI: 10.1051/0004-6361:200809447

A new probe of magnetic fields during high-mass star formation

Zeeman splitting of 6.7 GHz methanol masers

W. H. T. Vlemmings

Argelander Institute for Astronomy, University of Bonn, Auf dem Hügel 71, 53121 Bonn, Germany

Received 24 January 2008 / Accepted 30 March 2008

Abstract
Context. The role of magnetic fields during high-mass star formation is a matter of fierce debate, yet only a few direct probes of magnetic field strengths are available.
Aims. The magnetic field is detected in a number of massive star-forming regions through polarization observations of 6.7 GHz methanol masers. Although these masers are the most abundant of the maser species occurring during high-mass star formation, most magnetic field measurements in the high-density gas currently come from OH and H_2O maser observations.
Methods. The 100-m Effelsberg telescope was used to measure the Zeeman splitting of 6.7 GHz methanol masers for the first time. The observations were performed on a sample of 24 bright northern maser sources.
Results. Significant Zeeman splitting is detected in 17 of the sources with an average magnitude of 0.56 m s^{-1}. Using the current best estimate of the 6.7 GHz methanol maser Zeeman splitting coefficient and a geometrical correction, this corresponds to an absolute magnetic field strength of 23 mG in the methanol maser region.
Conclusions. The magnetic field is dynamically important in the dense maser regions. No clear relation is found with the available OH maser magnetic field measurements. The general sense of direction of the magnetic field is consistent with other Galactic magnetic field measurements, although a few of the masers display a change of direction between different maser features. Due to the abundance of methanol masers, measuring their Zeeman splitting provides the opportunity to construct a comprehensive sample of magnetic fields in high-mass star-forming regions.

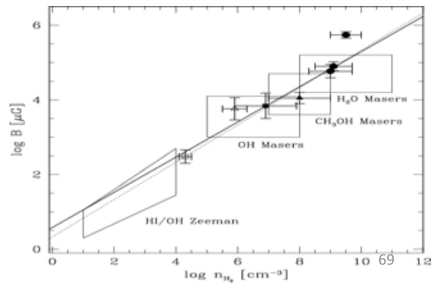

69

$\vec{B}$ confines motion of charged particles.

Molecular clouds → most neutral with only a tiny fraction of particles; ionized by cosmic rays or by natural radioactivity

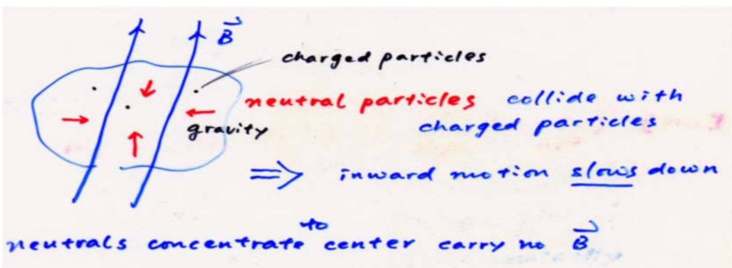

= decoupling of neutral particles from plasma in the initial stage of star formation

→ 1. leakage of $\vec{B}$
2. charged particles escaped from magnetic poles
(ampipolar diffusion=plasma drift)

70

If $\mathcal{M}_{\text{cloud}} > \mathcal{M}_{\text{crit}}$ → <u>supercritical</u> → Cloud will collapse dynamically

➔ Massive star formation

If $\mathcal{M}_{\text{cloud}} < \mathcal{M}_{\text{crit}}$ → <u>subcritical</u> → Cloud collapses, if ever, quasi-statically

➔ Low-mass star formation

Clouds tend to condense with $\mathcal{M} \sim 10^4 M_\odot$, but observed stellar mass ranges $0.05 \leq \mathcal{M}/M_\odot \leq 100$

Why is there a lower mass limit and an upper mass limit for stars?

Cloud collapse → (local) density increase → (local) M_J decrease
→ easier to satisfy $M > M_J$, i.e., cloud becomes more unstable
➔ <u>fragmentation</u>

Formation of a cluster of stars ~~

71

Recall Jeans mass $M_J \approx 1.2 \times 10^5 \left(\frac{T}{100\ K}\right)^{3/2} \left(\frac{\rho_0}{10^{-24}\ \text{g cm}^{-3}}\right)^{-1/2} \frac{1}{\mu^{3/2}}\ [M_\odot]$

$$\propto T^{2/3} / \rho^{1/2}$$

If during collapse, $M_J \downarrow$ → subregions become unstable and continue to collapse to smaller and smaller scales (fragmentation).

Since during collapse ρ always ↑, the behavior of M_J depends on T.

If gravitational energy is radiated away, i.e., $\tau_{\text{cooling}} \ll \tau_{\text{ff}}$ and collapse is <u>isothermal</u>, T = const, so $M_J \propto \rho^{-1/2}$ ➔ collapse continues

72

However, once the isothermal condition is no longer valid, e.g., when the cloud becomes optically thick, the collapse is **adiabatical**.

$$T \propto P^{2/5} \propto \rho^{2/3}$$

So $M_J \propto \frac{\rho}{\rho^{1/2}} = \rho^{1/2}$, i.e., grows with time (ever more difficult to overcome/collapse), so the collapse halts

For a monatomic idea gas, the adabatic index $\gamma \equiv c_p/c_v = \frac{f+2}{f} = {}^{5/2}/_{3/2} = 5/3$

$$PV^\gamma = \text{const; } TV^{\gamma-1} = \text{const;}$$

73

Equation of motion for a spherical surface at r is

$$\frac{d^2r}{dt^2} = -\frac{Gm}{r^2}$$

with initial condition $r(0) = r_0, \frac{dr}{dt}(0) = 0, m = 4\pi {r_0}^3 \rho_0/3$.

Multiplying both sides by dr/dt, and since $\frac{d}{dt}(\frac{dr}{dt})^2 = 2\frac{dr}{dt}\frac{d^2r}{dt^2}$,

$$\frac{d}{dt}(\frac{dr}{dt})^2 = -\frac{2Gm}{r^2}\frac{dr}{dt}$$

Integrating both sides, we get

$$\left(\frac{dr}{dt}\right)^2 = 2Gm\left(\frac{1}{r} - \frac{1}{r_0}\right)$$

74

Substituting m, we get

$$\frac{dr}{dt} = -\left[\frac{8\pi G \rho_0 {r_0}^2}{3}\left(\frac{r_0}{r} - 1\right)\right]^{\frac{1}{2}}$$

Define a new variable θ, so that $r(t) = r_0 \cos^2\theta$, ($\theta = 0$ at $t = 0$) then

$$\frac{d\theta}{dt}\cos^2\theta = \frac{1}{2}\left(\frac{8\pi G \rho_0}{3}\right)^{1/2}$$

Integrating this, we obtain $\theta + \frac{1}{2}\sin 2\theta = \left(\frac{8\pi G \rho_0}{3}\right)^{1/2} t$

The free-fall time is when $\theta = \pi/2$, $t_{\mathrm{ff}} = \left(\frac{3\pi}{32\, G\rho_0}\right)^{\frac{1}{2}} = \frac{3.4\times 10^7}{\sqrt{n_0}}$ [yr]

Bodenheimer p.34 ... when density becomes ∞ for all m.

75

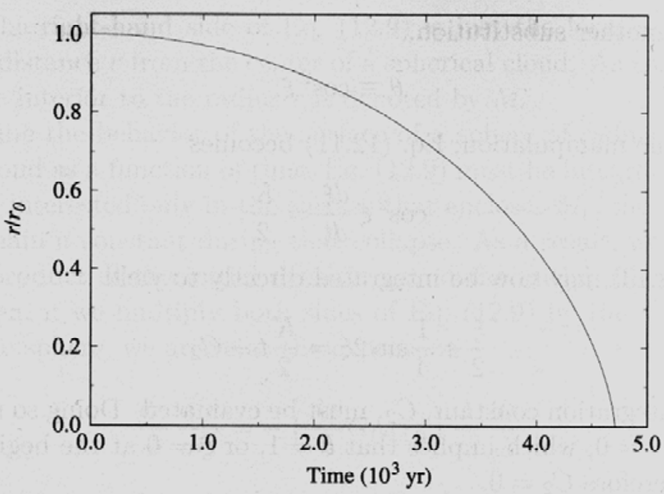

Figure 12.5 The ratio of the radius relative to its initial value as a function of time for the homologous collapse of a molecular cloud. The collapse is assumed to be isothermal, beginning with a density of $\rho_0 = 2\times10^{-16}$ g cm^{-3}.

Carroll & Ostlie

76

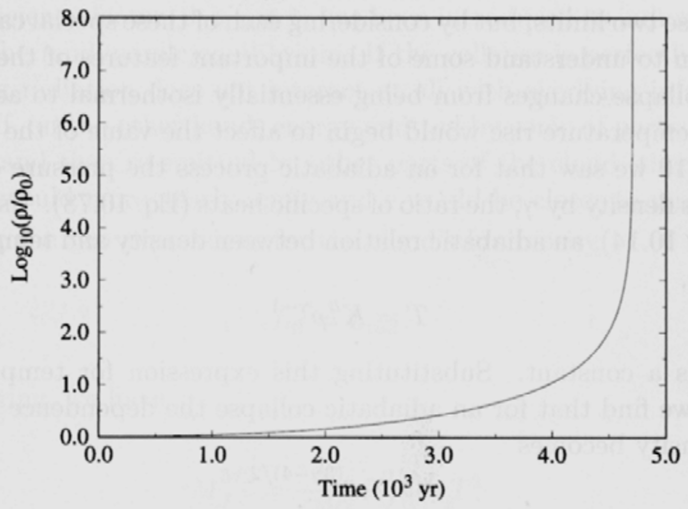

Figure 12.6 The ratio of the cloud's density relative to its initial value as a function of time for the isothermal, homologous collapse of a molecular cloud with an initial density of $\rho_0 = 2 \times 10^{-16}$ g cm^{-3}.

Carroll & Ostlie

77

Note that $t_{ff} \propto \frac{1}{\sqrt{G\rho_0}}$ has no dependence on r_0.

If ρ_0 is uniform, all m collapse to the center at the same time

→ homologous collapse

If ρ_0 is somewhat centrally condensed, as observed,
e.g., $\rho_0 \propto r^{-1}$ to r^{-2}, inner region (small r), t_{ff} ↓↓

→ inside-out collapse

78

Gravitational energy available $E_g \sim \frac{GM^2}{R}$
which is released during the contraction of mass M from ∞ to R

$$t_{KH} \sim \frac{GM^2}{R} \Big/ L \sim R^{-3} \quad (\because L \sim R^2 T^4,\ T\ \text{const})$$

$$t_{ff} \sim \frac{1}{\sqrt{G\rho}} \sim R^{3/2}$$

For an object already on the main sequence

$$t_{ff} \ll t_{KH}$$

Ex. For $1 M_\odot$, $1 L_\odot$ $\quad t_{ff} \sim 10^{-4}$ yr
$\quad t_{KH} \sim 2\times10^{7}$ yr $\qquad t_{ff} \ll t_{KH}$

$\therefore$ When $R \gtrsim 300 R_\odot$ $\quad t_{ff} \gtrsim t_{KH}$

$\Rightarrow$ protostellar collapse is a dynamical process.

$$\tau_{ff} \sim 66120/\sqrt{\rho_{MKS}} \sim 35/\sqrt{\rho_{cgs}} [\text{min}]$$

79

Free-Fall Collapse

$$m\frac{d^2r}{dt^2} = \frac{GMm}{r^2}$$

Dimension analysis

$$\frac{R}{t^2} \sim \frac{GM}{R^2} \Rightarrow t_{ff} \sim \frac{1}{\sqrt{G\rho}} \approx \frac{4.3\times10^7}{\sqrt{n_{H_0}}} \text{ [yrs]}$$

---

or

$$2E_K + E_P = \cdots < 0$$

$$t_s = \frac{R}{v_{sound}} \sim \frac{1}{\sqrt{G\rho}}, \quad v_s \sim \sqrt{\frac{RT}{\mu}}$$

---

e.g. $\rho \sim 10^3 \times 1.6\times10^{-24}$, $\quad t_{ff} \sim \frac{1}{\sqrt{6.6\times10^{-8}\times10^{-21}}} \sim 10^{14}$ s $\sim 3\times10^{6}$ yr

In reality, $\rho \uparrow$ as $r \downarrow$ (i.e., density concentration, e.g. $\rho \sim r^{-1.5}$)

$\therefore$ t_{ff} shorter for smaller r

$\Rightarrow$ Collapse proceeds in an inside-out fashion.

→ → core ← ← accretion

$$L_{acc} \sim GM_* \dot{M}_{acc}/R_*$$

80

Recall the relation between a circular motion and a simple harmonic motion.

Acceleration to the center
Time scale = ¼ period

Applications:
- Gas in a collapsing cloud
- Stars in a globular cluster
- Galaxies in a galaxy cluster

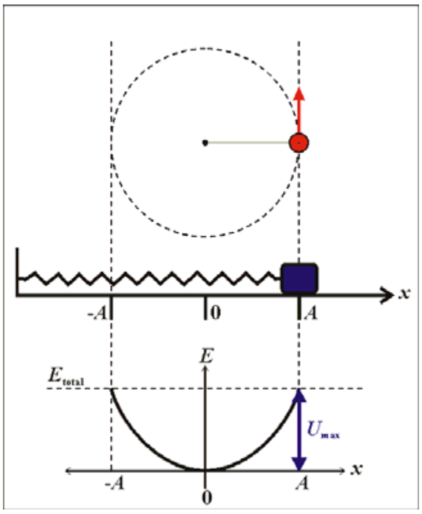

http://prism.texarkanacollege.edu/physicsbook/shm-ucm.gif

81

Exercise

1. For a the sun, i.e., a mass $\mathcal{M} = 1\,\mathcal{M}_\odot$, a luminosity $\mathcal{L} = 1\,\mathcal{L}_\odot$, and a radius $\mathcal{R} = 1\,\mathcal{R}_\odot$, compute the free-fall time scale τ_{ff} and the Kevin-Helmholtz time scale $\tau_{\mathrm{KH}} \approx {G\mathcal{M}^2}/{RL}$. Which time scale is longer?
2. Note that both time scales have different dependence on the size scale. At what size, do the two time scales equal?

82

Ann. Rev. Astron. Astrophys. 1987. 25: 23–81

STAR FORMATION IN MOLECULAR CLOUDS: OBSERVATION AND THEORY

Frank H. Shu, Fred C. Adams, and Susana Lizano

Astronomy Department, University of California, Berkeley, California 94720

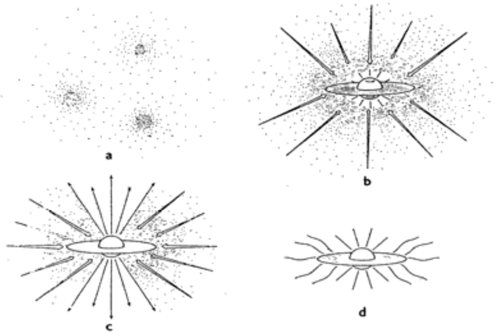

Figure 7 The four stages of star formation. (*a*) Cores form within molecular clouds as magnetic and turbulent support is lost through ambipolar diffusion. (*b*) A protostar with a surrounding nebular disk forms at the center of a cloud core collapsing from inside-out. (*c*) A stellar wind breaks out along the rotational axis of the system, creating a bipolar flow. (*d*) The infall terminates, revealing a newly formed star with a circumstellar disk.

83

THE ASTRONOMICAL JOURNAL VOLUME 98, NUMBER 4 OCTOBER 1989

A TWO MICRON POLARIZATION SURVEY OF T TAURI STARS

MOTOHIDE TAMURA[a)]
Department of Physics, Kyoto University, Sakyo-ku, Kyoto 606, Japan
and
Department of Astronomy, University of Massachusetts, Amherst, Massachusetts 01003

SHUJI SATO
National Astronomical Observatory, Mitaka, Tokyo 181, Japan

Received 30 September 1988; revised 23 May 1989

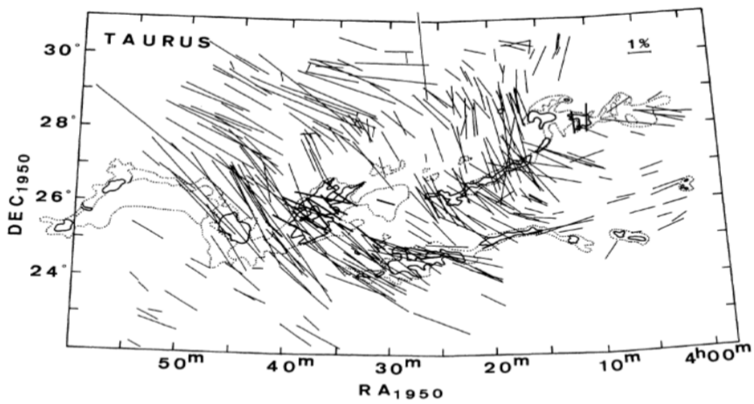

FIG. 2. Polarization map at optical (thin vectors) and at infrared (thick vectors) towards background stars in the Taurus dark cloud complex, compiled from the data in the literature (Moneti *et al.* 1984; Hsu 1984; Heyer *et al.* 1987; Tamura *et al.* 1987).

84

Evolution from a circumstellar toroid (geometrically thick) to a disk; opening angle of the outflow widened

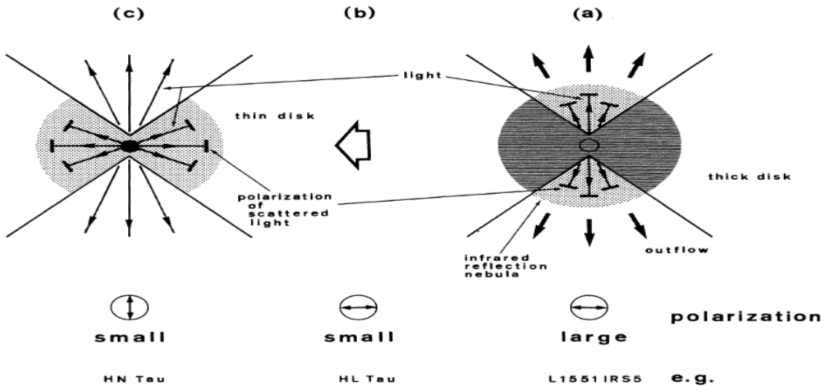

FIG. 10. Model of infrared polarization of (a) young stellar objects with mass outflows, (b) T Tauri stars with extreme mass-outflow phenomena, and (c) T Tauri stars without extreme mass outflow.

85

1980ApJ...239L..17S

OBSERVATIONS OF CO IN L1551: EVIDENCE FOR STELLAR WIND DRIVEN SHOCKS

RONALD L. SNELL
Astronomy Department and Electrical Engineering Research Laboratory, University of Texas at Austin; and Five College Radio Astronomy Observatory, University of Massachusetts at Amherst

ROBERT B. LOREN
Electrical Engineering Research Laboratory and McDonald Observatory, University of Texas at Austin

RICHARD L. PLAMBECK
Radio Astronomy Laboratory, University of California at Berkeley

ABSTRACT

CO observations reveal the presence of a remarkable, double-lobed structure in the molecular cloud L1551. The two lobes extend for ~0.5 pc in opposite directions from an infrared source buried within the cloud; one lobe is associated with the Herbig-Haro objects HH28, HH29, and HH102. We suggest that the CO emission in the double-lobed structure arises from a dense shell of material which has been swept up by a strong stellar wind from the infrared source. This wind has a velocity of $\sim$200 km s^{-1}, and evidently is channeled into two oppositely directed streams. The CO observations indicate that the shell has a velocity of $\sim$15 km s^{-1}, a mass of 0.3 $M_\odot$, and a kinetic temperature of 8–35 K. Its age is roughly 3×10^4 years. A stellar mass-loss rate of $\sim 8 \times 10^{-7}$ $M_\odot$ yr^{-1} would be sufficient to create such a shell.

86

Data cube
(sky position
and frequency)

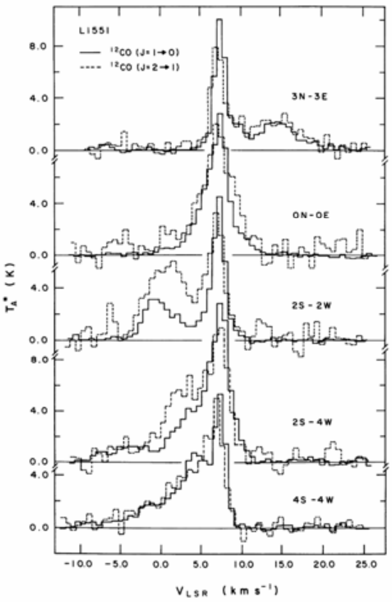

Fig. 1.—Spectra of the J = 1-0 (*solid*) and J = 2-1 (*dashed*) lines of ^{12}CO taken toward five selected positions in L1551. Offsets are measured in arcmin relative to the position of IRS-5 at α(1950) = 04^{h}28^{m}40^s, δ(1950) = 18°01′52″. The J = 1-0 spectra were taken at NRAO with a 1′.1 beam; the J = 2-1 spectra were taken at the MWO with a 1′.2 beam. The ratio of the 2-1 and 1-0 antenna temperatures in the broad velocity features can be used to infer the kinetic temperature of the gas responsible for these features.

87

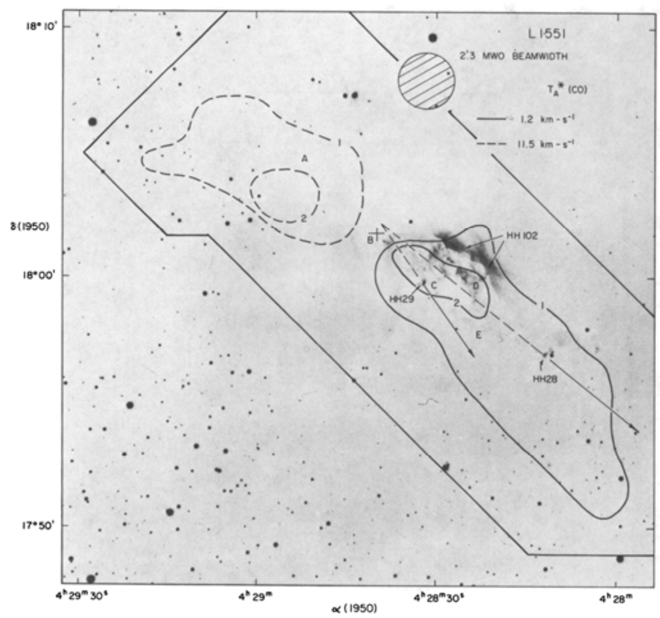

Fig. 2.—Contour map of the J = 1-0 ^{12}CO antenna temperatures in the broad velocity components, superposed on an optical photo of the region taken by Strom with the 4 m telescope at KPNO. The map is based on CO spectra taken at 115 positions within the enclosed border with 1′-2′ spacings. A cross indicates the position of IRS-5; letters A-E indicate the positions of the five spectra in Fig. 1 from top to bottom. Also shown are the directions of the proper motions of the two compact Herbig-Haro objects, HH28 and HH29; tracing their motion backward suggests a common origin at the infrared source.

Snell et al. (1980)

88

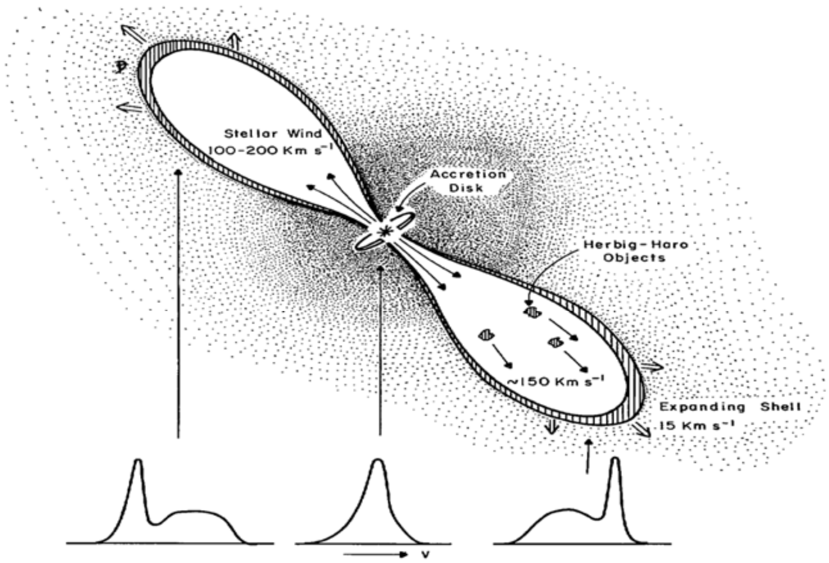

FIG. 5.—A schematic picture of the stellar wind driven shock model for L1551, indicating the CO line profiles which would be expected at different positions across the source. The Herbig-Haro objects are not necessarily located inside the shell; because of their high velocities, they may have been ejected through the shell and into the surrounding medium.

Snell et al. (1980)

89

Annu. Rev. Astron. Astrophys. 1996. 34:111–54

BIPOLAR MOLECULAR OUTFLOWS FROM YOUNG STARS AND PROTOSTARS

Rafael Bachiller

Observatorio Astronómico Nacional (IGN), Campus Universitario, Apartado 1143, E–28800 Alcalá de Henares (Madrid), Spain

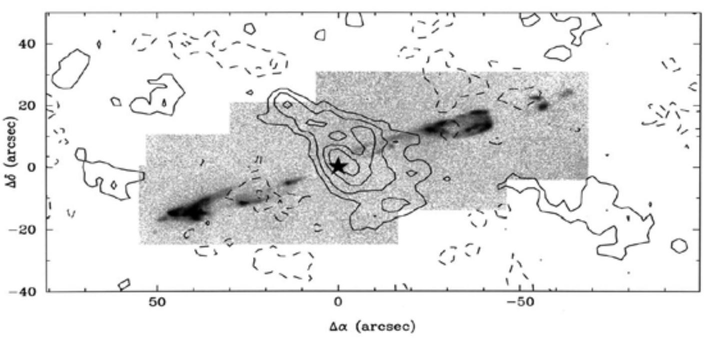

Figure 4 Superposition of a gray-scaled image of the HH 211 jet taken in the H_2 $v = 1{-}0$ S(1) line at 2.122 μm (from McCaughrean et al 1994) with a NH_3 (1,1) image obtained with the VLA at its D configuration (6″ angular resolution) (R Bachiller & M Tafalla 1995, unpublished data). The star marks the position of the jet source HH 211-mm (see also Table 1).

90

Herbig-Haro (HH) Objects

-- (shock) *excited nebulosity*

HH 34

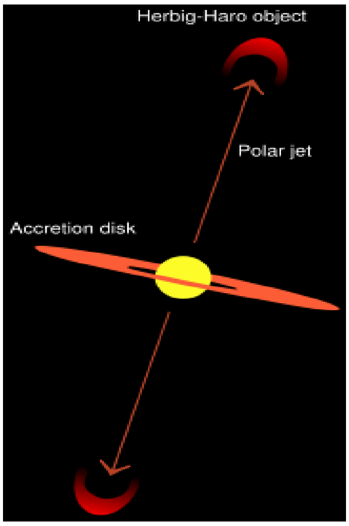

HH 47

91

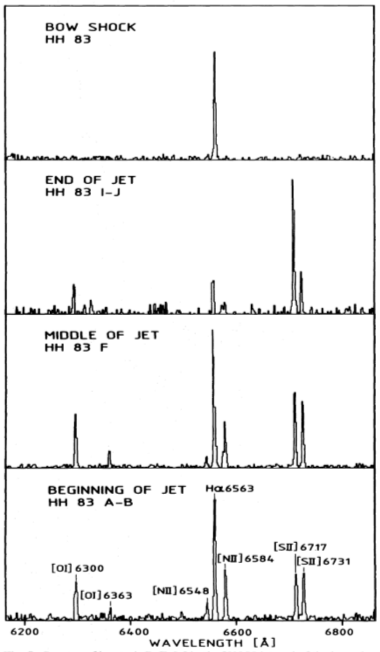

Fig. 5. Spectra of knots A-B, F, I-J in the HH 83 jet and of the bow shock in the wavelength range approx. 6200 Å to 6800 Å. Note the increasing [S II] 6717/Hα ratio as one moves out along the jet, as well as the changing sulphur line ratio, indicating decreasing electron density. The bow shock is pure Hα emission

Reipurth (1989)

92

M. Cohen, The T Tauri stars

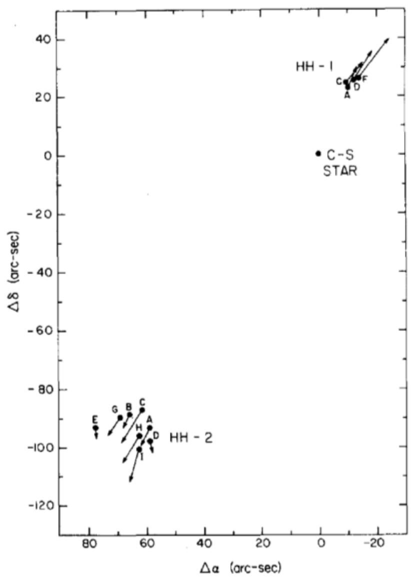

Fig. 39. Proper motions for individual knots of HH1, 2 and the Cohen–Schwartz star [161].

93

Molecular Hydrogen Objects (MHOs) 1000+ now known

Infrared image of molecular bow shocks (MHO 27) associated with bipolar outflows in Orion. Credit: UKIRT/Joint Astronomy Centre

94

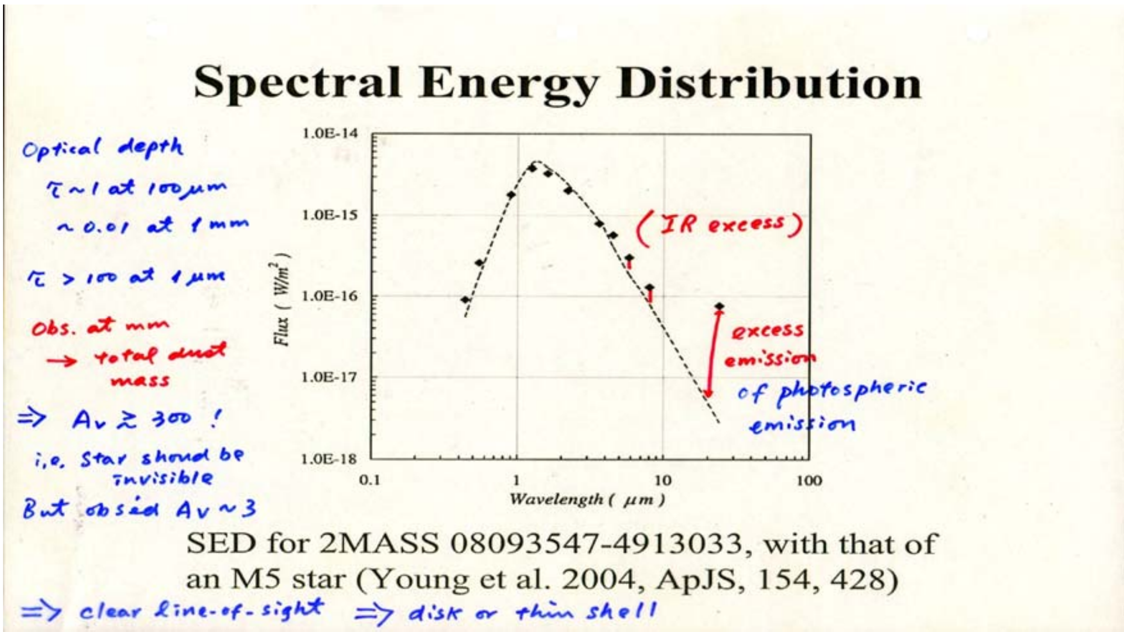

95

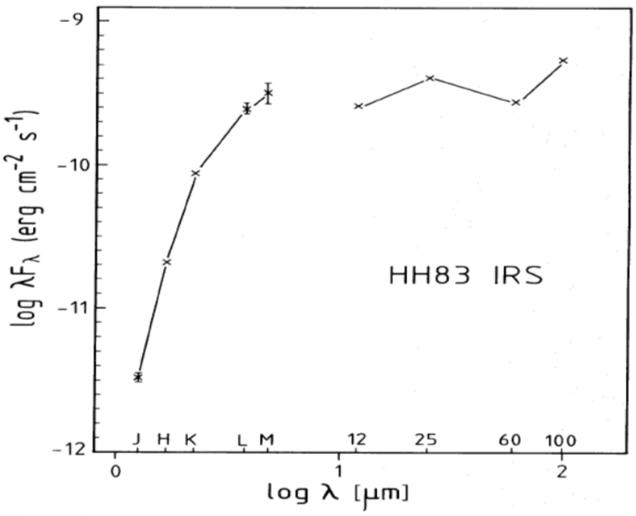

Fig. 6. The energy distribution of the infrared source of HH 83 based on near- and far-infrared photometry. Error bars are shown for the near-infrared data points where the errors are larger than the extent of the crosses. No error bars are given for the far-infrared IRAS data

Exciting source of an HH object = protostar

very prominent IR excess; lots of dust; a very young age

96

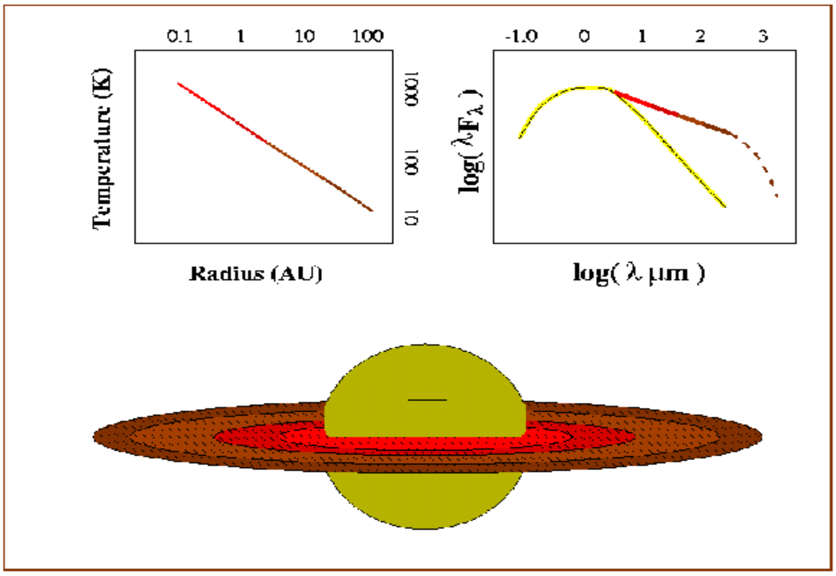

97

Accretion Disks

- Found in YSOs, supermassive BHs in AGB, binaries, Saturnian rings
- Turbulent viscosity important
  - generating heat
  - transporting angular momentum <u>outwards</u>
  - transporting matter <u>inwards</u>

<u>Fact</u>: The Sun has > 99% of the total mass in the solar system, but accounts for ~3% of the total angular momentum (rotation), whereas Jupiter's orbital angular moment accounts for 60%.

<u>Fact</u>: Outer planets rotate fast (thus are flattened.)

98

Exercise

1. Compare the angular momenta of the Sun, Jupiter, and Earth.
2. What is the specific angular momentum of the Earth versus Jupiter?
3. How round (or flat) is the shape of the Earth, of Jupiter, and of the Sun?

http://www.zipcon.net/~swhite/docs/astronomy/Angular_Momentum.html

99

Water and carbon dioxide in <u>solid</u> form
→ cold materials near the protostar

Silicate feature → thick dusty cocoon

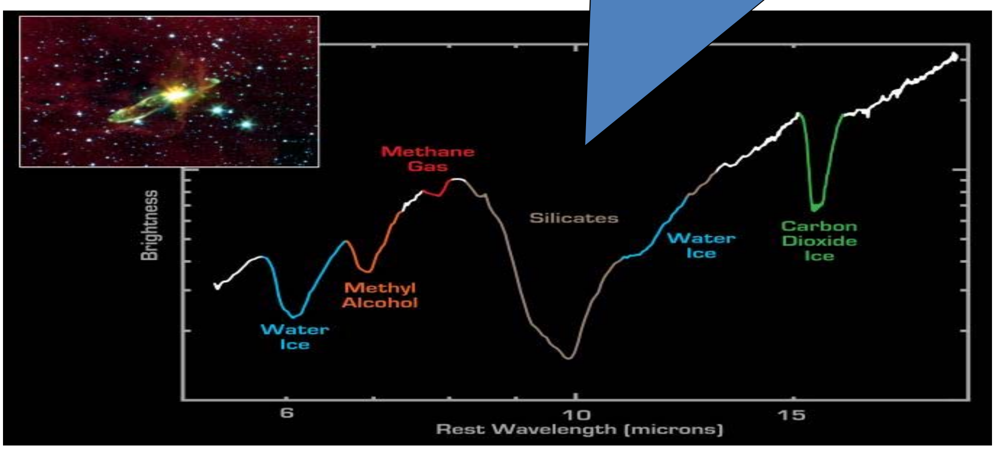

Spitzer IRS

100

T Tauri stars (= PMS sun-like stars) are seen against dark nebulosity and characterized by emission-line spectra.

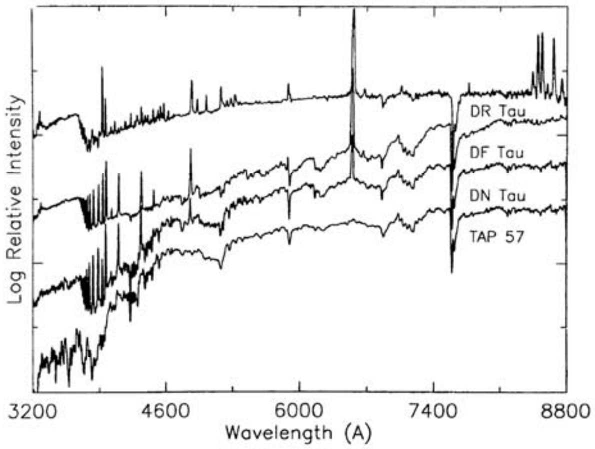

Figure 2 Medium-resolution spectrograms covering the spectral range 3200–8800 Å of four late-K or early-M T Tauri stars, shown in order of increasing emission levels. The relative intensity is displayed in wavelength units.

Bertout (1989) 101

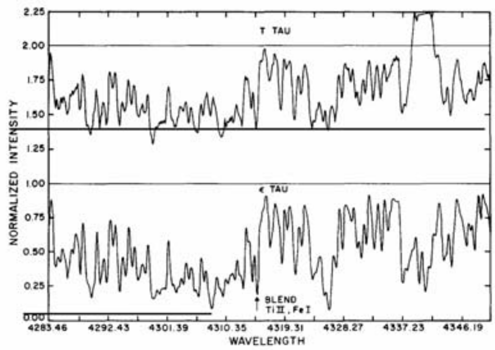

Fig. 3a. Spectrum of T Tau and of ε Tau, a standard star of the same temperature.

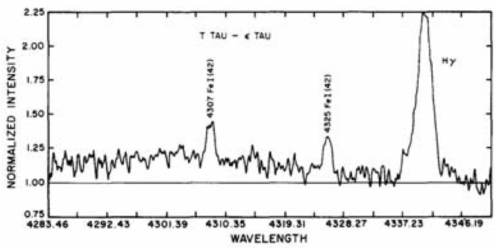

Fig. 3b. The result of subtracting the optical spectrum of a standard stellar spectrum from that of a T Tau star, suitably normalised, having the same photospheric temperature. Note the set of discrete emission lines in the T Tau spectrum. (From [17].)

Cohen (1984) 102

P Cygni profile → A spectral profile showing an expanding envelope

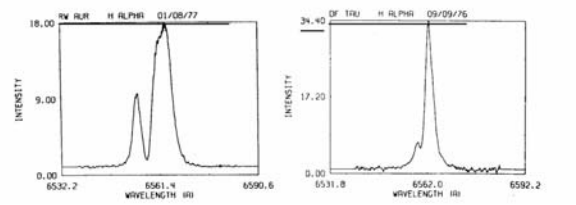

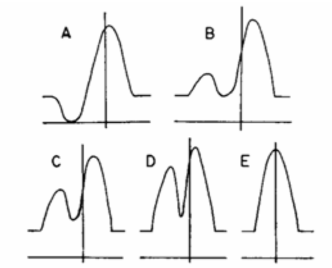

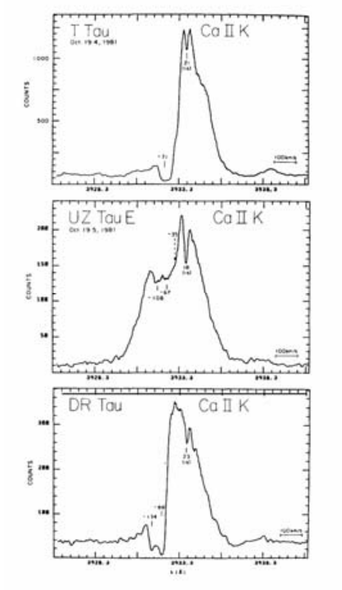

Stellar velocity

Cohen (1984)

103

T Tauri stars also show <u>infrared excess</u> in the SEDs.

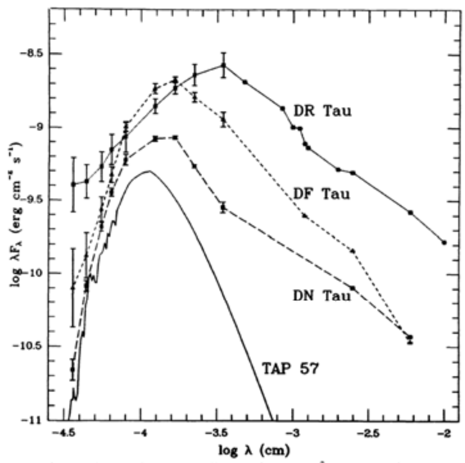

Figure 3 Observed spectral energy distributions from 3600 Å to 100 μm of the stars whose spectra are shown in Figure 2. The energy distribution of the K7V WTTS TAP 57, shown as a solid line, has been displaced downward by 0.3 dex. The filled symbols are simultaneous (for DN Tau and DF Tau) or averaged (for DR Tau) photometric data (cf. Bertout et al. 1988) supplemented by *IRAS* data (Rucinski 1985). When available, observed variability is indicated by error bars. When compared with WTTSs such as TAP 57, CTTSs display prominent ultraviolet and infrared excesses. Excess continuum flux and optical emission-line activity are often correlated.

… and also <u>UV excess</u>

→ spectral "veiling"

Bertout (1989)

104

INTERPRETATION OF T TAURI STARS

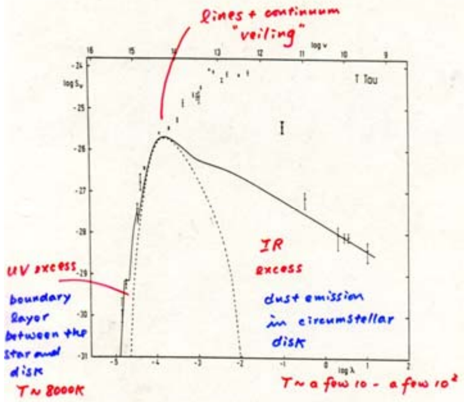

Figure 3: Continuum energy distribution of the star T Tau (according to Bertout 1980). The λ = 1 mm point is a new measurement by Chini et al. (1983). The units of S_ν are $Wm^{-2}Hz^{-1}$, λ is given in cm, ν in Hz. The broken line indicates the contribution of the star's photosphere, the solid line the combined contribution of the photosphere and the ionized part of the circumstellar gaseous envelope. The remaining IR excess is attributed to dust emission.

Appenzeller (1983) RMAA

105

CS Cha K4Ve CTTS

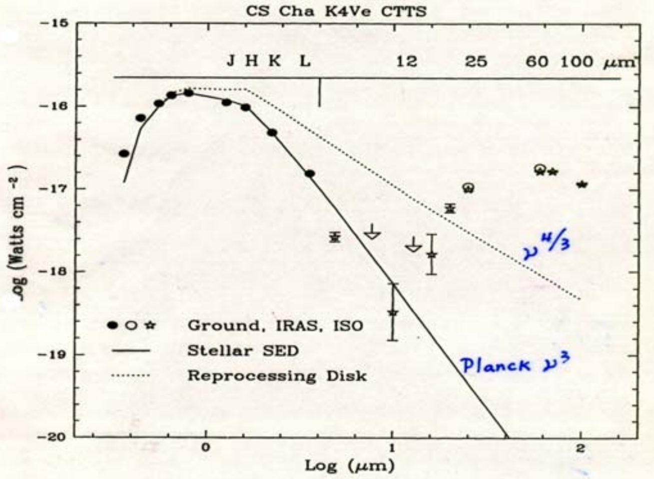

Figure 2. CS Cha SED. The ISO measurements are shown by stars. The two arrows denote upper limits from ISO observations. Filled circles are ground-based photometry. Open circles are IRAS measurements at 60 and 100 μm. The solid curve shows the SED of the stellar photosphere; the dotted curve the model prediction for a standard reprocessing disk seen face-on.

106

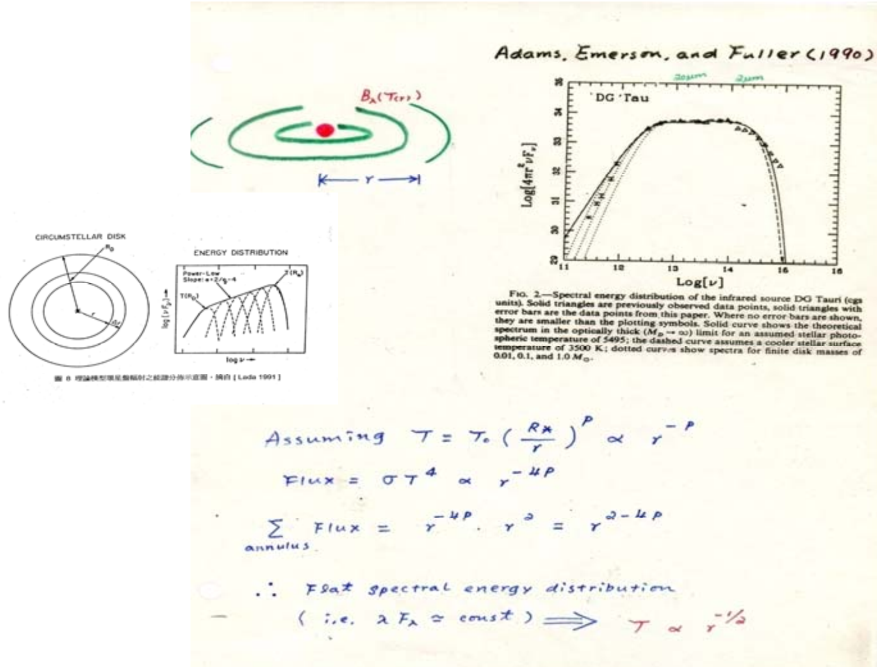

107

Spectral index useful to classify a young stellar object (YSO)

$$\alpha = \frac{d\log(\lambda F_\lambda)}{d\log(\lambda)}$$

Where λ=wavelength, between 2.2 and 20 μm; F_λ=flux density

Class 0 sources --- undetectable at $\lambda < 20$ μm
Class I sources --- $\alpha > 0.3$
Flat spectrum sources --- $0.3 > \alpha > -0.3$
Class II sources --- $0.3 > \alpha > -1.6$
Class III sources --- $\alpha < -1.6$

➔ Evolutionary sequence in decreasing amounts of circumstellar material (disk clearing)

108

Annu. Rev. Astron. Astrophys. 1996. 34:111–54

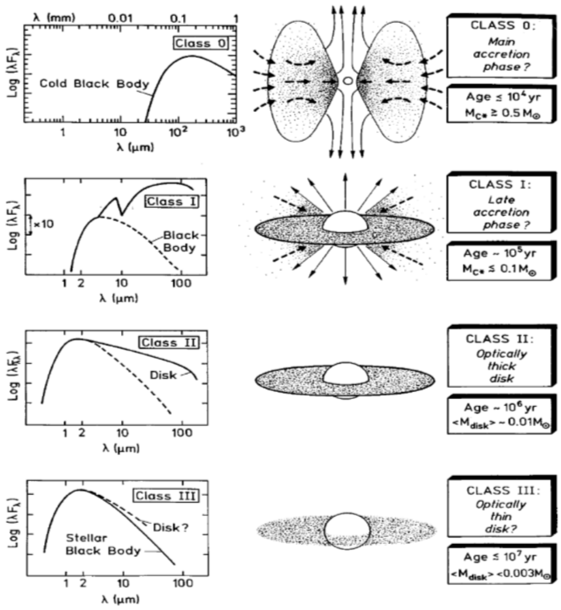

Figure 11 Evolutionary sequence of the spectral energy distributions for low-mass YSOs as proposed by André (1994). The four classes 0, I, II, and III correspond to successive stages of evolution.

Submilimeter cores

Protostars

Classical T Tauri stars

Weak-lined T Tauri stars

Rafael Bachiller

109

T Tauri stars are PMS objects, contracting toward the **zero-age main sequence (ZAMS).**

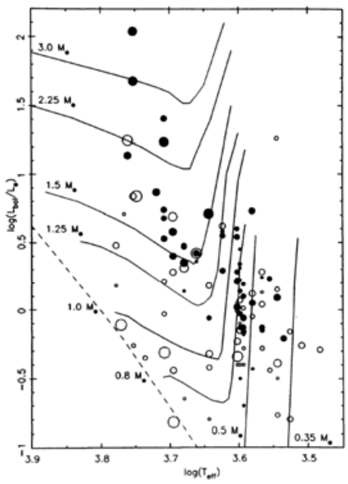

Figure 4 Position in the Hertzsprung-Russell diagram of all CTTSs and WTTSs with known $v \sin i$. WTTSs are represented by open circles, and CTTSs by dark circles. In both cases, the circle area is proportional to the stellar $v \sin i$. Approximate pre-main-sequence quasi-static evolutionary tracks for various masses are also plotted together with the zero-age main sequence (dashed line).

Bertout (1989)

110

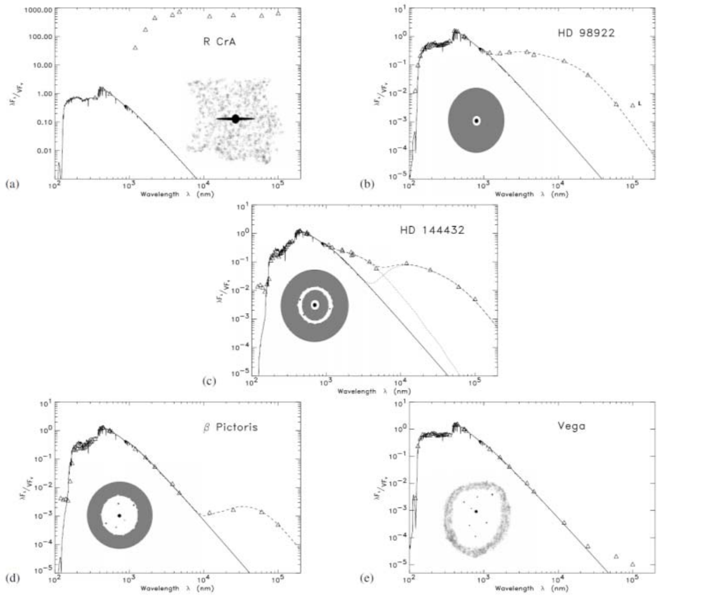

Fig. 3a–e. Evolutionary scenario: **a** embedded source (R CrA); **b** single dust disk causing near-IR and far-IR excess (HD 98922); **c** double dust disk (HD 144432); **d** single dust disk causing far-IR excess (β Pictoris); **e** more evolved dust disk (Vega)

Malfait+1998

111

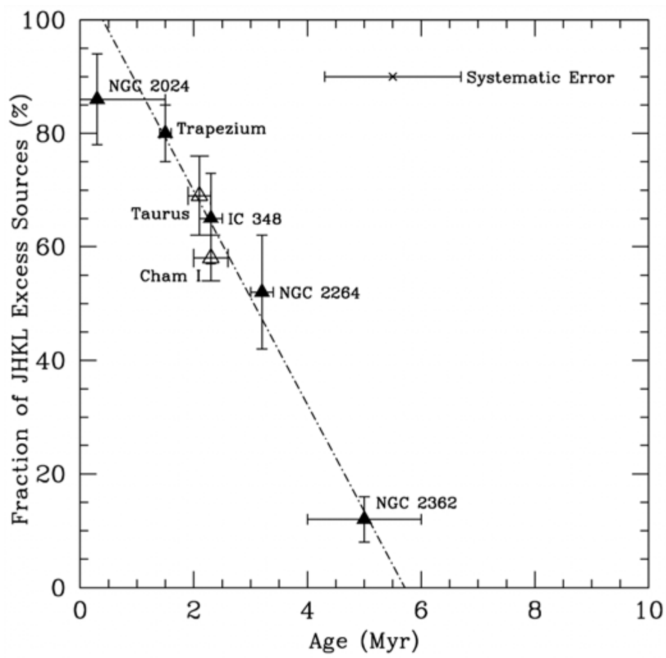

One half of stars lose disks within 3 Myr

Disk disposed in ~6 Myr: planet formation timescale

Haisch+ 2001

112

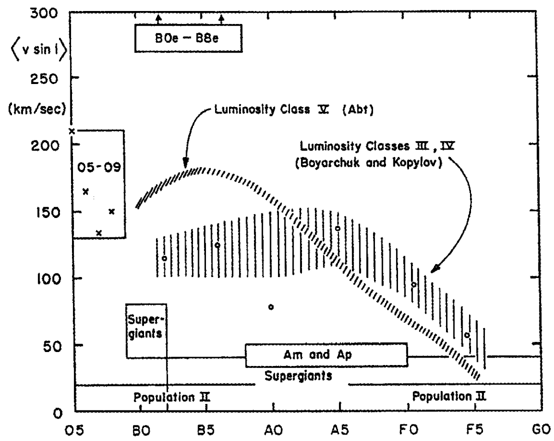

Fig. 3. Projected equatorial velocities, averaged over all possible inclinations, as a function of spectral type. On the main sequence (luminosity class V), early-type stars have rotational velocities that reach and even exceed 200 km/s; these velocities drop to a few km/s for late-type stars, such as the Sun (type G2) (Slettebak [20]; courtesy Gordon & Breach)

- Early-type stars are fast rotators
- Stars later than ~F5 rotate very slowly
- Disk/planet formation?

113

Annu. Rev. Astron. Astrophys. 1996. 34:207–40

THE FU ORIONIS PHENOMENON[1]

Lee Hartmann and Scott J. Kenyon

Harvard-Smithsonian Center for Astrophysics, 60 Garden Street, Cambridge, Massachusetts 01238

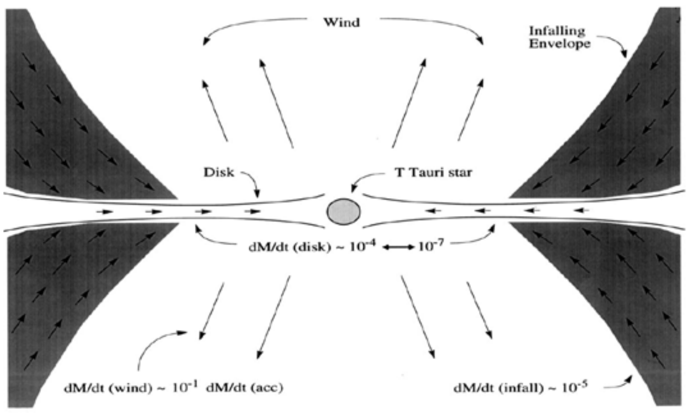

Figure 1 Schematic picture of FU Ori objects. FU Ori outbursts are caused by disk accretion increasing from $\sim 10^{-7}\ M_\odot\ yr^{-1}$ to $\sim 10^{-4}\ M_\odot\ yr^{-1}$, adding $\sim 10^{-2}\ M_\odot$ to the central T Tauri star during the event. Mass is fed into the disk by the remanant collapsing protostellar envelope with an infall rate $\lesssim 10^{-5}\ M_\odot\ yr^{-1}$; the disk ejects roughly 10% of the accreted material in a high-velocity wind.

114

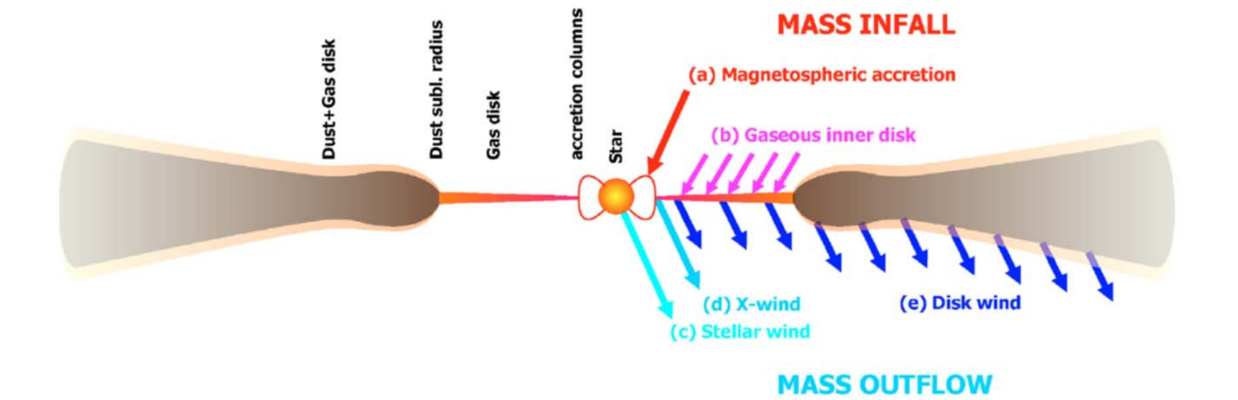

Fig. 1. Illustration of the regions which have been proposed as the origin of the permitted hydrogen recombination line emission observed towards HAeBe stars (this sketch is not to scale; read Sect. 1 for details about the individual mechanisms).

Kraus+08

115

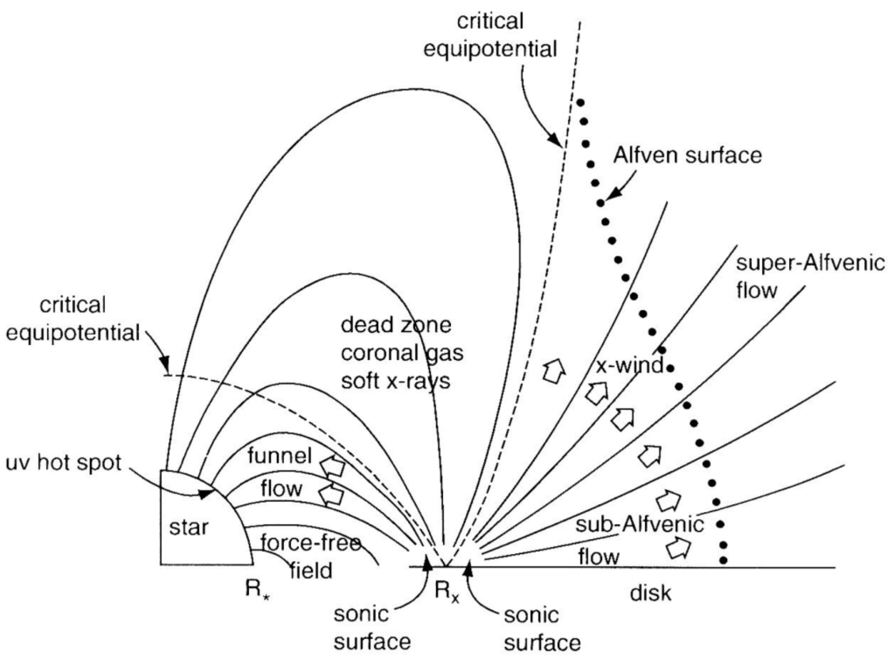

116

Annu. Rev. Astron. Astrophys. 1996. 34:111–54

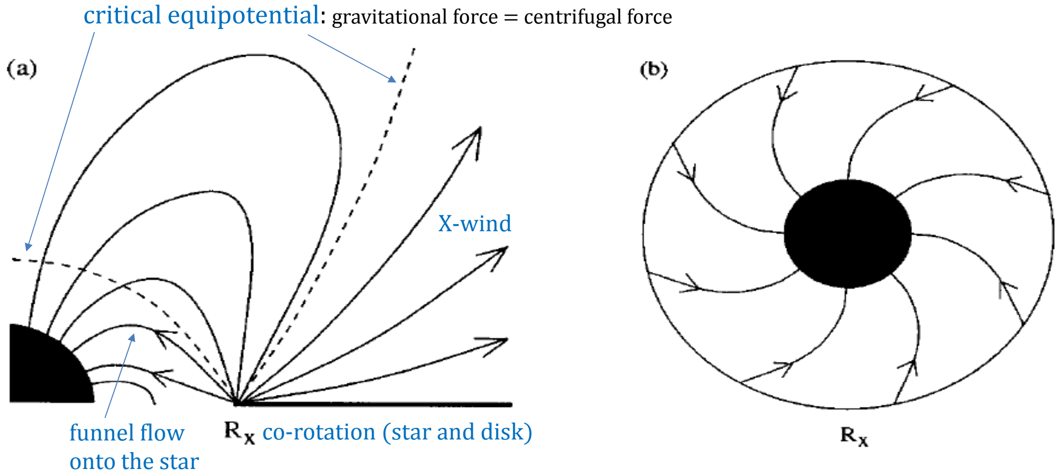

Figure 13 Schematic views of the (*a*) meridional plane and (*b*) equatorial plane of the configuration modeled by Shu et al (1994a,b) for the origin of bipolar outflows. The circumstellar disk is truncated at a distance R_X from the star. Both energetic outflows and funnel flows emerge from the disk truncation region. Gas accreting from the disk onto the star in a funnel flow drags the stellar field into a trailing spiral pattern. (From Najita 1995.)

Rafael Bachiller

117

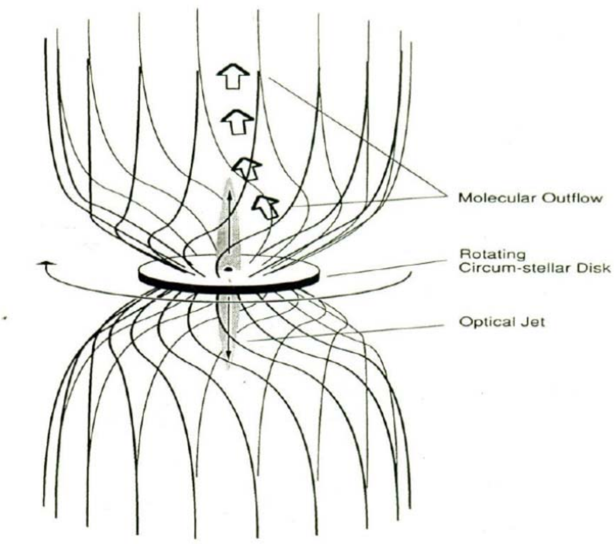

Figure 6. A schematic drawing of the magnetohydrodynamical model.

118

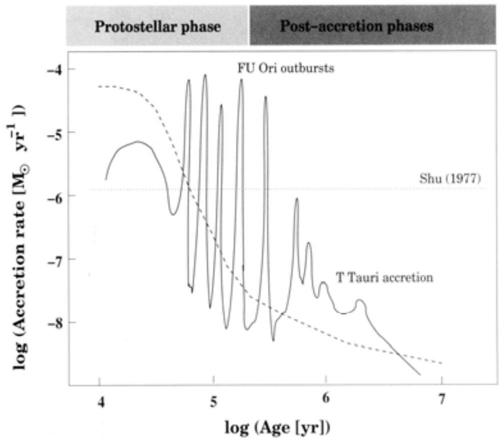

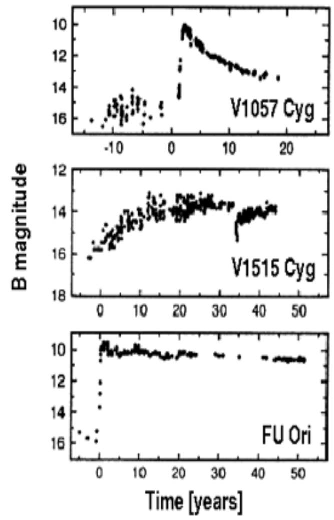

Fig. 6.1. The diagram schematically shows the time development of the accretion rates as they appear in various calculations and in relation to observed phenomena. The dotted straight line resembles the result from standard star formation [777], which does not depend on time and is based on infinitely large radius and mass and thus appears as a flat line throughout the entire time interval. The hatched curve represents an approximation to the results of the many more realistic calculations. The thick line was adapted from Hartmann [344] and shows additional features such as outbursts of FU Ori type protostars and T Tauri disk accretion. All rates apply for typical low-mass ($\sim M_\odot$) stars only.

Inside-out collapse (Shu 1977) isothermal sound speed → constant accretion rate

Collision

Gas (hydrogen atoms) root-mean-squared speed

$$m_{\rm H}\sqrt{<v^2>} = 3kT$$

For H I regions,

$$T \sim 100 \text{ K}, <v>_{\rm HI} \sim 1 \text{ km s}^{-1}$$

$$\text{For } e^-, <v>_{e^-} \sim 50 \text{ km s}^{-1}$$

Cross sections σ

- Hard sphere OK for neutral atoms, i.e., 'physical' cross section

$$\sigma = \pi(a_1 + a_2)^2$$

$$\sigma_{\rm HI,HI} \leftarrow a \sim 5.6 \times 10^{-9} \text{ cm}$$

$$\text{c.f., Bohr radius (first orbit)} = 5.3 \times 10^{-9} \text{ cm}$$

120

Cross sections σ

- For free e^-, p^+

$$\sigma >> \sigma_{\rm physical} \text{ because of Coulomb force, need QM}$$

$$a \sim \frac{2.5\times10^{-2}}{v^2} \text{ cm } (v \text{ in km})$$

$$\text{If } v_{e^-} \sim 50 \text{ km s}^{-1},\ a \sim 10^{-5} \text{ cm for } e^-\text{-}e^- \text{ collision}$$

$$T = 3\times10^4 \text{ K},\ <v>\sim 10^3 \text{ km s}^{-1}$$

$$\longrightarrow \quad a \sim 2.5\times10^{-8} \text{ cm}$$

$$\text{c.f., classical electron radius} \sim 2.8\times10^{-13} \text{ cm}$$

$$\frac{e^2}{r_0} = m\,c^2$$

$$r_0 = \frac{e^2}{m\,c^2} \sim 2.8\times10^{-13} \text{ cm}$$

Conventional unit for cross section

$$1 \text{ barn} = 10^{-24} \text{ cm}^2$$

$$\sigma_{\rm HI,HI} =\sim 10^8 \text{ barns } (\sim 10^{-16} \text{ cm}^2)$$

121

Collision

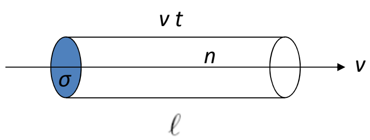

\# of collisions = # of particles in the (moving) volume

$$N = n\sigma\,v\,t$$

\# of collisions per unit time = $N/t = n\,\sigma\,v$

Time (mean-free time) between 2 consecutive collisions (N=1) = $t_{\rm collision} = \frac{1}{n\,\sigma\,v}$

Mean-free path $\ell = v\,t_{\rm col}$, i.e., $\ell = \frac{1}{N\,\sigma}$

122

Ex 1 between hydrogen atoms in an H I region

$$n_{\rm HI} \sim 10\ {\rm cm}^{-3};\ v_{\rm HI} \sim 1\ {\rm km\ s}^{-1};\ \sigma_{\rm HI,HI} \sim 10^{-16}\ {\rm cm}^2$$

$$t_{\rm HI,HI} \sim 10^{10}\ {\rm s} \sim 300\ {\rm years}$$

$$\ell \sim 10^{15}\ {\rm cm} \sim 100\ {\rm AU}$$

∴ Collisions are indeed very rare.

Ex 2 between a hydrogen atom and an electron

$$\sigma_{\rm e^-,HI} \sim 10^{-15}\ {\rm cm}^2\ {\rm (polarization)}$$

$$t_{\rm e^-,HI} \sim \frac{1}{10\times10^{-15}\times10^5} \sim 30\ {\rm years}$$

Ex 3 between electrons

$$\sigma_{\rm e^-,e^-} \sim 10^{-12}\ {\rm cm}^2;\ n_e \sim 0.2\ {\rm cm}^{-3}$$

$$t_{\rm e^-,e^-} \sim \frac{1}{0.2\times10^{-12}\times50\times10^5} \sim 10\ {\rm days}$$

123

Stellar Structure

Structure Equations

What does each of these equations means?

$$\frac{dP}{dr} = -\frac{Gm(r)\rho}{r^2}$$ Hydrostatic equilibrium

$$\frac{dm}{dr} = 4\pi r^2 \rho$$ Mass continuity (distribution)

$$\frac{dL}{dr} = 4\pi r^2 \rho q$$ Energy generation

$$\frac{dT}{dr} = \frac{-3\kappa\rho L}{4ac4\pi r^2 T^3}$$ by radiation

Energy transport

$$\frac{dT}{dr} = (\frac{\gamma - 1}{\gamma})\frac{T}{P}\frac{dP}{dr}$$ by convection

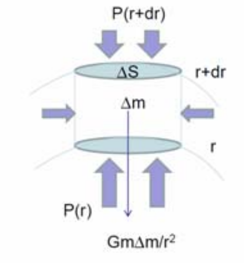

$$P = P(\rho, T, \mu)$$ Equation of state

$$\kappa = \kappa(\rho, T, \mu)$$ Opacity

$$q = q(\rho, T, \mu)$$ Nuclear reaction rate

Variables (7): *m, ρ, T, P, κ, L*, and *q*

Vogt-Russell theorem

the structure of a star is uniquely determined by its mass and the chemical abundance.

In fact, … by any two variables above, cf. the HRD. It is not really a "theorem" in the mathematical sense, i.e., not strictly valid. It is a "rule of thumb".

In general, the equation of motion is

$$\ddot{r} = -\frac{Gm}{r^2} - \frac{1}{\rho}\frac{\partial P}{\partial r} = -\frac{Gm}{r^2} - 4\pi r^2 \frac{\partial P}{\partial m}$$

Mean molecular weight

In a fully ionized gas (in stellar interior),

$\mu = 1/2$ (H) … 2 particles per m_H

$= 4/3$ (He) … 3 particles per 4 m_H

$\cong 2$ (metals) … 2 particles per m_H

$\mu = 4/(6X + Y + 2)$ for a fully ionized gas

Adopting the solar composition,

$X_\odot = 0.747, Y_\odot = 0.236, Z_\odot = 0.017$

→ $\mu \simeq 0.6$

Note recent revision $Z_\odot = 0.0152$ (Caffau+11)

At the center of a star in hydrostatic equilibrium

$$\frac{dP}{dm} = -\frac{Gm}{4\pi r^4}$$

Integrating from the center to the surface

$$P(M) - P(0) = -\int_0^M \frac{Gm\,dm}{4\pi r^4}$$

With the boundary conditions,

$$P(M) \approx 0 \quad P(0) = P_c$$

Thus,

$$P_c = \int_0^M \frac{Gm\,dm}{4\pi r^4} > \int_0^M \frac{Gm\,dm}{4\pi R^4} = \frac{GM^2}{8\pi R^4} = 4.4\times 10^{13} (\frac{M}{M_\odot})^2 (\frac{R_\odot}{R})^4 \text{ N m}^{-2}$$

Hydrostatic equilibrium

$$\frac{dP}{dr} = -\frac{Gm(r)}{r^2}\rho, \text{so } \frac{P}{R} = \frac{GM}{R^2}\frac{M}{R^3} \rightarrow P = \frac{GM^2}{R^4}$$

Ideal gas law $P = \frac{\rho}{\mu m_H} kT;\ \rho = \frac{M}{R^3}$

So $P = \frac{M}{R^3}\frac{T}{\mu}$, and $T \sim \frac{\mu GM}{R}$

This should be valid at the star's center, thus

$$T_* \sim \frac{\mu\, GM_*}{R_*}$$

Luminosity

Ohm's law *in circuit I = V / R, hydraulic analogy*

[flow] ∝ [pressure gradient] / [resistance]

(unit) Pressure = [energy] / [volume]

$$L \sim 4\pi R^2 \frac{d\left(\frac{1}{3}aT^4\right)/dr}{\kappa\rho}$$
$$\sim 4\pi R^2 \frac{4}{3}\frac{aT^3}{\kappa\rho}\frac{dT}{dr}$$
$$\sim \frac{R^2T^3}{\kappa\rho}\frac{dT}{dr}$$

Blackbody radiation
Energy density $u = aT^4$
Radiation pressure $P = (1/3)\, u$

Exercise: Derive Ohm's law.

For a given structure,

$$T \sim T_c, \frac{dT}{dr} \sim \frac{T_c}{R}, T_c \sim \frac{\mu GM}{R}.$$

$$L \sim \frac{R^2T^4/R}{\kappa(M/R^3)} \sim \frac{R^4T^4}{\kappa M} \sim \frac{R^4}{\kappa M}\left(\frac{\mu GM}{R}\right)^4$$

$$L \sim \frac{\mu^4 G^4 M^3}{\kappa}$$

The opacity $\kappa = \kappa(\rho, T, \mu)$

$$L \sim \frac{\mu^4 G^4 M^3}{\kappa}$$

- For solar composision, Kramers opacity

$$\kappa \sim \rho T^{-3.5} \quad \text{valid for } 10^4\text{–}10^6 \text{ K.}$$

$$T \sim \frac{\mu\, GM}{R}$$

So $\kappa \sim \mu^{-3.5} G^{-3.5} M^{-2.5} R^{0.5}$

and $L \sim \mu^{7.5} G^{7.5} M^{5.5} R^{-0.5}$

- For high-mass stars, i.e., high temperature and low density, opacity by electron scattering

$$\kappa = 0.2\,(1+X)\ \text{cm}^2\text{g}^{-1} = \text{const.}$$

and $L \sim \mu^4 G^4 M^3$

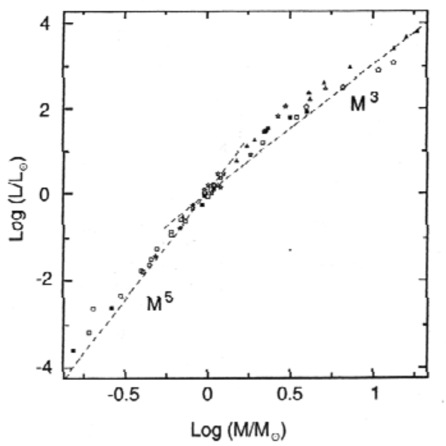

Figure 1.6 The mass–luminosity relation for main-sequence stars. Symbols denote ordinary binary stars (squares); eclipsing variables (triangles); Cepheids (pentagons); double-star statistics (stars).

Opacity

- Bound-bound absorption Excitation of an electron of an atom to a higher energy state by the absorption of a photon. The excited atom then will be de-excited spontaneously, emitting a photon, or by collision with another particle.
- Bound-free absorption Photoionization of an electron from an atom (ion) by the absorption of a photon. The inverse process is radiative recombination.
- Free-free absorption Transition of a free electron to a higher energy state, via interaction of a nucleus or ion, by the absorption of a photon. The inverse process is bremsstrahlung.
- Electron scattering Scattering of a photon by a free electron, also known as Thomson (common in stellar interior) or Compton (if relativistic) scattering.
- H^- absorption Important when $< 10^4$ K, i.e., dominant in the outer layer of low-mass stars (such as the Sun)

- Bound-bound, bound-free, and free-free opacities are collectively called Kramers opacity, named after the Dutch physicist H. A. Kramers (1894-1952).
- All have similar dependence $\kappa \propto \rho\, T^{-3.5}$.
- Kramers opacity is the main source of opacity in gases of temperature $10^4 \sim 10^6$ K, i.e., in the interior of stars up to $\sim 1\ M_{\odot}$.
- In a star much more massive, the electron scattering process dominates the opacity, and the Kramers opacity is important only in the surface layer.

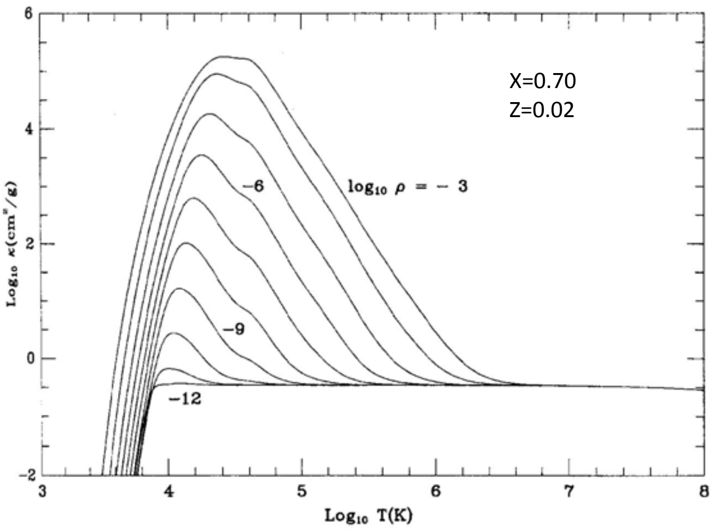

Data from Iglesias & Rogers (1996)

Opacity

κ in cm^2 g^{-2}

$$\kappa\rho = \Sigma_i n_i \sigma_i$$

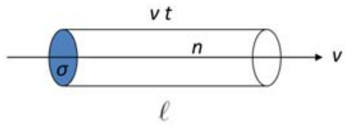

$\int \kappa\rho ds$ gives the optical depth

The Rossland mean opacity

$$\frac{1}{<\kappa>} = \frac{1}{B}\int_0^\infty \frac{B_\nu}{\kappa_\nu}\, d\nu$$

For Kramers opacity

$$\kappa_{Kr} \approx 4 \times 10^{25}\,(1+X)(Z+0.001)\,\rho\, T^{-3.5}\ \ [\mathrm{cm^2 g^{-1}}]$$

For Thomson scattering,

$$\kappa_\nu = \frac{8\pi}{3}\frac{r_e^2}{\mu_e m} = 0.20\,(1+X)\ \ [\mathrm{cm^2 g^{-1}}]$$

is frequency independent, so is the Rossland mean.

$$\kappa_{es} = 0.20\,(1+X)\ \ [\mathrm{cm^2 g^{-1}}]$$

Here r_e is the electron classical radius, X is the H mass fraction, and $\mu_e = 2/(1+X)$

the electron cross section $\sigma = 0.665 \times 10^{-24}$ [cm^2]

- For H^- opacity, $E_{\mathrm{ion}} = 0.754$ eV
  important for $4 \times 10^3 < T < 8 \times 10^3$ K

$$\kappa_{H^-} \approx 2.5 \times 10^{-31} \left(\frac{Z}{0.02}\right) \rho^{0.5} T^9\ [\mathrm{cm^2\ g^{-1}}]$$

is temperature and metallicity (providing electrons) dependent.

- For $T > 10^4$ K, H^- is ionized.

- At $T < 3500$ K, molecular opacity dominates.

Main sequence = a mass sequence defined by hydrogen fusion at the center of a star

Radius does not vary much; but the luminosity does.

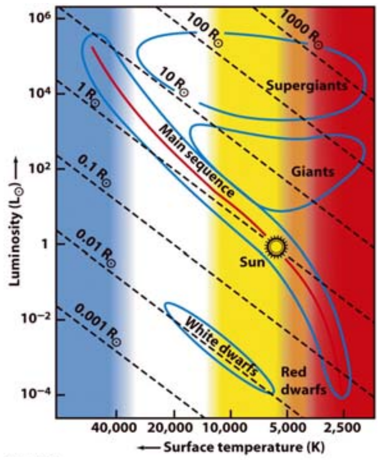

$\log L \propto \log T$

$$T_c \approx \frac{\mu\, GM}{R}$$

So for a given $T_c, M \rightarrow R$, $\rightarrow L$ } $L\,(\propto R^2\, T^4)$ and T

Main sequence is a run of L and T_c as a function of stellar mass, with T_c nearly constant.

Why $T_c \approx$ constant?
Because H burning at $\sim 10^7$ K regardless of the stellar mass

Gas Thermodynamics

Heat capacity: heat supplied to increase one degree in temperature; C_P and C_V

Specific heat capacity (=per unit mass), c_P and c_V

$c_P - c_V = k_B$

$c_P \,/\, c_V = \gamma$

γ: the adiabatic index or heat capacity ratio

e.g., dry air, =1.403 (0°C), =1.400 (20°C)

O_2, =1.400 (20°C), =1.397 (200°C)

H_2O, = 1.330 (20°C), =1.310 (200°C)

To Determine γ of a Star

For an ideal gas, $u_i = \frac{1}{2}kT$ per degree of freedom
Equipartition of energy $\to u = \Sigma u_i = \frac{n}{2}kT$ for n dof

Since $c_V = \left(\frac{\partial u}{\partial T}\right)_V = \frac{n}{2}k$, and $\frac{c_P}{c_V} \equiv \gamma = \frac{nk/2+k}{nk/2} = 1 + \frac{2}{n}$

For an ideal gas, $n = 3, \gamma = 5/3$
For a photon gas, $n = 6, \gamma = 4/3$
(3 propagation directions, each with 2 polarizations)

For a monatomic gas, dof=3 $\to \gamma = 5/3 = 1.67$
For a diatomic gas, dof =5 $\to \gamma = 7/5 = 1.4$

Equation of State

Stability of a star: $2E_K + E_P = 0$

$$\begin{aligned} E_{\text{thermal}} &= \frac{3}{2}kT = \frac{3}{2}(c_P - c_V)T \\ &= \frac{3}{2}(\gamma - 1)\, c_V T \\ &= \frac{3}{2}(\gamma - 1)\, U \end{aligned}$$

$$E_P = \Omega$$

So, $3(\gamma - 1)U + \Omega = 0$

$$E_{\text{total}} = U + \Omega = \left[\frac{-1}{3(\gamma - 1)} + 1\right] \Omega = \frac{3\gamma - 4}{3(\gamma - 1)}\Omega$$

Because $\Omega < 0$, in order to be stable, $E_{\text{total}} < 0 \rightarrow \gamma > 4/3$

In general, for a stable star with a mixture of gas and radiation,

$$\frac{4}{3} \leq \gamma \leq \frac{5}{3}$$

$\gamma \rightarrow 4/3$, radiation pressure dominates.

$\gamma \rightarrow 5/3$, gas pressure dominates.

For an ideal gas, $P = \frac{N}{V}kT = \frac{\rho}{\mu m_H}kT$

$$\frac{dP}{P} = \frac{d\rho}{\rho} + \frac{dT}{T} \quad \text{and} \quad PdV + VdP = NkdT$$

First law of thermodynamics (conservation of energy)

$$dQ = dU + PdV$$

For constant V, $c_V = \left(\frac{dQ}{dT}\right)_V = \frac{dU}{dT}$

$$dQ = dU + NkdT - VdP = \left(\frac{dU}{dT} + Nk\right)dT - VdP$$

So for constant P, $c_P = \left(\frac{dQ}{dT}\right)_P = \frac{dU}{dT} + Nk = c_V + Nk$

Hence $c_P = c_V + Nk$,

and $\gamma = c_P/c_V = (Nk + c_V)/c_V$

An isothermal (= constant in temperature) process:
internal energy does not change

An adiabatic process: $dQ = 0$

$$dQ = c_V dT + PdV = c_V dT + (NkT/V)dV$$
$$= dT/T + (c_P - c_V)/c_V(dV/V) = 0$$

$$\log T + (\gamma - 1)\log V = \text{constant}$$

$TV^{\gamma-1} = \text{constant}$

$PV^{\gamma} = \text{constant}$

$P^{1-\gamma}T^{\gamma} = \text{constant}$

Convective equilibrium (stability vs instability)

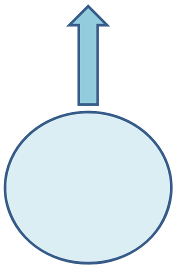

A fluid convective "cell" is buoyed upwards.

If temperature inside is higher than surroundings, the cell keeps rising. E_{kin} of particles higher → dissipates

Otherwise it sinks back (convectively stable).

The rising height is typified by the mixing length ℓ, or parameterized as the scale height H, defined as the pressure (or density) varies by a factor of e. Usually

$$0.5 \lesssim \ell/H \lesssim 2.0$$

Convective stability/instability

How good is energy transportation by radiation?

cf. Schwarzschild

Convective stability: a fluid resisting vertical motion

atmosphere in radiative equilibrium $T\downarrow$ as $r\uparrow$

Consider a mass of gas

Rises → expands adiabatically

∴ $T\downarrow$

⇒ denser than the surroundings

→ sinks back

∴ Stable in rad. equil.

So, vertical perturbation dampens out

But if rises, adiabatically cooling, but still warmer than the surroundings

⇒ less denser than surr.

→ keeps rising

⇒ Convection sets in when the adiabatic temp. gradient is smaller than temp. gradient by radiative equil.

i.e., $$\left(\frac{dT}{dr}\right)_{ad} < \left(\frac{dT}{dr}\right)_{rad}$$

Compared with surrounding temperature gradient

Radiation can no longer transport the energy efficiently enough
→ Convective instability

For an adiabatic process, $PV^{\gamma} = constant$

Since $\frac{dP}{dr} = -\rho g$ and $P = \rho k T$

$dT \cdot \frac{dP}{dr}\frac{1}{P} \propto \frac{1}{T} \cdot dT$

$$\therefore \frac{dT}{dr} \propto \frac{dT/T}{dP/P} = \frac{d\ln T}{d\ln P}$$

⇒ Criterion for convection equilibrium becomes

$$\left(\frac{d\ln T}{d\ln P}\right)_{ad} < \left(\frac{d\ln T}{d\ln P}\right)_{rad}$$

With the notation ∇ (nabla)

$$\nabla_{ad} < \nabla_{rad}$$

Convection takes place when the temperature gradient is "sufficiently" high (compared with the adiabatic condition) or the pressure gradient is low enough.

Such condition also exists when the gas absorbs a great deal of energy without temperature increase, e.g., with phase change or ionization
➔ when c_V is large or γ is small

In meteorology, dry and cool air tends to be stable, whereas wet and warm air (smaller gamma values) is vulnerable to convection → thunderstorm

How to calculate ∇_{rad} ?

$$\frac{dT}{dr} = -\frac{3}{4ac} \cdot \frac{\kappa\rho}{T^3} \frac{L_r}{4\pi r^2} \qquad \text{but} \quad \frac{dP}{dr} = -g\rho$$

$$\therefore \frac{dT}{dP} \propto \frac{\kappa}{T^3} \frac{L_r}{r^2}$$

$$\nabla_{rad} \equiv \left(\frac{d\ln T}{d\ln P}\right)_{rad} = \frac{dT/T}{dP/P} = \cdots = \frac{3\kappa}{16\pi ac} \frac{P}{T^4} \frac{L_r}{GM_r}$$

For an adiabatic process for an ideal gas

① $P = nkT \propto \rho T$

$$\frac{dP}{P} = \frac{d\rho}{\rho} + \frac{dT}{T}$$

② $nR = c_p - c_v$

③ $\gamma = \frac{c_p}{c_v} = \frac{1+c_v}{c_v} = \frac{1+n/2}{n/2} = 1 + \frac{2}{n}$

n: d.o.f.

$$dQ = c_v\,dT + P\,d\left(\frac{1}{\rho}\right) = c_v\,dT - \frac{P}{\rho^2}\,d\rho = 0$$

$$\therefore\ c_v\,dT = \frac{P}{\rho^2}\,d\rho$$

$$c_v\frac{dT}{T} = \frac{P}{\rho T}\cdot\frac{d\rho}{\rho}$$

$$c_v\frac{dT}{T} = (c_p - c_v)\left(\frac{dP}{P} - \frac{dT}{T}\right)$$

$$\Rightarrow\ c_p\frac{dT}{T} = (c_p - c_v)\frac{dP}{P}$$

n: d.o.f

$$\nabla_{ad} \equiv \left(\frac{d\ln T}{d\ln P}\right)_{ad} = \left(\frac{dT/T}{dP/P}\right)_{ad} = 1 - \frac{c_v}{c_p} = 1 - \frac{1}{\gamma}$$

e.g., for monatomic gases, $\gamma = 5/3$ $\nabla_{ad} = 0.4$

In practice, if $\gamma = {}^5/_3$, the condition for convective stability (no convective) is $\left(\frac{d\log T}{d\log P}\right) < 0.4$

Note. $\nabla_{rad} \propto P$

At surface $\nabla_{rad} \to 0$

$\therefore\ \nabla_{ad} \overset{\text{always}}{>} \nabla_{rad} \Rightarrow$ no convection!

The outermost layers of a star are always in radiative equilibrium.

$\therefore$ Convection occurs either

① large temperature gradient for radiative equilibrium

② small adiabatic temperature gradient

Ionization satisfies both conditions because

① Opacity ↑

② e^- receive energy → d.o.f. ↑, so γ ↓ → ∇_{ad} ↓

→ Development of hydrogen convective zones

Similarly, there are 1st and 2nd helium convective zones.

For a **very low-mass star**, ionization of H and He leads to a fully convective star → H completely burns off.

For a **sun-like star**, ionization of H and He, and also the large opacity of H^- ions → a convective envelope (outer 30% radius).

For a **massive star**, the core produces fierce amount of energy → convective core
→ a large fraction of material to take part in the thermonuclear reactions

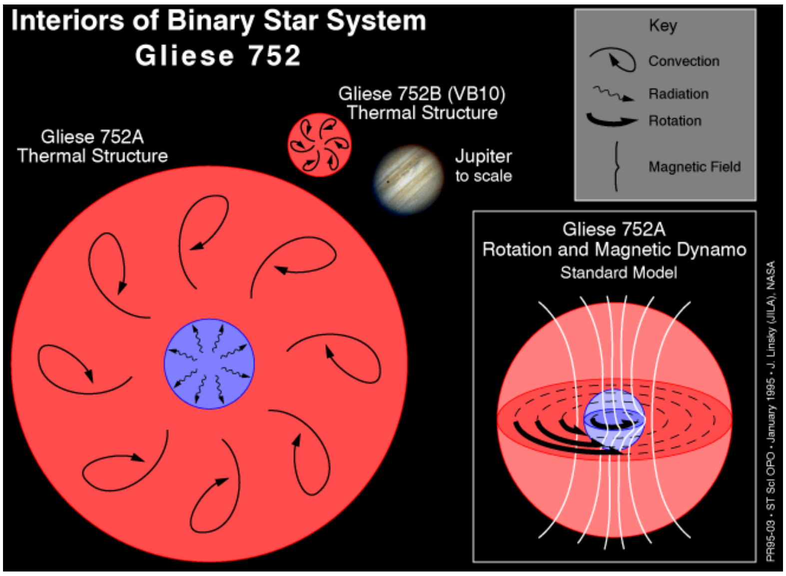

A binary system at 5.74 pc. Gliese 752A (=Wolf 1055) is an M2.5 red dwarf (mass ~0.46 solar, m_V~9.13), whereas Gliese 752B (VB 10) is an M8V (mass ~0.075 solar, m_V~17.30).

Energy Transport

By radiation

$$\frac{dT}{dr} = \frac{-3}{4ac}\frac{\kappa\rho}{T^3}\frac{L_r}{4\pi r^2}$$

L_r: luminosity

κ: opacity

(electron scattering, b-f, f-f, H^-)

Note: For radiative transport

$$\nabla_{rad} \equiv \left(\frac{d\ln T}{d\ln P}\right)_{rad} = \frac{3\kappa}{16\pi a c}\frac{P}{T^4}\left(\frac{L_r}{G M_r}\right)$$

If temperature gradient is too large, then

By convection (unstable to convection; convective instability)

criterion $\nabla > \nabla_{ad}$

$$\nabla \equiv \frac{d\ln T}{d\ln P} \qquad \nabla_{ad} \equiv \left(\frac{d\ln T}{d\ln P}\right)_{ad} = \frac{\gamma - 1}{\gamma}$$

γ: adiabatic index

In case of convection

$$\nabla \equiv \frac{d\ln T}{d\ln P} = \frac{P}{T}\frac{dT/dr}{dP/dr} \overset{\text{hydrostatic equil}}{=} -\frac{r^2}{GM_r}\left(\frac{P}{\rho T}\right)\frac{dT}{dr} \simeq \nabla_{ad}$$

$$\therefore \frac{dT}{dr} = -\nabla_{ad}\frac{GM_r}{r^2}\frac{\rho T}{P} = -\frac{\gamma-1}{\gamma}\frac{GM_r}{r^2}\frac{\rho T}{P}$$

Hayashi Track

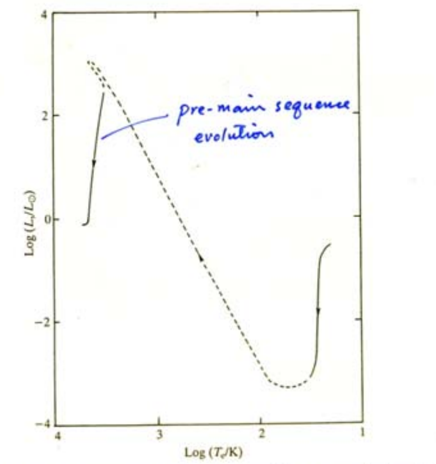

Fig. 53. The complete pre-main-sequence evolution of a star of solar mass.

Chushiro HAYASHI 1920-2010

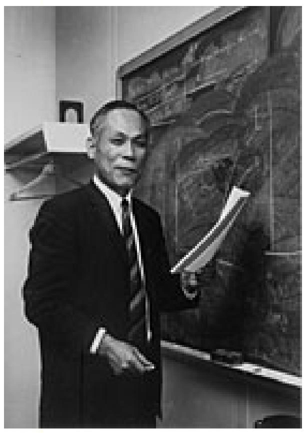

A convection evolutionary track for low-mass pre-main sequence stars

When a protostar reaches hydrostatic equilibrium, there is a minimum effective temperature (~4000 K) cooler than which (the **Hayashi boundary**) a stable configuration is not possible (Chushiro Hayashi 1961).

A protostar

- contracts on the Kevin-Helmholtz timescale
- is cool and highly opaque → fully convective → homogenizes the composition

A star < 0.5 $M_\odot$ remains on the Hayashi track throughout the entire PMS phase.

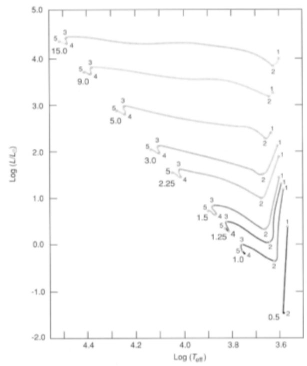

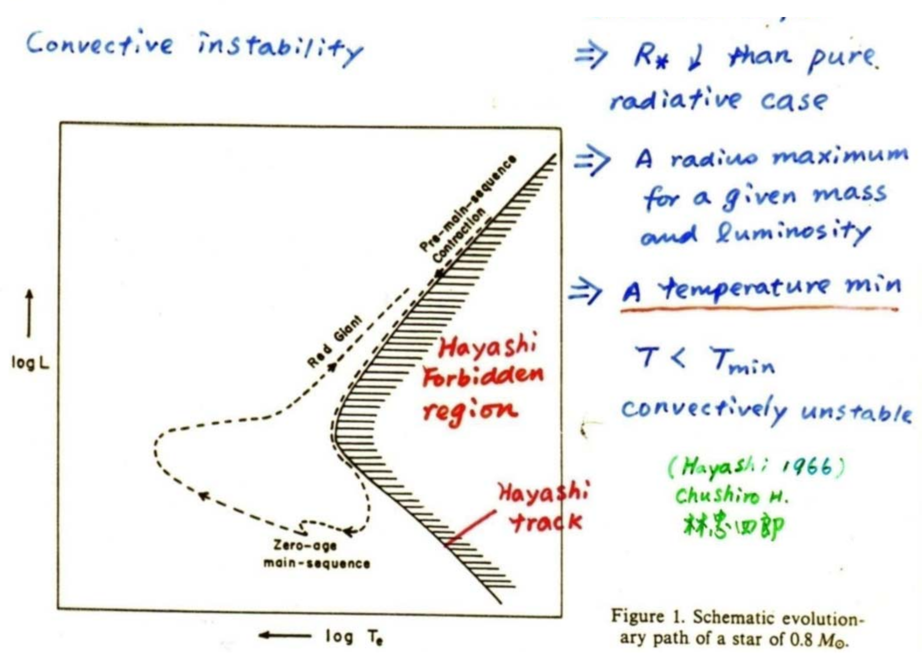

Figure 1. Schematic evolutionary path of a star of 0.8 $M_\odot$.

Convection occurs when $\nabla_{\mathrm{rad}} > \nabla_{\mathrm{ad}}$

That is, when ∇_{rad} is large, or when ∇_{ad} is small.

Recall $\nabla_{\mathrm{rad}} = \frac{dT}{dr} = \frac{L_r}{r^2}\frac{\kappa\rho}{\sigma T^3}$

$\nabla_{\mathrm{ad}} = 1 - \frac{1}{\gamma}$ where $\gamma = {}^{c_p}/_{c_v}$

→ ∇_{ad} small = c_v large → H_2 dissociation
H ionization, T~6,000 K
He ionization, T~20,000 K
He II ionization, T~50,000 K

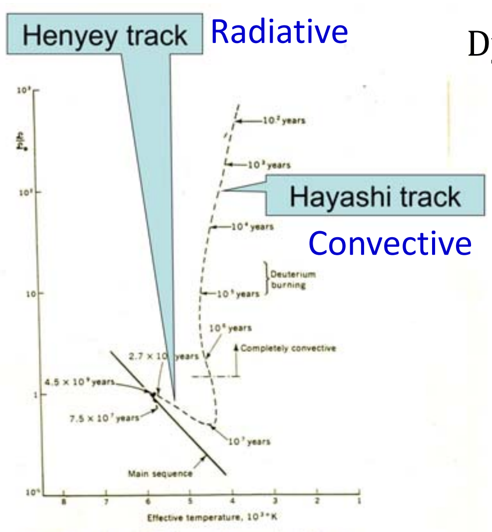

Fig. 5-1 The path on the H-R diagram of the contraction of the sun to the main sequence. The interior has become sufficiently hot to burn deuterium after about 10^6 years. The contraction ceases near the main sequence when the core has become hot enough to replenish the solar luminosity with the thermonuclear power generated by the fusion of hydrogen into helium. [*After D. Ezer and A. G. W. Cameron, The Contraction Phase of Stellar Evolution, in R. F. Stein and A. G. W. Cameron (eds.), "Stellar Evolution," Plenum Press, New York,* 1966.]

Dynamical collapse → quasi-static contraction

- half of E_{grav} becomes particle E_{kin} (internal energy); half radiated away
- Matter optically thin to thick → thermodynamical equilibrium, $T_{\mathrm{rad}} = T_{\mathrm{kin}}$
- Energy used for ionization (for H, $T < 10^4$ K), so surface temperature remains almost constant. Protosun now size was 60 $R_\odot$
- Star fully convective

→ Hayashi track

Check out http://www.peripatus.gen.nz/Astronomy/HerRusDia.html for a good summary

Astron. & Astrophys. 40, 397—399 (1975)

On the Luminosity of Spherical Protostars

I. Appenzeller*
Universitäts-Sternwarte Göttingen

W. Tscharnuter
Universitäts-Sternwarte Göttingen and Max-Planck-Institut für Physik und Astrophysik München

Summary. Hydrodynamic model computations have been carried out for a spherically symmetric $1\,M_\odot$ protostar. Compared to similar computations by Larson (1969) we used a different treatment of the accretion shock front. Our computations basically confirm Larsons results and show that Larson's disputed shock jump conditions have little influence on the protostellar models.

Key words: star formation — protostars — YY Orionis stars

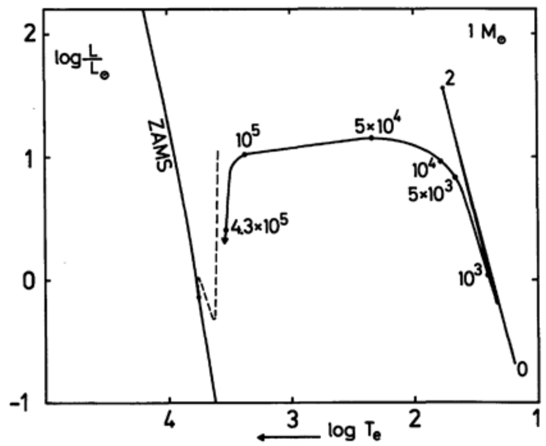

Fig. 1. Evolutionary path of a $1\,M_\odot$ protostar in an infrared HR diagram (solid line). The numbers indicate the time (in years) since the formation of the (final) hydrostatic core. For comparison, the evolutionary path of a conventional fully hydrostatic $1\,M_\odot$ pre-main sequence star is also included (broken line)

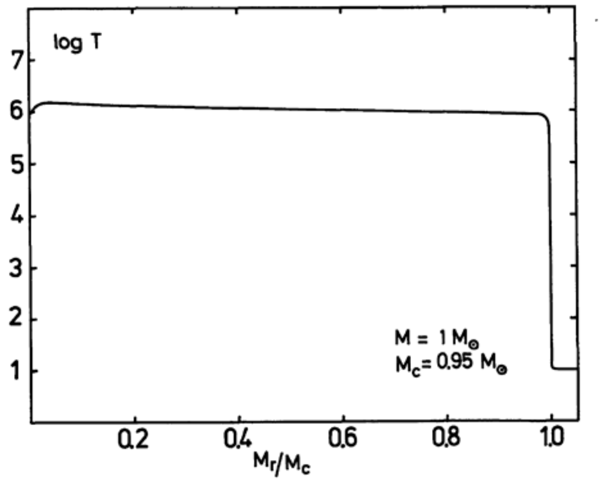

Fig. 2. Temperature distribution in the hydrostatic core of a $1\,M_\odot$ protostellar model after 95% of the total mass has accumulated in the core

The Evolution of a Massive Protostar

I. Appenzeller and W. Tscharnuter
Universitäts-Sternwarte Göttingen

Astron. & Astrophys. 30, 423 – 430 (1974)

Summary. The hydrodynamic evolution of a massive protostar has been calculated starting from a homogeneous gas and dust cloud of $60\,M_\odot$ and an initial density of $10^{-19}\,\mathrm{g\,cm^{-3}}$. Initially the collapsing gas cloud evolved similar to protostar models of lower mass. About 3.6×10^5 years after the beginning of the collapse a small hydrostatic core was formed. About 2×10^4 years later hydrogen burning started in the center of the hydrostatic core. After another 2.5×10^4 years the collapse of the envelope was stopped and reversed by the heat flow from the interior and the entire envelope was blown off, leaving behind an almost normal main-sequence star of about $17\,M_\odot$. During most of the core's evolution the central region of the protostar would have looked like a cool but luminous infrared point source to an outside observer.

Read this paper!

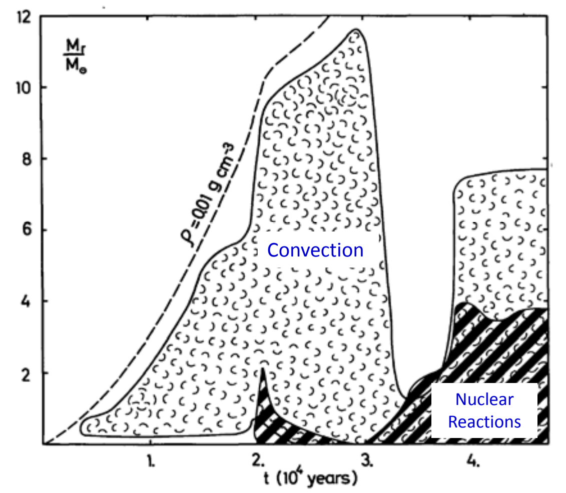

Fig. 5. The variation of the internal structure of the evolving hydrostatic core. The abscissa gives the time since the formation of the (final) hydrostatic core. ($t=0$ corresponds to an age of the protostar of 361 473 years.) "Cloudy" regions represent convection. Cross-hatched regions represent nuclear energy generation at a rate exceeding 10^3 erg g^{-1} s^{-1}. The approximate extent of the hydrostatic core is indicated by the line $\varrho = 0.01$ g cm^{-1}

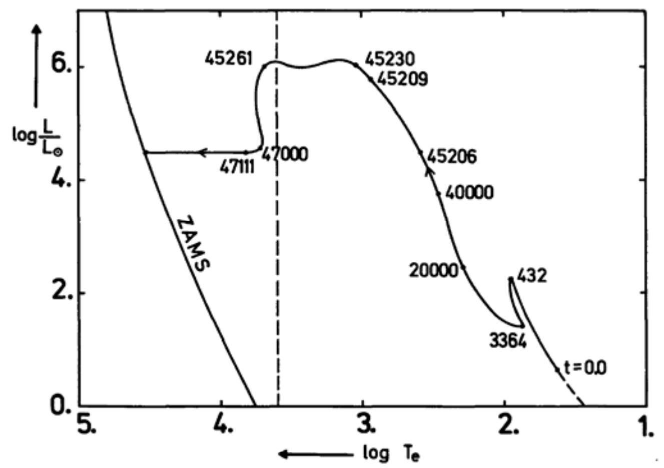

Fig. 6. Approximate evolutionary path of the optically thick central region of the 60 $M_\odot$ protostar in an infrared HR diagram. The numbers indicate the time t since the formation of the final hydrostatic core (c.f. Fig. 5). For comparison we also included the position of the zero-age main-sequence (ZAMS). The broken line gives the approximate lower limit of the effective temperature of hydrostatic configurations (Hayashi *et al.*, 1962)

Pre-Main Sequence Evolutionary Tracks

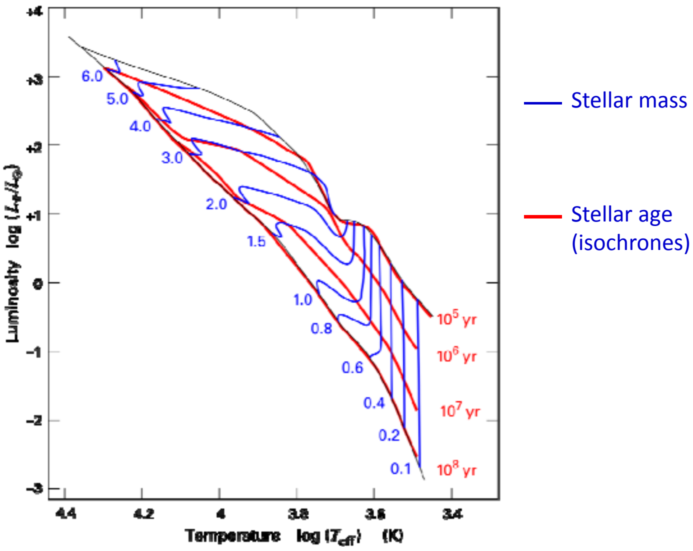

http://en.wikipedia.org/wiki/File:PMS_evolution_tracks.svg

Theoretical evolutionary tracks

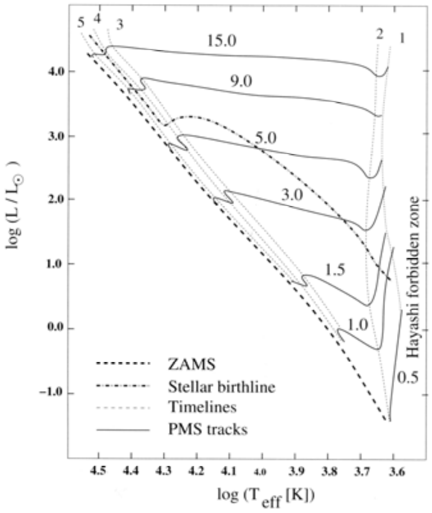

Fig. 6.6. Evolutionary paths in the HR-diagram for stellar masses ranging from 0.5 to 15 $M_\odot$ (solid tracks, adapted from Iben [420]). These paths are marked by thin hatched lines marking time periods labeled 1 to 5. The thick hatched line to the left approximately indicates the location of the ZAMS. The line across the tracks is the stellar birthline approximated from [76] for an accretion rate of $\dot{M}_{acc} = 10^{-5} M_\odot \ yr^{-1}$.

1965ApJ...141..993

STELLAR EVOLUTION. I. THE APPROACH TO THE MAIN SEQUENCE*

ICKO IBEN, JR.
California Institute of Technology, Pasadena, California
Received August 18, 1964; revised November 23, 1964

ABSTRACT

The manner in which nuclear reactions replace gravitational contraction as the major source of stellar luminosity is investigated for model stars of population I composition in the mass range $0.5 < M/M_\odot < 15.0$. By following in detail the depletion of C^{12} from high initial values down to values corresponding to equilibrium with N^{14} in the C-N cycle, the approach to the main sequence in the Hertzsprung-Russell diagram and the time to reach the main sequence, for stars with $M \geq 1.25\, M_\odot$, are found to differ significantly from data reported previously.

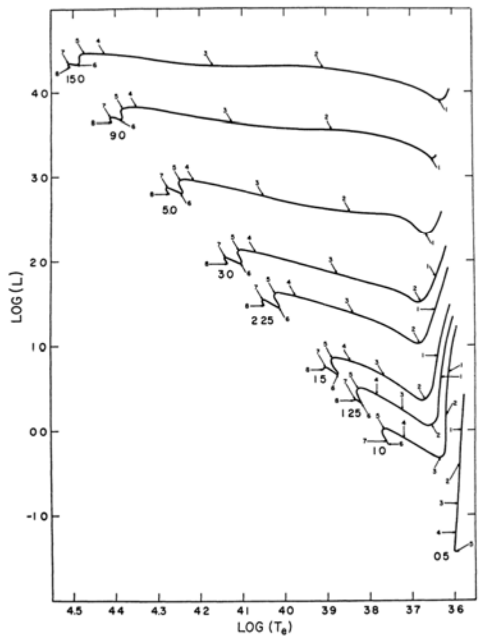

FIG. 17.—Paths in the Hertzsprung-Russell diagram for models of mass $(M/M_\odot)$ = 0.5, 1.0, 1.25, 1.5, 2.25, 3.0, 5.0, 9.0, and 15.0. Units of luminosity and surface temperature are the same as those in Fig. 1

Effects of chemical abundances and "metals" in determination of stellar structure

Metal poorer → hotter

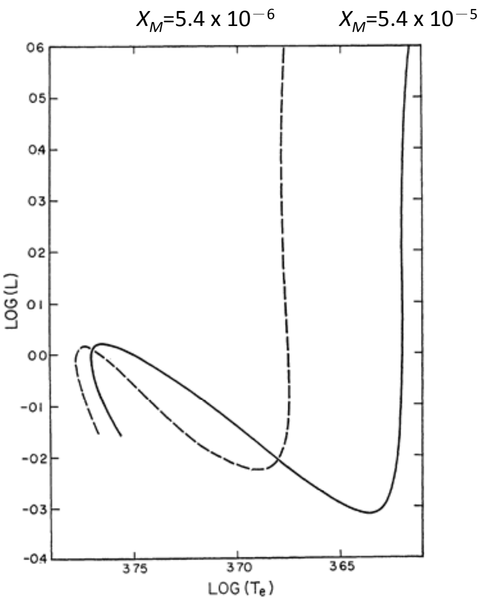

FIG. 1.—Paths in the theoretical Hertzsprung-Russell diagram for $M = M_\odot$. Luminosity in units of $L_\odot = 3.86 \times 10^{33}$ erg/sec and surface temperature T_e in units of °K. Solid curve constructed using a mass fraction of metals with 7.5-eV ionization potential, $X_M = 5.4 \times 10^{-5}$. Dashed curve constructed with $X_M = 5.4 \times 10^{-6}$.

Exercise

A useful site to download theoretical evolutionary tracks (the "Padova tracks") is the CMD/PARSEC isochrones
http://stev.oapd.inaf.it/cgi-bin/cmd

As homework

1. Plot V versus $(B-V)$ for an ensemble of stars (i.e., a star cluster) of ages 1 Myrs, 10 Myr, 100 Myr, and 1 Gyr.
2. Compare the V versus $(B-V)$ CMDs of two 100 Myr old star clusters, one with Z=0.01 and the other with Z=0.0001 (extremely metal poor).

Thermonuclear Reactions

- Eddington in 1920s hypothesized that fusion reactions between light elements were the energy source of the stars.
- Stellar evolution = (con) sequence of nuclear reactions
- $E_{\text{kinetic}} \approx kT_c \approx 8.62 \times 10^{-8}\, T \sim$ keV,

  but $E_{\text{Coulomb barrier}} = \frac{Z_1 Z_2 e^2}{r} = \frac{1.44\, Z_1 Z_2}{r[\text{fm}]} \sim$ MeV, 3 orders higher than the kinetic energy of the particles.

- Tunneling effect in QM proposed by Gamow (1928, Z. Physik, **52**, 510); applied to energy source in stars by Atkinson & Houtermans (1929, Z. Physik, **54**, 656)

2

George Gamow (1904-1968)

Russian-born physicist, stellar and big bang nucleosynthesis, CMB, DNA, Mr. Thompkins series

1929 U Copenhagen

1960s U Colorado

3

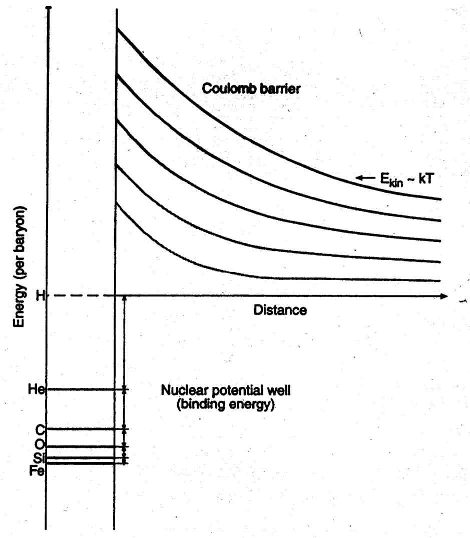

Figure 4.2 Schematic representation of the Coulomb barrier – the repulsive potential encountered by a nucleus in motion relative to another – and the short-range negative potential well that is due to the nuclear force. The height of the barrier and the depth of the well depend on the nuclear charge (atomic number).

4

Quantum mechanics
tunneling effect

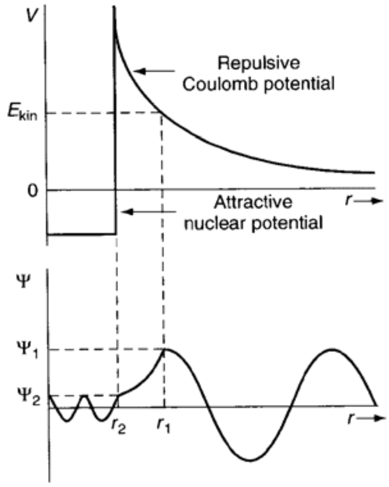

Figure 3.4 Illustration of the potential seen by particle b when approaching particle A with a kinetic energy E_{kin}, and the corresponding wavefunction Ψ; classically, particle b would reach only a distance r_1 from particle A before being repelled by the Coulomb force

5

Cross section for nuclear reactions (penetrating probability)

$$\propto\ e^{-\pi Z_1 Z_2 e^2/\varepsilon_0 h v}$$

This ↗ as v ↗

Velocity probability distribution (Maxwellian)

$$\propto\ e^{-mv^2/2kT}$$

This ↘ as v ↗

∴ **Product of these 2 factors ➔ <u>Gamow peak</u>**

6

D. Clayton "Principles of Stellar Evolution and Nucleosynthesis"

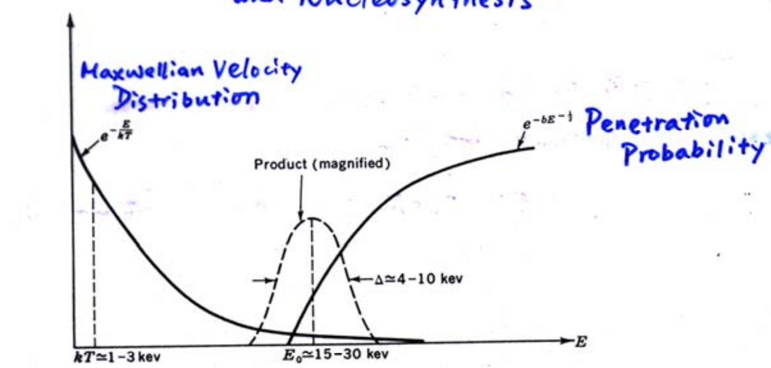

Fig. 4-6 The dominant energy-dependent factors in thermonuclear reactions. Most of the reactions occur in the high-energy tail of the maxwellian energy distribution, which introduces the rapidly falling factor $\exp(-E/kT)$. Penetration through the coulomb barrier introduces the factor $\exp(-bE^{-\frac{1}{2}})$, which vanishes strongly at low energy. Their product is a fairly sharp peak near an energy designated by E_0, which is generally much larger than kT. The peak is pushed out to this energy by the penetration factor, and it is therefore commonly called the *Gamow peak* in honor of the physicist who first studied the penetration through the coulomb barrier.

Clayton 7

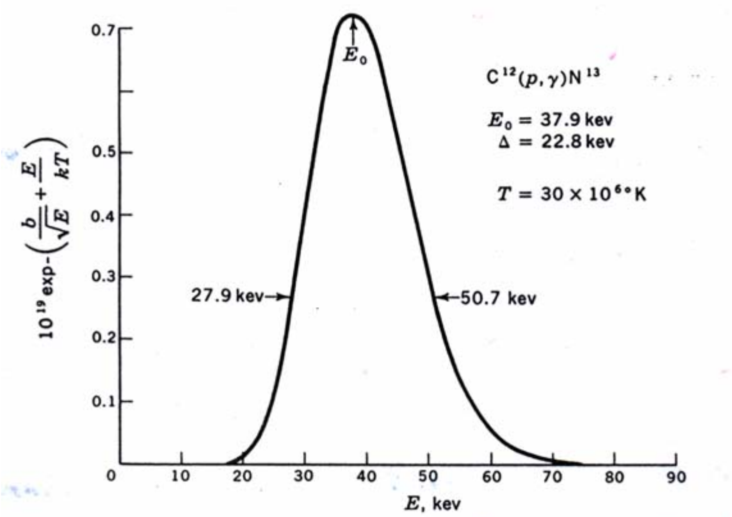

Fig. 4-7 The Gamow peak for the reaction $C^{12}(p,\gamma)N^{13}$ at $T = 30 \times 10^6$ °K. The curve is actually somewhat asymmetric about E_0, but it is nonetheless adequately approximated by a gaussian.

Clayton 8

Resonance → very sharp peak in the reaction rate
➔ 'ignition' of a nuclear reaction

Resonance reactions
Energy of interacting particles ≈ Energy level of compound nucleus

So there exists a narrow range of temperature in which the reaction rate ↑↑
→ a power law
→ an ignition (threshold) temperature

For a thermonuclear reaction or a nucleosynthesis (fusion) process, the reaction rate is expressed as

$$q \text{ [energy released per mass]} \propto \rho^m T^n$$

9

Collision

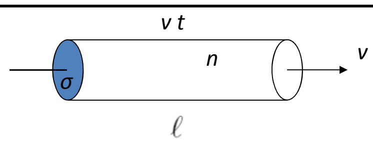

A two-body encounter,
[# of collisions] = [total # of particles in the (moving) volume], so $N = n\,(\sigma v t)$

- ✓ **# of collisions per unit time** $= {}^{N}/_{t} = n\,\sigma v$
- ✓ **Time between 2 consecutive collisions, mean free time (*N*=1),** $t_{\text{col}} = 1/\,n\,\sigma v$
- ✓ **Mean free path** $\ell = v t_{\text{col}} = 1/n\,\sigma$

10

Nuclear reaction rate

- ✓ $r_{12} \propto n_1 n_2 \langle \sigma v \rangle \propto n_1 n_2 \exp\left[-C\left(\frac{z_1^2 z_2^2}{T_6}\right)^{1/3}\right]$ [cm^{-3}s^{-1}]
- ✓ **As $T \nearrow$, $r_{12} \nearrow \nearrow$**
- ✓ **Major reactions are those with smallest $Z_1 Z_2$**
- ✓ n_i **is the particle volume number density,** $n_i m_i = \rho X_i$, **where** X_i **is the mass fraction**
- ✓ $q_{12} \propto Q\, \rho\, X_1\, X_2 / m_1 m_2$ [erg g^{-1}s^{-1}]

11

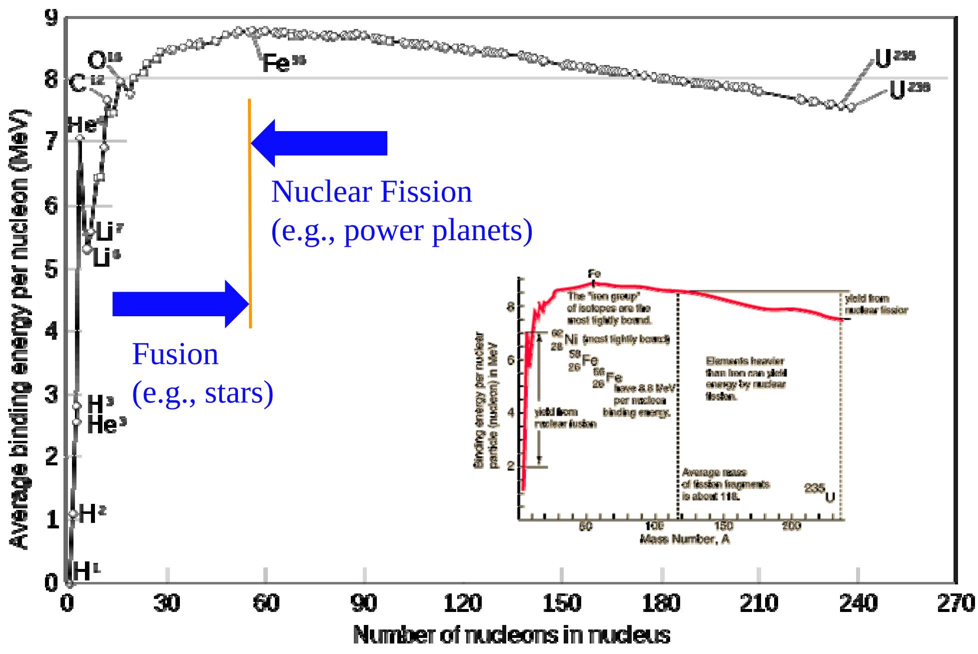

12

Planets — form in circumstellar disks by aggregation of ever larger dust grains (and gas)

Brown dwarfs — form like stars but evolve like planets

In terms of nuclear reactions

- Stars, $M > 0.08\ M_\odot$, core H burning
- BDs, $M > 0.01\ M_\odot$, short D burning — flat $L(t)$ for $t = 10^6 - 10^8$ yr
  - ↳ also for low-mass PMS stars
- Planets, no nuclear burning ever — $L(t) \downarrow$ continuously

13

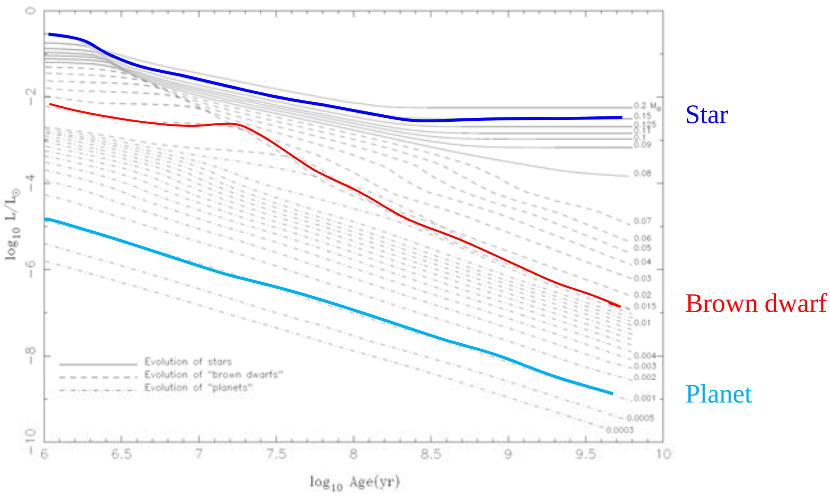

FIG. 7.—Evolution of the luminosity (in $L_\odot$) of solar-metallicity M dwarfs and substellar objects vs. time (in yr) after formation. The stars, "brown dwarfs" and "planets" are shown as solid, dashed, and dot-dashed curves, respectively. In this figure, we arbitrarily designate as "brown dwarfs" those objects that burn deuterium, while we designate those that do not as "planets." The masses (in $M_\odot$) label most of the curves, with the lowest three corresponding to the mass of Saturn, half the mass of Jupiter, and the mass of Jupiter.

Burrows 14

Stars	$\mathcal{M}/M_\odot > 0.08$, core H fusion Spectral types O, B, A, F, G, K, M
Brown Dwarfs	$0.065 > \mathcal{M}/M_\odot > 0.013$, core D fusion $0.080 > \mathcal{M}/M_\odot > 0.065$, core Li fusion Spectral types M6.5–9, L, T, Y Electron degenerate core ✓$10\ \mathrm{g\ cm^{-3}} < \rho_c < 10^3\ \mathrm{g\ cm^{-3}}$ ✓$T_c < 3 \times 10^6$ K
Planets	$\mathcal{M}/M_\odot < 0.013$, no fusion ever

15

THE ASTROPHYSICAL JOURNAL, Vol. 158, November 1969

THE MASS-RADIUS RELATION FOR COLD SPHERES OF LOW MASS*

H. S. ZAPOLSKY
University of Maryland, College Park, and Center for Theoretical Physics
AND
E. E. SALPETER
Laboratory of Nuclear Studies, Physics Department, and Center for Radiophysics and Space Research, Cornell University, Ithaca, New York
Received 1969 March 14

ABSTRACT

The relationship between mass and radius for zero-temperature spheres is determined for each of a number of chemical elements by using a previously derived equation of state and numerical integration. The maximum radius of a cold sphere is thus found as a function of chemical composition, and a semi-empirical formula for the mass-radius curve is derived.

16

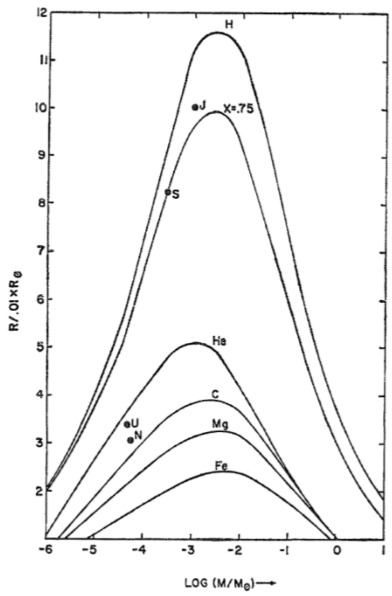

FIG. 1.—Mass-radius plot for homogeneous spheres of various chemical compositions. The points J, S, U, N are the observed values for the Jovian planets.

17

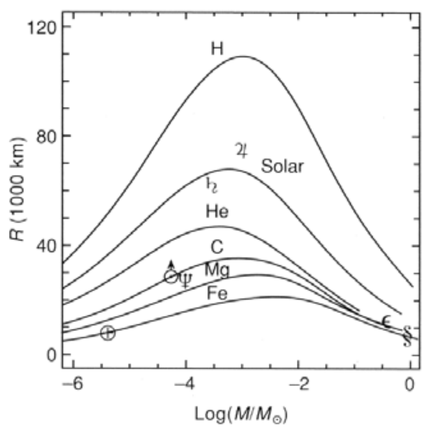

Figure 12.4 Mass-radius relation for low-mass objects (following H. S. Zapolsky & E. E. Salpeter, *Astrophys. J.* 158). Different curves correspond to different compositions, as indicated. The locations of several planets – Earth, Jupiter, Saturn, Uranus and Neptune – are marked by the planets' symbols. Also marked are the locations of two white dwarfs, Sirius B (§) and 40 Eridani B (ϵ) (data from D. Koester (1987), *Astrophys. J.*, 322).

Brown dwarfs and very low-mass stars … partial P_{deg}^{e-}

White dwarfs
≈ completely degenerate,
R↘ as M↗

Terrestrial planets
R ↗ as M↗ ← complicated EoSs

Mass-radius relation max @ $M_{\text{Jupiter}} \approx (1/1000)\, M_{\odot}$

18

$M_{\odot}c^2 = 2 \times 10^{54}$ ergs
1 amu = 931 Mev/c^2

Deuterium Burning

$$^2H + {}^1H \longrightarrow {}^3He + \gamma \quad (T > 10^6 K)$$

$$^2H({}^1H, \gamma)\,{}^3He$$

$$Q_{DP} = 5.5 \text{ MeV}$$

$$q_{DP} = 4.19 \times 10^7 \, [D/H] \left(\frac{\rho}{1\, g\, cm^{-3}}\right)\left(\frac{T}{10^6 K}\right)^{11.8} [erg\, g^{-1} s^{-1}]$$

ISM value, $\langle D/H \rangle \sim 2 \times 10^{-5}$

19

$n + p \rightarrow D + \gamma$ (production of D)
$D + D \rightarrow {}^4He + \gamma$ (destruction) → faster

The lower the mass density, the more the D abundant → D as a sensitive tracer of the density of the early Universe

Before the Big Bang nucleosynthesis, there were plenty of neutrons, but much less abundant than protons, so all neutrons go into making ^4He

$$\rightarrow {}^4He \approx \frac{n/2}{(n+p)/4} = \frac{2n}{n+p}$$

Current value $n/p \approx 0.12$, so $^4He \approx 2/9$, as observed today.

20

D/H

- 156 ppm … Terrestrial seawater (1.56×10^{-4})
- 22~26 ppm … Jupiter
- 17 ppm … Saturn
- 55 ppm … Uranus
- 200 ppm … Halley's Comet

21

Recall a star's central temperature

$$T_c \sim \frac{\mu G M}{R} \cdot \alpha$$

(α: mass distr.)

Numerically

$$T_c = 7.5 \times 10^6 \, K \left(\frac{M_*}{M_\odot}\right)\left(\frac{R_*}{R_\odot}\right)^{-1}$$

$$\therefore \quad M_* = 0.4\, M_\odot \longrightarrow T_c \sim 10^6\, K$$

22

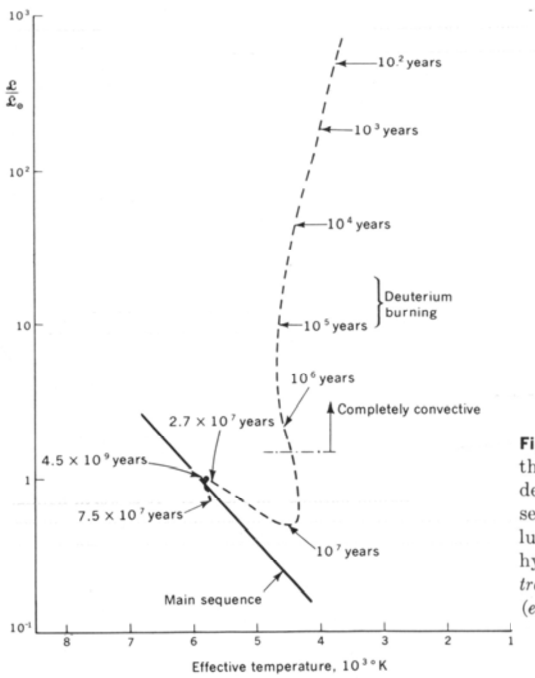

Fig. 5-1 The path on the H-R diagram of the contraction of the sun to the main sequence. The interior has become sufficiently hot to burn deuterium after about 10^5 years. The contraction ceases near the main sequence when the core has become hot enough to replenish the solar luminosity with the thermonuclear power generated by the fusion of hydrogen into helium. [*After D. Ezer and A. G. W. Cameron, The Contraction Phase of Stellar Evolution, in R. F. Stein and A. G. W. Cameron (eds.), "Stellar Evolution," Plenum Press, New York,* 1966.]

Clayton 23

THE ASTROPHYSICAL JOURNAL, **274**:822–829, 1983 November 15

THE BIRTHLINE FOR LOW-MASS STARS

STEVEN W. STAHLER
Harvard-Smithsonian Center for Astrophysics, Cambridge, Massachusetts
Received 1983 January 19; accepted 1983 May 4

ABSTRACT

Using the results of protostar theory, I find the locus in the Hertzsprung-Russell diagram where pre-main-sequence stars of subsolar mass should begin their quasi-static contraction phase and first appear as visible objects. This "birthline" is in striking agreement with observations of T Tauri stars, providing a strong confirmation of the fact that these stars are indeed contracting along Hayashi tracks. The assumption that most T Tauri stars first appear along this line forces a recalibration of their ages. This recalibration removes the puzzling dip in present-day star formation seen in age histograms of several cloud complexes. Since the underlying protostar calculation assumes that the parent cloud was only thermally supported prior to its collapse, the observed location of the birthline places severe restrictions on the degree of extrathermal support provided by rotation, magnetic fields, or turbulence. In addition, the hypothesis that the collapse from thermally supported clouds to low-mass stars proceeds through protostellar disks appears untenable, since the disk accretion process almost certainly produces pre-main-sequence stars with radii well below the observed birthline.

Protostars are heavily embedded in clouds, so obscured, with no definition of T_{eff}

Birthline=beginning of PMS; star becomes optically visible ≈ deuterium main sequence

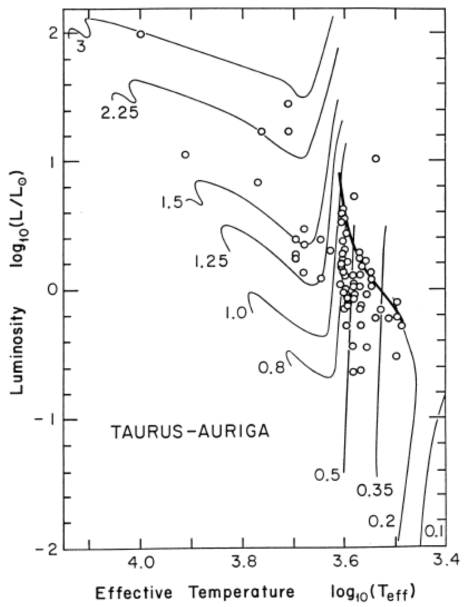

Stahler (1983, 1988), Palla & Stahler (1990)

… compared with observations

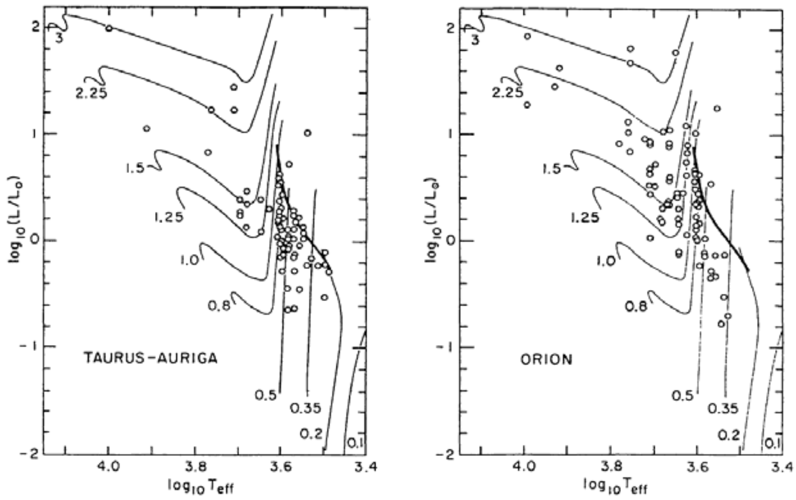

Figure 4 Hertzsprung-Russell diagrams from Cohen & Kuhi (1979) showing theoretical pre-main-sequence contraction tracks and T Tauri stars in the Taurus-Auriga and Orion cloud complexes. The heavy solid curve is the theoretical "birthline" of Stahler (1983).

25

Lithium Burning

$^7Li + {}^1H \longrightarrow {}^4He + {}^4He \quad (T > 3 \times 10^6 K)$

ISM $[Li/H] \sim 2 \times 10^{-9}$

Primordial abundance 10 x lower,
produced by cosmic rays α hitting 4He
(inverse reaction)

Li measurable in stellar spectra

Li I 6708 Å absorption

(actually doublet 6707.78 and 6707.93
but difficult to resolve

26

Presence of Li I λ6707 absorption → stellar youth

Ca I λ6718 prominent in late-type stars

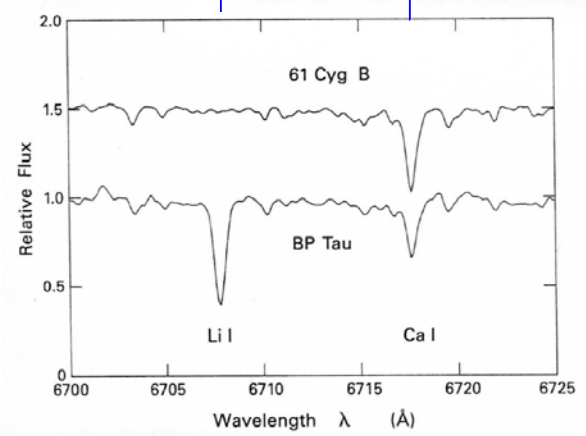

Figure 16.9 Lithium absorption in a pre-main-sequence star. Shown is a portion of the optical spectrum of BP Tau, a T Tauri star of spectral type K7, corresponding to an effective temperature of 4000 K. Also shown, for comparison, is a main-sequence star of the same spectral type, 61 Cyg B. Only in the first star do we see the Li I absorption line at 6708 Å. Both objects also have a strong line due to neutral calcium.

Stahler & Palla 27

M > 1.2 M_sun → shallow convection → surface Li does not deplete during contraction

For protostars with $T_c \geq 3 \times 10^6$K, the central lithium is readily destroyed.

Stars $\geq 0.9\ M_\odot$ become radiative at the core, so Li not fully depleted.

Li abundance → age clock

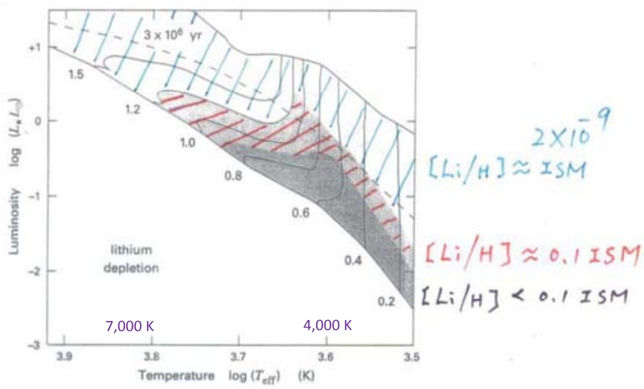

Figure 16.10 Theoretical prediction of pre-main-sequence lithium depletion. Within the white area between the birthline and the ZAMS, the surface [Li/H] is equal to its interstellar value of 2×10^{-9}. Stars in the lightly shaded region have depleted the element down to 0.1 times the interstellar value. The darker shading indicates depletion by at least this amount. Note also the masses on the ZAMS, in solar units, and the indicated isochrone.

Stahler & Palla 28

Older → depletion at higher T_{eff}

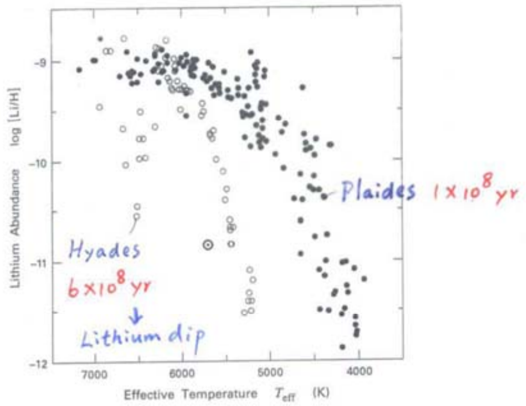

[Li/H] ↓ as T_{eff} ↓

Stahler & Palla

29

A hydrogen gas — proton-proton chains

$4\,H \rightarrow {}^4He$ unlikely ⇒ a chain of reactions

baryon #, lepton #, charges all conserved

$p^+ + p^+ \rightarrow {}^2D^+ + e^+ + \nu$ ⟨1.4×10^{10} yr⟩
(1.44 MeV) neutrino → 0.26 MeV escaped

${}^2D + p \rightarrow {}^3He + \gamma$ ⟨6 s⟩
(5.49 MeV)

0.420 MeV to the positron and neutrino; position and electron (each 0.511 MeV rest energy) annihilate
➔ 1.442 MeV

${}^3He + {}^3He \rightarrow {}^4He + 2p$ ⟨10^6 yr⟩
(12.85 MeV) PP I chain

Note : net $6p \rightarrow {}^4He + 2p$

${}^3He + {}^4He \rightarrow {}^7Be + \gamma$

... but the nucleus of deuterium, a deuteron, consists of a proton and a neutron!

30

- ✓ $p + p \rightarrow {}^{2}He$ (unstable)$\rightarrow p + p$
- ✓ **Hans Bethe (1939) realized that the weak interaction was capable of converting a proton to a neutron (!) first**
- ✓ **Weak interaction → very small cross section**
- ✓ **The neutron is more massive, so this requires energy, i.e., it is an endothermic process, but neutron + proton → deuteron (releasing binding energy, so exothermic)**

31

$^{3}He + {}^{3}He \rightarrow {}^{4}He + 2p$ (12.85 MeV) $< 10^{6}$ yr $>$

Note: net $6p \rightarrow {}^{4}He + 2p$

PP I chain

$^{3}He + {}^{4}He \rightarrow {}^{7}Be + \gamma$

$^{7}Be + e^{-} \rightarrow {}^{7}Li + \nu$

$^{7}Li + p \rightarrow 2\,{}^{4}He$

PP II chain

All 3 branches operate simultaneously.

$^{7}Be + p^{+} \rightarrow {}^{8}B + \gamma$

$^{8}B \rightarrow {}^{8}Be + e^{+} + \nu$

$^{8}Be \rightarrow 2\,{}^{4}He$

PP III chain

32

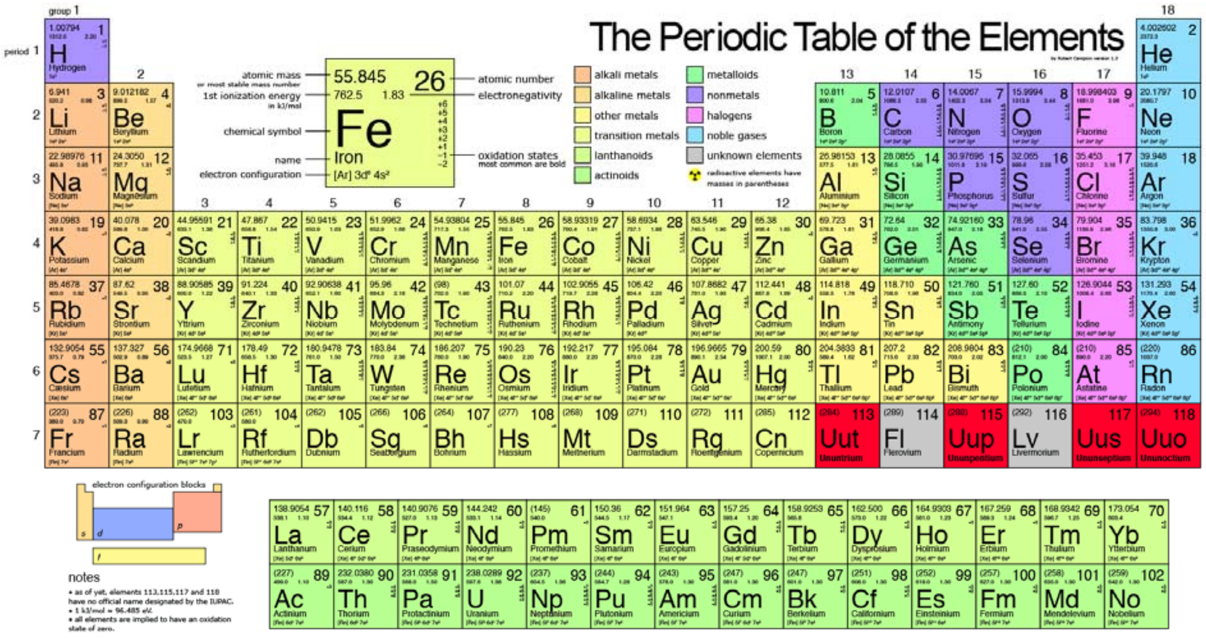

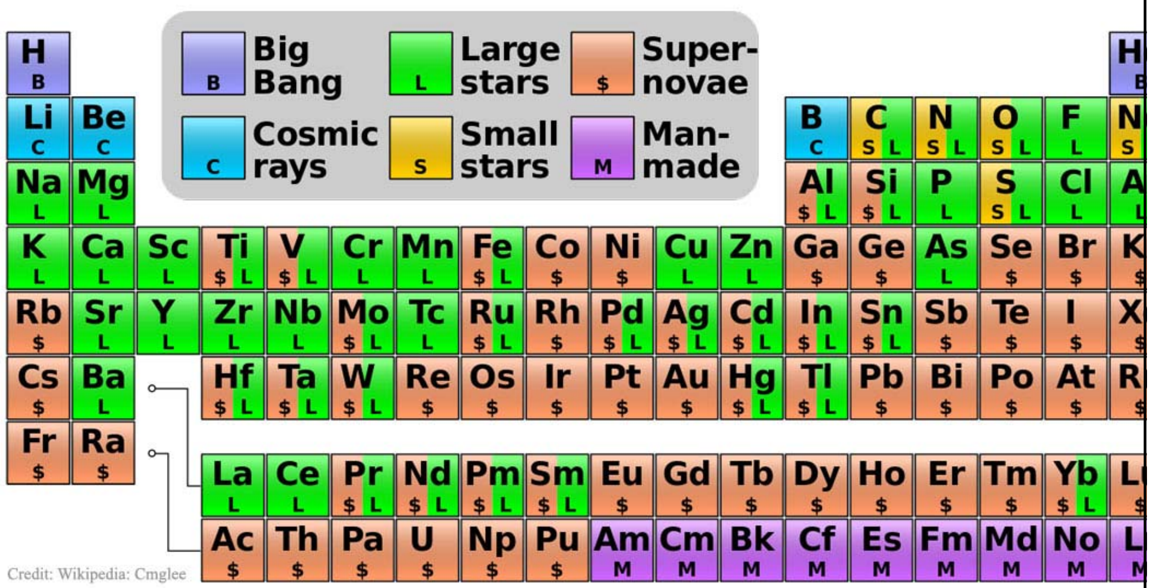

https://apod.nasa.gov/apod/ap160125.html

34

The proton-proton chain

$^1H + {}^1H \rightarrow {}^2D + e^+ + \nu_e$ (1.44 MeV, 1.4×10^{10} yr)
$^2D + {}^1H \rightarrow {}^3He + \gamma$ (5.49 MeV, 6 s)

pp I important when
$T_c > 5 \times 10^6$K

pp I chain

$^3He + {}^3He \rightarrow {}^4He + {}^1H + {}^1H$ (12.85 MeV, 10^6 yr)
Note: net $6\ {}^1H \rightarrow {}^4He + 2\ {}^1H$

$Q_{total} = 1.44 \times 2 + 5.49 \times 2 + 12.85 = 27.7$ MeV
$Q_{net} = 27.7 - 0.26 \times 2 = 26.2$ MeV

pp II chain

$^3He + {}^4He \rightarrow {}^7Be + \gamma$
$^7Be + e^- \rightarrow {}^7Li + \nu_e$
$^7Li + {}^1H \rightarrow {}^4He + {}^4He$

pp III chain

$^3He + {}^4He \rightarrow {}^7Be + \gamma$
$^7Be + {}^1H \rightarrow {}^8B + \gamma$
$^8B + \rightarrow {}^8Be + e^+ + \nu_e$
$^8Be \rightarrow {}^4He + {}^4He$

The baryon number, lepton number, and charges are all conserved.

All 3 branches operate simultaneously.

pp I is responsible for > 90% stellar luminosity

35

Exercise

Assuming that the solar luminosity if provided by $4\ {}^1H \rightarrow {}^4He$, liberating 26.73 MeV, and that the neutrinos carry off about 2% of the total energy. Estimate how many neutrinos are produced each second from the sun? What is the solar neutrino flux at the earth? (How many neutrinos pass through your body per second?)

36

Solution

2% is carried away by neutrinos, so the actual energy produced for radiation

$$E = (0.98 \times 26.731 \text{ MeV}) \times 1.6 \times 10^{-12} \text{ erg/eV}$$

Each alpha particle produced → 2 neutrinos, so with $L_{\odot} = 3.846 \times 10^{33}$ ergs/s, *the neutrino production rate is* $2 \times 10^{38}\ \nu/\text{s}$, *and the flux at earth is* $2 \times 10^{38} / 4\pi\ (1\ \text{AU})^2 \approx 6.6 \times 10^{10}\ \nu\ \text{cm}^{-2}\text{s}^{-1}$

37

The thermonuclear reaction rate,

$$r_{pp} = 3.09 \times 10^{-37}\ n_p^2\ T_6^{-2/3} \exp\left(-33.81\ T_6^{-1/3}\right)$$

$$(1 + 0.0123\ T_6^{1/3} + 0.0109\ T_6^{2/3} + 0.0009\ T_6)\quad [\text{cm}^{-3}\text{s}^{-1}],$$

where the factor $3.09 \times 10^{-37}\ n_p^2 = 11.05 \times 10^{10}\ \rho^2 X_H^2$

$$q_{pp} = 2.38 \times 10^{6}\ \rho\ X_H^2\ T_6^{-2/3} \exp\left(-33.81\ T_6^{-1/3}\right)$$

$$(1 + 0.0123\ T_6^{1/3} + 0.0109\ T_6^{2/3} + 0.0009\ T_6)\quad [\text{erg g}^{-1}\text{s}^{-1}]$$

38

PP I vs PP II

i.e., ^3He to react with ^3He — lower temp.

or with ^4He — $T > 1.4 \times 10^7 K$

Relative importance of each chain

i.e. branching ratio $\longleftrightarrow T, \rho, \mu$

$T > 3 \times 10^7 K$, PP III dominates

but in reality, at this temperature, CNO reactions take over.

Overall rate of energy generation is determined by the slowest reaction, i.e., the 1st one, $\tau \sim 10^{10}$ yr

$\varepsilon_{pp} \sim \rho^1 T^n$, $n \sim 4-6$

$Q_{pp} \sim 26.73$ MeV ≈ 6.54 MeV per proton

$n \sim 6$ for $T \approx 5 \times 10^6$ K
$n \sim 3.8$ for $T \approx 15 \times 10^6$ K (Sun)
$n \sim 3.5$ for $T \approx 20 \times 10^6$ K

39

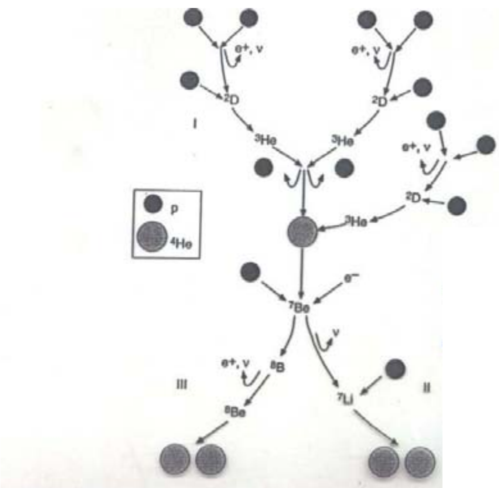

Figure 4.3 The nuclear reactions of the p–p I, II, and III chains.

Among all fusion processes, the p-p chain has the lower temperature threshold, and the weakest temperature dependence.

$$Q_{pp} = (M_{4H} - M_{He})\, c^2 = 26.73 \text{ MeV}$$

But some energy (up to a few MeV) is carried away by neutrinos.

40

CNO cycle

(bi-cycle)

C, N, O as catalysts

$^{12}C + {}^{1}H \rightarrow {}^{13}N + \gamma$ 10^{6} y

$^{13}N \rightarrow {}^{13}C + e^{+} + \nu$ 14 min

$^{13}C + {}^{1}H \rightarrow {}^{14}N + \gamma$ 3×10^{5} y

$^{14}N + {}^{1}H \rightarrow {}^{15}O + \gamma$ 3×10^{8} y

$^{15}O \rightarrow {}^{15}N + e^{+} + \nu$ 82 s

→ $^{15}N + {}^{1}H \rightarrow {}^{12}C + {}^{4}He$ 10^{4} y

$^{14}N + {}^{1}H \rightarrow {}^{15}O + \gamma$

$^{15}O \rightarrow {}^{15}N + e^{+} + \nu$

$^{15}N + {}^{1}H \rightarrow {}^{16}O + \gamma$ ←

$^{16}O + {}^{1}H \rightarrow {}^{17}F + \gamma$

$^{17}F \rightarrow {}^{17}O + e^{+} + \nu$

$^{17}O + {}^{1}H \rightarrow {}^{14}N + {}^{4}He$

CN cycle more significant

NO cycle efficient only when $T > 20 \times 10^{6}$ K

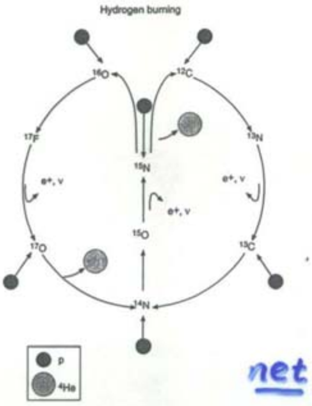

Figure 4.4 The nuclear reactions of the CNO bi-cycle.

Recognized by Bethe and independently by von Weizsäcker

CN cycle + NO cycle

Cycle can start from any reaction as long as the involved isotope is present.

$Q_{CNO} \sim 25$ MeV

after that carried away by the neutrinos

net

$4H \rightarrow {}^{4}He$

$\varepsilon_{CNO} \sim \rho T^{16}$

41

表 6.2 氢燃烧的核反应

序号 r	反应式	Q_r(MeV)	$(q_\nu)_r$(MeV)	速率 $N_A<\sigma v>$ ($cm^3 mol^{-1} s^{-1}$)
1	$^{1}H(p,e^{+}\nu)^{2}H$	1.442	0.265	1.26×10^{-20}
2	$^{2}H(p,\gamma)^{3}He$	5.494		1.85×10^{-3}
3	$^{3}He(^{3}He,2p)^{4}He$	12.860		2.29×10^{-13}
4	$^{3}He(\alpha,\gamma)^{7}Be$	1.588		1.67×10^{-18}
5	$^{7}Be(e^{-},\nu)^{7}Li$	0.862	0.862	* 4.59×10^{6} s
6	$^{7}Li(p,\gamma)^{8}Be(\alpha)^{4}He$	17.346		3.21×10^{-11}
7	$^{7}Be(p,\gamma)^{8}B$	0.137		1.38×10^{-14}
8	$^{8}B(e^{+}\nu)^{8}Be(\alpha)^{4}He$	18.072	6.710	* 0.77s
9	$^{12}C(p,\gamma)^{13}N$	1.944		1.26×10^{-12}
10	$^{13}N(e^{+}\nu)^{13}C$	2.221		* 870s
11	$^{13}C(p,\gamma)^{14}N$	7.551		4.59×10^{-12}
12	$^{14}N(p,\gamma)^{15}O$	7.297		1.30×10^{-14}
13	$^{15}O(e^{+}\nu)^{15}N$	2.754	0.9965	* 178s
14	$^{15}N(p,\alpha)^{12}C$	4.966		3.62×10^{-10}
15	$^{15}N(p,\gamma)^{16}O$	12.128		2.76×10^{-13}
16	$^{16}O(p,\gamma)^{17}F$	0.600		2.51×10^{-16}
17	$^{17}F(e^{+}\nu)^{17}O$	2.762	0.9994	* 95s
18	$^{17}O(p,\alpha)^{14}N$	1.191		4.07×10^{-16}
19	$^{17}O(p,\gamma)^{18}F$	5.607		3.05×10^{-16}
20	$^{18}F(e^{+}\nu)^{18}O$	1.655	0.3965	* 1.67s
21	$^{18}O(p,\alpha)^{15}N$	3.980		7.63×10^{-13}
22	$^{18}O(p,\gamma)^{19}F$	7.994		8.43×10^{-16}
23	$^{19}F(p,\alpha)^{16}O$	8.114		6.25×10^{-15}

* 表示 β 衰变的半周期.

(根据 Caughlan and Fowler, 1988; Harris, et al. 1983; Fowler, et al., 1975; 弱相互作用过程的快慢用原子半衰期表示，根据 Fuller, et al., 1980, 1982, 1985; Clayton, 1968). 表中的速率为典型温度下的速率，p—p 链的典型温度为 1×10^{7}K, CNO 循环的典型温度为 2.5×10^{7}K.

Huang 42

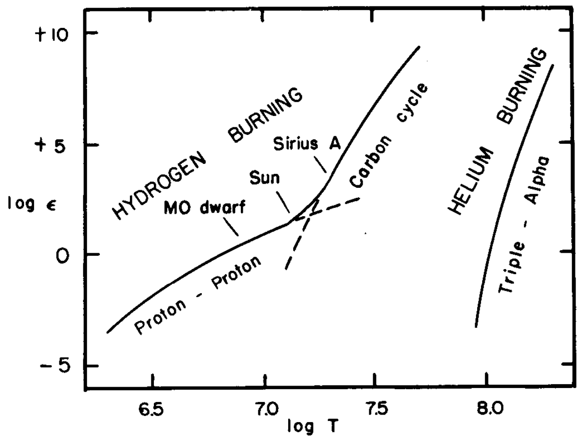

Fig. 10.1. Nuclear energy generation as a function of temperature (with $\rho X^2 = 100$ and $X_{CN} = 0.005X$ for the proton-proton reaction and the carbon cycle, but $\rho^2 Y^3 = 10^8$ for the triple-alpha process).

Schwarzschild

At the center of the Sun,
$q_{CNO}/q_{pp} \approx 0.1$

CNO dominates in stars > 1.2 $M_\odot$, i.e., of a spectral type F7 or earlier

→ large energy outflux

➔ a convective core

This separates the lower and upper MS.

CN cycle takes over the PP chains near T_6=18.
Helium burning starts ~10^8 K.

43

The Solar Standard Model (SSM)

Best structural and evolutionary model to reproduce the observational properties of the Sun

- $L_\odot = 3.842 \times 10^{33}$ [ergs/s]
- $R_\odot = 6.9599 \times 10^{10}$ [cm]
- $M_\odot = 1.9891 \times 10^{33}$ [gm]
- Spectroscopic observations → Z/X =0.0245
  (latest value seems to indicate $Z_\odot = 0.013$)

Neglecting rotation, magnetic fields, and mass loss ($dM/dt \sim 10^{-14}\, M_\odot$/yr)

Sun Fact Sheet
http://nssdc.gsfc.nasa.gov/planetary/factsheet/sunfact.html

44

A He Gas — the triple-alpha process

He-burning ignites at Tc ~ 10^8 K

$^4He + {}^4He \to {}^8Be$ (−95 keV, i.e., endothermic)

The lifetime of ^8Be is 2.6×10^{-16} s but is still longer than the mean-free time between α particles at T_8 (Edwin Salpeter, 1952)

$^8Be + {}^4He \to {}^{12}C + \gamma$ (7.4 MeV) ← bottleneck

Note: net $3\ {}^4He \to {}^{12}C$

$Q_{3\alpha} = 7.275$ MeV net $3\ {}^4He \to {}^{12}C$

↪ 5.8×10^{17} erg g^{-1} ~ 0.1 of H → He

$\varepsilon_{3\alpha} \sim \rho^2 T^{40}$ ∵ bottleneck: 2nd reaction ↔ ^8Be

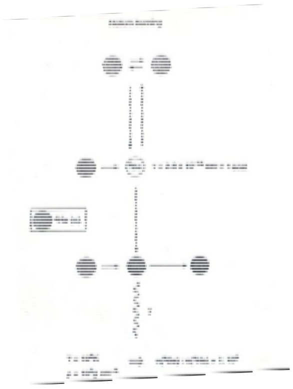

Nucleosynthesis during helium burning

$C^{12}(\alpha, \gamma)O^{16}$ Q = 7.162 MeV

$O^{16}(\alpha, \gamma)Ne^{20}$

A succession of (α, γ) processes

→ ^{16}O, ^{20}Ne, ^{24}Mg … (the α-process)

A carbon/oxygen Gas

$^{12}C + {}^{12}C$

$T \gtrsim 5 \times 10^8$ K

$Q_{CC} \sim 13$ MeV

$^{12}C + {}^{12}C \to {}^{24}Mg + \gamma$
$\to {}^{23}Mg + n$
$\to {}^{23}Na + p$
$\to {}^{20}Ne + \alpha$
$\to {}^{16}O + 2\alpha$

$^{16}O + {}^{16}O \to {}^{32}S + \gamma$
$\to {}^{31}S + n$
$\to {}^{31}P + p$
$\to {}^{28}Si + \alpha$
$\to {}^{24}Mg + 2\alpha$

$^{16}O + {}^{16}O$

$T \gtrsim 10^9$ K

$Q_{OO} \sim 16$ MeV

C-burning ignites when Tc ~ (0.3-1.2) × 10^9 K, i.e., for stars 15-30 $M_\odot$

O-burning ignites when Tc ~ (1.5-2.6) × 10^9 K, i.e., for stars > 15-30 $M_\odot$

The p and α particles produced are captured immediately (because of the low Coulomb barriers) by heavy elements

➔ isotopes

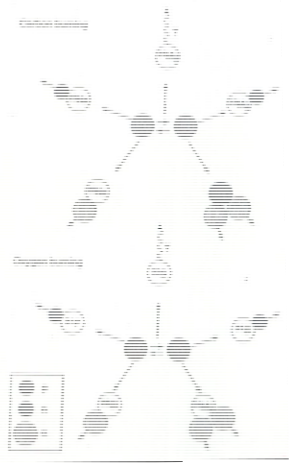

O burning → Si

46

$$q_{PP} = 2.4 \times 10^{6}\, \rho\, X^{2}\, T_6^{\;-2/3} \exp\left[-33.8\, T_6^{\;-1/3}\right] \quad [\mathrm{erg\, g^{-1}\, s^{-1}}]$$

$$q \propto \rho\, X_H^2\ T^4$$

$$q_{CN} = 8 \times 10^{27}\, \rho\, X\, X_{CN}\, T_6^{\;-2/3} \exp\left[-152.3\, T_6^{\;-1/3}\right] \quad [\mathrm{erg\, g^{-1}\, s^{-1}}]$$

$$q \propto \rho\, X_H X_{CN}\, T^{16}$$

$\frac{X_{CN}}{X_H} = 0.02$ ok for Pop I

$$q_{3\alpha} = 3.9 \times 10^{11}\, \rho^2 X_\alpha^{\;3}\, T_8^{\;-3} \exp[-42.9\, T_8] \quad [\mathrm{erg\, g^{-1}\, s^{-1}}]$$
$$\approx 4.4 \times 10^{-8}\, \rho^2 X_\alpha^{\;3}\, T_8^{\;40} \quad [\mathrm{erg\, g^{-1}\, s^{-1}}] \quad (\text{if } T_8 \approx 1)$$

Clayton

47

Does ^{28}Si follow the same scenario?

$^{28}Si + {}^{28}Si \xrightarrow{?} {}^{56}Fe$?

C+C 6×10^8 K
O+O 10^9 K

No ! Coulomb barrier becomes extremly high; another nuclear reaction takes place

cf.

Photoionization

Likewise

Photodisintegration

48

For example, $^{16}O + \alpha \leftrightarrow {}^{20}Ne + \gamma$
If $T < 10^9$ K $\rightarrow$
but if $T \geq 1.5 \times 10^9$ K (in radiation field) $\leftarrow$

So ^{28}Si disintegrates at $\approx 3 \times 10^9$ K to lighter elements
(then recaptured ...)
Until a nuclear statistical equilibrium is reached

But the equilibrium is not exact
→ pileup of the iron group nuclei (Fe, Co, Ni)
which can resist photodisintegration until 7×10^9 K

49

Nuclear Fuel	Process	$T_{threshold}$ (10^6 K)	Products	Energy per nucleon (MeV)
H	p-p	~4	He	6.55
H	CNO	15	He	6.25
He	3α	100	C, O	0.61
C	C + C	600	O, Ne, Na, Mg	0.54
O	O + O	1,000	Mg, S, P, Si	~0.3
Si	Nuc. Equil.	3,000	Co, Fe, Ni	<0.18

From Prialnik Table 4.1

50

$^{56}Fe + 100\ \text{MeV} \rightarrow 13\ ^{4}He + 4\ n$

If T ↑↑↑, even $^{4}He \rightarrow p^{+} + n^{0}$

So stellar interior has to be between a few T_6 and a few T_9.

Lesson: Nuclear reaction that absorb energy from ambient radiation field (in stellar interior) can lead to catastrophic consequences.

51

Alternative Energy --- Accretion Energy

Accretion Energy

$$L = \frac{GM}{R}\dot{M}$$

in terms of the Schwarzschild radius $R_S \equiv \frac{2GM}{c^2}$

$$\Rightarrow L = \left[\frac{R_S}{2R}\right]\dot{M}c^2$$

'efficiency'; ↑ as R ↓

Accretion is highly efficient onto a compact object.

52

For chemical reactions typically ~ a few eV

e.g., H_2 dissociation, $E \sim 4.48$ eV

$\therefore \frac{4.48\,\text{eV}}{2m_p} \sim 10^{12}\ \text{erg}\ g^{-1} \rightarrow 10^{-9}$ eff.

For nuclear reactions typically ~ a few MeV

e.g., $4H \rightarrow He$, $E \sim 7$ MeV

$\therefore \frac{7\,\text{MeV}}{m_p} \sim 10^{19}\ \text{erg}\ g^{-1} \rightarrow 10^{-2}$ eff.

For accretion process $E \sim 10^{21}\ \text{erg}\ g^{-1}$

Ex. a neutron star $R \sim 15$ km, $\frac{R_s}{2R} \sim 0.1$

Longair "High-Energy Astrophysics"

53

Time Scales

Different physical processes inside a star,
e.g., nuclear reactions (changing chemical composition) are slow (longer time scales); structural adjustments (dP/dt) take places on relatively shorter time scales.

- ✓ Dynamical timescale
- ✓ Thermal timescale
- ✓ Nuclear timescale
- ✓ Diffusion timescale

54

Dynamical Timescale

hydrostatic equilibrium $\xrightarrow{\text{perturbation}}$ motion $\xrightarrow{\text{adjustment}}$ hydrostatic equilibrium

Free-fall collapse

Equation of motion $\ddot{r} = -\frac{GM_r}{r^2} - \frac{1}{\varrho}\frac{dP}{dr}$

Near the star's surface $r = R, M_r = M$, so $\ddot{R} = -\frac{GM}{R^2} - \frac{1}{\varrho}\frac{dP}{dR}$

Free-fall means pressure ≪ gravity, so $\ddot{R} \approx -\frac{GM}{R^2}$

Assuming a constant acceleration $R = -(\ddot{R}/2)\,\tau_{\rm ff}^2$, so

$$\tau_{\rm ff} = (2R^3/GM)^{1/2} = \frac{1}{\left(\frac{2}{3}\pi G\bar{\rho}\right)^{1/2}} \approx 0.04\left(\frac{\rho_\odot}{\bar{\rho}}\right)^{1/2} [\mathrm{d}]$$

55

Stellar Pulsation

The star pulsates about the equilibrium configuration
→ same as dynamical timescale

$$\tau_{\rm pul} \propto 1/\sqrt{\bar{\rho}}$$

Propagation of Sound Speed (pressure wave)

Pressure induced perturbation,

$$R/\tau_{\rm ff}^2 = -\frac{\ddot{R}}{2} = \frac{GM}{R^2} + \frac{1}{\varrho}\frac{dP}{dR} \approx \frac{1}{\varrho}\frac{dP}{dR} \approx \frac{1}{\varrho}\frac{P}{R}$$

so $\frac{R}{\tau_{\rm ff}} \approx \sqrt{\frac{P}{\rho}} \approx c_s$ (sound speed) $\propto \sqrt{T}$ (for ideal gas)

$$\tau_{\rm s} \approx \frac{R}{c_s}$$

In general, $\tau_{\rm dyn} \approx \frac{1}{\sqrt{G\bar{\rho}}} \approx \frac{1.6\times10^{15}}{\sqrt{n}}\,[\mathrm{s}] = 1000\sqrt{\left(\frac{R}{R_\odot}\right)^3\left(\frac{M_\odot}{M}\right)}\,[\mathrm{S}]$

56

Thermal Timescale

Kelvin-Helmholtz timescale (radiation by gravitational contraction)

$$E_{\text{total}} = E_{\text{grav}} + \mathrm{E}_{\text{thermal}} = \frac{1}{2} E_{\text{grav}} = -\frac{1}{2} \alpha GM^2/R$$

This amount of energy is radiated away at a rate L, so timescale

$$\tau_{\text{KH}} = \frac{E_{\text{total}}}{L} = \frac{1}{2} \alpha GM^2/RL$$
$$= 2 \times 10^7 M^2/RL \quad \text{[yr] in solar units}$$

$$\boxed{\tau_{\text{KH}} \approx 2 \times 10^7 \left(\frac{M}{M_\odot}\right)^2 \left(\frac{R_\odot}{R}\right) \left(\frac{L_\odot}{L}\right) \text{ [yr]}}$$

57

$M = 1\,\mathcal{M}_\odot, R = 1$ pc	$M = 1\,\mathcal{M}_\odot, R = 1\,\mathcal{R}_\odot$
$\tau_{\text{dyn}} \approx 1.6 \times 10^7$ yr	$\tau_{\text{dyn}} \approx 1.6 \times 10^3$ s ≈ 30 min
$\tau_{\text{ther}} \approx 1$ yr	$\tau_{\text{ther}} \approx 3 \times 10^7$ yr

58

Nuclear Timescale

Time taken to radiate at a rate of L on nuclear energy

$4\ {}^{1}H \rightarrow\ {}^{4}He\ (Q = 6.3 \times 10^{18}\text{erg/g})$

$$\tau_{\text{nuc}} = \frac{E_{\text{nuc}}}{L} = 6.3 \times 10^{18}\,\frac{M}{L}$$

$$\tau_{\text{nuc}} \approx 10^{11}\left(\frac{M}{M_\odot}\right)\left(\frac{L_\odot}{L}\right)\ [\text{yr}]$$

From the discussion above, $\tau_{\text{nuc}} \gg \tau_{\text{KH}} \gg \tau_{\text{dyn}}$

59

Main-Sequence Lifetime of the Sun

Energy Gained in a PP Chain

- 4H → 1 He + neutrinos + energy
- Mass of 4 H = 6.693×10^{-27} kg
  – Mass of 1 He = 6.645×10^{-27} kg

Mass deficit → 0.048×10^{-27} kg = 0.7%

$M_\odot \approx 2 \times 10^{33}$ [g]

$L_\odot \approx 4 \times 10^{33}$ [ergs/s]

Fusion efficiency

Nuclear physics

Stellar physics

$$\tau_\odot^{\text{MS}} \approx \text{M}_\odot\,\frac{(0.007)(0.1)\,c^2}{\text{L}_\odot} = 3.15 \times 10^{17}[\text{s}] = 10^{10}\ [\text{yr}]$$

Given $L_{\text{MS}}/L_\odot \approx (M/M_\odot)^4 \rightarrow \tau^{\text{MS}} \approx 10^{10}\,(M_\odot/M)^3$ [yr]

60

Diffusion Timescale

Time taken for photons to randomly walk out from the stellar interior to eventual radiation from the surface

$r_e = \frac{1}{4\pi\epsilon_0}\frac{e^2}{m_e c^2}$ ("classical" radius of the electron)

$\sigma_{\text{Thomson}} = \frac{8\pi}{3}{r_e}^2 = 6.6525 \times 10^{-29}$ [m^2] for interactions with photon energy $h\nu \ll m_e c^2$ (electron rest energy)

Thus, mean free path $\ell = 1/(\sigma_T n_e)$, where for complete ionization of a hydrogen gas, $n_e = M/(m_p R^3)$.

So, $\ell \approx m_p R^3/\sigma_T M = 4$ [mm] for the mean density.

At the core, it is 100 times shorter.

$\tau_{\text{dif}} \approx 10^4$ [yr] (Exercise: Show this.)

61

For an isotropic gas

$$P = \frac{1}{3}\int_0^\infty p\, v_p\, n(p)\, dp$$

- p and v_p: relativistic case
- $n(p)$: particle type & quantum statistics

For a photon gas, $p = h\nu/c$, so

$$P_{rad} = \frac{1}{3}\int_0^\infty h\nu\, n(\nu)\, d\nu = \frac{1}{3}u = \frac{1}{3}aT^4,$$

$$a = 7.565 \times 10^{15} \text{ ergs cm}^{-3}\text{ K}^{-4}$$

62

Radiation Pressure

$P_{\text{total}} = P_{\text{radiation}} + P_{\text{gas}}$

Since $P_{\text{rad}} \sim T^4 \sim M^4/R^4$

But $P_{\text{tot}} \sim M^2/R^4$

➔ $P_{\text{rad}}/P_{\text{tot}} \sim M^2$

So the more massive of a star, the higher relative contribution by radiation pressure (and γ decreases to 4/3.)

63

When P_{rad} dominates

$$\mathcal{F} = \frac{-d\,P_{\text{rad}}/dr}{\kappa\rho} = \frac{4ac}{3} T^3 \frac{dT}{dr} = \frac{L}{4\pi r^2}$$

$$\frac{d\text{P}_{\text{rad}}}{dr} \sim \frac{\kappa\rho}{c}\frac{L}{4\pi r^2}$$

On the other hand, by definition

$$\frac{dP_{\text{tot}}}{dr} = -\rho\frac{Gm}{r^2}$$

$$\Rightarrow \frac{d\text{P}_{\text{rad}}}{dP_{\text{tot}}} = \frac{\kappa L}{4\pi cGm}$$

64

Toward the outer layers, both $P_{\text{gas}} \searrow$ **and** $\text{P}_{\text{rad}} \searrow$, **so** $P_{\text{tot}} \searrow\searrow$, **and** $dP_{\text{tot}} > dP_{\text{rad}}$. **This leads to**

$$\kappa L \leq 4\pi c G m$$

At the surface, $m = M, P = 0$, **it is always radiative, so**

$$L < \frac{4\pi c G M}{\kappa}$$

This is the Eddington luminosity limit = Maximum luminosity of a celestial object in balance between the radiation and gravitational force.

Numerically,

$$L_{Edd}/L_{\odot} = 3.27 \times 10^4 \ \mu_e \, M/M_{\odot}$$

For X-ray luminosity, scattered by electrons in an optically thin gas, $L_X < 10^{38}$ erg sec^{-1}

65

Eddington limit is the upper limit on the luminosity of an object of mass M, $L \leq \left(\frac{4\pi G m_p}{\sigma_T}\right) M$

$$\equiv L_{\text{Edd}} \approx 10^{38} \, {}^{M}/_{M_{\odot}} \ [\text{erg s}^{-1}]$$

For 1 $M_{\odot}$, $L_{\text{Edd}} \approx 5 \times 10^4 L_{\odot}, M_{\text{bol}} = -7.0$
For 40 $M_{\odot}$, $M_{\text{bol}} = -11.0$

Eta Carina, $L \approx 5 \times 10^6 L_{\odot}$, $M_{\text{bol}} = -11.6$, $M \approx 120 \, M_{\odot}$

66

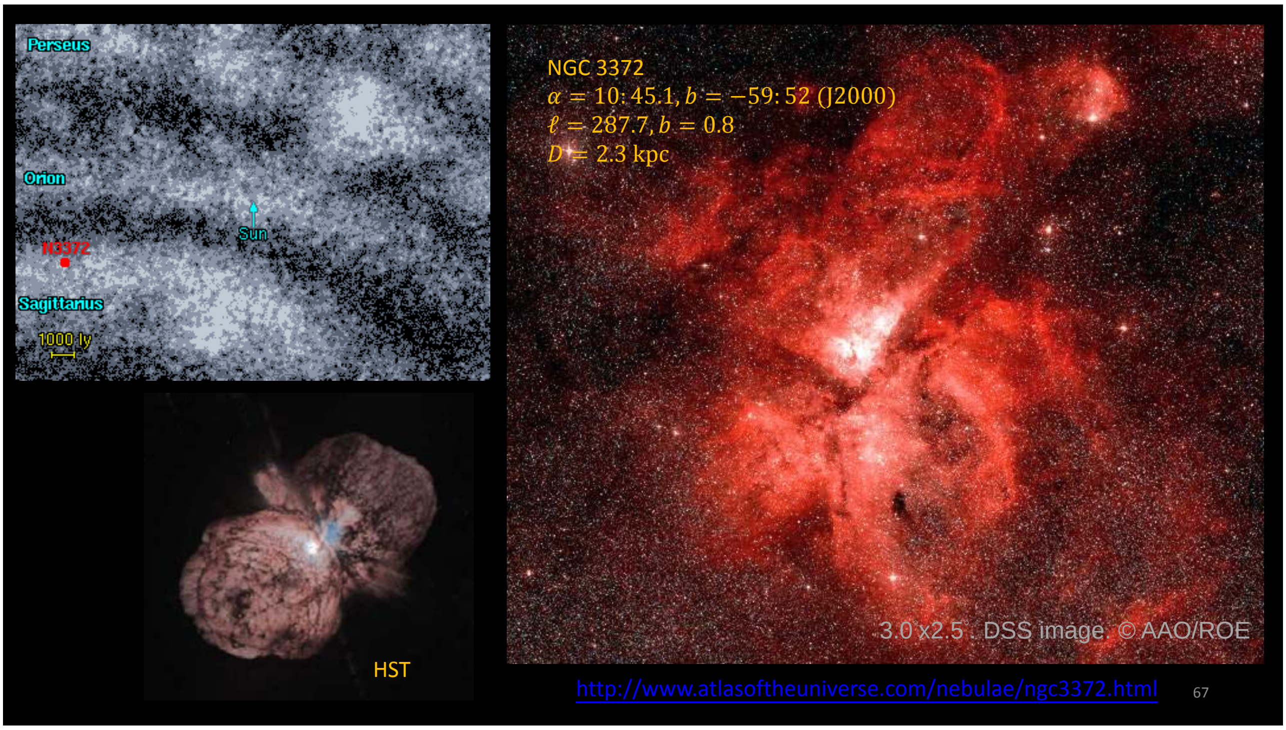

In general,

$$L_{Edd} \simeq 3.2 \times 10^4 \frac{M}{M_\odot} \frac{\kappa_e}{\kappa} \; [L_\odot]$$

inequality is violated

L_{Edd} can be exceeded if

① $L \uparrow\uparrow$, e.g., intense thermonuclear burning

② $\kappa \uparrow\uparrow$, e.g. H or He ionization

$\Rightarrow$ Hydrostatic equilibrium can no longer maintained

$\therefore$ need a different heat transfer mechanism

68

Comparison of 1, 5, and 25 $\mathcal{M}_{\odot}$ stars

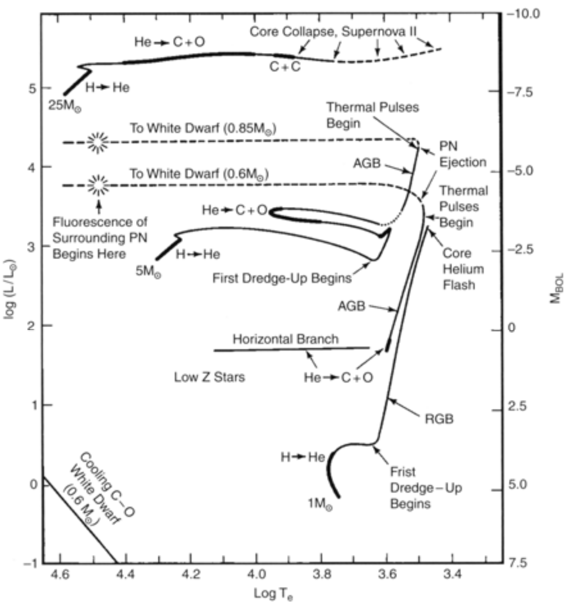

Evolutionary tracks of theoretical model stars in the HR diagram (Iben, 1985)

69

Stellar Evolution onto and off the Main Sequence

Stellar Structure

$$\frac{dP}{dM_r} = -\frac{GM_r}{4\pi r^4}$$

$$\frac{dr}{dM_r} = \frac{1}{4\pi r^2 \rho}$$

$$\frac{dT}{dM_r} = \begin{cases} -\frac{3\kappa}{64\pi^2 ac}\left(\frac{1}{T^3}\right)\left(\frac{L_r}{r^4}\right), & \nabla_{rad} < \nabla_{ad} \\ -\frac{\nabla_{ad}}{4\pi}\left(\frac{T}{P}\right)\left(\frac{GM_r}{r^4}\right), & \nabla_{rad} > \nabla_{ad} \end{cases}$$

$$\frac{dL_r}{dM_r} = \epsilon(\rho, T, X)$$

Boundary Conditions

At stellar center, $M_r = 0$, $r \doteq L_r = 0$

At stellar surface, $M_r = M$, $\rho = T = 0$

Given $M \Rightarrow L, T_c, P_c$

$$\begin{cases} \frac{dr}{dM} = \frac{1}{4\pi r^2 \rho} \\ \frac{dP}{dM} = -\frac{GM}{4\pi r^2} \\ \frac{dL}{dM} = \epsilon - T\frac{dS}{dT} \\ \frac{dT}{dM} = -\frac{3}{4}\frac{\kappa}{ac}\frac{L}{T^3}\frac{1}{16\pi^2 r^4} \quad (\text{rad.}) \end{cases}$$

$$= \frac{\gamma - 1}{\gamma}\frac{d\ln T}{d\ln P} \quad (\text{conv.})$$

Given M, μ

→ a stable structure, uniquely determined

Russell - Vogt theorem

⇒ a unique position in H-R diagram for a MS star

⇒ mass-radius & mass-lum. relations

$$\kappa \equiv \kappa(\rho, T, \mu)$$

$$\gamma \equiv \gamma(\rho, T, \mu)$$

B.C. $\begin{cases} M(r=0) = 0; \; L(r=0) = 0 \\ \rho(r=R) = 0; \; T(r=R) \rightarrow T_{eff} \simeq c \end{cases}$

∴ Stellar evolution → μ changes

To compute structural changes with appropriate time steps

At a given time, with a given mass

→ set of $(r, T, \rho, \epsilon, L, \mu)$

→ plotted as evolutionary tracks on HRD

e.g. T_{eff}, L

Luminosity

$$\frac{L}{L_\odot} = \frac{L}{L_\odot}(M/M_\odot)$$

$$\frac{L}{L_\odot} \propto \begin{cases} 7^{1.75}(M/M_\odot)^3, & M \gtrsim 7M_\odot \\ (M/M_\odot)^{4.8}, & 0.4M_\odot \lesssim M_\odot \lesssim 7M_\odot \\ 0.4^{2.35}(M/M_\odot)^{1.9}, & M \lesssim 0.4M_\odot \end{cases}$$

Approximately, for $M \gtrsim M_\odot$, $\boxed{L \propto M^{3.5}}$

Main sequence lifetime ($H \rightarrow He$)

$$\tau_{MS} \sim 0.1\,\epsilon \frac{XM}{L}$$

→ After this fraction stellar evolution becomes important, so star not in stable state

$$\approx 10^{10}\left(\frac{M}{M_\odot}\right)/(L/L_\odot) \quad [yr]$$

$$\approx 10^{10}(M/M_\odot)^{-2.5} \quad [yr]$$

Note: M-L, Strong dependence on mass (index of 3.5) ⇐ strong dep of ϵ on T for $M \gtrsim M_\odot$

Radius $\frac{R}{R_\odot} = \frac{R}{R_\odot}(M/M_\odot)$

$R \sim M^{0.85}$ $M \lesssim M_\odot$
$R \propto M^{0.56}$ $M \gtrsim M_\odot$
> different structure

Temperature

$$\frac{T_c}{T_{\odot,c}} = \frac{T_c}{T_{\odot,c}}(M/M_\odot)$$

$T_{\odot,c} \sim 1.44 \times 10^7 K$

For $M \gtrsim M_\odot$, T_c changes 2-3x.

For $M \lesssim M_\odot$, $T_c \uparrow$ as $M \uparrow$

For $T_c \gtrsim 1.4 \times 10^7 K$, CNO cycle starts to dominate nuclear reaction process in the core of a star

$T_c < 1.4 \times 10^7 K$, PP chain dominates

$$\epsilon_{pp}(\rho, T) \sim \frac{2.4 \times 10^{4}\rho X^2}{(T/10^9)^{2/3}} e^{-3.380/(T/10^9)^{1/3}} \quad [erg\,s^{-1}g^{-1}]$$

$$\epsilon_{CNO}(\rho, T) \sim \frac{4.4 \times 10^{25}\rho XZ}{(T/10^9)^{2/3}} e^{-15.228/(T/10^9)^{1/3}} \quad [erg\,s^{-1}g^{-1}]$$

Evolution Equations

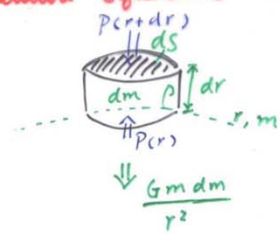

$$dm = \rho\, dr dS = \rho 4\pi r^2\, dr$$

$$\frac{\partial^2 r}{\partial t^2} = \ddot{r}\, dm$$
$$= -\frac{Gmdm}{r^2} + P(r)dS - \underline{P(r+dr)}dS$$

$$P(r) + \frac{\partial P}{\partial r} \cdot dr$$

The equation of motion is

$$\ddot{r} = -\frac{Gm}{r^2} - \frac{1}{\rho}\frac{\partial P}{\partial r} \quad \text{or} \quad \ddot{r} = \frac{Gm}{r^2} - 4\pi r^2 \frac{\partial P}{\partial m}$$

In case of hydrostatic equilibrium, i.e., $\ddot{r} \rightarrow 0$

$$\frac{dP}{dr} = -\rho\frac{Gm}{r^2} < 0$$

X = 0.708, Y = 0.272, Z = 0.020

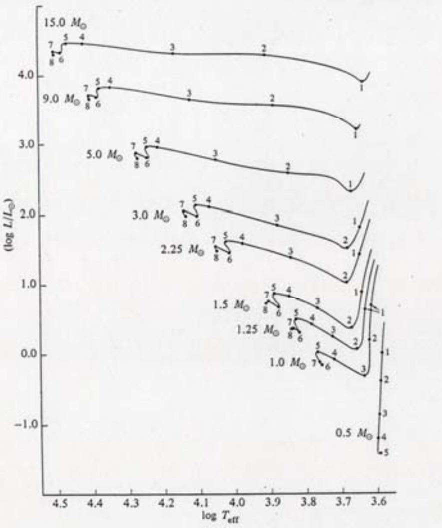

Fig. 7-3A Evolutionary Tracks of Pre-Main-Sequence Stars in the Hertzsprung-Russell Diagram. The mass, in units of the solar mass, is given at the left of each track. The small numbers correspond to the points in Table 7-4A, which give the time measured from the initial model for each mass. The units of T_{eff} are degrees Kelvin. [After I. Iben, Jr., 1965 (321).] ApJ 141, 993

Table 7-4A Time *t* in Years Measured from the Initial Model for Each Mass. The last point for each mass represents the main sequence.* [From I. Iben, Jr., 1965 (321).]

POINT IN FIG. 7-3A	MASS OF MODEL (UNITS OF THE SOLAR MASS)								
	15	9	5	3	2.25	1.5	1.25	1.0	0.5
	10^4	10^5	10^5	10^6	10^6	10^7	10^7	10^7	10^8
1	0.067	0.014	0.294	0.034	0.079	0.023	0.045	0.012	0.003
2	0.377	0.015	1.069	0.208	0.594	0.236	0.396	0.106	0.018
3	0.935	0.364	2.001	0.763	1.883	0.580	0.880	0.891	0.087
4	2.203	0.699	2.860	1.135	2.505	0.758	1.115	1.821	0.309
5	2.657	0.792	3.137	1.250	2.818	0.862	1.404	2.529	1.550
6	3.984	1.019	3.880	1.465	3.319	1.043	1.755	3.418	—
7	4.585	1.915	4.559	1.741	3.993	1.339	2.796	5.016	—
8	6.170	1.505	5.759	2.514	5.855	1.821	2.954	—	—

* Each entry must be multiplied by 10^n as given at the head of each column.

Table 7-4B The Logarithm of the Time in Seconds, log *t*, Measured From the Initial Models for Masses 1 $M_\odot$ and 15 $M_\odot$. [From data of I. Iben, Jr., 1965 (321).]

POINT IN FIG. 7-3A	MASS OF MODEL (UNITS OF THE SOLAR MASS)	
	15	1.0
1	10.33	12.57
2	11.07	13.52
3	11.47	14.45
4	11.84	14.76
5	11.92	14.90
6	12.10	15.03
7	12.16	15.20
8	12.29	—

$\log\tau \approx 14.5$

$\log\tau \approx 15.0$

"Introduction to Stellar Atmospheres and Interiors" by Eva Novotny

STELLAR EVOLUTION. I. THE APPROACH TO THE MAIN SEQUENCE*

ICKO IBEN, JR.
California Institute of Technology, Pasadena, California
Received August 18, 1964; revised November 23, 1964

ABSTRACT

The manner in which nuclear reactions replace gravitational contraction as the major source of stellar luminosity is investigated for model stars of population I composition in the mass range $0.5 < M/M_\odot < 15.0$. By following in detail the depletion of C^{12} from high initial values down to values corresponding to equilibrium with N^{14} in the C-N cycle, the approach to the main sequence in the Hertzsprung-Russell diagram and the time to reach the main sequence, for stars with $M \geq 1.25\ M_\odot$, are found to differ significantly from data reported previously.

$1\ M_{\odot}$

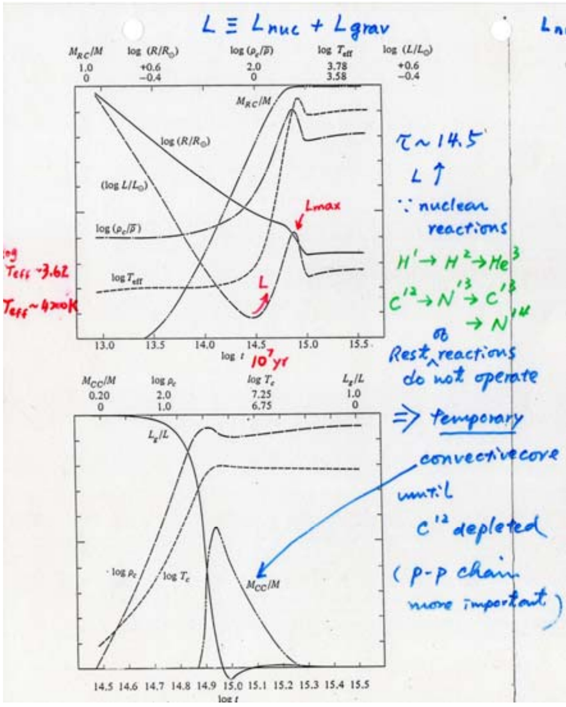

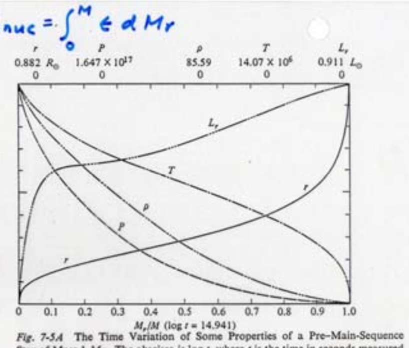

Fig. 7-5A The Time Variation of Some Properties of a Pre–Main-Sequence Star of Mass $1\ M_{\odot}$. The abscissa is log t, where t is the time in seconds measured from the initial model of the series for this mass. The upper and lower limits of each ordinate are given. The ordinates are: M_{RC}/M, the fraction of the total mass contained in a radiative core; $\log(R/R_{\odot})$, where $R/R_{\odot}$ is the total radius relative to that of the Sun ($R_{\odot} = 6.96 \times 10^{10}$ cm); $\log(\rho_c/\bar{\rho})$, where ρ_c is the central density and $\bar{\rho}$ is the mean density; $\log T_{eff}$, where T_{eff} is the effective temperature in degrees Kelvin; and $\log(L/L_{\odot})$, where $L/L_{\odot}$ is the luminosity relative to that of the Sun ($L_{\odot} = 3.86 \times 10^{33}$ erg sec^{-1}). [After I. Iben, Jr., 1965 (321).]

Fig. 7-5B The Time Variation of Some Properties of a Pre–Main-Sequence Star of Mass $1\ M_{\odot}$. The abscissa is log t, where t is the time in seconds measured from the initial model of the series for this mass. The upper and lower limits of the scale for each curve are given. The ordinates are M_{CC}/M, the fraction of the mass contained in a convective core; $\log \rho_c$, where ρ_c is the central density in gm cm^{-3}; $\log T_c$, where T_c is the central temperature in degrees Kelvin; and L_g/L, the net fraction of the luminosity that is generated by gravitational contraction (but not necessarily the fraction of the *emitted* radiation that is due to gravitational contraction—see text). The value of L_g/L becomes negative near log t = 15.0: zero for this ordinate is on the horizontal axis. [Adapted from I. Iben, Jr., 1965 (321).]

Fig. 7-5C A Model of Mass $1\ M_{\odot}$ During the Pre–Main-Sequence Phase at Time log t = 14.941. The time is measured in seconds from the initial model of the series for this mass. The abscissa is the fractional mass M_r/M. The upper and lower limits of each ordinate are given. Each upper limit is the maximum value in the model. The ordinates are r, the radius in units of the solar radius ($R_{\odot} = 6.96 \times 10^{10}$ cm); P, the pressure in dyne cm^{-2}; ρ, the density in gm cm^{-3}; T, the temperature in degrees Kelvin; and L_r, the net luminosity in units of the solar luminosity ($L_{\odot} = 3.86 \times 10^{33}$ erg sec^{-1}). [Adapted from I. Iben, Jr., 1965 (321).]

Pre-main Sequence Evolution of a $1\ M_{\odot}$ Star

$\tau < 2 \times 10^{14}$ s (i.e. 7×10^6 yr)

$T_{eff} \sim$ const ~ 4200 K $R \downarrow \Rightarrow L \downarrow$

due to ionization of H & He

a deep convective envelope

$\rho_c / \bar{\rho} \sim$ const   (Hayashi track)

Star completely convective in the first 10^6 yr

L_g / L : energy from gravitational contraction

$\tau \sim 14.5$ $(10^7 yr)$, $L \uparrow$ $\Rightarrow$ nuclear reactions (cont.)

~ 15 $\Rightarrow$ expanding the core

$\rho_c \downarrow$, $T_c \downarrow$

But T_c not high enough

only ${}^1H \rightarrow {}^2D \rightarrow {}^3He$

${}^{12}C \rightarrow {}^{13}N \rightarrow {}^{13}C \rightarrow {}^{14}N$

The rest of PP chains or CNO cycle do not operate yet

Note $L_{nuc} + L_g \equiv L$

$\tau \sim 15$, $L_g < 0$ ($\because$ core expansion)

$\epsilon_{nuc} \uparrow \rightarrow \nabla T \uparrow$

$\Rightarrow$ A temporary convective core ($\tau \sim 14.9$)

until ${}^{12}C$ is depleted and

PP chains become important

Eventually $\nabla T \downarrow$ at core, convective core $\downarrow$

($\tau \sim 15.3$)

$\tau \sim 15$, $L \rightarrow L_{max}$

Structure of star adjusts

∵ Energy sources from gravitational to nuclear processes

⇒ ^{12}C main sequence ! Point 5

short lasting, depletion rapidly

→ slight contraction

T_c, ρ_c high enough for pp reactions to be the sole energy source.

For all stars $M \gtrsim M_\odot$ ⇒ convective core

^{12}C burning → recedes

For stars $M \gtrsim 1.25\, M_\odot$ ⇒ double luminosity maxima and minima

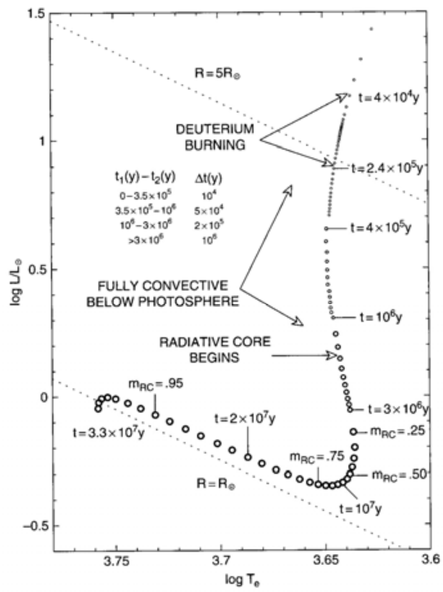

Pre main sequence evolution in the HR diagram of a low mass model ($M = 1M_\odot, Z = 0.01, Y = 0.25$)

Iben 2013

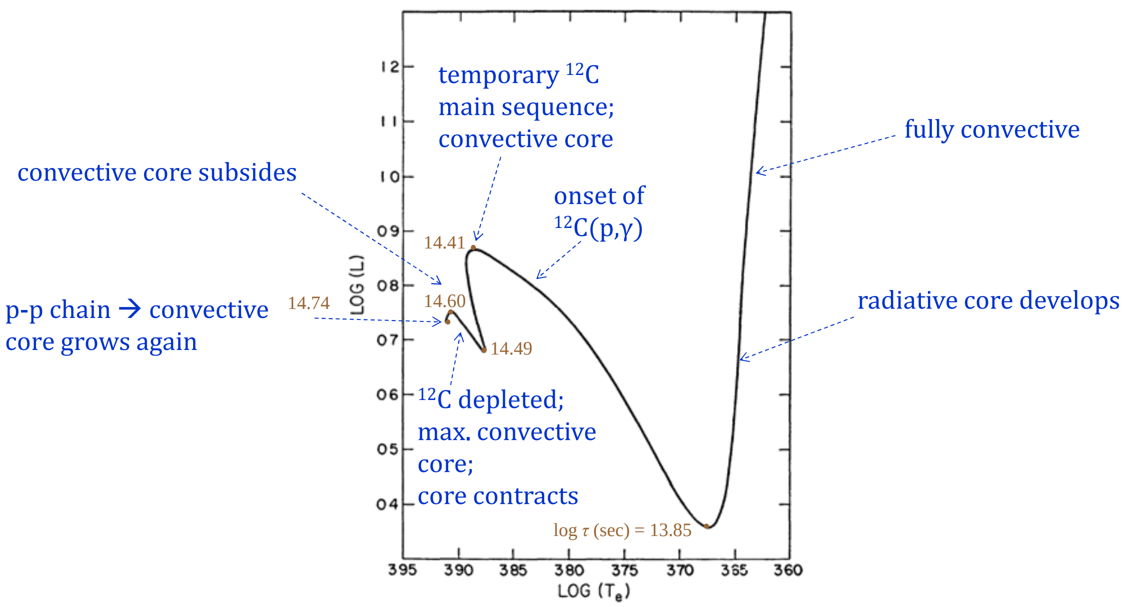

FIG. 6—The path in the Hertzsprung-Russell diagram for $M = 1.5\ M_\odot$. Units of luminosity and surface temperature are the same as in Fig. 1.

For 0.5 $M_\odot$ Stars,

ρ_c, T_c not high enough for ^{12}C burning

For $M \lesssim 0.1\ M_\odot$ (dependent on μ)

T_c not high enough for even H burning

$\Rightarrow$ contraction continues

$\rightarrow$ degenerate core

$\Rightarrow$ black dwarfs ... nowadays called brown dwarfs

only the initial, nearly vertical descent

$\because$ T_c, ρ_c never high enough to ignite ^{12}C

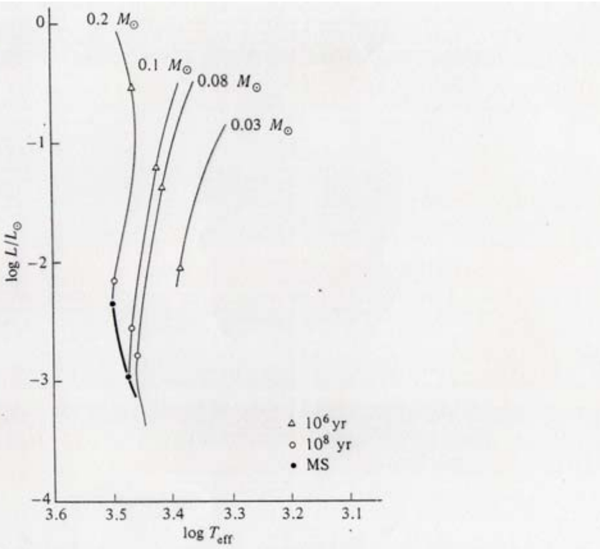

Fig. 7-3B Evolutionary Tracks of Pre-Main-Sequence Stars of Low Mass in the Hertzsprung–Russell Diagram. The masses, and the ages at two points on each track, are indicated. The heavy curve (*MS*) is the hydrogen-burning main sequence. The convective parameter is assumed to have the value $l/H = 1.0$. [Adapted from A. S. Grossman and H. C. Graboske, Jr., 1971 (400).]

Parameters at the stellar cores for non-rotating single MS stars

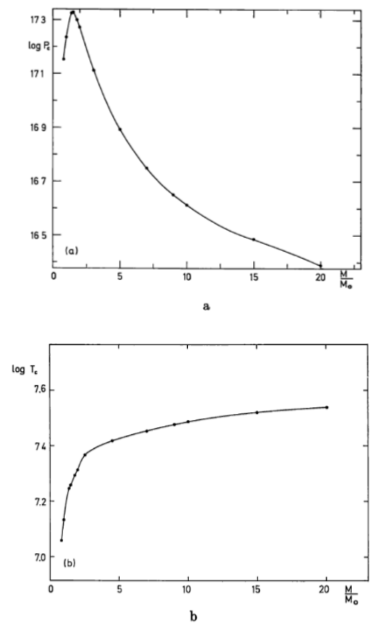

Figs. 3a and 3b. For non-rotating stars, the central pressure and central temperature variation with mass along the main-sequence

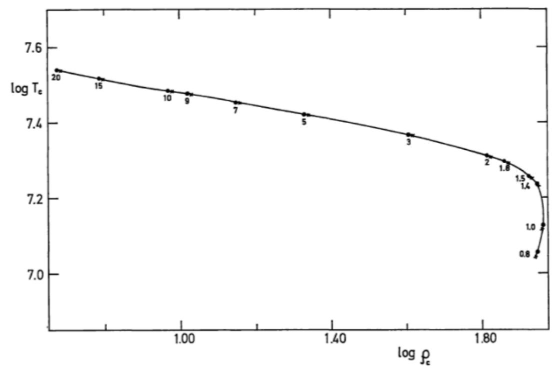

Fig. 4. The central temperature versus the central density for main-sequence stars. The curve is drawn through the data referring to non-rotating stars (dots). The crosses refer to critically, uniformly rotating stars. The Arabic numeral refers to the mass of the model

Sackman (1970) A&A, **8**, 76

Effect of Stellar Rotation

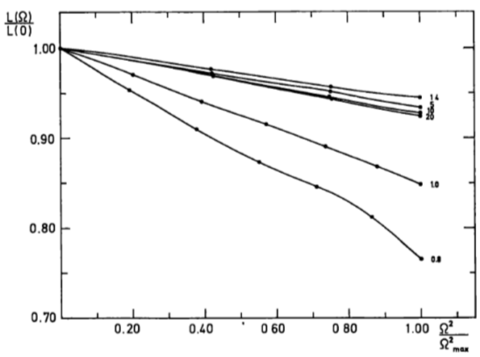

Fig. 1. The decrease of the luminosity with increasing rotation measured by Ω^2/Ω^2_{max}, where Ω refers to the angular velocity of rotation and the subscript max to the critical case. The Arabic numeral refers to the mass of each sequence in solar units

$\frac{\Omega}{\Omega_{crit}} \nearrow \Rightarrow L \searrow$

More so for lower-mass stars

Rotation effectively lowers the stellar mass.

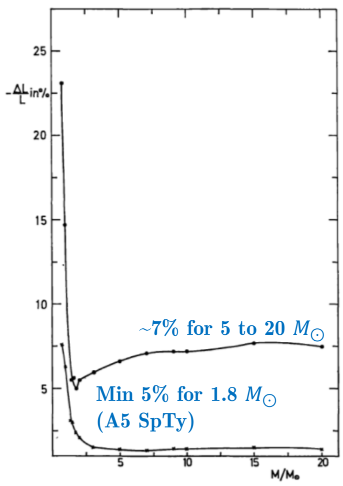

Fig. 5. The maximum change in the luminosity of a critically rotating star from that of a non-rotating star of the same mass, expressed in percent, against the mass of the main-sequence model. The dots refer to the actual results of the Stellar Interior models, while the crosses refer to the approximations made for Eq. (12)

Sackman (1970) ApJ, **8**, 76

Rotation → star cooler and fainter

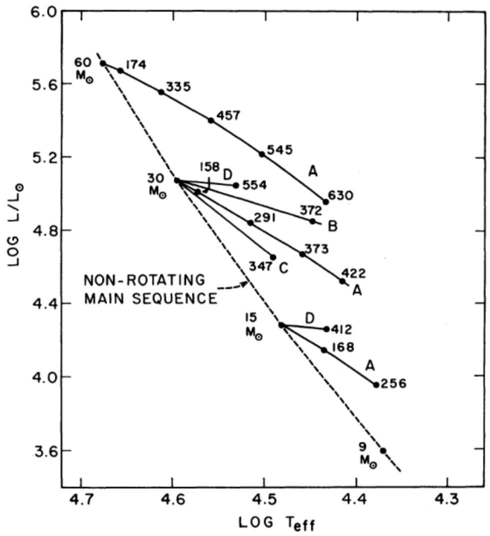

FIG. 2.—Theoretical H-R diagram showing model sequences of increasing angular momentum (*solid curves*). Numbers on curves give calculated velocities at the equator in km sec^{-1}. The distribution of angular momentum for each sequence is indicated by the letter A, B, C, or D.

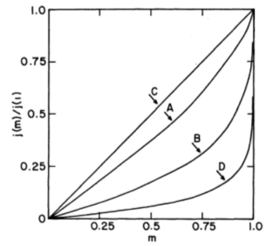

FIG. 1.—Angular momentum per unit mass, as a function of mass fraction interior to a given cylinder about the axis of rotation, for three assumed laws of differential rotation (Cases A, B, and C) and for a uniformly rotating model (Case D) of 30 $\mathfrak{M}_{\odot}$, log J = 52.73.

D: solid body rotation

Rotation law:
angular momentum distribution $j(m_\varpi)$ as a function of, m_ϖ, the mass fraction interior to the cylinder of radius ϖ about the rotation axis.

Bodenheimer (1971) ApJ, **167**, 153

Rotation → line broadening

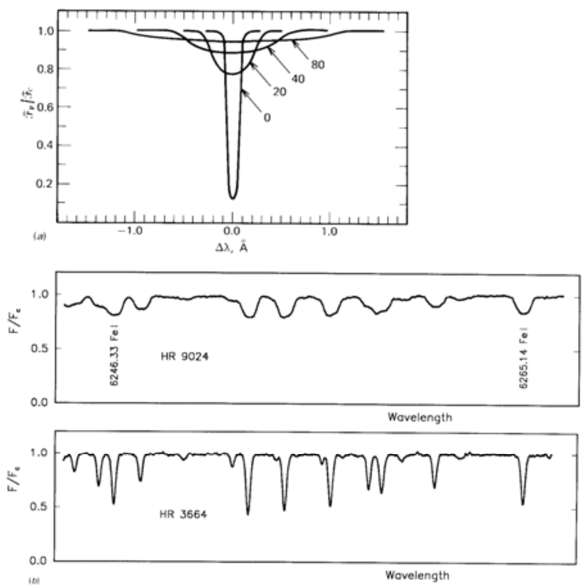

Fig. 17.7. (*a*) Computed profiles illustrate the broadening effect of rotation. The profiles are labeled with $v \sin i$. the wavelength is 4243 Å, and the line has an equivalent width of 100 mÅ. (*b*) These two early-G giants illustrate the Doppler broadening of the line profiles by rotation.

Gray p. 376

Rotation vs Spectral Type

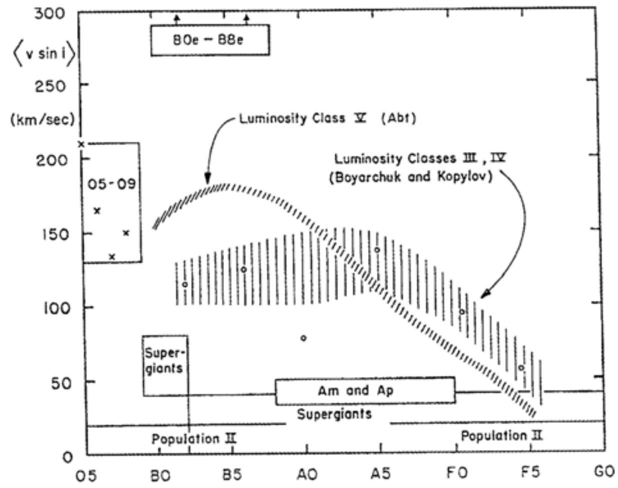

Fig. 3. Projected equatorial velocities, averaged over all possible inclinations, as a function of spectral type. On the main sequence (luminosity class V), early-type stars have rotational velocities that reach and even exceed 200 km/s; these velocities drop to a few km/s for late-type stars, such as the Sun (type G2) (Slettebak [20]; courtesy Gordon & Breach)

15 $M_\odot$

Fig. 7-6 The Time Variation of Some Properties of a Pre-Main-Sequence Star of Mass 15 $M_\odot$. The abscissa is log t, where t is the time in seconds measured from the initial model of the series for this mass. The upper and lower limits of each ordinate are given. The ordinates are M_{CC}/M, the fraction of the total mass contained in a convective core; log ρ_c, where ρ_c is the central density in gm cm^{-3}; log T_c, where T_c is the central temperature in degrees Kelvin; log $(L/L_\odot)$, where $L/L_\odot$ is the luminosity relative to the solar luminosity ($L_\odot = 3.86 \times 10^{33}$ erg sec^{-1}); and L_g/L, the net fraction of the luminosity that is generated by gravitational contraction (but not necessarily the fraction of the *emitted* radiation that is due to gravitational contraction—see text). [Adapted from I. Iben, Jr., 1965 (321).]

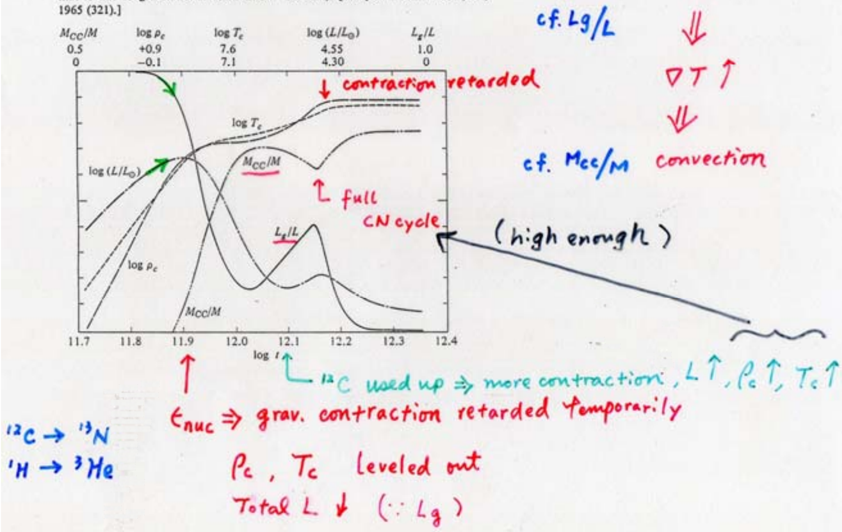

1997AJ....113.1733H

1747 L. A. HILLENBRAND: ORION NEBULA CLUSTER 1747

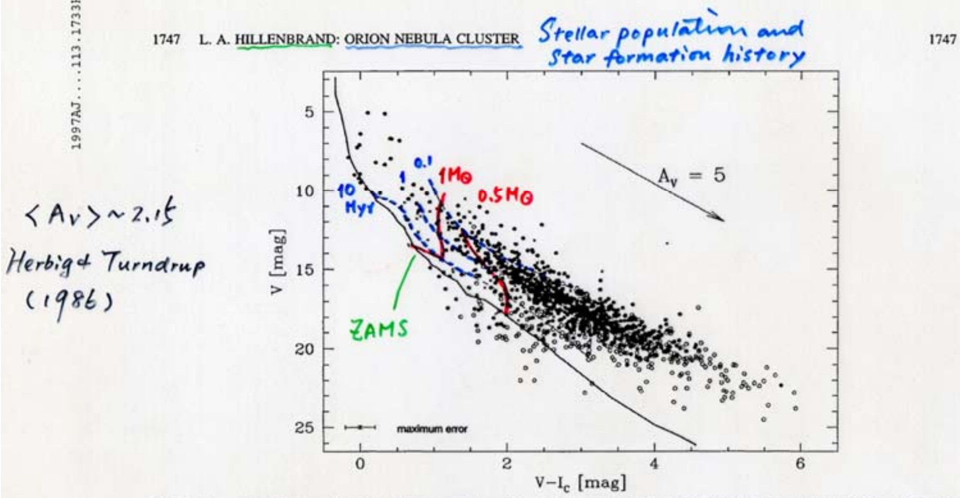

FIG. 7. *Color-magnitude diagram for all stars with measured V- and I-band photometry.* Errors for the new photometry are smaller than 0.05 mag in V and 0.1 mag in $V-I_C$ in 90% of the cases and are restricted in all cases to 0.1 mag in V and 0.2 mag in $V-I_C$, corresponding to the error bar shown. Also shown is the reddening vector corresponding to 5 magnitudes of visual extinction and the zero-age main sequence over the range O5–M7, as well as the 0.1, 1, and 10 Myr isochrones and the 0.5 and 1 $M_\odot$ evolutionary tracks from the calculations of D'Antona & Mazzitelli (1994) translated into this color-magnitude plane. Filled circles indicate proper motion cluster members plus all sources which have been identified as being externally ionized; open circles indicate that no proper motion information is available; crosses indicate proper motion nonmembers.

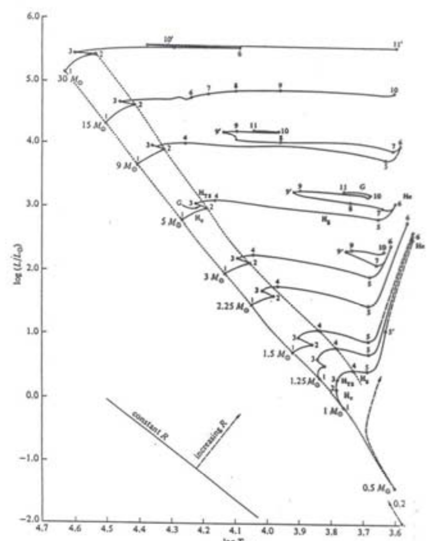

Table 7-7 Evolutionary Times. The times, expressed in years, refer tervals between the points in Fig. 7-25.* [Adapted from I. Iben, Jr., 1967 (327).]

MASS ($M_\odot$) \ INTERVAL	1–2	2–3	3–4	4–5	5–6
30	4.80 (6)	8.64 (4)	←	~1.0 (4)	→
15	1.010 (7)	2.270 (5)	←	7.55 (4)	→
9	2.144 (7)	6.053 (5)	9.113 (4)	1.477 (5)	6.552 (4)
5	6.547 (7)	2.173 (6)	1.372 (6)	7.532 (5)	4.857 (5)
3	2.212 (8)	1.042 (7)	1.033 (7)	4.505 (6)	4.238 (6)
2.25	4.802 (8)	1.647 (7)	3.696 (7)	1.310 (7)	3.829 (7)
1.5	1.553 (9)	8.10 (7)	3.490 (8)	1.049 (8)	≥2 (8)
1.25	2.803 (9)	1.824 (8)	1.045 (9)	1.463 (8)	≥4 (8)
1.0	7 (9)	2 (9)	1.20 (9)	1.57 (8)	≥1 (9)

MASS ($M_\odot$) \ INTERVAL	6–7	7–8	8–9	9–10(?)	10(?)–11(?)
30	←	53.1 (4)	→		1.3 (4)
15	7.17 (5)	6.20 (5)	1.9 (5)	3.5 (4)	
9	4.90 (5)	9.50 (4)	3.28 (6)	1.55 (5)	2.86 (4)
5	6.05 (6)	1.02 (6)	9.00 (6)	9.30 (5)	7.69 (4)
3	2.51 (7)	4.08 (7)		6.00 (6)	

* A number in parentheses is the power of 10 by which an entry is to be multiplied.

Fig. 7-25 Evolutionary Tracks in the Hertzsprung–Russell Diagram. The mass of each star is given at the left of the track. The composition is $X = 0.708$, $Y = 0.272$, and $Z = 0.020$ for all masses except 30 $M_\odot$, for which the composition is $X = 0.70$, $Y = 0.27$, $Z = 0.03$. *Dashed portions* of the curves are estimates. The *letters* along the tracks for 1 $M_\odot$ and 5 $M_\odot$ have the following significance: H_c = hydrogen-burning near the center; G = gravitational contraction of the entire star; H_{TS} = hydrogen-burning in a thick shell; H_s = hydrogen-burning in a thin shell; He = helium-burning near the center plus hydrogen-burning in a thin shell. The times required to reach the encircled points are given in Table 7-7.

The *dotted lines* indicate the boundaries of the main sequence. The *line* (*lower left*) shows the slope of a path along which the radius remains constant. The track for 15 $M_\odot$ does not turn back as do the other tracks because the semi-convective zone was treated as fully convective [see R. Stothers and C.-W. Chin, 1968 (377)]. [Adapted from I. Iben, Jr., 1967 (327). The track for 30 $M_\odot$ is given by R. Stothers, 1966 (333).]

H_c : H core burning
H_{TS} : H thick shell
T_s : H thin shell

Evolution on the Main Sequence

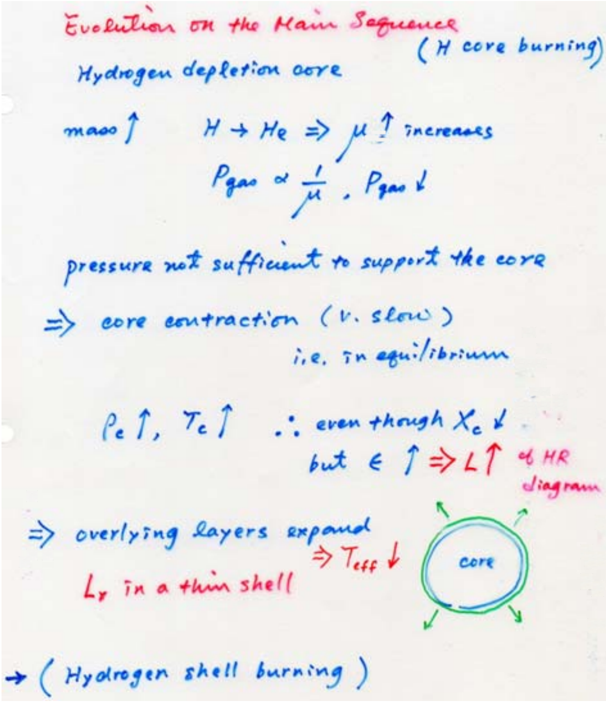
Evolution on the Main Sequence (H core burning)

Hydrogen depletion core

mass ↑ H → He ⇒ μ ↑ increases

$P_{gas} \propto \frac{1}{\mu}$, P_{gas} ↓

pressure not sufficient to support the core

⇒ core contraction (v. slow)

i.e. in equilibrium

ρ_c ↑, T_c ↑ ∴ even though X_c ↓

but ε ↑ ⇒ L ↑ of HR diagram

⇒ overlying layers expand

⇒ T_{eff} ↓

L_r in a thin shell

→ (Hydrogen shell burning)

1-2 main sequence

2-3 overall contraction

3-4 H thick shell burning

5-6 H thin shell burning

6-7 red giant

7-10 core He burning

8-9 envelope contraction

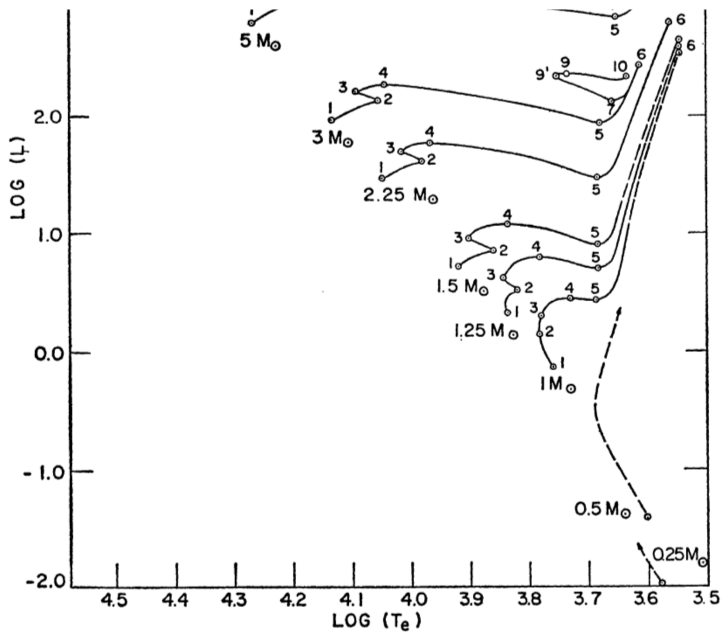

$\frac{dL_r}{dM_r} = \epsilon$ v. high near center

↓ slope

298 Stellar Interiors

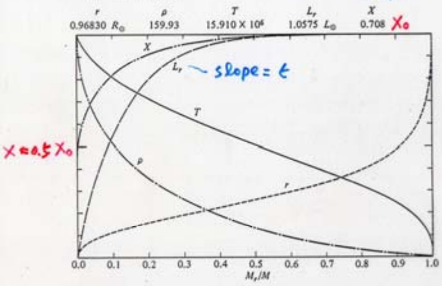

Fig. 7-10A A Model of Mass 1 $M_\odot$ during the Main-Sequence Phase at Time $t = 4.26990 \times 10^9$ Years. Radius r, density ρ, temperature T, net luminosity L_r, and hydrogen abundance X are shown as functions of fractional mass M_r/M. The lower limit of the ordinate is zero for all variables. The upper limits, given in the figure, are the total radius R (units of $R_\odot = 6.96 \times 10^{10}$ cm), central density ρ_c (gm cm^{-3}), central temperature T_c in degrees Kelvin, total luminosity L (units of $L_\odot = 3.86 \times 10^{33}$ erg sec^{-1}), and initial hydrogen abundance $X = 0.708$. The central pressure (not shown) is 2.5186×10^{17} dyne cm^{-2}. The time t is measured from the initial model calculated for the pre-main-sequence phase (see Section 2). [Adapted from I. Iben, Jr., 1967 (326).]

Zero-age Main Sequence (ZAMS)
≡ homogeneous chemical composition

Termination of MS
≡ end of H burning at core

H depletion core
$X \simeq 0$, $L_r \simeq 0$, $\nabla T \simeq 0$
⇒ ϵ_{nuc} in a thin shell

299 Stellar Evolution

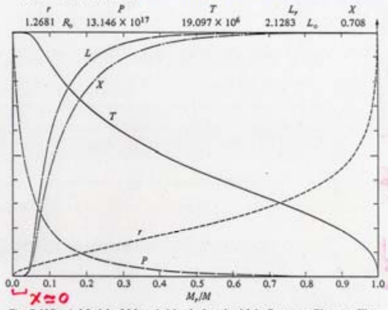

Fig. 7-10B A Model of Mass 1 $M_\odot$ during the Main-Sequence Phase at Time $t = 9.20150 \times 10^9$ Years. Radius r, pressure P, temperature T, net luminosity L_r, and hydrogen abundance X are shown as functions of fractional mass M_r/M. The lower limit of the ordinate is zero for all variables. The upper limits, given in the figure, are 1.2681 $R_\odot$ (with $R_\odot = 6.96 \times 10^{10}$ cm; however, the total radius is 1.3526 $R_\odot$), central pressure P_c (dyne cm^{-2}), central temperature T_c in degrees Kelvin, total luminosity L (units of $L_\odot = 3.86 \times 10^{33}$ erg sec^{-1}), and initial hydrogen abundance $X = 0.708$. The central density (not shown) is 1026.0 gm cm^{-3}. The time t is measured from the initial model calculated for the pre-main-sequence phase (see Section 2). [Adapted from I. Iben, Jr., 1967 (326).]

As τ goes on, $M_{core}^{H=0}$ ↑, until $M_c \sim 0.1\, M_\odot$

Schönberg-Chandrasekhar limit (1942) ApJ 96, 16

maximum fraction of total mass maintainable within an isothermal core

1 $M_\odot$ Stars on the Main Sequence

$4H \rightarrow He$ $n \downarrow \rightarrow P \downarrow \rightarrow$ core contracts (slowly)

$q_{pp} \sim \rho X^2 T_6^4$

H depletion $X \downarrow$ but $T \uparrow$, $\rho \uparrow$

$\therefore q \uparrow \Rightarrow L \uparrow$

(Faint distant sun dilemma)

→ envelope $R \uparrow$

H depleted core $L_r = 0$, but ϵ_{nuc} in a thick shell around the core

$$L_{TS} > L_{core}(MS)$$

$$\Rightarrow L \uparrow \rightarrow R \uparrow \Rightarrow T_{eff} \downarrow$$

Point 4 ≡ End of M.S

Star → subgiant branch

until M_{sc} is reached (~8-10%)

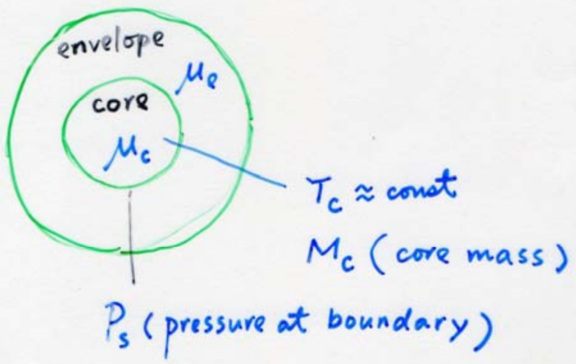

THE ASTROPHYSICAL JOURNAL
AN INTERNATIONAL REVIEW OF SPECTROSCOPY AND ASTRONOMICAL PHYSICS

VOLUME 96 SEPTEMBER 1942 NUMBER 2

ON THE EVOLUTION OF THE MAIN-SEQUENCE STARS

M. Schönberg[1] and S. Chandrasekhar

ABSTRACT

The evolution of the stars on the main sequence consequent to the gradual burning of the hydrogen in the central regions is examined. It is shown that, as a result of the decrease in the hydrogen content in these regions, the convective core (normally present in a star) eventually gives place to an isothermal core. It is further shown that there is an upper limit (∼ 10 per cent) to the fraction of the total mass of hydrogen which can thus be exhausted. Some further remarks on what is to be expected beyond this point are also made.

$$\frac{M_c}{M} \approx 0.37 \left(\frac{\mu_e}{\mu_c}\right)^2 \quad (\sim 10\text{-}15\% \text{ in reality})$$

Take ionized H in env ($\mu = 0.61$); pure He in core $\mu = 1.34$

$M_c \sim 8\text{-}9\%\ M$ $\mu_c \sim 2\,\mu_e$

Beech 1988

(Point 4, 5) Shortly after the MS

- ϵ_{nuc} in a thin shell

L_r ↑↑ between 13% - 20%

core experiences gravitational contraction $L_g > 0$

$\Rightarrow \nabla T$

$\rho_c \to 1.5 \times 10^4\ g\,cm^{-3}$, P_{deg} important ($= 0.46\, P_{total}$)

- convection beyond 63% M → mixing → $X \approx$ const

(Point 5′) $P_{deg} = 76\%\ P_{total}$

$T_{shell}\uparrow\uparrow$ $\epsilon_{CN} > \epsilon_{pp} \Rightarrow R\uparrow\uparrow,\ T_{eff}\downarrow\downarrow$

$\kappa\uparrow$ in envelope → convection for outer 71 ~~20~~ 71% M

X ≈ const ~~for outer~~ 29% M beyond

∇T in core ← grav. contraction

$\rho_c = 1.5\times10^4\ g\,cm^{-3} \Rightarrow P_{deg} = 46\%$ of P_{total}

ϵ in a shell

So $M_c > M_{sc}$ OK

L_r used to push envelope

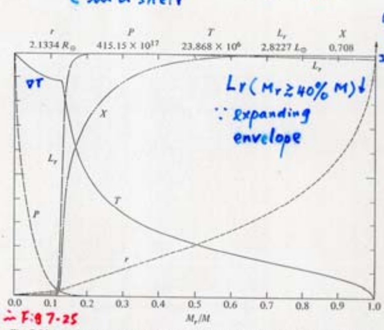

H-5 ≐ Fig 7-25

Fig. 7-26A A Model of Mass 1 $M_\odot$ Shortly after Leaving the Main Sequence, at $t = 10.3059 \times 10^9$ Years. Radius r, pressure P, temperature T, net luminosity L_r, and hydrogen abundance X are shown as functions of fractional mass M_r/M. The lower limit of the ordinate is zero for all variables. The upper limits, given in the figure, are 2.1334 $R_\odot$ (with $R_\odot = 6.96 \times 10^{10}$ cm; however, the total radius is 2.2179 $R_\odot$), central pressure P_c (dyne cm^{-2}), central temperature T_c (°K), total luminosity L (units of $L_\odot = 3.86 \times 10^{33}$ erg sec^{-1}), and initial hydrogen abundance $X = 0.708$. The central density (not shown) is 15,214 gm cm^{-3}. The time is measured from the initial model calculated for the pre-main-sequence phase (see Section 2). [Adapted from I. Iben, Jr., 1967 (326).]

X ≈ const > 63% M ∵ convection (mixing)

$\rho_c \sim 10^5\ g\,cm^{-3}$ $\frac{P_{deg}}{P_{tot}} \sim 76\%$

$T_s\uparrow\uparrow \Rightarrow \epsilon_{CN} > \epsilon_{pp}$

X(M > 30%) ≈ const ∵ convection

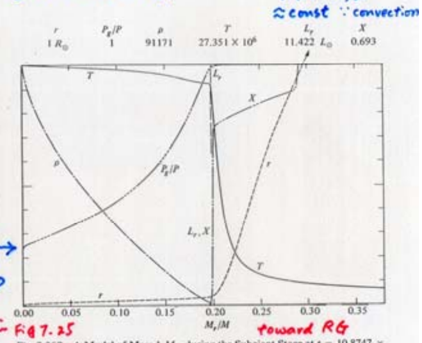

5′ ≐ Fig 7.25 toward RG

Fig. 7-26B A Model of Mass 1 $M_\odot$ during the Subgiant Stage at $t = 10.8747 \times 10^9$ Years. Radius r, ratio P_g/P of gas pressure computed from the perfect gas law to the actual pressure with degeneracy included, temperature T, net luminosity L_r, and hydrogen abundance X are shown as functions of fractional mass M_r/M in the range 0 to 0.38. The distribution of L_r is a step function rising from zero to maximum scale with the initial rise in X. The lower limit of the ordinate is zero for all variables. The upper limits, given in the figure, are 1 $R_\odot$ (with $R_\odot = 6.96 \times 10^{10}$ cm; however, the total radius is 6.1784 $R_\odot$), unity for the ratio of pressures, central density ρ_c (gm cm^{-3}), central temperature T_c (°K), total luminosity L (units of $L_\odot = 3.86 \times 10^{33}$ erg sec^{-1}), and hydrogen abundance $X = 0.693$. The central pressure (not shown) is 6552.2 dyne cm^{-2}. The time is measured from the initial model calculated for the pre-main-sequence phase (see Section 2). [Adapted from I. Iben, Jr., 1967 (326).]

Envelope expands and cools

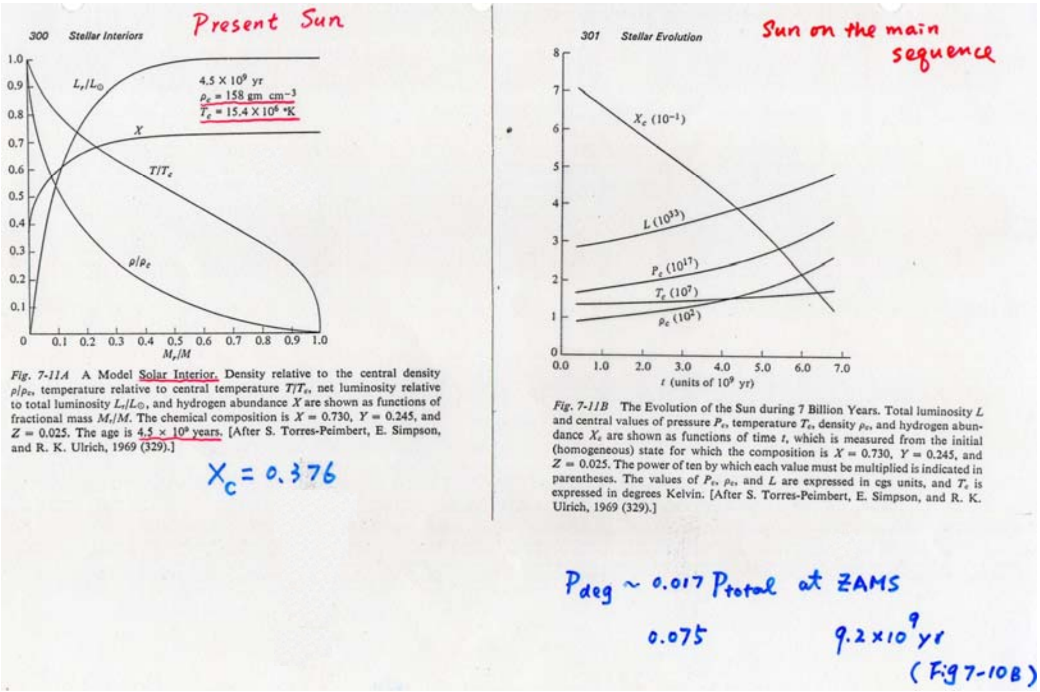

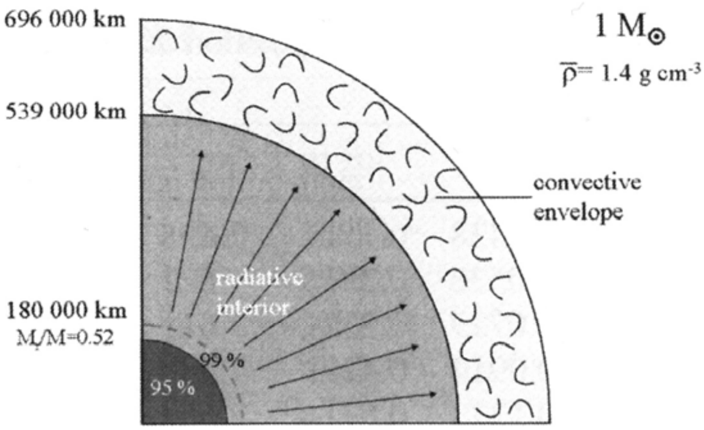

T_6 = 15.5	7.5	1.5	T= 5 800 K
ρ = 160	19	0.09	g cm^{-3}

Figure 3.2. The present structure of the Sun. The physical parameters are indicated in the figure. The temperature T_6 is in million K. *From Maeder (2009).*

Lequeux 2013

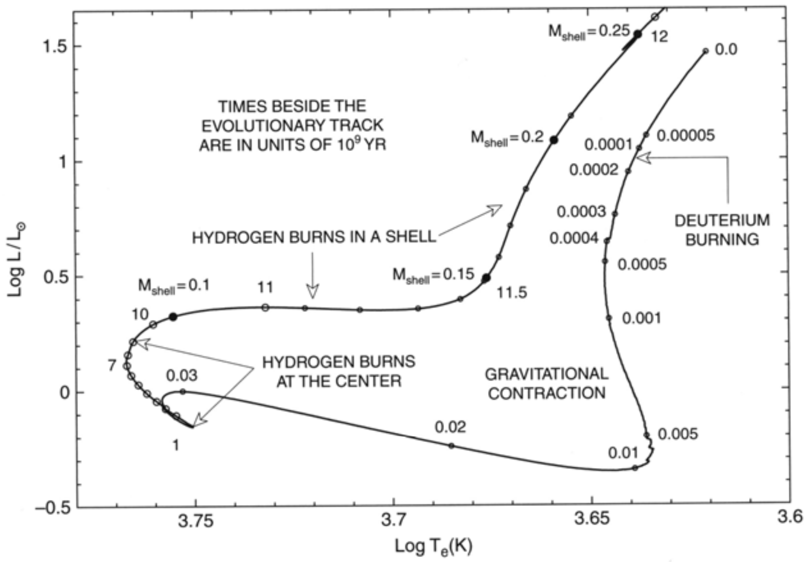

Evolutionary track of a $1M_\odot$ model ($Z = 0.015$, $Y = 0.275$) during gravitational contraction and central and shell hydrogen-burning phases

Iben 2013

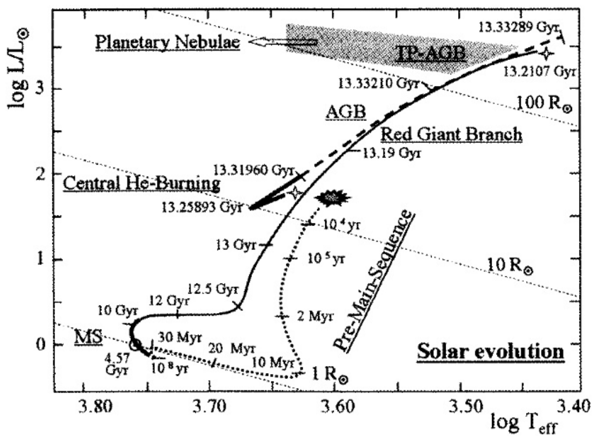

Figure 3.1. The evolution of the Sun. The evolution track of a solar-mass star is shown in the HR diagram from its formation to its death as a planetary nebula. Time is indicated at different steps along the track. The two 4-branch stars correspond to the helium flash and to the subsequent rapid rearrangement of the structure of the star. *From Maeder (2009), data from Corinne Charbonnel.*

Lequeux 2013

Effect of Chemical Composition

As $X\uparrow$ a $Z\uparrow$

$\Rightarrow$ MS shifts upwards

Given a mass, shifted to the right and downwards

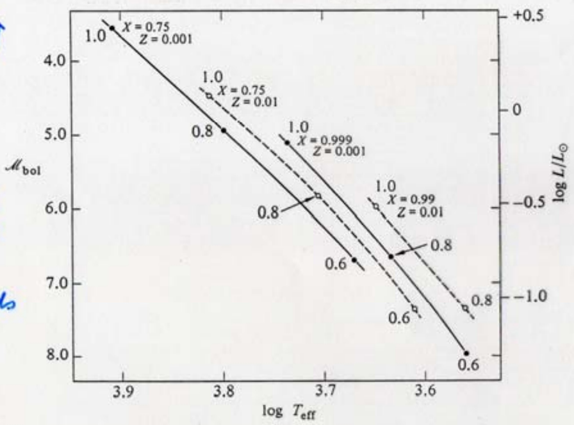

Fig. 7-15A The Effect of Chemical Composition on the Main Sequence in the Hertzsprung–Russell Diagram. Each curve is calculated for a different chemical composition. The masses 0.6 $M_\odot$, 0.8 $M_\odot$, and 1.0 $M_\odot$ are indicated. [From P. Demarque, 1960 (369).]

For Pop I $\left(\begin{array}{c} 0.57 \lesssim X \lesssim 0.77 \\ 0.01 \lesssim Z \lesssim 0.03 \end{array} \right)$ $\Delta m_{bol} \sim 0.8$ mag for 1 $M_\odot$

Pop II similar range in Δm_{bol}

Main Sequence phase = core H burning

Evidence of thermonuclear reactions at a star's center, i.e., stellar evolution

- (solar) neutrinos
- heavy elements in evolved stars
  (isotope ratios ≠ YSOs)

  'dredge-up' ← convective zone to bring processed materials to surface
- Stars "disappear", e.g., supernovae

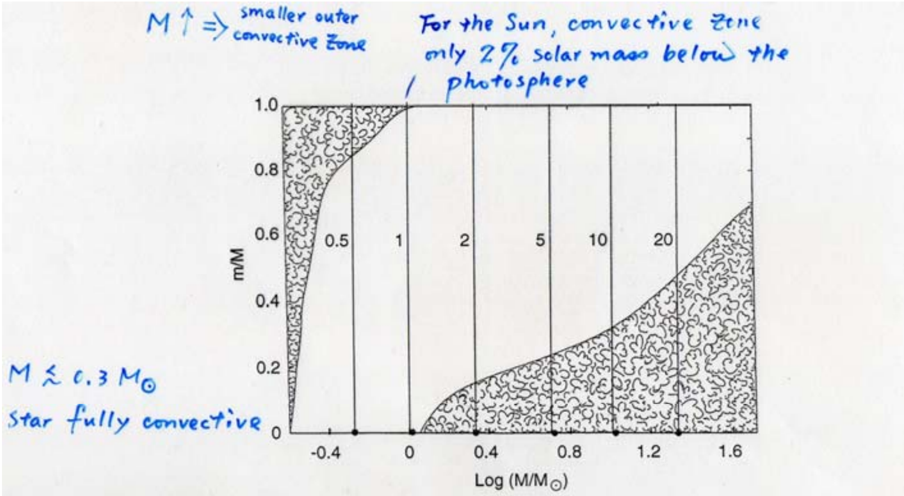

Figure 8.4 The extent of convective zones (shaded areas) in main-sequence star models as a function of the stellar mass [adapted from R. Kippenhahn & A. Weigert (1990), *Stellar Structure and Evolution*, Springer-Verlag].

Subdwarfs: The Pop II Main Sequence

- Luminosity class VI
- 1.5 to 2 mag fainter than a Pop I MS stars o the same spectral type
- Low metallicity → low opacity → (UV excess) → low radiation pressure, so smaller, hotter for the same stellar mass

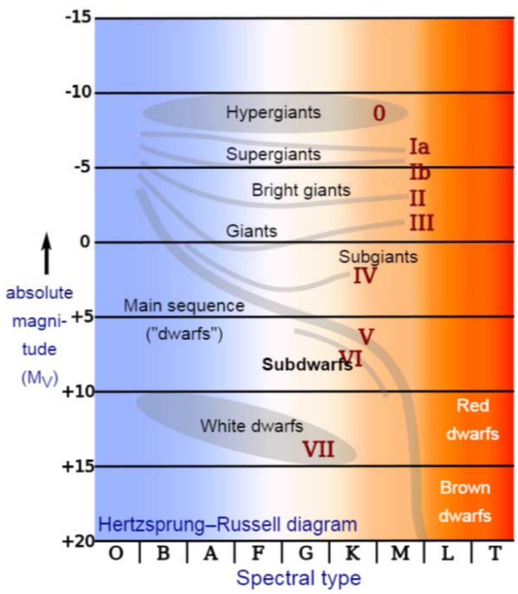

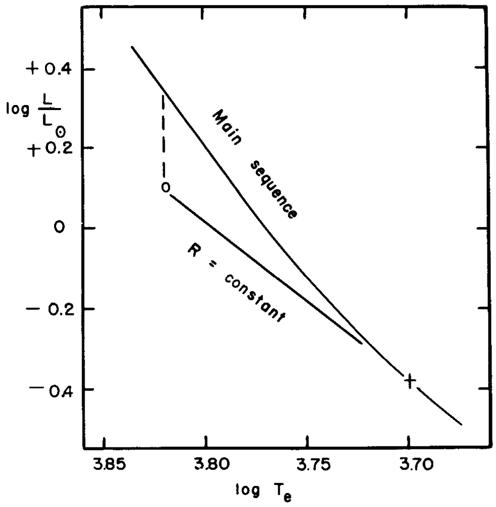

Fig. 17.1. Relation of subdwarfs to the main-sequence in the Hertzsprung-Russell diagram.

Schwarzschild

Post-main Sequence Evolution

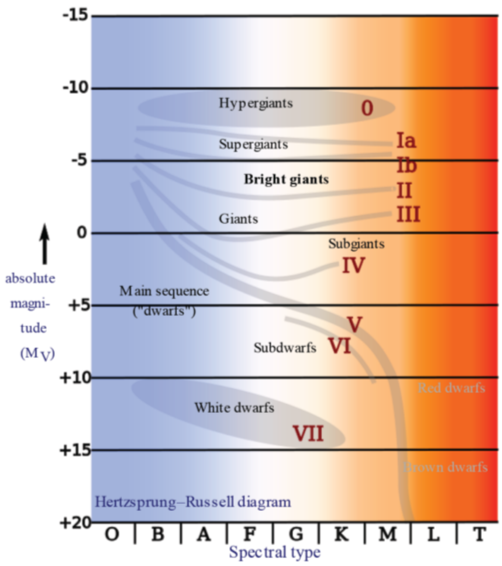

http://en.wikipedia.org/wiki/File:HR-diag-no-text-2.svg

Hypergiants
luminosity class 0; excessive mass loss

Supergiants
Ia luminous supergiants;
Ib supergiants; $Ia^{+} = 0$

Subgiants
luminous class IV; between MS turn-off and the red giant branch

Dwarfs
luminosity class V = MS stars

Subdwarfs (sd)
luminosity class VI, 1.5 to 2 mag lower than MS; lower metallicity

2

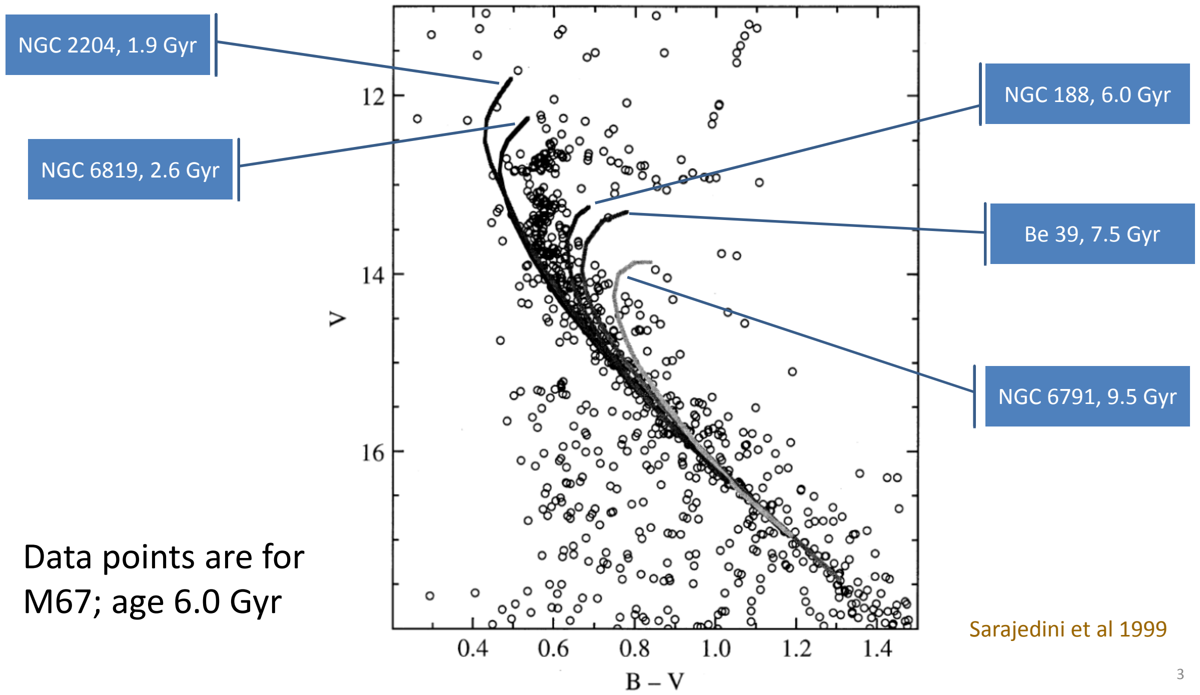

Data points are for M67; age 6.0 Gyr

3

Mass Loss during Stellar Evolution

- Stars lose mass at all evolutionary stages.
- Pre-main sequence: protostellar (bipolar) outflows

  YSO jets, (star/disk) winds
- Main sequence: solar wind $\dot{\mathcal{M}} = 10^{-14}\ M_\odot\ \mathrm{yr}^{-1}$

  For $\tau_{\rm MS} \approx 10^{10}$ yr → $\tau_{\rm loss,MS} \approx 10^{-4}\ M_\odot$

  Some stars, e.g., WR stars $\dot{\mathcal{M}} = 10^{-5}\ M_\odot\ \mathrm{yr}^{-1}$
- Post-main sequence: $R \uparrow \longrightarrow g \downarrow$, and $P_{\rm rad} \uparrow \Longrightarrow \dot{\mathcal{M}} \uparrow$

4

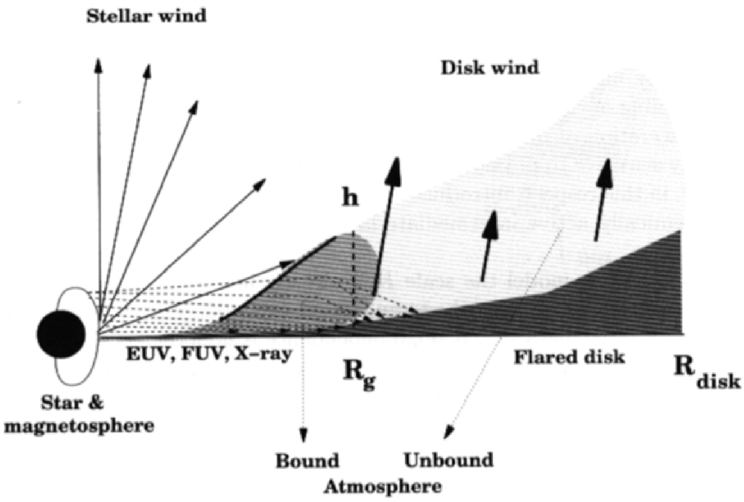

Fig. 7.6. Schematic representation of an irradiated flared disk. Below the radius R_g where matter remains bound by the gravity of the central star an optically thin atmosphere develops. Above this radius flared matter may escape and form some kind of slow wind. Adapted from Hollenbach et al. [403].

Schulz

5

- For a stationary, isotropic wind, the mass loss rate

$$\dot{\mathcal{M}} = 4\,\pi r^2\,\rho(r)\,\frac{\mathrm{dr}}{\mathrm{d}t} = 4\,\pi r^2\,\rho(r)\,v(r)$$ $v(r)$: velocity law

- $v(r)\uparrow$, at $r \to \infty$, $v_\infty \equiv v(r \to \infty)$ terminal velocity

Often $v(r) \approx v_0 + (v_\infty - v_0)\left(1 - \frac{R_*}{r}\right)^\beta$, where

$v_0 = v(R_*)$ at photosphere

- $\beta \le 1, v \to v_\infty$ gradually $\quad \beta \ge 1, v \to v_\infty$ slowly
- For hot stars, $\beta \approx 0.8$. Cool stars experience slower acceleration, so have larger β.

6

$$\dot{\mathcal{M}} = 4\,\pi r^2\,\rho(r)\,v(r)$$ mass conservation

$$\ddot{r} = -\frac{1}{\rho}\frac{\mathrm{d}P}{\mathrm{d}r} - \frac{GM}{r^2} = \frac{\mathrm{d}v}{\mathrm{d}t} = \frac{\mathrm{d}v}{\mathrm{d}r}\frac{\mathrm{d}r}{\mathrm{d}t} = v\frac{\mathrm{d}v}{\mathrm{d}r}$$ momentum conservation

Massive stars → radiation pressure → outer atmosphere expands supersonically → winds driven by spectral-line opacity in UV.

7

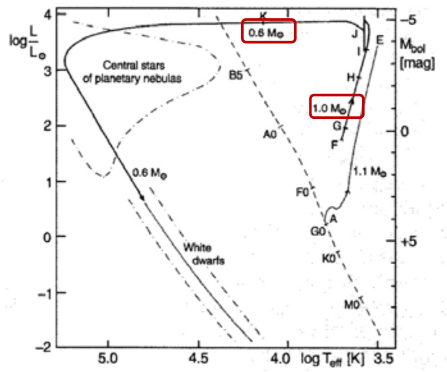

Fig. 8.8. The evolutionary paths in the Hertzsprung–Russell diagram of Population I stars having 1.0 $\mathcal{M}_\odot$ and 1.1 $\mathcal{M}_\odot$, from central hydrogen burning (A) to the helium flash (E), without taking mass losses into account. After A. V. Sweigart and P. G. Gross (1978). The ejection of a mass of 0.1 $\mathcal{M}_\odot$ during the helium flash was assumed. The further evolution of the star of 1.0 $\mathcal{M}_\odot$ was calculated taking the mass loss according to (7.105) into account, after D. Schönberner (1979). F → G: the asymptotic giant branch; only one of the thermal pulses (helium flashes) which occur after I is drawn in, at J. The mass loss becomes important at H and leads to a final mass of 0.6 $\mathcal{M}_\odot$, which is reached at K

Mass loss (Reimers 1975)

$$\dot{M} \approx 4\times10^{-13}\,\frac{L/L_\odot}{(g/g_\odot)\;(R/R_\odot)}\;[\mathrm{M}_\odot\,\mathrm{yr}^{-1}]$$

$$g = GM/R^2$$

Sun now $\dot{M} \approx 2\times10^{-14}\ \mathrm{M}_\odot\,\mathrm{yr}^{-1}$

Cool supergiant $\dot{M} \approx 10^{-7}$ to $10^{-5}\ \mathrm{M}_\odot\,\mathrm{yr}^{-1}$

Unsöld

8

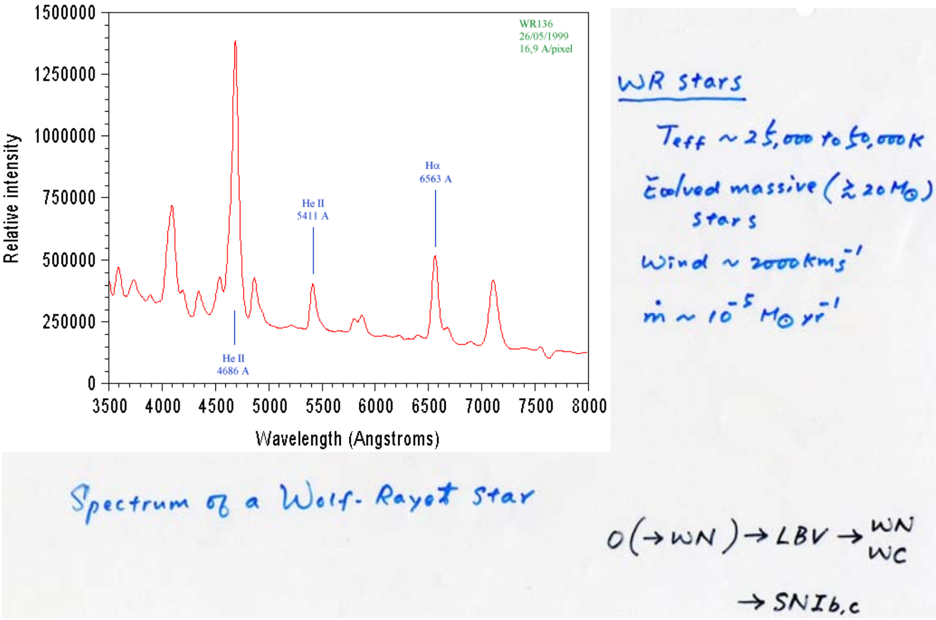

9

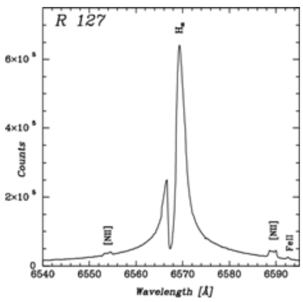

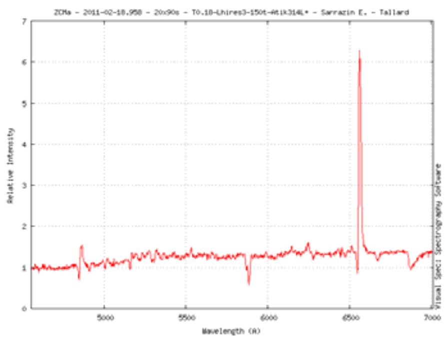

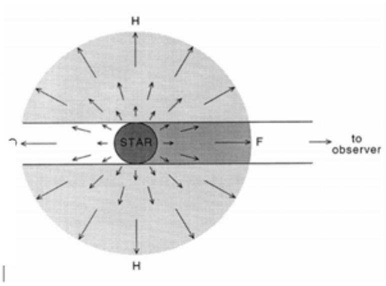

P Cygni profile of a spectral line --- a blue-shifted absorption superimposed on an emission line → **mass loss** (cool gas toward us)

Lamers and Cassinelli, *Introduction to Stellar Winds*, Cambridge, 1999

10

P Cygni stars

- Higher mass-loss rate, $> 10^{-5}\,\mathrm{M_\odot\,yr^{-1}}$
- Lower terminal velocity, $v_\infty < 10^{2.5}\,\mathrm{km\,s^{-1}}$
- Higher wind density, $n_H > 10^{10}\,\mathrm{cm^{-3}}$ at 2 R_*

than normal stars (Lamers 1986).

11

Effects of metallicity

RGB for a Pop II 1.2 $\mathrm{M_\odot}$ star

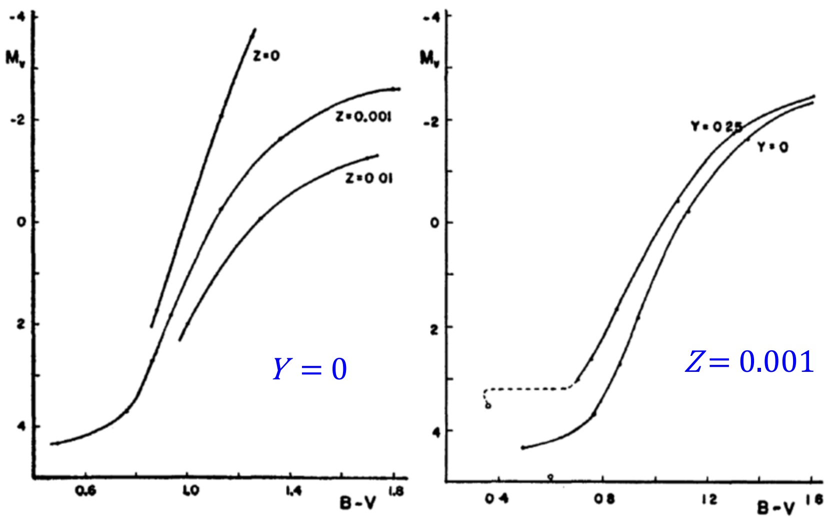

Demarque & Geisler (1963)

12

Next Tuesday (May 30) is a holiday, again.

A make-up class on June 5 (Monday) at 3 pm? June 7 (Wednesday) at 3 pm?

13

Stellar Pulsation

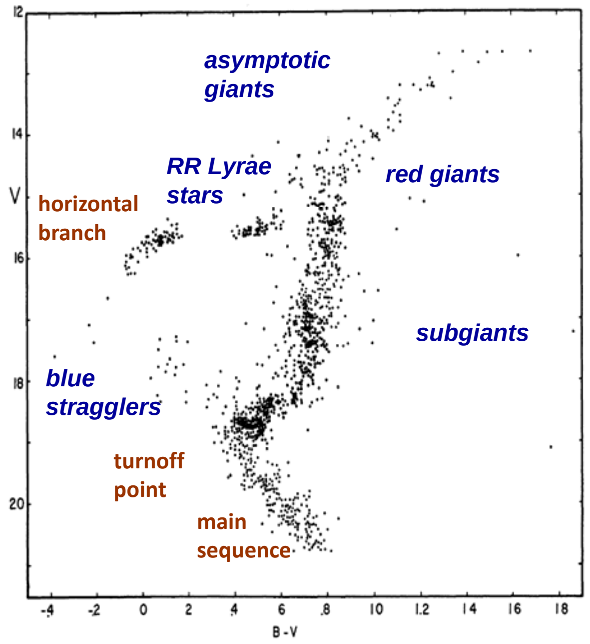

FIG. 5.—Color-magnitude diagram for M3 stars in the arguments V and $B - V$

15

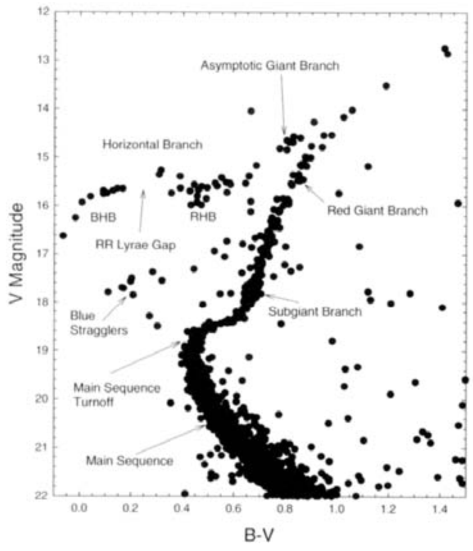

Figure 5.26 A color-magnitude (H–R) diagram of the globular cluster M3, with features mentioned in the text pointed out. Data from Rey et al. (2001).

16

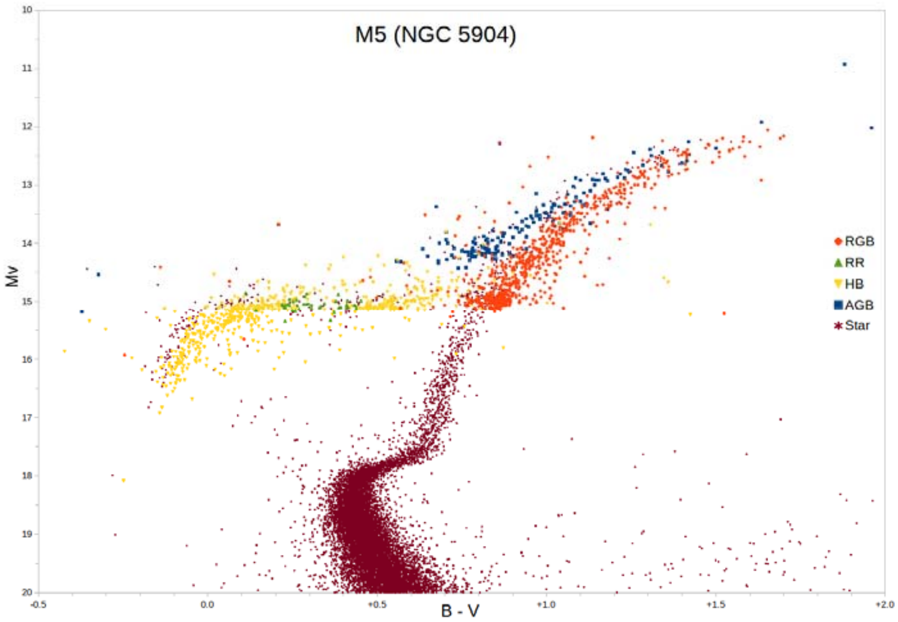

https://en.wikipedia.org/wiki/Subgiant#/media/File:M5_colour_magnitude_diagram.png

17

Stellar Variability

- Time to transmit a perturbation of pressure changes across the star

$$t_{\text{vib}} \sim \frac{2R}{\bar{v}_s} \quad \text{where} \quad v_s = \sqrt{\gamma \frac{P_g}{\rho}}$$

$\gamma = c_P/c_V = 5/3$ for monatomic gas.

- Virial theorem, $2K + \Omega = 0$, $\therefore$ $\quad v_s^2 = \frac{GM}{R}$

$$t_{\text{vib}} \sim \frac{2R}{\sqrt{GM/R}} \sim \frac{1}{\sqrt{G\rho}}$$

cf. free-fall time

18

Approximate Relation between Stellar Density, Pulsation and Minimum Rotational Period

Star	Density g cm^{-3}	t_{vib} sec	$t_{rot, min}$ sec
Neutron star	10^{15}	10^{-4}	3×10^{-4}
White Dwarf	10^{7}	1	3
RR Lyrae star	10^{-2}	$10^{4.5}$	10^{5}
Cepheid Variable	10^{-6}	$10^{6.5}$	10^{7}

t (Crab Nebula) ~ 33 ms → cannot be a white dwarf

- ❖ **Rotational Variation** --- sub-seconds .. weeks
- ❖ **Pulsational Variation** --- hours .. weeks
- ❖ **Orbital (Eclipsing Binaries)** --- hours .. days

19

Valve mechanism (Eddington)

- Heating → P↑ → expansion → cooling

  ∴ Self-regulated stability

- Absorption of radiation
- Usually $\kappa \propto T^{-n}$

  ∴ Heating $\xrightarrow{IF}$ T↑ → κ↓ → cooling

- contraction → releases energy

  expansion → absorbs energy

Normally T ↗ → κ ↘

Recall Kramers opacity

20

κ mechanism — a partially ionized layer to absorb energy during compression (and release energy during expansion)

In stars, there are 2 ionization zones

— $T \sim (1-1.5)\times 10^4$ K hydrogen ionization zone

HI → HII, HeI → HeII

— $T \sim (4-5)\times 10^4$ K

HeII → HeIII helium ionization zone

But if there is an ionization layer, e.g., $He^+ \rightarrow He^{++}$

$T \nearrow \rightarrow \kappa \nearrow$
energy trapped
→ expansion

Energy escaped
→ Contraction

➔ <u>pulsation</u>

21

Depths of ionization zones

e.g. $T_{eff} \gtrsim 7500$ K, zones near surface

→ not enough mass available to drive the oscillation.

$T_{eff} \gtrsim 5500$ K, zones deeper

⇒ significant <u>pulsation</u>

$T_{eff} < 5500$ K, convective outer layer

→ pulsation suppresses

∴ $T_{eff} \sim 5500-7500$ K for pulsation to take place. Instability "strip"

There is a certain surface temperature range for stellar pulsation …

22

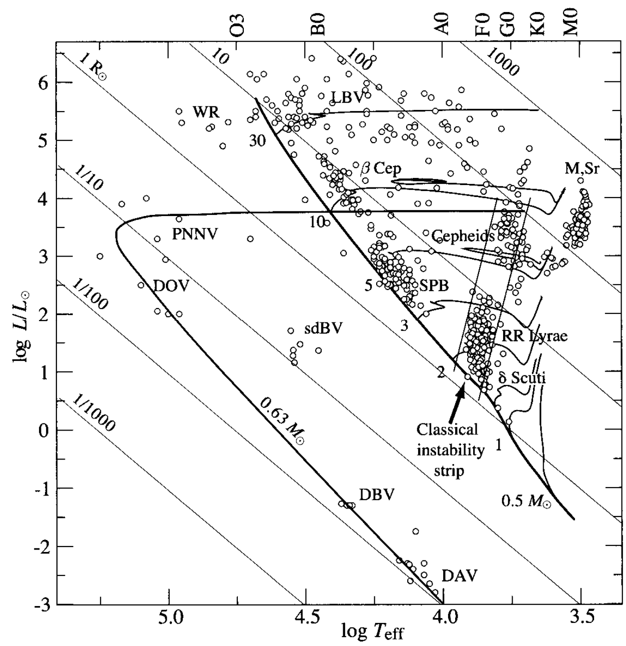

Figure 4.9. Examples of various types of pulsating variable stars plotted as small circles on the Hertzsprung–Russell diagram. The dark line to the right is the main sequence with evolutionary tracks branching off to the right for different stellar masses. The ultimate evolutionary track of a star that ends its life as a compact star of 0.63 $M_\odot$ is shown. It moves leftward through the planetary nebulae nuclei variables (PNNV) and then downward as a cooling white dwarf, passing through regions of pulsational instability sequentially classified as DOV, DBV, and DAV (DAV = Dwarf + type/temperature A + Variable). Other types of intrinsic variables are shown: β Cephei stars, Mira (M), Semiregular (Sr), luminous blue (LBV), Wolf–Rayet (WR), slowly pulsating B stars (SPB), and subdwarf B stars (sdBV). The *classical instability strip* is shown as two parallel lines encompassing Cepheid, RR Lyrae, and δ Scuti variables; if extended, it intersects the pulsating DAV stars. The thin lines represent loci of constant radius. [Provided by A. Gautschy; see Gautschy H. Saio, *ARAA* **33**, 77 (1995)]

Bradt "Astrophycs Processes"

23

Normally, $T \uparrow \Rightarrow \kappa \downarrow$

plays a role also in red giants

Core → increased energy output

Envelope → expansion, cooling → $\kappa \uparrow$

⇒ Red giants have convective envelopes.

cf PMS Hayashi tracks

The envelope extends from just outside of the H-burning shell to the surface.

→ 'Dredge-up' of processed material from deep interior to surface

24

e.g., observations of heavy elements or
isotope ratios in evolved stars different
from (enrichment) young stars
(in a star cluster)

⇒ Evidence of stellar evolution
" of nuclear reactions.

Convection → chemical mixing

Much more efficient than the slow change of chemical composition produced by nuclear reaction.

In a convection region, $\frac{\partial X_i}{\partial m} = 0$

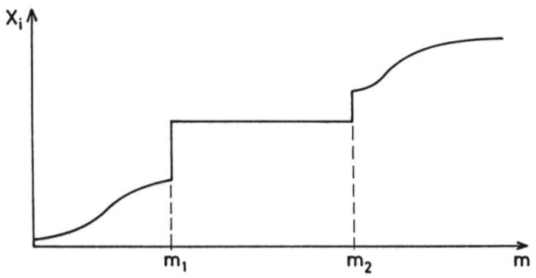

Fig. 8.1. The abundances X_i are smeared out owing to rapid mixing inside a convection zone extending from m_1 to m_2. At these borders X_i can be discontinuous

Kippenhahn & Weigert

The Dredge-ups

When H shell burning begins, the He core contracts and heats up, making the shell burn furiously. The input of energy forces the envelope to expand and the star moves up the "red giant branch" (RGB). But the furiously burning shell runs on the CNO cycle and now the envelope becomes convective because of the low temperature, high opacity, and high temperature gradient, and processed material from the core mixes for the first time with the envelope. We call this the first dredge-up which should be visible in the spectrum of the photosphere as an increase in N at the expense of C and O.

27

For stars more than half a solar mass, the (gravitationally) contracting and heating He core will reach ignition temperature for triple alpha, and the star will (after a possibly traumatic He-flash start) begin life on the "helium burning main sequence". When the He is exhausted in the core (the H-burning shell never provides enough He to keep the core going very long) the He begins shell burning, and now the star rapidly moves up **the AGB, the Asymptotic Giant Branch**. Now begins a **second dredge-up** where for the first time new elements (C N and O) appear in the star's photosphere. The triple alpha shell is really unstable and generates thermal pulses rather than a clean burn. The C core is nearly degenerate at the C-He boundary. The boundary shrinks, heats up, triple alpha starts, pulses, and the explosion may shut

28

itself down. The pulse is quite muffled by the outer layers of the star. But during a pulse the process can actually initiate more complicated fusion processes including neutron generation which can synthesize heavier elements. So for the first time new elements can be dredged up during the AGB phase of stellar evolution. Now these giant stars all have associated strong stellar winds and so can contribute to the chemical evolution of the cosmos.

29

But why wait for a dredge-up? Really massive O stars evolve in a really short time and lose their outer layers due to strong stellar winds really fast. There is a class of stars, the **Wolf-Rayet** or WR stars whose spectra are helium-rich and hydrogen-deficient which are thought to have lost their outer layers revealing directly the by-products of the CNO cycle (original CNO recycled to mostly N -- WN stars) or even the triple alpha (first production of new elements, mainly C -- WC stars). Almost all WR stars are binary stars which may help the envelope stripping process.

30

The Dredge-ups

H shell burning → He core ↓, T ↑ (feeds back to H shell burning)

⇓

envelope expands → red giant branch (RGB)

↓

CNO cycle → low T, high opacity, ∇T ↑

∴ convective envelope

↓

Material in the core brought up and mixed with envelope

⇒ The (first) dredge-up

Photosphere observed N ↑ at the expenses of C and O

31

He flash

If $M > 0.5 M_\odot$ → He core burning (He "main sequence")

(lasting v. short)

He shell burning → asymptotic giant branch (AGB)

⇒ The second dredge-up

3 α process → unstable → thermal pulses

Heavy elements in spectra of evolved stars ↔ YSOs ⇒ obs. test of stellar evolution

32

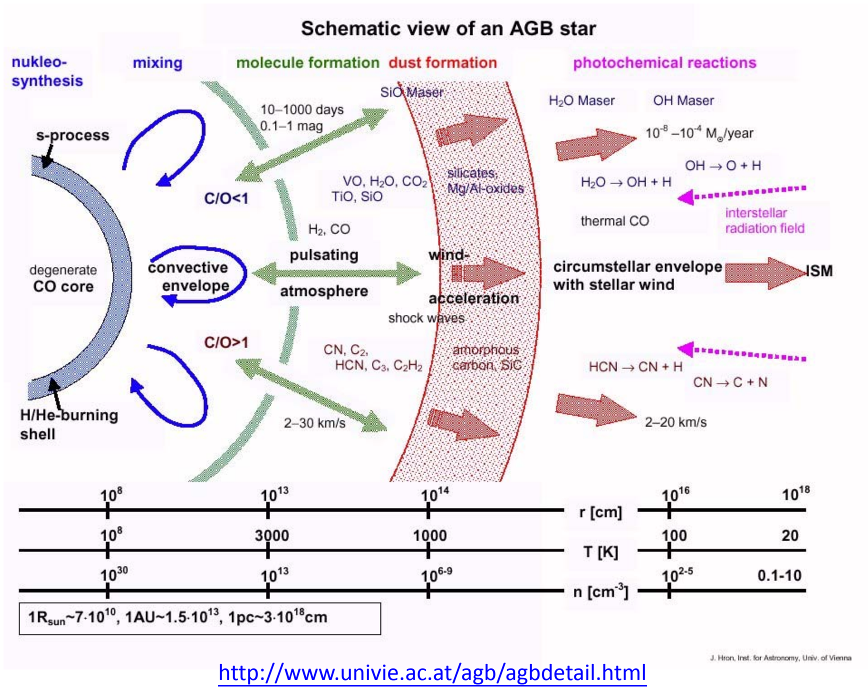

http://www.univie.ac.at/agb/agbdetail.html

33

Electron Degeneracy

34

Fermi-Dirac distribution for non-interacting, indistinguishable particles obeying Pauli exclusion principle; applicable to half-integer spin in TE. Examples of fermions include the electron, proton, neutrons, ^{3}He (2 e^{-}, 2 p^{+}, 1 n^{0})

Bose-Einstein distribution for particles not limited to single occupancy of the same energy state. i.e., that do not obey Pauli exclusion principle; with integer values of spin. Example bosons include ^{4}He, the Higgs boson, gauge boson, graviton, meson.

35

A Fermi gas is called degenerate if the temperature is low in comparison with the Fermi temperature/energy.

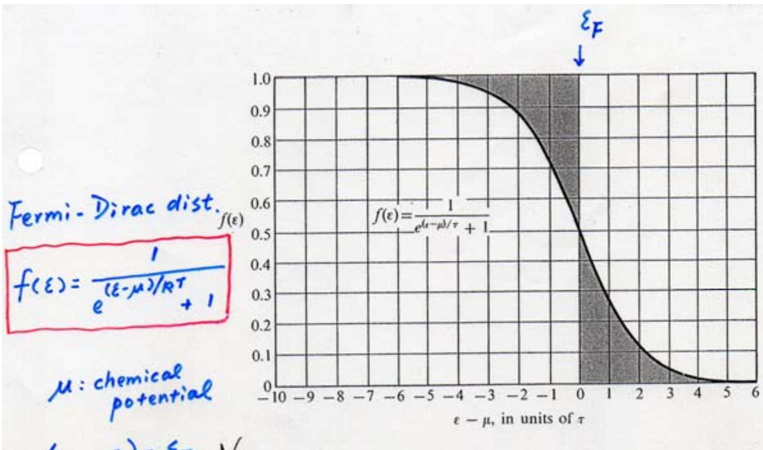

Figure 6.3 Plot of the Fermi-Dirac distribution function $f(\varepsilon)$ versus $\varepsilon - \mu$ in units of the temperature τ. The value of $f(\varepsilon)$ gives the fraction of orbitals at a given energy which are occupied when the system is in thermal equilibrium. When the system is heated from absolute zero, fermions are transferred from the shaded region at $\varepsilon/\mu < 1$ to the shaded region at $\varepsilon/\mu > 1$. For conduction electrons in a metal, μ might correspond to 50 000 K.

36

Chemical Potential (μ)

- Temperature governs the flow of energy between two systems.
- Chemical potential governs the flow of particles; from higher chemical potential to the lower

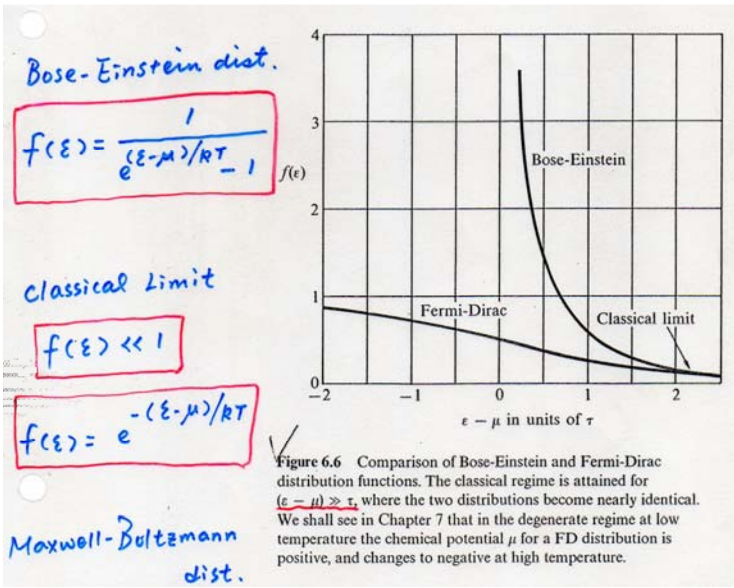

Figure 6.6 Comparison of Bose-Einstein and Fermi-Dirac distribution functions. The classical regime is attained for $(\varepsilon - \mu) \gg \tau$, where the two distributions become nearly identical. We shall see in Chapter 7 that in the degenerate regime at low temperature the chemical potential μ for a FD distribution is positive, and changes to negative at high temperature.

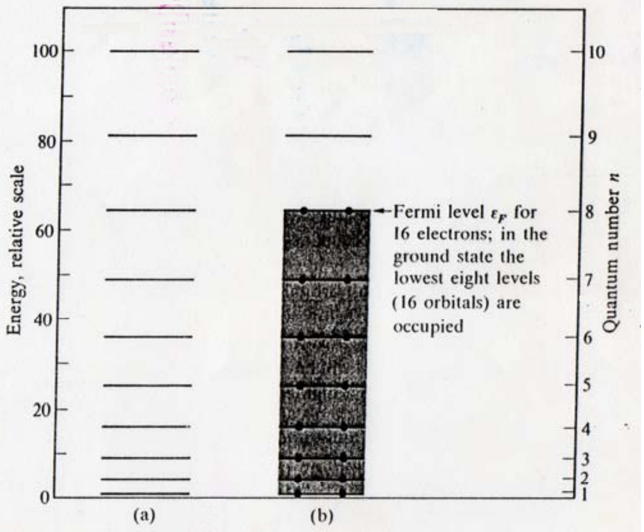

Figure 7.1 (a) The energies of the orbitals $n = 1, 2, \ldots, 10$ for an electron confined to a line of length L. Each level corresponds to two orbitals, one for spin up and one for spin down. (b) The ground state of a system of 16 electrons. Orbitals above the shaded region are vacant in the ground state.

39

As time goes on, electron degeneracy becomes increasingly important,

e.g. $P_e^{deg} \sim 1.7\%$ of total pressure at $\tau \sim 0$

$\sim 7.5\%$ " $\tau \sim 9.2 \times 10^9$ yr

Taking electron deg. pressure into account,

$M_{isothermal\ core} \sim 0.13\ M_\odot$

⇒ pressure insufficient to support overlying layers

⇒ core contraction ⇒ heated, ϵ_{nuc} ↑

⇒ Overlying layers pushed outwards

⇒ ϵ_{nuc} in a narrowing shell

End of main-sequence phase

40

Structural changes during Post-Main Sequence

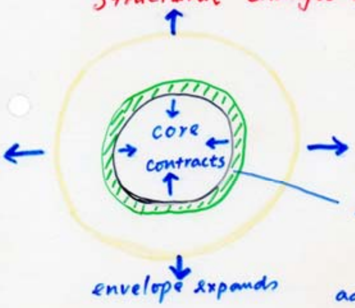

Shell burning, $\epsilon_{shell} \rightarrow L_{shell}$

$\Downarrow$

adds mass to core

$\Downarrow$

core contracts $\Rightarrow T_c \uparrow$

envelope expands

$T_{eff} \downarrow$

$L_* \approx L_{shell}$

L_{shell} heats core $\longrightarrow$ core $\approx$ isothermal

$\therefore$ needs density gradient to support against gravity

41

For low-mass stars ($0.7 - 2 M_\odot$)

ρ_c is high $\longrightarrow$ e^- degeneracy sets in <u>before</u> core He burning begins

When He burning starts $\longrightarrow T_c \uparrow$ (but P_c does <u>not</u>)

$\longrightarrow \epsilon \uparrow\uparrow$

$\Rightarrow$ <u>He flash</u>

$E_{release} \sim 10^{11} L_\odot$ in a few seconds

Energy absorbed by envelope (being pushed)

no observable effects !

42

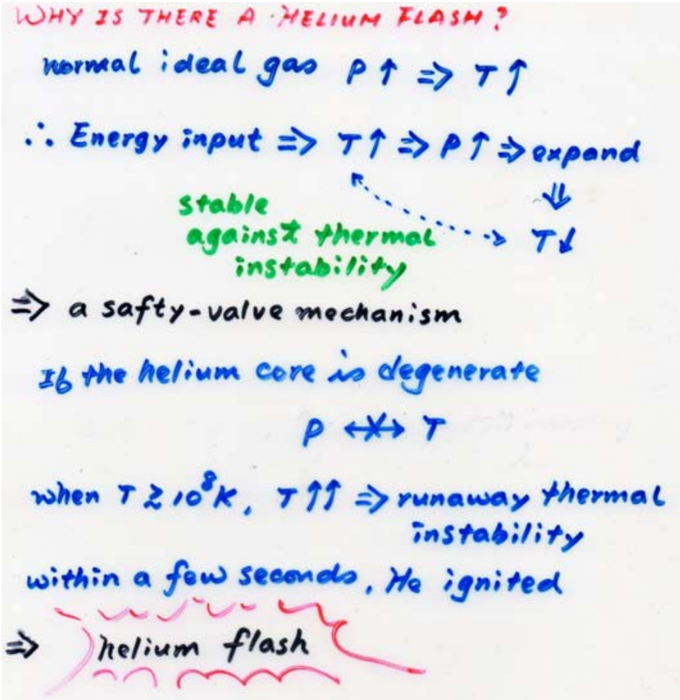

WHY IS THERE A HELIUM FLASH?

normal ideal gas $P\uparrow \Rightarrow T\uparrow$

$\therefore$ Energy input $\Rightarrow T\uparrow \Rightarrow P\uparrow \Rightarrow$ expand $\Rightarrow T\downarrow$

stable against thermal instability

$\Rightarrow$ a safty-valve mechanism

If the helium core is degenerate

$P \not\leftrightarrow T$

when $T \gtrsim 10^8$ K, $T\uparrow\uparrow \Rightarrow$ runaway thermal instability

within a few seconds, He ignited

$\Rightarrow$ helium flash

43

The helium flash occurs for $M_{\text{core}} \approx 1\ M_\odot$

If $\mathcal{M} \le 0.5\ \mathcal{M}_\odot$ $\rightarrow$ core never hot enough

If $\mathcal{M} \ge 2.25\ \mathcal{M}_\odot$ $\rightarrow$ core too hot, He ignited before a degenerate core develops

➔ Only $\mathcal{M} \approx 0.5 - 2.25\ \mathcal{M}_\odot$ stars experience the He flash.

44

After the helium flash

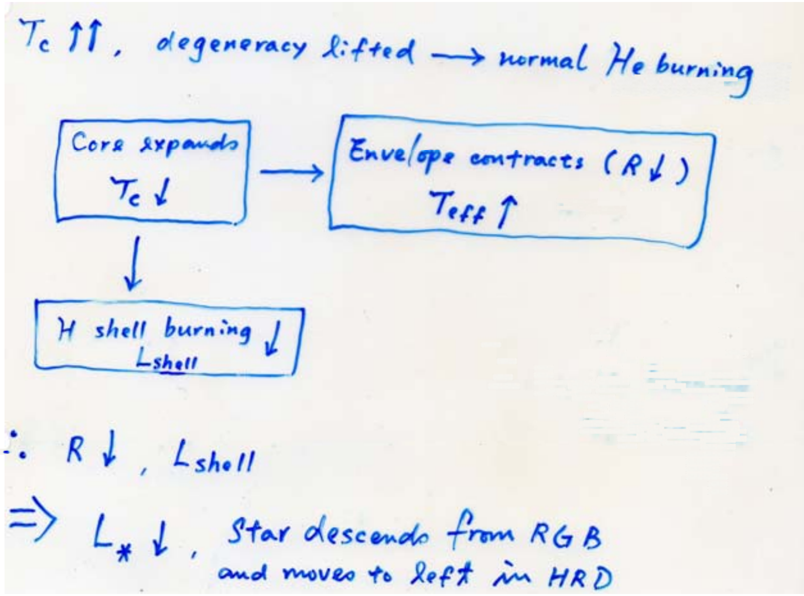

45

Core He burning is much shorter than the MS phase of core H burning, because He is short in abundance, not as efficient in energy supply (1/10 per mass), and the stellar luminosity is higher.

46

HB: L~50-100 $L_\odot$, $\tau \sim 10^8$ yrs

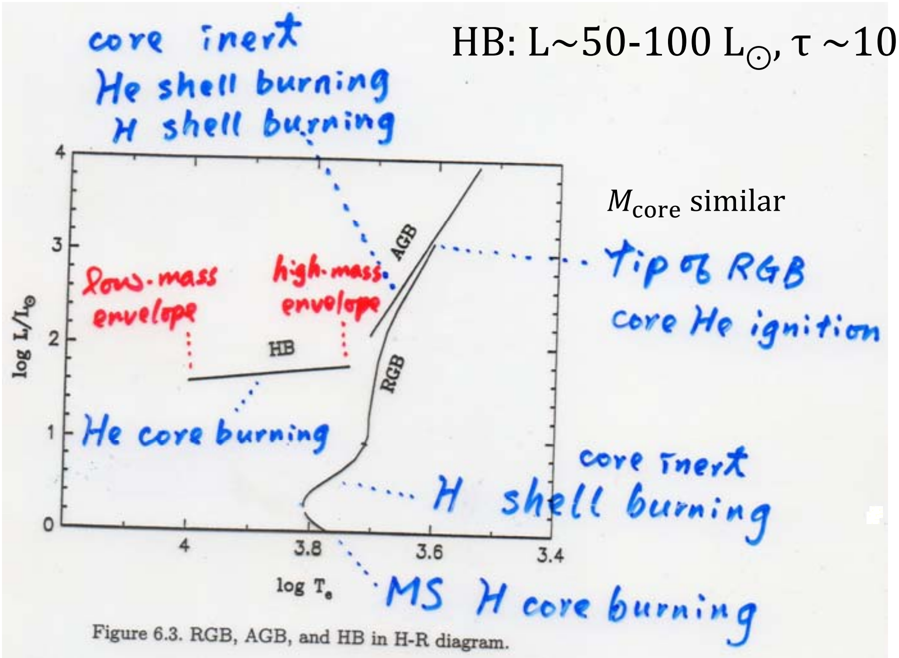

Figure 6.3. RGB, AGB, and HB in H-R diagram.

M_{core} similar

47

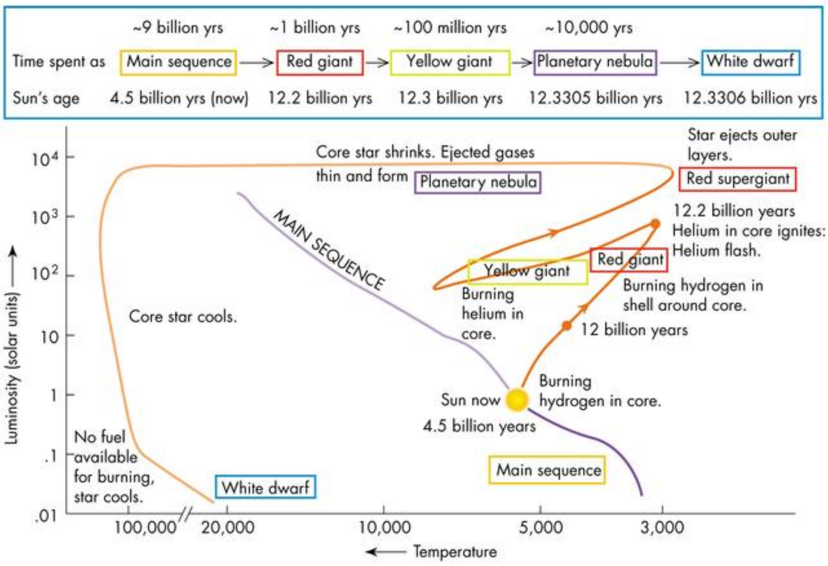

Evolution of the Sun in the HRD

- MS (core H burning)
- Subgiant branch (shell H burning)
- Red giant branch (shell H burning)
- Red giant (core He flash)
- Horizontal branch (core He burning)
- Asymptotic giant branch (shell He burning)
- Red supergiant
- Protoplanetary nebula
- Planetary nebula
- White/black dwarf

48

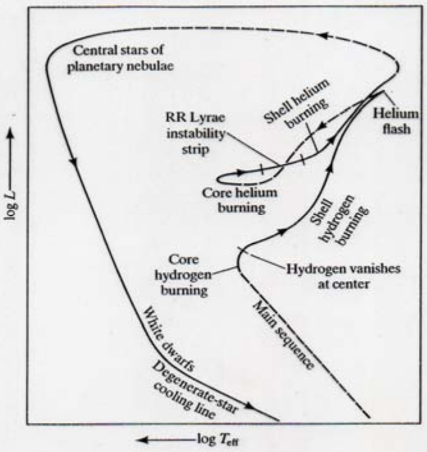

Figure 3-18. Schematic evolution track for a representative low-mass, globular-cluster star from the main sequence to its ultimate demise as a white dwarf. The major energy sources are indicated at several key phases. Dashed lines indicate episodes of very rapid evolution, during which details of the structure of the star are, at present, not too well known. Compare this figure with Figure 3-13.

Mihalas & Binney

49

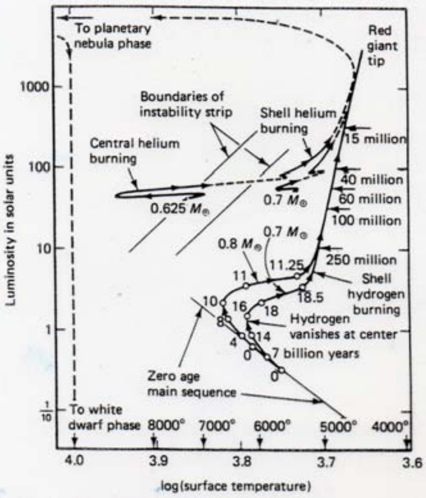

Fig. 14.11. Evolutionary tracks for population II stars with 0.7 and 0.8 $M_\odot$. A helium abundance of $Y = 0.30$ and a heavy element abundance of $Z = 10^{-3}$ was used. On the main sequence and subgiant branches evolution times since arrival on the zero age main sequence are given in billions of years. On the red giant branch evolution times from one arrow to the next are given in millions of years. Also indicated is the instability strip, the T_{eff}, L domain in which stars start to pulsate (see Chapter 17). From the tip of the asymptotic giant branch the stars probably evolve through the planetary nebula stage to become white dwarfs as indicated by the long dashed lines. From Iben (1971).

50

The red clump = HB (core He burning) of metal-rich stars

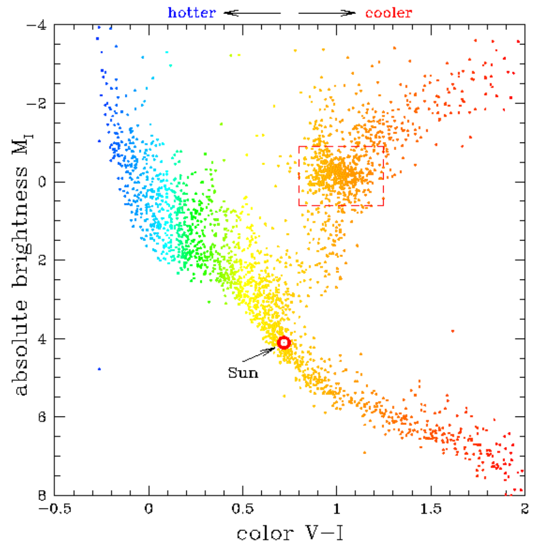

http://www.astronomy.ohio-state.edu/~kstanek/CfA/RedClump/

51

L_{RC} independent of composition or age ➔ standard candles

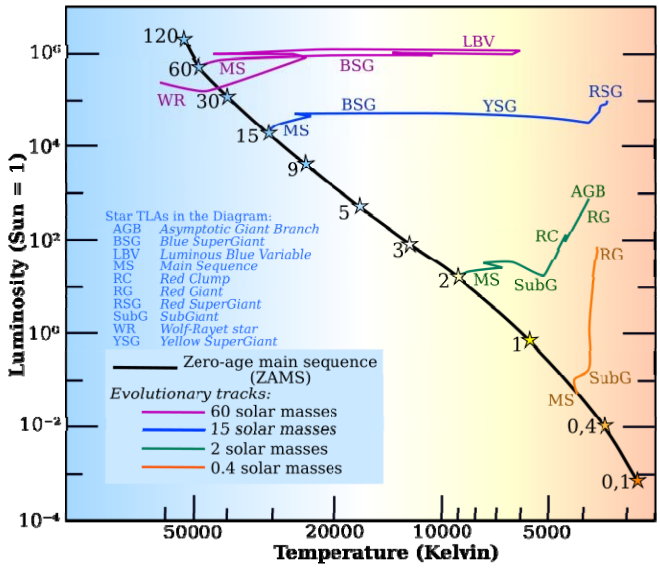

52

Distance to M31 With the *HST* and *Hipparcos* Red Clump Stars (1998)

K. Z. Stanek & P. M. Garnavich

$M_I = -0.23$

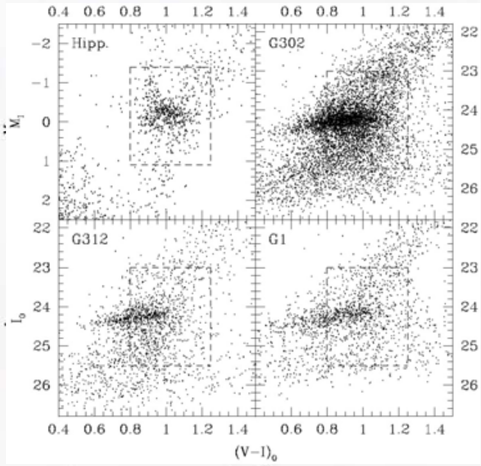

Using the red clump stars to determine the distance to M31

$R_{M31} = 784 \pm 13 \pm 17$ kpc

Systematic

Statistical error

Fig. 2.— The red clump dominated parts of CMDs for the *Hipparcos* stars (upper-left panel) and for three fields in M31 observed with the HST. The dashed rectangles surround the red clump regions used for the comparison between the local and the M31 red clump stars.

53

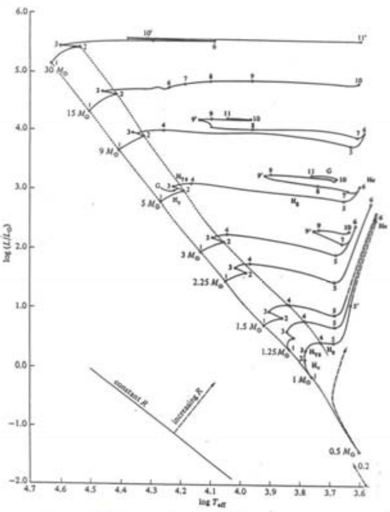

Table 7-7 Evolutionary Times. The times, expressed in years, refer tervals between the points in Fig. 7-25.* [Adapted from I. Iben, Jr., 1967 (327).]

MASS ($M_\odot$) \ INTERVAL	1–2	2–3	3–4	4–5	5–6
30	4.80 (6)	8.64 (4)	←	~1.0 (4)	→
15	1.010 (7)	2.270 (5)	←	7.55 (4)	→
9	2.144 (7)	6.053 (5)	9.113 (4)	1.477 (5)	6.552 (4)
5	6.547 (7)	2.173 (6)	1.372 (6)	7.532 (5)	4.857 (5)
3	2.212 (8)	1.042 (7)	1.033 (7)	4.505 (6)	4.238 (6)
2.25	4.802 (8)	1.647 (7)	3.696 (7)	1.310 (7)	3.829 (7)
1.5	1.553 (9)	8.10 (7)	3.490 (8)	1.049 (8)	≥2 (8)
1.25	2.803 (9)	1.824 (8)	1.045 (9)	1.463 (8)	≥4 (8)
1.0	7 (9)	2 (9)	1.20 (9)	1.57 (8)	≥1 (9)

MASS ($M_\odot$) \ INTERVAL	6–7	7–8	8–9	9–10[a]	10[a]–11[a]
30	←		53.1 (4)	→	1.3 (4)
15	7.17 (5)	6.20 (5)	1.9 (5)	3.5 (4)	
9	4.90 (5)	9.50 (4)	3.28 (6)	1.55 (5)	2.86 (4)
5	6.05 (6)	1.02 (6)	9.00 (6)	9.30 (5)	7.69 (4)
3	2.51 (7)	4.08 (7)		6.00 (6)	

* A number in parentheses is the power of 10 by which an entry is to be multiplied.

Fig. 7-25 Evolutionary Tracks in the Hertzsprung–Russell Diagram. The mass of each star is given at the left of the track. The composition is $X = 0.708$, $Y = 0.272$, and $Z = 0.020$ for all masses except 30 $M_\odot$, for which the composition is $X = 0.70$, $Y = 0.27$, $Z = 0.03$. *Dashed portions* of the curves are estimates. The *letters* along the tracks for 1 $M_\odot$ and 5 $M_\odot$ have the following significance: H_c = hydrogen-burning near the center; G = gravitational contraction of the entire star; H_{TS} = hydrogen-burning in a thick shell; H_s = hydrogen-burning in a thin shell; He = helium-burning near the center plus hydrogen-burning in a thin shell. The times required to reach the encircled points are given in Table 7-7.

The *dotted lines* indicate the boundaries of the main sequence. The *line* (*lower left*) shows the slope of a path along which the radius remains constant. The track for 15 $M_\odot$ does not turn back as do the other tracks because the semi-convective zone was treated as fully convective [see R. Stothers and C.-W. Chin, 1968 (377)]. [Adapted from I. Iben, Jr., 1967 (327). The track for 30 $M_\odot$ is given by R. Stothers, 1966 (333).]

H_c : H core burning

H_{TS} : H thick shell

T_s : H thin shell

54

For high-mass stars, e.g., $5 M_\odot$

③

L_{grav} contributes ; $L_r \uparrow$ for $M_r < 0.1 M$

$\Rightarrow \nabla T \Rightarrow$ later He burning begins <u>before</u> e^- deg. sets in

Shell burning pushes the core and envelope → L_r (r > 0.2) ↓

$\epsilon_{shell} \uparrow\uparrow \Rightarrow$ envelope expands $\uparrow\uparrow$

↳ adds mass until Schönberg-Chandrasekhar limit ④

$\Rightarrow$ core contracts, $T_c \uparrow \longrightarrow \epsilon_{shell} \uparrow\uparrow\uparrow$

pushes envelope, $T_{eff} \downarrow$, $L_r \lesssim$ const

55

End of core contraction

③

Fig. 7-28A A Model of Mass 5 $M_\odot$ Shortly after Leaving the Main Sequence, at $t = 6.82461 \times 10^7$ Years. Radius r, pressure P, density ρ, temperature T, net luminosity L_r, and hydrogen abundance X are shown as functions of fractional mass M_r/M. The lower limit of the ordinate is zero for all variables. The upper limits, given in the figure, are 2.9198 $R_\odot$ (with $R_\odot = 6.96 \times 10^{10}$ cm; however, the total radius is 3.9429 $R_\odot$), central pressure P_c (dyne cm^{-2}), central density ρ_c (gm cm^{-3}), central temperature T_c (°K), total luminosity L (units of $L_\odot = 3.86 \times 10^{33}$ erg sec^{-1}), and initial hydrogen abundance $X = 0.708$. The time is measured from the initial model calculated for the pre-main-sequence phase. [Adapted from I. Iben, Jr., 1966 (331).]

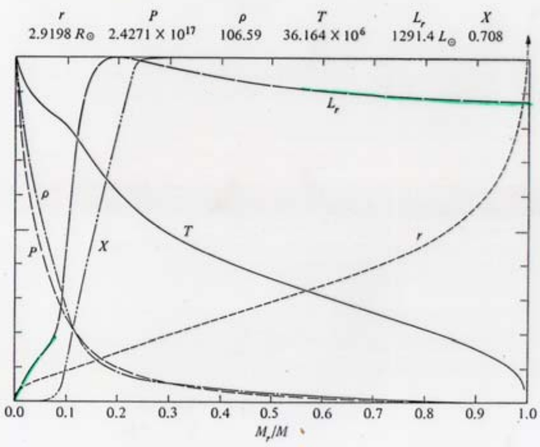

56

$\tau_{④-⑤} \sim 7.5 \times 10^5$ yr (i.e., v. short)

→ Hertzsprung gap

$\tau_{⑤-⑥} \sim 5 \times 10^5$ yr

⑥ = tip of RGB
= onset of He burning
$T_c \sim 2 \times 10^8$ K

But core is nondegenerate

∴ core expands, ϵ_{core} ↓
↓
envelope contracts, T_{eff} ↑

57

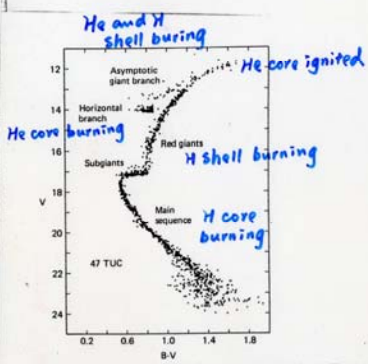

Fig. 1.7. The color apparent magnitude diagram for 47 Tucanae. The new measurements go down to stars as faint as 23rd magnitude, though for the faint stars the scatter becomes large. The main sequence and the giant and subgiant branches are surprisingly sharp, showing that there are very few or no binaries in this globular cluster. The red stub of the horizontal branch is seen at V ~ 14 and B − V ~ 0.8. The asymptotic giant branch (see Chapter 14) is seen above the horizontal branch. From Hesser *et al.* (1987).

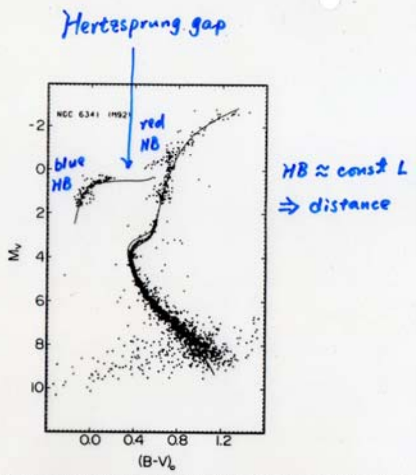

Fig. 1.8. The color absolute magnitude diagram for the globular cluster M92 (cluster 92 in the Messier catalog of nebulous objects). The new observations for M92, like those for 47 Tuc, go to very faint magnitudes. For M92 the main sequence is now clearly recog-izable. In addition the subgiant, red giant and horizontal branches are clearly seen. Also seen is the so-called asymptotic branch, for $(B-V)_0 \sim 0.6$ above the horizontal branch. The thin lines shown are the theoretical isochrones, i.e. the location where stars are expected to be seen at a given time. From Hesser *et al.* (1987).

HB morphology differs from one GC to another.

58

After ⑤

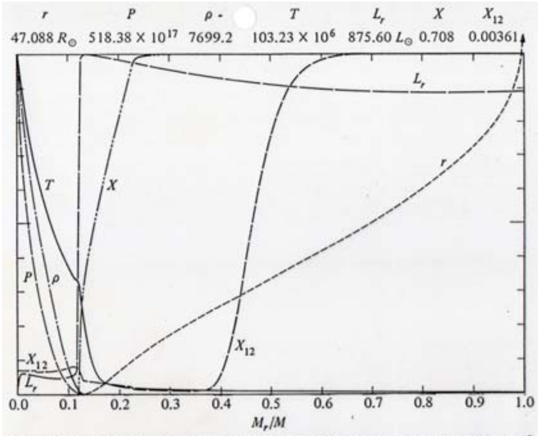

Fig. 7-28B A Model of Mass 5 $M_\odot$ during the Giant Stage at $t = 7.03776 \times 10^7$ Years. Radius r, pressure P, density ρ, temperature T, net luminosity L_r, hydrogen abundance X, and carbon-12 abundance X_{12} are shown as functions of fractional mass M_r/M. The lower limit of the ordinate is zero for all variables. The upper limits, given in the figure, are 47.088 $R_\odot$ (with $R_\odot = 6.96 \times 10^{10}$ cm; however, the total radius is 51.328 $R_\odot$), central pressure P_c (dyne cm^{-2}), central density ρ_c (gm cm^{-3}), central temperature T_c (°K), total luminosity L (units of $L_\odot = 3.86 \times 10^{33}$ erg sec^{-1}), initial hydrogen abundance $X = 0.708$, and carbon-12 abundance $X_{12} = 0.003610$. The time is measured from the initial model calculated for the pre-main-sequence phase. [Adapted from I. Iben, Jr., 1966 (331).]

At the center, $N^{14}(\alpha,\gamma)F^{18}(\beta^+,\nu)O^{18}$

59

5 $M_\odot$ (continued)

From ⑥ → ⑦

$\epsilon_{core} \downarrow \rightarrow L_* \downarrow$

$T_{eff} \uparrow$

But as $T_{envelope} \uparrow \rightarrow$ opacity $\downarrow \Rightarrow L_* \uparrow$

60

Between points ⑦ and ⑧

Fig. 7-28C A Model of Mass 5 $M_\odot$ during the Giant Stage at $t = 7.73665 \times 10^7$ Years. Radius r, pressure P, density ρ, temperature T, net luminosity L_r, and helium-4 abundance X_4 are shown as functions of fractional mass M_r/M. The lower limit of the ordinate is zero for all variables. The upper limits, given in the figure, are 35.852 $R_\odot$ (with $R_\odot = 6.96 \times 10^{10}$ cm; however, the total radius is 50.612 $R_\odot$), central pressure P_c (dyne cm^{-2}), central density ρ_c (gm cm^{-3}), central temperature T_c (°K), total luminosity L (units of $L_\odot = 3.86 \times 10^{33}$ erg sec^{-1}), and helium-4 abundance $X_4 = 0.9763$. The time is measured from the initial model calculated for the pre-main-sequence phase (see Section 2). [Adapted from I. Iben, Jr., 1966 (331).]

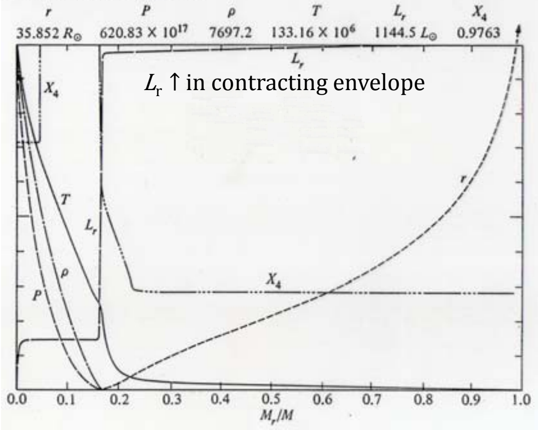

61

Point 11 Two shells at M_r=0.07 (He) and 0.22 (H)

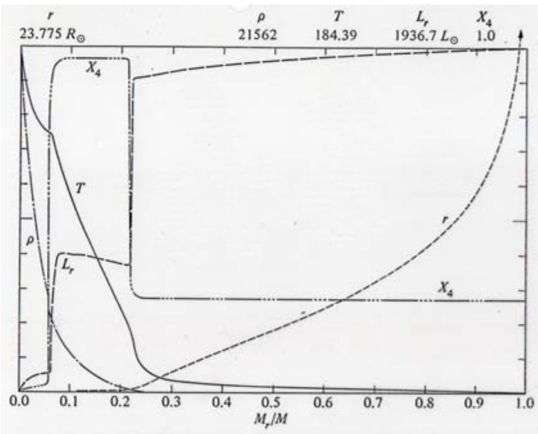

Fig. 7-28D A Model of Mass 5 $M_\odot$ during the Giant Stage at $t = 8.79060 \times 10^7$ Years. Radius r, density ρ, temperature T, net luminosity L_r, and helium-4 abundance X_4 are shown as functions of fractional mass M_r/M. The lower limit of the ordinate is zero for all variables. The upper limits, given in the figure, are 23.775 $R_\odot$ (with $R_\odot = 6.96 \times 10^{10}$ cm; however, the total radius is 44.141 $R_\odot$), central density ρ_c (gm cm^{-3}), central temperature T_c (°K), total luminosity L (units of $L_\odot = 3.86 \times 10^{33}$ erg sec^{-1}), and helium-4 abundance $X_4 = 1.0$. The time is measured from the initial model calculated for the pre-main-sequence phase. [Adapted from I. Iben, Jr., 1966 (331).]

62

MS Stars

AGB

wind → envelope

$M = 1-9 M_\odot$ ⟶ C-O core $0.6-1.1 M_\odot$ — WD

roughly core mass ↔ MS mass

⇒ expect WD mostly $0.6 M_\odot$

During AGB, H-shell and He-shell burning

bottom of He layer

Envelope shed = a random process in pulses

63

If H-shell burning → WD w/ a thin layer of H

80% of all DA white dwarfs (H lines, no He lines nor metal lines)

If He-shell burning — WD He layer

↓ less freq.

DB (He I lines, no H, metals) 16%

⇒ expect more DA white dwarfs than DBs

obs 25% He lines

DC (continuous, no lines)

DO (He II lines)

DQ (C dominated)

64

- Origins of DA and non-DA uncertain: (1) exact phase when the last thermal pulse takes place after the AGB phase, or (2) convective mixing, radiative levitation, or diffusion.

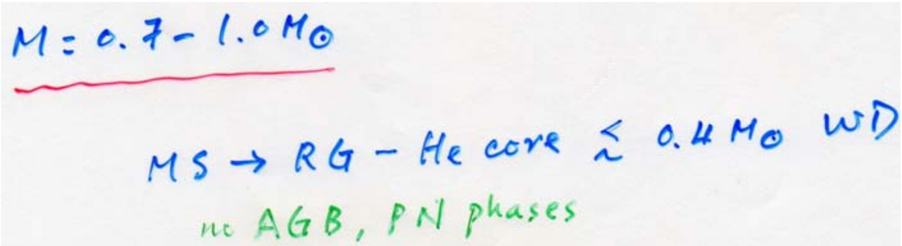

65

A&A 419, L5–L8 (2004)

Mass distribution of DA white dwarfs in the First Data Release of the Sloan Digital Sky Survey

J. Madej[1], M. Należyty[1], and L. G. Althaus[2]

[1] Astronomical Observatory, University of Warsaw, Al. Ujazdowskie 4, 00-478 Warsaw, Poland
[2] Departament de Fisica Aplicada, Universitat Politecnica de Catalunya, Av. del Canal Olimpic s/n, 08860, Castelldefels, Spain

Received 4 March 2004 / Accepted 23 March 2004

Abstract. We investigate the sample of 1175 new nonmagnetic DA white dwarfs with the effective temperatures $T_{\rm eff} \geq$ 12 000 K, which were extracted from the Data Release 1 of the Sloan Digital Sky Survey. We determined masses, radii, and bolometric luminosities of stars in the sample. The above parameters were derived from the effective temperatures $T_{\rm eff}$ and surface gravities $\log g$ published in the DR1, and the new theoretical $M - R$ relations for carbon-core and oxygen-core white dwarfs. Mass distribution of white dwarfs in this sample exhibits the peak at $M = 0.562\ M_{\odot}$ (carbon-core stars), and the tail towards higher masses. Both the shape of the mass distribution function and the empirical mass-radius relation are practically identical for white dwarfs with either pure carbon or pure oxygen cores.

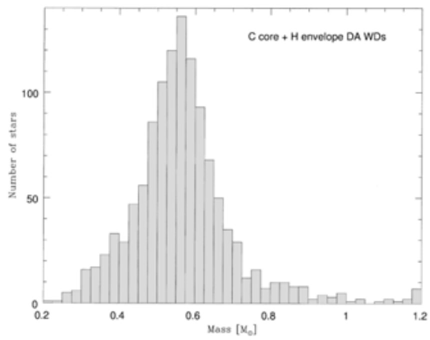

66

$\mathcal{M} < 0.7\ M_{\odot}$

$< 0.16\ M_{\odot}$ → no RGB
$< 0.5\ M_{\odot}$ → $\tau_{MS} > \tau_{Universe}$
$< 0.5 \sim 0.7\ M_{\odot}$ → no core He burning

Very low-mass stars are completely convective
→ more H to burn → τ_{MS} lengthened

67

A 1 $M_{\odot}$ main sequence star

- $\tau_{MS} \sim 10^{10}$ yrs
- $\tau_{RGB} \sim 10^{9}$ yrs
- $\tau_{HB} \sim 10^{8}$ yrs
- $\tau_{AGB} \sim 2 \times 10^{7}$ yrs
- $\tau_{PS} \sim 5 \times 10^{4}$ yrs

A remnant of a 0.6 WD

68

$\mathcal{M} < 25\ \mathrm{M}_\odot$

Mass loss rate low

$\boldsymbol{\mathcal{M} = 20 - 25}\ \mathrm{M}_\odot$
O type star → red supergiant → supernova

$\boldsymbol{\mathcal{M} < 20}$
O type star → red supergiant → Cepheid
→ red supergiant → supernova

69

$\mathcal{M} = 25 - 60\ \mathrm{M}_\odot$

Mass loss not sufficient to remove the entire envelope

$\boldsymbol{\mathcal{M} = 40 - 60}\ \mathrm{M}_\odot$
O type star → blue super giant → yellow supergiant
→ red supergiant
→ blue supergiant → WN → supernova

$\boldsymbol{\mathcal{M} = 25 - 40}\ \mathrm{M}_\odot$
O type star → blue super giant → yellow supergiant
→ red supergiant
→ supernova

70

$\mathcal{M} > 60\ M_\odot$

Mass loss fierce $\approx 10^{-1}\ M_\odot\ yr^{-1}$, rid of almost entire envelope during the LBV stage, left with a WR star, evolving toward a SN.

O type star → Of star → blue super giant

→ luminous blue variable → WN star
→ WC star → supernova

71

A&A 564, A30 (2014)

The evolution of massive stars and their spectra

I. A non-rotating 60 $M_\odot$ star from the zero-age main sequence to the pre-supernova stage⋆,⋆⋆

Jose H. Groh[1], Georges Meynet[1], Sylvia Ekström[1], and Cyril Georgy[2]

[1] Geneva Observatory, Geneva University, Chemin des Maillettes 51, 1290 Sauverny, Switzerland
e-mail: jose.groh@unige.ch
[2] Astrophysics group, EPSAM, Keele University, Lennard-Jones Labs, Keele, ST5 5BG, UK

ABSTRACT

For the first time, the interior and spectroscopic evolution of a massive star is analyzed from the zero-age main sequence (ZAMS) to the pre-supernova (SN) stage. For this purpose, we combined stellar evolution models using the Geneva code and stellar atmospheric/wind models using CMFGEN. With our approach, we were able to produce observables, such as a synthetic high-resolution spectrum and photometry, thereby aiding the comparison between evolution models and observed data. Here we analyze the evolution of a non-rotating 60 $M_\odot$ star and its spectrum throughout its lifetime. Interestingly, the star has a supergiant appearance (luminosity class I) even at the ZAMS. We find the following evolutionary sequence of spectral types: O3 I (at the ZAMS), O4 I (middle of the H-core burning phase), B supergiant (BSG), B hypergiant (BHG), hot luminous blue variable (LBV; end of H-core burning), cool LBV (H-shell burning through the beginning of the He-core burning phase), rapid evolution through late WN and early WN, early WC (middle of He-core burning), and WO (end of He-core burning until core collapse). We find the following spectroscopic phase lifetimes: 3.22×10^6 yr for the O-type, 0.34×10^5 yr (BSG), 0.79×10^5 yr (BHG), 2.35×10^5 yr (LBV), 1.05×10^5 yr (WN), 2.57×10^5 yr (WC), and 3.80×10^4 yr (WO). Compared to previous studies, we find a much longer (shorter) duration for the early WN (late WN) phase, as well as a long-lived LBV phase. We show that LBVs arise naturally in single-star evolution models at the end of the MS when the mass-loss rate increases as a consequence of crossing the bistability limit. We discuss the evolution of the spectra, magnitudes, colors, and ionizing flux across the star's lifetime, and the way they are related to the evolution of the interior. We find that the absolute magnitude of the star typically changes by ~6 mag in optical filters across the evolution, with the star becoming significantly fainter in optical filters at the end of the evolution, when it becomes a WO just a few 10^4 years before the SN explosion. We also discuss the origin of the different spectroscopic phases (i.e., O-type, LBV, WR) and how they are related to evolutionary phases (H-core burning, H-shell burning, He-core burning).

Read the first 4 paragraphs of this paper.

72

Stellar Rotation

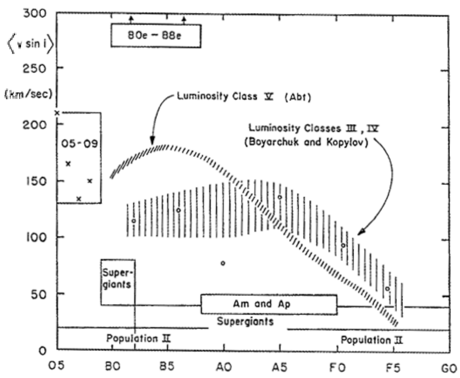

Fig. 3. Projected equatorial velocities, averaged over all possible inclinations, as a function of spectral type. On the main sequence (luminosity class V), early-type stars have rotational velocities that reach and even exceed 200 km/s; these velocities drop to a few km/s for late-type stars, such as the Sun (type G2) (Slettebak [20]; courtesy Gordon & Breach)

Fig. 2.2 *Panel A* The *blue curve* is the median equatorial velocity $(4/\pi)\langle v \sin i \rangle$ for each spectral type from Glebocki and Gnacinski (2005). The *green curve* shows the equatorial velocity of the *Kepler* targets, $\bar{v}$(s.t.), derived from the measured rotation periods and the KIC radii. The *black points* show measurements by Reiners and Mohanty (2012). In this sample 201 stars have an upper $v \sin i$ limit of 4 km/s (due to instrumental limitations), these stars are represented by the *solid bar*. *Panel B* The rotation periods P_{rot} of the stars in our sample, averaged within each spectral type. *Panel C* The same as panel B, but for comparison we show the median of the rotation periods measured by McQuillan et al. (2013) (*black points* with *errorbars*), for the stars overlapping with our sample. Similarly, the *red curve* shows the median of the rotation periods found by Debosscher et al. (2011). *Shaded areas* and *error bars* span the *upper* and *lower* 34th percentile values from the median. Reproduced with permission from Astronomy & Astrophysics, © ESO

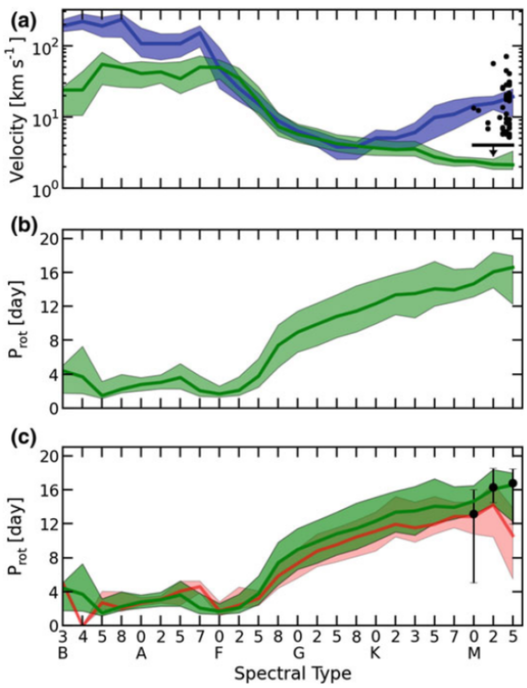

Rotation → star cooler and fainter

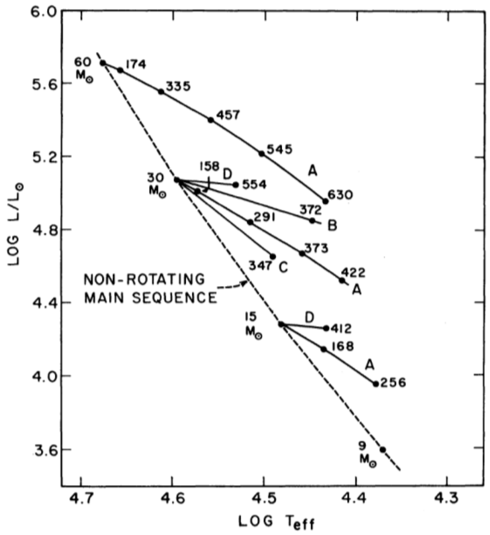

FIG. 2.—Theoretical H-R diagram showing model sequences of increasing angular momentum (*solid curves*). Numbers on curves give calculated velocities at the equator in km sec^{-1}. The distribution of angular momentum for each sequence is indicated by the letter A, B, C, or D.

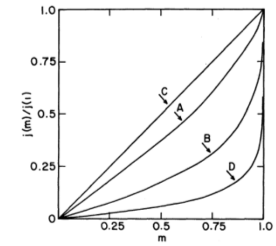

FIG. 1.—Angular momentum per unit mass, as a function of mass fraction interior to a given cylinder about the axis of rotation, for three assumed laws of differential rotation (Cases A, B, and C) and for a uniformly rotating model (Case D) of 30 $\mathfrak{M}_{\odot}$, log J = 52.73.

D: solid body rotation

Rotation law:
angular momentum distribution $j(m_{\varpi})$ as a function of, m_{ϖ}, the mass fraction interior to the cylinder of radius ϖ about the rotation axis.

Bodenheimer (1971) ApJ, **167**, 153

1. Introduction

Massive stars are essential constituents of stellar populations and galaxies in the near and far Universe. They are among the most important sources of ionizing photons, energy, and some chemical species, which are ejected into the interstellar medium through powerful stellar winds and during their extraordinary deaths as supernovae (SN) and long gamma-ray bursts (GRB). For these reasons, massive stars are often depicted as cosmic engines, because they are directly or indirectly related to most of the major areas of astrophysical research.

Despite their importance, our current understanding of massive stars is still limited. This inconvenient shortcoming can be explained by many reasons on which we elaborate below. First, the physics of star formation mean that massive stars are rare (Salpeter 1955). Moreover, their lifetime is short, of a few to tens of millions of years (e.g., Ekström et al. 2012; Langer 2012). These factors make it challenging to construct evolutionary sequences and relate different classes of massive stars. This is in sharp contrast to what can be done for low-mass stars.

Second, one can also argue that the evolution of massive stars is extremely sensitive to the effects of some physical processes, such as mass loss and rotation (Maeder & Meynet 2000; Heger et al. 2000), that have relatively less impact on the evolution of low-mass stars. However, the current implementation of rotation in one-dimensional codes relies on parametrized formulas, and the choice of the diffusion coefficients has a key impact on the evolution (Meynet et al. 2013). Likewise, mass-loss recipes arising from first principles are only available for main sequence (MS) objects (Vink et al. 2000, 2001) and a restricted range of Wolf-Rayet (WR) star parameters (Gräfener & Hamann 2008). Third, binarity seems to affect the evolution of massive stars, given that a large portion of them are in binary systems that will interact during the evolution (Sana et al. 2012).

Fourth, our understanding of different classes of stars is often built by comparing evolutionary models and observations. However, mass loss may affect the spectra, magnitudes, and colors of massive stars, thus making the comparison between evolutionary models and observations a challenge. In addition to luminosity, effective temperature, and surface gravity, the

76

observables of massive stars can be strongly influenced by a radiatively driven stellar wind that is characteristic of these stars. The effects of mass loss on the observables depend on the initial mass and metallicity, since they are in general more noticeable in MS stars with large initial masses, during the post-MS phase, and at high metallicities. When the wind density is significant, the mass-loss rate, wind clumping, wind terminal velocity, and velocity law have a strong impact on the spectral morphology. This makes the analysis of a fraction of massive stars a difficult task, and obtaining their fundamental parameters, such as luminosity and effective temperature, is subject to the uncertainties that comes from our limited understanding of mass loss and clumping. Furthermore, the definition of effective temperature of massive stars with dense winds is problematic and, while referring to an optical depth surface, it does not relate to a hydrostatic surface. This is caused by the atmosphere becoming extended, with the extension being larger the stronger the wind is. Stellar evolution models are able to predict the stellar parameters only up to the stellar hydrostatic surface, which is not directly reached by the observations of massive stars when a dense stellar wind is present. Since current evolutionary models do not thoroughly simulate the physical mechanisms happening at the atmosphere and wind, model predictions of the evolution of massive stars are difficult to be directly compared to observed quantities, such as a spectrum or a photometric measurement.

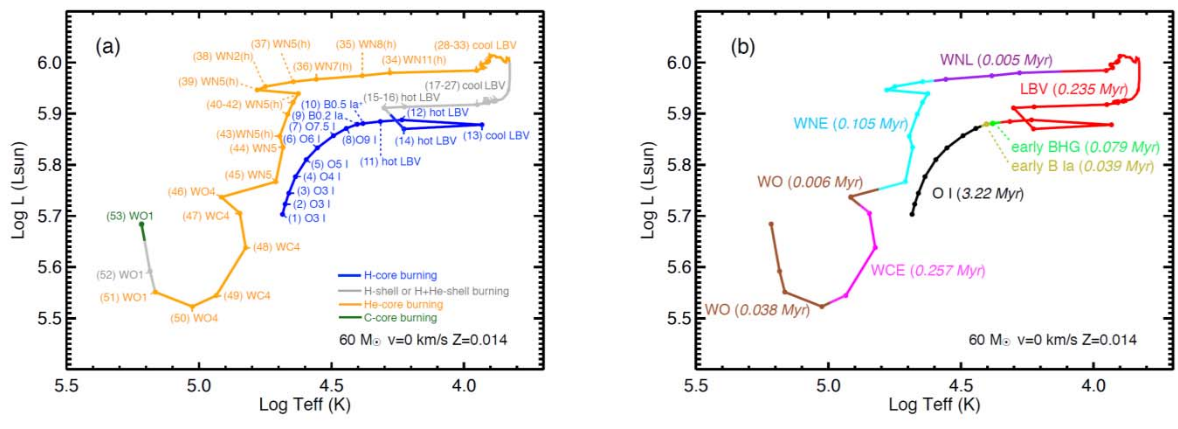

Fig. 3. **a)** HR diagram showing the evolutionary track of a non-rotating star with initial mass of 60 $M_{\odot}$ at metallicity $Z = 0.014$, using our revised values of $T_{\rm eff}$. The color code corresponds to the evolutionary phases of a massive star, with H-core burning in blue, He-core burning in orange, C-core burning in green, and H and/or He-shell burning in gray. **b)** Similar to **a)**, but color coded according to the spectroscopic phases. Lifetimes of each phase are indicated in parenthesis. **c)** Evolution of $T_{\rm eff}$ as a function of age. The color code is the same as in **a)**. **d)** Surface abundances

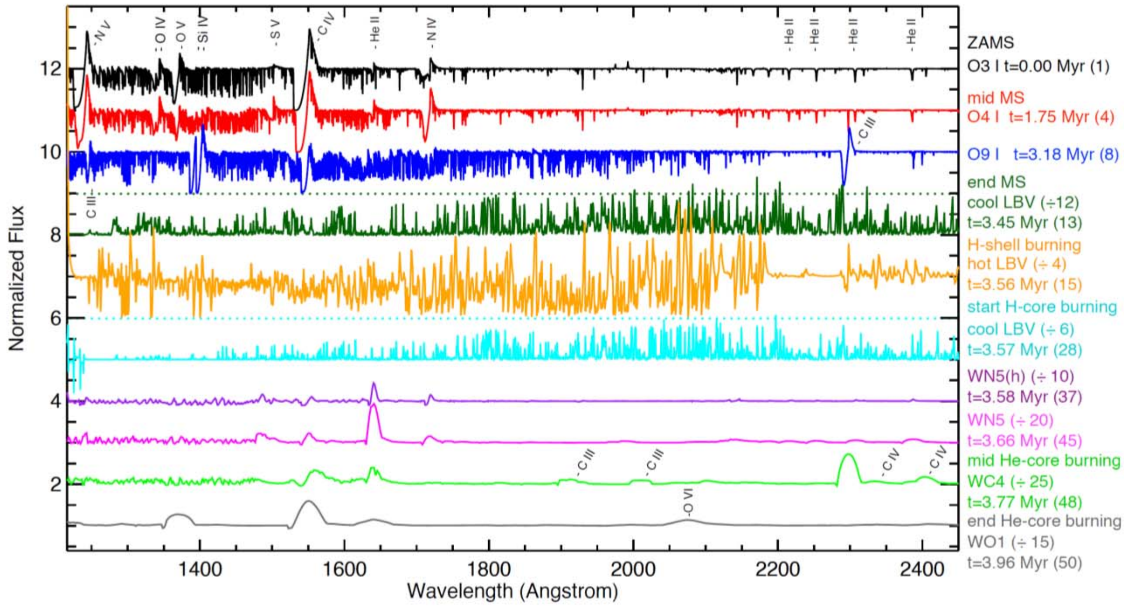

79

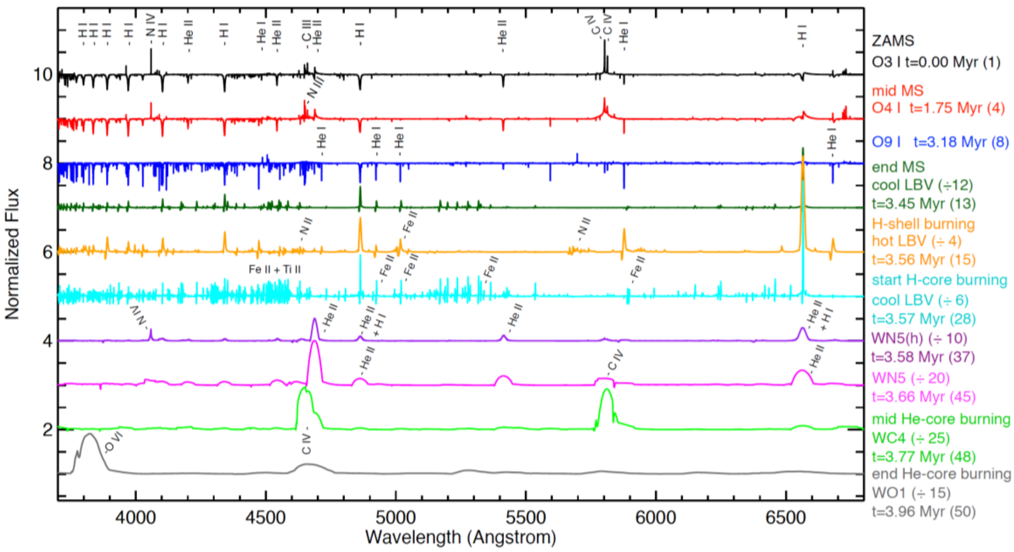

Fig. 4. Evolution of the ultraviolet **a)** (*top*) and optical spectra **b)** (*bottom*) of a non-rotating 60 $M_\odot$ star. The evolution proceeds from top to bottom, with labels indicating the evolutionary phase, spectral type, scale factor when appropriate, age, and model stage according to Table 1. Note that certain spectra have been scaled for the sake of displaying the full range of UV and optical emission lines.

80

Test of Stellar Evolution by Star Clusters

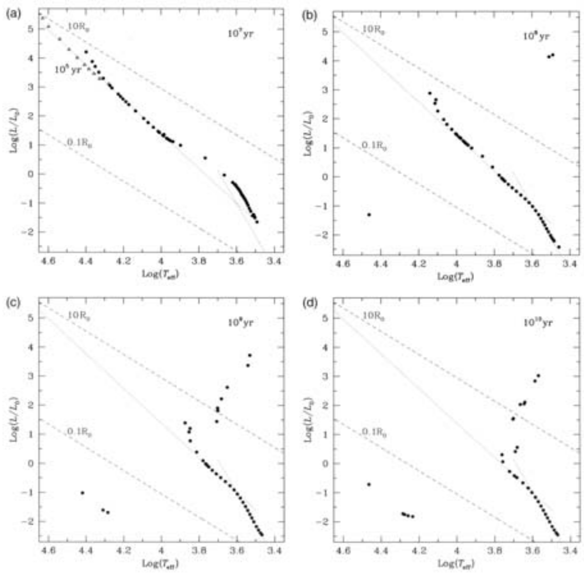

Figure 9.21 Evolutionary calculations for stars of different masses forming a hypothetical cluster result in an evolving H–R diagram, shown at four ages. The number of stars and their mass distribution is arbitrary. The dashed lines are lines of constant radius. The dotted lines mark the main-sequence slopes. We note that at 10^7 years (a), the low-mass stars are not yet settled on the main sequence, while the very massive ones have already left it: the open triangles show the main sequence of massive stars at a much earlier epoch, 10^5 years. The Hertzsprung gap is conspicuous at 10^8 years (b) resembling the Hyades-cluster H–R diagram shown in Figure 1.5. By contrast, the continuously-populated track toward the red giant branch is clearly seen at later epochs (c and d), when low-mass stars leave the main sequence.

Prialnik

81

82

Initial Mass Function

The birthrate function $B(M, t)$ is the number of stars per unit volume, with masses between M and $M + dM$ that are formed out of ISM during time interval t and $t + dt$.

$$B(M, t)\, dM\, dt = \psi(t)\, \xi(M)\, dM\, dt,$$

where $\psi(t)$ is the **star formation rate** (SFR),
and $\xi(M)$ is the **initial mass function** (IMF).

For the Galactic disk, SFR is $5.0 \pm 0.5\ M_\odot \mathrm{pc}^{-2}\ \mathrm{Gyr}^{-1}$ integrated over the z direction.

IMF: many more low-mass stars than higher mass stars as a result of cloud fragmentation?

83

The IMF specifies the fractional distribution in mass of a newly formed stellar system. It is often assumed to have a simple power law $\xi(M) = c\, M^{-\alpha} = c\, M^{-(1+\Gamma)}$

In general, $\xi(M)$ extends from a lower to an upper cutoff, e.g., from 0.1 to 125 solar masses. Commonly used IMFs are those of Salpeter (1955), Scalo (1986), and Miller and Scalo (1979).

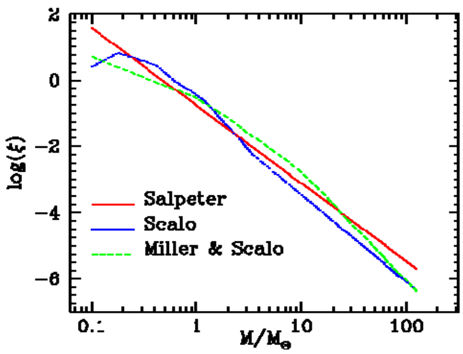

http://webast.ast.obs-mip.fr/hyperz/hyperz_manual1/node7.html

- Edwin Salpeter (1955) on solar-neighborhood stars (ApJ, 121, 161)
  Present-day LF → mass-luminosity relation → present-day mass function → stellar evolution → initial mass function
  α=2.35 or Γ = 1.35
- Glenn E. Miller and John M. Scalo extended work below 1 $M_\odot$
  (1979, ApJS, 41, 513) $\alpha \approx 0$ for $M < 1\ M_\odot$
- Pavel Kroupa (2002, Sci, 295, 82)
  $\alpha = 2.3$ for $M > 0.5\ M_\odot$
  $\alpha = 1.3$ for $0.08\ M_\odot < M < 0.5\ M_\odot$
  $\alpha = 0.3$ for $M < 0.08\ M_\odot$
- A universal IMF among stellar systems (SFRs, star clusters, galaxies) (Bastian et al. 2010, ARAA). But why?

85

THE LUMINOSITY FUNCTION AND STELLAR EVOLUTION

EDWIN E. SALPETER*
Australian National University, Canberra, and Cornell University
Received July 29, 1954

ABSTRACT

The evolutionary significance of the observed luminosity function for main-sequence stars in the solar neighborhood is discussed. The hypothesis is made that stars move off the main sequence after burning about 10 per cent of their hydrogen mass and that stars have been created at a uniform rate in the solar neighborhood for the last five billion years.

Using this hypothesis and the observed luminosity function, the rate of star creation as a function of stellar mass is calculated. The total number and mass of stars which have moved off the main sequence is found to be comparable with the total number of white dwarfs and with the total mass of all fainter main-sequence stars, respectively.

86

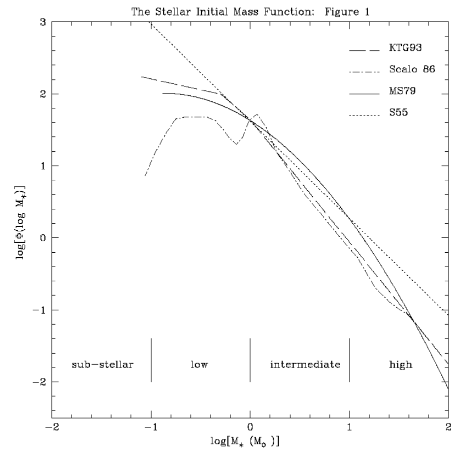

Figure 1. Initial mass function for field stars in the solar neighborhood taken from a variety of recent studies. These results have been normalized at 1 M⊙. For both the MS79 and Scalo 86 IMFs we have adopted 15 Gyr as the age of the Milky Way. Current work suggests that the upper end of the IMF (> 5M⊙) is best represented by a power–law similar to Salpeter (1955) while the low mass end (< 1M⊙) is flatter (Kroupa, Tout, and Gilmore 1993). The shape of the IMF from 1–5 M⊙ is highly uncertain.

From Meyer et al. (2000) Protostars & Planets IV

87

Orion Nebula Cluster

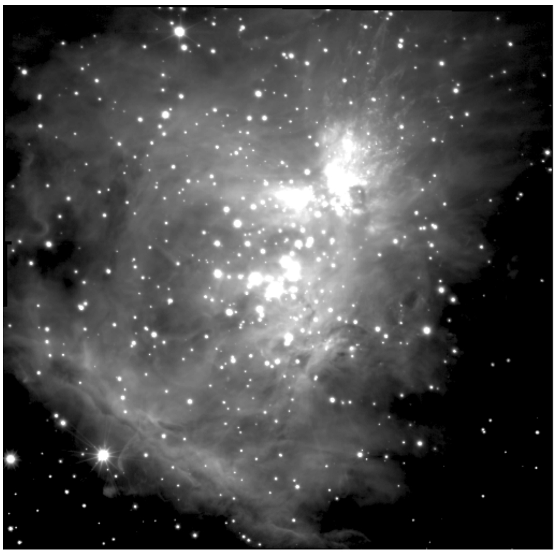

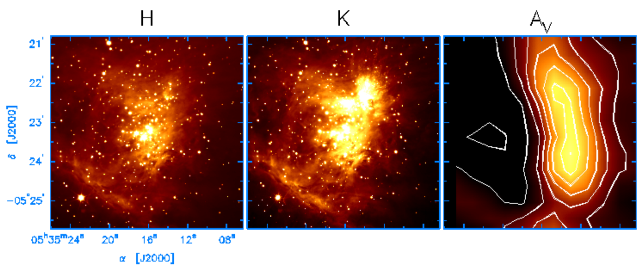

http://www.astro.caltech.edu/~jmc/papers/onc/gif/figure1.gif

88

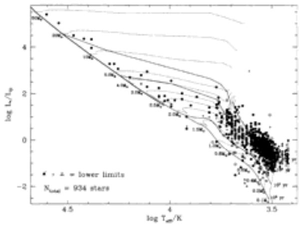

FIG. 12. *HR diagram for the Orion Nebula Cluster.* Triangles indicate lower limits in luminosity. Filled circles/triangles indicate proper motion cluster members plus all sources which have been identified as being externally ionized; open circles/triangles indicate that no proper motion information is available; crosses indicate proper motion nonmembers. Typical errors are ≤0.02 in log T_{eff} for late-type (K-M) stars but increase towards earlier spectral types, and ≤0.2 in $\log(L_*/L_\odot)$ at all spectral types. Two luminosities are plotted for all stars later than M7, with the asterisk indicating the luminosity calculated assuming the star has the $V-I$ color and bolometric correction of an M7 star; see text. Superimposed are the zero-age main sequence and the pre-main sequence evolutionary tracks of D'Antona & Mazzitelli (1994, model 1); over the mass range from 0.1 $M_\odot$ to 2.5 $M_\odot$; Swenson *et al.* (1994, model F) from 3 $M_\odot$ to 5 $M_\odot$; and Iben & Cameron (1967) from 10 $M_\odot$ to 50 $M_\odot$. The apparent trend of increasing stellar age with mass suggests errors in the zero point of the pre-main-sequence evolutionary tracks, i.e., the initial mass-radius relationship with which the calculations begin.

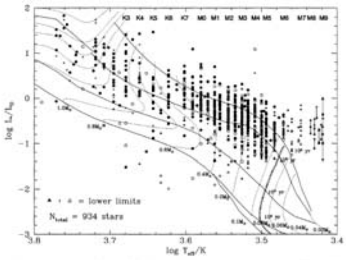

FIG. 13. *Low-mass end of the HR diagram for the Orion Nebula Cluster.* All lines and symbols are the same as in Fig. 12, with the pre-main sequence evolutionary calculations of D'Antona & Mazzitelli now shown down to 0.02 $M_\odot$. The hydrogen-burning mass limit of 0.08 $M_\odot$ is emphasized. The temperature-spectral-type relationship over the range from K3–M9 is denoted. Note the locations of stars M6.5 and later relative to the tracks. These are probably young brown dwarfs. For a magnitude-limited sample restricted to I_c<17.5 mag, our data begin to become incomplete at ages older than 1 Myr and masses less than 0.1 $M_\odot$, assuming a typical extinction of A_V=2 mag.

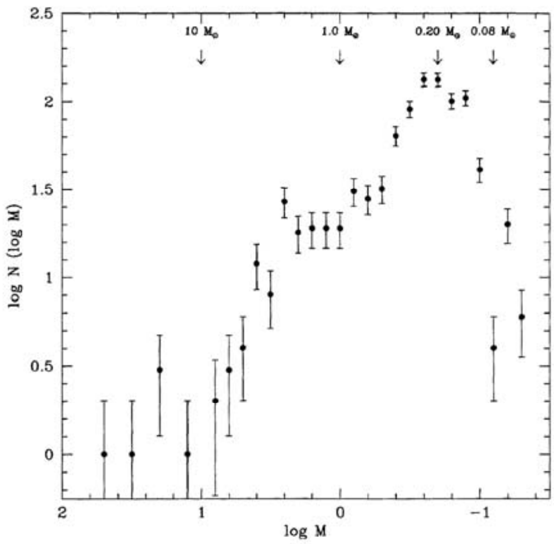

FIG. 17. *The Initial Mass Function as measured in the Orion Nebula Cluster.*

Hillenbrand 1997, AJ, 113, 1733

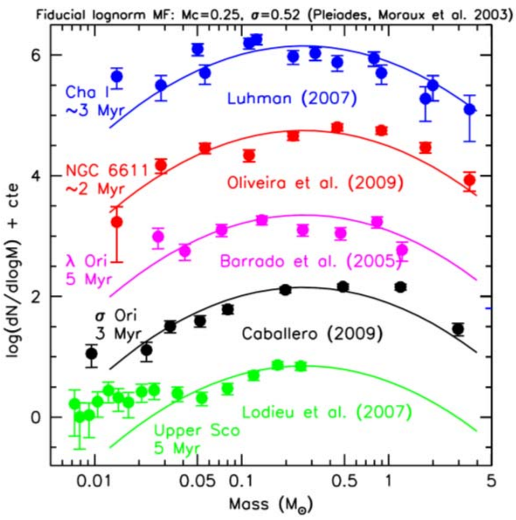

Fig. 9. The IMF determined in a number of young (< 10 Myr) clusters and star forming regions (offset for clarity). The solid lines show the log-normal model that best fits the Pleiades (see Fig. 8). The MFs may be generally consistent with that of the Pleiades but the MF of Upper Sco is quite different. Figure constructed by Bouvier & Moraux.

Jeffries 2012

Stellar Initial Mass Function and Dense Core Mass Function

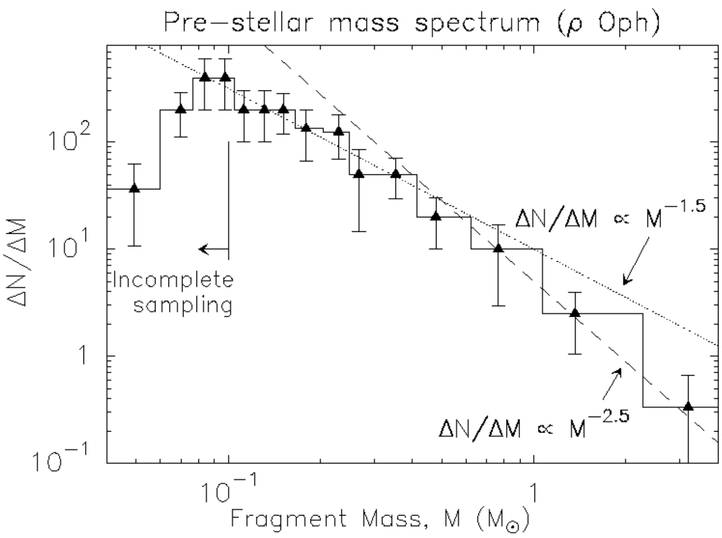

Andre et al. (2000) Protostars & Planets IV

91

Formation of Massive Stars

- **Competitive accretion (of cloud cores)**

  ... low-mass protostars competing with each other, and accrete matter from the parent molecular cloud

- **Coalescence of two or more stars with lower masses**

92

SUBMITTED ON FEBRUARY 17TH, 2015
Preprint typeset using LaTeX style emulateapj v. 12/16/11

THE HIGH-MASS STELLAR INITIAL MASS FUNCTION IN M31 CLUSTERS*

DANIEL R. WEISZ[1,12], L. CLIFTON JOHNSON[1], DANIEL FOREMAN-MACKEY[2], ANDREW E. DOLPHIN[3], LORI C. BEERMAN[1], BENJAMIN F. WILLIAMS[1], JULIANNE J. DALCANTON[1], HANS-WALTER RIX[4], DAVID W. HOGG[2,4], MORGAN FOUESNEAU[4], BENJAMIN D. JOHNSON[5], ERIC F. BELL[6], MARTHA L. BOYER[7], DIMITRIOS GOULIERMIS[4,8], PURAGRA GUHATHAKURTA[9], JASON S. KALIRAI[7], ALEXIA R. LEWIS[1], ANIL C. SETH[10], EVAN D. SKILLMAN[11]

Submitted on February 17th, 2015

ABSTRACT

We have undertaken the largest systematic study of the high-mass stellar initial mass function (IMF) to date using the optical color-magnitude diagrams (CMDs) of 85 resolved, young (4 Myr < t < 25 Myr), intermediate mass star clusters (10^3-10^4 $M_\odot$), observed as part of the Panchromatic Hubble Andromeda Treasury (PHAT) program. We fit each cluster's CMD to measure its mass function (MF) slope for stars $\gtrsim 2$ $M_\odot$. By modeling the ensemble of clusters, we find the distribution of MF slopes is best described by $\Gamma = +1.45^{+0.03}_{-0.06}$ with a very small intrinsic scatter. This model allows the MF slope to depend on cluster mass, size, and age, but the data imply no significant dependencies within this regime of cluster properties. The lack of an age dependence suggests that the MF slope has not significantly evolved over the first ~ 25 Myr, and provides direct observational evidence that the measured MF represents the IMF. Taken together, this analysis — based on an unprecedented large sample of young clusters, homogeneously constructed CMDs, well-defined selection criteria, and consistent principled modeling — implies that the high-mass IMF slope in M31 clusters is universal. The IMF has a slope ($\Gamma = +1.45^{+0.03}_{-0.06}$) that is slightly steeper than the canonical Kroupa (+1.30) and Salpeter (+1.35) values, with no drastic outliers in this sample of nearly 100 clusters. Using our inference model on select Milky Way (MW) and LMC high-mass IMF studies from the literature, we find $\Gamma_{MW} \sim +1.15 \pm 0.1$ and $\Gamma_{LMC} \sim +1.3 \pm 0.1$, both with intrinsic scatter of $\sim$0.3–0.4 dex. Thus, while the high-mass IMF in the Local Group may be universal, systematics in literature IMF studies preclude any definitive conclusions; homogenous investigations of the high-mass IMF in the local universe are needed to overcome this limitation. *Consequently, the present study represents the most robust measurement of the high-mass IMF slope to date*. To facilitate practical use over the full stellar mass spectrum, we have grafted the M31 high-mass IMF slope onto widely used sub-solar mass Kroupa and Chabrier IMFs. The increased steepness in the M31 high-mass IMF slope implies that commonly used UV- and Hα-based star formation rates should be increased by a factor of $\sim$1.3–1.5 and the number of stars with masses > 8 $M_\odot$ are $\sim 25\%$ fewer than expected for a Salpeter/Kroupa IMF.

93

Compact Objects

Compact Objects

Nuclear energy $4\,{}^{m}H - {}^{m}He = 0.029\, m_H$

mass deficit $= 7 \times 10^{-3}$ g/g

$\therefore$ Energy available $= mc^2 = 6 \times 10^{18}\ \text{erg g}^{-1}$

Chemical energy $\lesssim 100$ kcal $\Rightarrow 4 \times 10^{12}\ \text{erg g}^{-1}$

Gravitational energy e.g. for $\odot$, $\frac{3}{5} \frac{M_\odot^2 G}{R_\odot} \sim 2 \times 10^{48}$ erg

$\Rightarrow 10^{15}\ \text{erg g}^{-1}$

Accretion $\frac{MG}{r} \cdot \dot{m}$

In general $\frac{\mathcal{E}_{nuc}}{mass} \sim 0.01c^2$ $\frac{\mathcal{E}_{grav}}{mass} \sim \frac{3GM}{5R}$,

$\uparrow\uparrow$ as $R \downarrow\downarrow$

For very compact objects, large amounts of gravitational energy can be released, perhaps even more than nuclear energy,

$$R \lesssim \frac{MG}{0.01c^2} \sim 10^7 \text{ cm} \sim 100 \text{ km, for } 1 M_\odot$$

cf. Schwarzschild radius $R_S \equiv \frac{2GM}{c^2} \sim 3$ km, for $1 M_\odot$

More about Degeneracy

Atoms in a white dwarf are fully ionized and the e^- gas is degenerate.

1844 Bessel observed the oscillated path of Sirius

1862 Sirius B discovered by Clark

$M(\text{Sirius B}) \sim 2\times10^{33}\ g$ ← orbit

$R(\text{Sirius B}) \sim 2\times10^{9}\ cm$ ← surface temp. and radiation

cf $R_\odot \sim 7\times10^{10}\ cm$

$$\bar{\rho}_{\text{Sirius B}} = \frac{M}{\frac{4}{3}\pi R^3} \sim 0.7\times10^{5}\ g\,cm^{-3}$$

cf $\bar{\rho}_{sun} \sim 1\ g\,cm^{-3}$

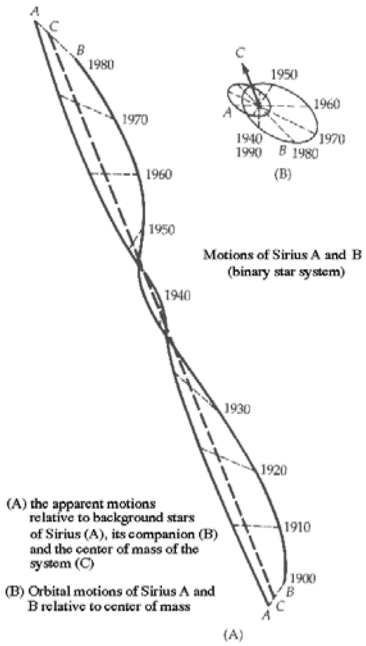

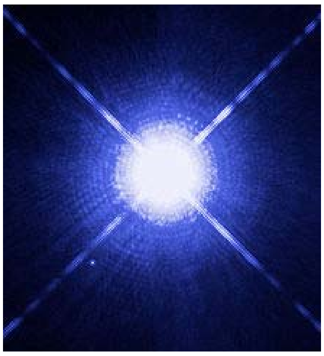

Sirius A and B by the *HST*

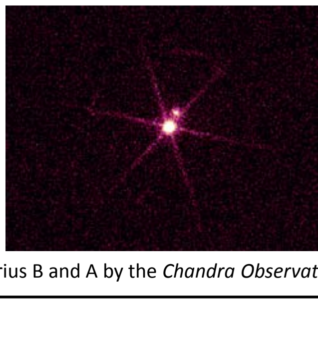

Sirius B and A by the *Chandra Observatory*

For WDs $\langle \rho \rangle \sim 10^5 - 10^6 \ g \ cm^{-3}$

mean separation of carbon ions

$$\langle d_{ii} \rangle \sim \left(\frac{\rho}{m_c} \right)^{-1/3} \approx 0.02 \text{ Å}$$

$$m_c \simeq 12 \, m_H$$

but the size of a normal carbon atom

$$r_c \simeq \frac{a_0}{Z} \simeq \frac{a_0}{6} \simeq 0.08 \text{ Å}$$

$\therefore$ complete ionization

$\rightarrow$ fermion gas of separate nuclei & e^-

electron gas

Mean separation of electrons

$$\langle d_{ee} \rangle \sim \left(\frac{Z\rho}{m_c} \right)^{-1/3} \approx 0.01 \text{ Å}$$

but $\lambda_e = [\hbar^2/m_e kT]^{1/2} \approx 10$ Å $\Rightarrow$ QM treatment!

Particle in a Box

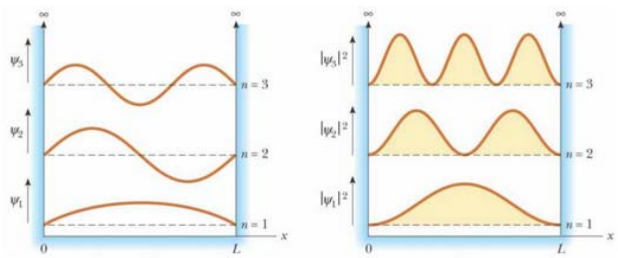

cf. standing wave in a string

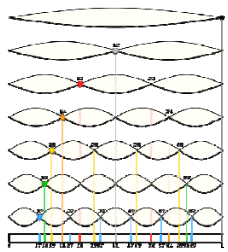

$\Psi = 0$ at the walls

→ De Broglie wavelength

$$\lambda_n = 2L/n\,, \quad n = 1, 2, 3, \ \ldots$$

Since $\lambda_n = {}^{h}/_{mv} \rightarrow E_K = {}^{1}/_{2} \, mv^2 = (mv)^2/2m = \dfrac{h^2}{2m\lambda^2}$

No potential ➔ $E_n = (mv)^2/2m = \dfrac{h^2}{2m\lambda_n^2} = \dfrac{n^2 h^2}{8mL^2} = \dfrac{1}{2m}\dfrac{n^2\pi^2\hbar^2}{L^2}$

Within the box, the Schrödinger equation

$$\frac{d^2\psi}{dx^2} + \frac{2m}{\hbar^2} E\psi = 0 \rightarrow \psi_n = \sqrt{\frac{2}{L}} \sin\frac{n\pi x}{L}$$

At the center, ψ_1, ψ_3 probability → max

ψ_2 probability $= 0$

c.f. classical physics → same probability everywhere in the box

Consider an atom in a box of volume $V = \ell^3$

wave equation $-\frac{\hbar^2}{2m}\nabla^2\psi = \varepsilon\,\psi$

energies, $\varepsilon_n = \frac{\hbar^2}{2m}\left(\frac{\pi}{\ell}\right)^2\left[n_x^2 + n_y^2 + n_z^2\right]$

where n_i's are quantum no's

any positive integer

In the phase space (n_i)

$$\varepsilon_F = \frac{\hbar^2}{2m}\left(\frac{\pi n_F}{\ell}\right)^2$$

n_F: radius that separates filled & empty states

$$\varepsilon_F = \frac{\hbar^2}{2m}\left(\frac{\pi\, n_F}{\ell}\right)^2$$

For N electrons (one octant; 2 spin states)

$$N_e = 2 \times \frac{1}{8} \times \frac{4}{3}\pi n_F^3 \qquad n_F = \left(\frac{3}{\pi} N_e\right)^{1/3}$$

$$\therefore\ \mathcal{E}_F = \frac{\hbar^2}{2m}\frac{\pi^2}{V^{2/3}}\left(\frac{3}{\pi}N_e\right)^{2/3} = \frac{\hbar^2}{2m}\left(3\pi^2\frac{N_e}{V}\right)^{2/3}$$

$$\boxed{\mathcal{E}_F = \frac{\hbar^2}{2m}\left(3\pi^2 n_e\right)^{2/3}} \sim n_e^{2/3}$$

n_e: electron concentration

Fermi energy: the <u>highest</u> filled energy level at temperature zero

The total energy of the system in the ground state

$$U_e = 2\sum_{n\le n_F}\mathcal{E}_n = 2\times\frac{1}{8}\times 4\pi\int_0^{n_F} n^2\mathcal{E}_n\, dn$$

$$= \frac{\pi^2}{2m}\left(\frac{\hbar}{\ell}\right)^2\int_0^{n_F} n^4\, dn \qquad \mathcal{E}_n = \frac{\hbar^2}{2m}\left(\frac{\pi n}{\ell}\right)^2$$

$$= \frac{\pi^3}{10m}\left(\frac{\hbar}{\ell}\right)^2 n_F^5 = \cdots = \frac{3}{5}N_e\mathcal{E}_F$$

Fermi energy of degenerate fermion gases

Phase of matter	Particles	E_F	$T_F = E_F/k_B$ [K]
Liquid ^{3}He	atoms	4×10^{-4} eV	4.9
Metal	electrons	2–10 eV	5×10^4
White dwarfs	electrons	0.3 MeV	3×10^9
Nuclear matter	nucleons	30 MeV	3×10^{11}
Neutron stars	neutrons	300 MeV	3×10^{12}

$$E_F = \frac{\hbar^2}{2m_e}(3\pi^2 n_e)^{2/3}$$

The average kinetic energy per fermion (e^-)

$$\frac{U_e}{N_e} = \frac{3}{5}\varepsilon_F$$ (Degenerate, nonrelativistic)

i.e. average kinetic energy per particle $= \frac{3}{5}\varepsilon_F$

For $N =$ const, if $n_e \uparrow$ (i.e. volume $\downarrow$) $\quad \varepsilon_e \propto n_e^{2/3}$

$\Rightarrow u_e \uparrow \Rightarrow$ repulsive effect

Fermi energy tends to increase the volume.

$$P = \frac{2}{3}u_e = \frac{2}{5} n \varepsilon_F$$

It can be shown (!) that for a relativistic, for which the energy $\varepsilon \sim pc$ $\quad p$: momentum

$$\varepsilon_F = \hbar \pi c \left(\frac{3}{\pi} n_e\right)^{1/3} \sim n_e^{1/3}$$

and

$$\frac{U_e}{N} = \frac{3}{4}\varepsilon_F$$ (Degenerate, relativistic)

For any nonrelativistic particles

$$PV = \frac{2}{3} N E_K \Rightarrow P = \frac{2}{3} n E_K$$

For nonrelativistic degenerate gas

$$E_K = \frac{3}{5}\varepsilon_F = \frac{3}{5}(3\pi^2)^{2/3}\frac{\hbar^2}{2m} n_e^{2/3}$$

$$\Rightarrow P_{deg} \sim 1.004\times 10^{13}\left(\frac{\rho}{\mu_e}\right)^{5/3} \text{ [dynes cm}^{-2}\text{]}$$

$\mu_e \approx 2$ with no H

Degenerate State

$$E_n = \frac{\hbar^2}{2m}\left(\frac{n\pi}{\ell}\right)^2 \Rightarrow E_f = \frac{\hbar^2}{2m}\left(\frac{n_F\pi}{\ell}\right)^2 = \frac{\hbar^2}{2m}(3\pi^2 n_e)^{2/3}$$

$$\text{Total } N_e = 2\cdot\frac{1}{8}\cdot\frac{4}{3}\pi n_F^3 = \frac{\pi}{3} n_F^3 \Rightarrow n_F = \left(\frac{3}{\pi} n_e\right)^{1/3}$$

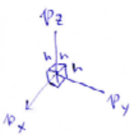

Uncertainty principle $\Delta V \Delta^3 p \lesssim h^3$

$$2\cdot 4\pi p^2 dp = h^3 \cdot n_e(p)\, dp$$

Considering the problem in terms of momentum

$$\text{Up to } p_F,\quad 2\cdot\frac{4}{3}\pi p_F^3 = N_e = n_e\cdot h^3 \Rightarrow p_F = \left(\frac{3h^3}{8\pi} n_e\right)^{1/3}$$

$$\text{Pressure integral } P = \frac{1}{3}\int_0^\infty n(p)\, v\, p\, dp \quad (\text{use } v = p/m_e)$$

Non-relativistic

$$= \frac{1}{3}\int_0^{p_F} \frac{8\pi p^2}{h^3}\frac{p}{m_e}\, p\, dp$$

$$= \frac{8\pi}{3m_e h^3}\frac{1}{5} p_F^5 = \frac{8\pi}{15 m_e h^3} p_F^5$$

$$\text{For electrons, } n_e = \frac{\rho}{\mu_e m_H} \quad \therefore P = \frac{h^2}{20 m_e}\left(\frac{3}{\pi}\right)^{2/3}\left(\frac{\rho}{\mu_e m_H}\right)^{5/3}$$

Pressure and Momentum

$$\boldsymbol{P} = \frac{1}{3}\int_0^\infty n(p)\, v\, p\, dp$$

In the non-relativistic case

$$P_{\mathrm{e,deg}}^{\mathrm{NR}} = \frac{h^2}{20 m_e}\left(\frac{3}{\pi}\right)^{2/3}\frac{1}{m_{\mathrm{H}}^{5/3}}\left(\frac{\rho}{\mu_e}\right)^{5/3}$$
$$= 1.00 \times 10^{13}\left(\frac{\rho}{\mu_e}\right)^{5/3} \quad [\mathrm{cgs}]$$
$$\propto \rho^{5/3}$$

In the **extremely** relativistic case $v \rightarrow c$ in the pressure integral

$$P_{\mathrm{e,deg}}^{\mathrm{ER}} = \frac{hc}{8}\left(\frac{3}{\pi}\right)^{1/3}\frac{1}{m_{\mathrm{H}}^{3/4}}\left(\frac{\rho}{\mu_e}\right)^{4/3}$$
$$= 1.24 \times 10^{15}\left(\frac{\rho}{\mu_e}\right)^{4/3} \quad [\mathrm{cgs}]$$
$$\propto \rho^{4/3}$$

For a composition devoid of hydrogen, and not very rich in extremely heavy elements, $\mu_e \approx 2$.

For Stars $M \lesssim 0.8 M_\odot$

P_{deg} enough to support the envelope

→ core contracts slowly, T↑ little

→ envelope expands gradually

Star moves upwards on H-R diagram

Originally, the structure of the star

↓T↑

$T \sim 5\times10^4$ K, atoms completely ionized

Why does a red giant puff off?

As envelope $\uparrow$, $T \downarrow$ (cooling), $E_K \downarrow$ and

$H^+ + e^-$ recombine

$$H^+ + e^- \longrightarrow H + \gamma$$

$\Rightarrow$ Energy source!

So outer envelope (beyond recombination layers)

$\Delta T / \Delta r \uparrow$ pushing the envelope

At the same time, gravity $F_g \propto 1/r^2 \downarrow\downarrow$

Recombination $\uparrow$ $\Rightarrow$ $L \uparrow$, $\nabla T \uparrow$, $F_g \downarrow$

$\Rightarrow$ $T \downarrow\downarrow$ $\Rightarrow$ Recombination $\uparrow\uparrow$ ...

'Runaway' process $\Rightarrow$ Envelope 'blown' away

Mechanical Pressure

$$P = P_{Ions} + P_{electrons} + P_{rad} + \cdots$$

- If the gas nondegenerate

$$P_I + P_e = P_{gas} = \frac{k}{\mu m_H} \rho T$$

- If gas degenerate (e^-) P_I : ideal gas

  P_e : degenerate eq. of state

- If photon gas $P_I + P_e \ll P_{rad} = \frac{1}{3} a T^4$, $a = \frac{4\sigma}{c}$

Note

Above needs modifications

- $T \uparrow\uparrow$, e.g. $T > 10^9$ K

  $p^+ - e^-$ pair production

- $\rho \uparrow\uparrow$, particle interaction $\not\Leftrightarrow$ ideal gas

- $\vec{B}$, addition of P_{mag}

Radiation pressure $P_{rad} = \frac{1}{3} a T^4$

For $P_{gas} = P_{rad} \Rightarrow T = 3.20 \times 10^7 (\rho/\mu)^{1/3} \sim 3.6 \times 10^7 \rho^{1/3}$

$$P_{\text{ideal gas}} \propto \rho\, T/\mu$$

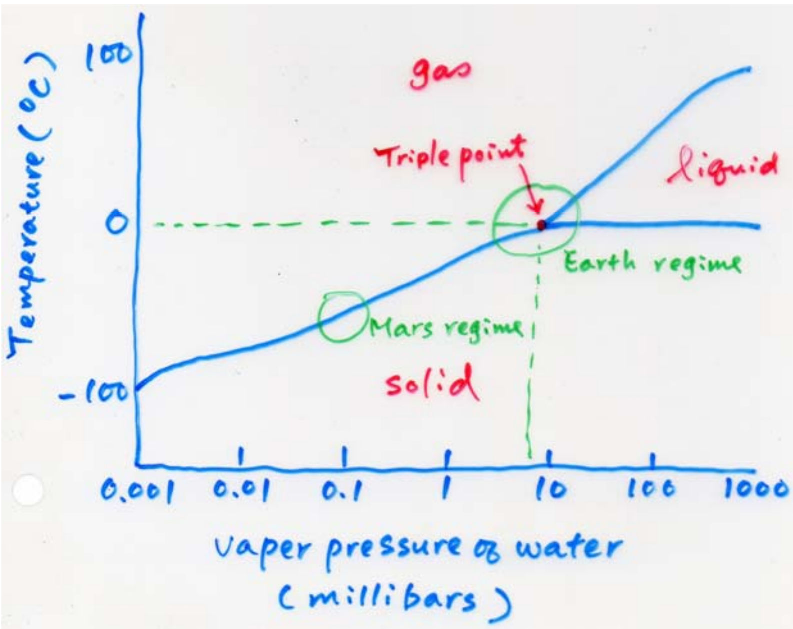

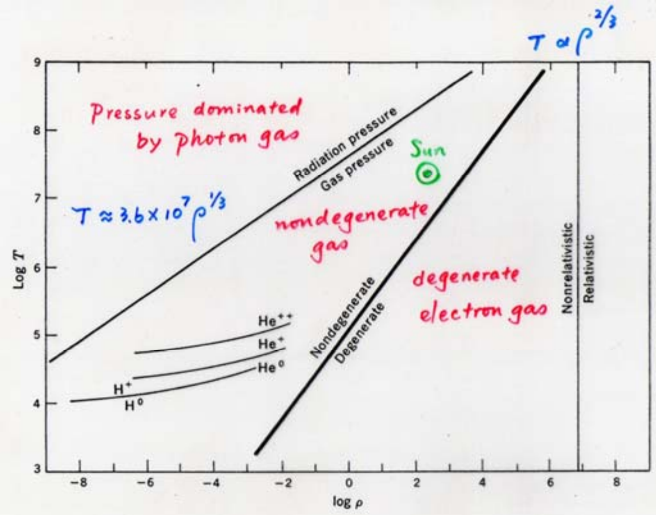

Fig. 2-11 Zones of the equation of state of a gas in thermodynamic equilibrium. Radiation pressure dominates the gas pressure in the upper left-hand corner. The remaining boundaries are similar to those in Fig. 2-7. Also included for comparison are the transition strips in a hydrogen-dominated gas between H^0 and H^+, between He^0 and He^+, and between He^+ and He^{++}.

From clayton

Nonrelativistic, complete degeneracy

- $P_{NR,e} \sim 1.004 \times 10^{13} \left(\rho/\mu_e\right)^{5/3}$ [dynes cm^{-2}]

cf NR, non-degenerate case, i.e., ideal gas

- $P_{ideal} \sim \rho T$

So, as $\rho \uparrow \Rightarrow P_{ideal} \longrightarrow P_{deg}$

and at relatively low temperature

$$P_{gas} = P_{ions} + P_{e^-} = \left(\frac{1}{\mu_I} + \frac{1}{\mu_e}\right)\cdots$$

$$\equiv \frac{1}{\mu}\cdots$$

$$\therefore \frac{1}{\mu} \equiv \frac{1}{\mu_I} + \frac{1}{\mu_e} = 0.61 \text{ for } \odot$$

cf. $\frac{1}{\mu_e} \approx \frac{1}{2}(1+X)$ for $\odot$

$\sum_i X_i \frac{Z_i}{A_i}$ [average # of free electrons per nucleon]

$$\left(\frac{\rho}{\mu_e}\right)^{5/3} \longleftrightarrow \rho T \quad \text{or} \quad T \sim \rho^{2/3}$$

$$\boxed{\frac{\rho_{crit}}{\mu_e} \gtrsim 2.4\times10^{-8}\, T^{3/2}\ [\mathrm{g\,cm^{-3}}]}$$ when degeneracy sets in

Relativistic complete degeneracy

Total energy $\sim m_0 c^2$
$p_0 c$

$$\boxed{\frac{\rho_{crit}}{\mu_e} \gtrsim 7.3\times10^{6}\ [\mathrm{g\,cm^{-3}}]}$$

where relativistic kinetics has to be used.

Note $\rho > 10^6\ \mathrm{g\,cm^{-3}}$ for a degenerate gas to be relativistic, $T > 10^9$ K to be completely degenerate.

Conditions that satisfy both $\rho > 10^6$, $T > 10^9$ probably exist only in very late stages of stellar evolution

Almost in all other cases, nonrelativistic is ok!

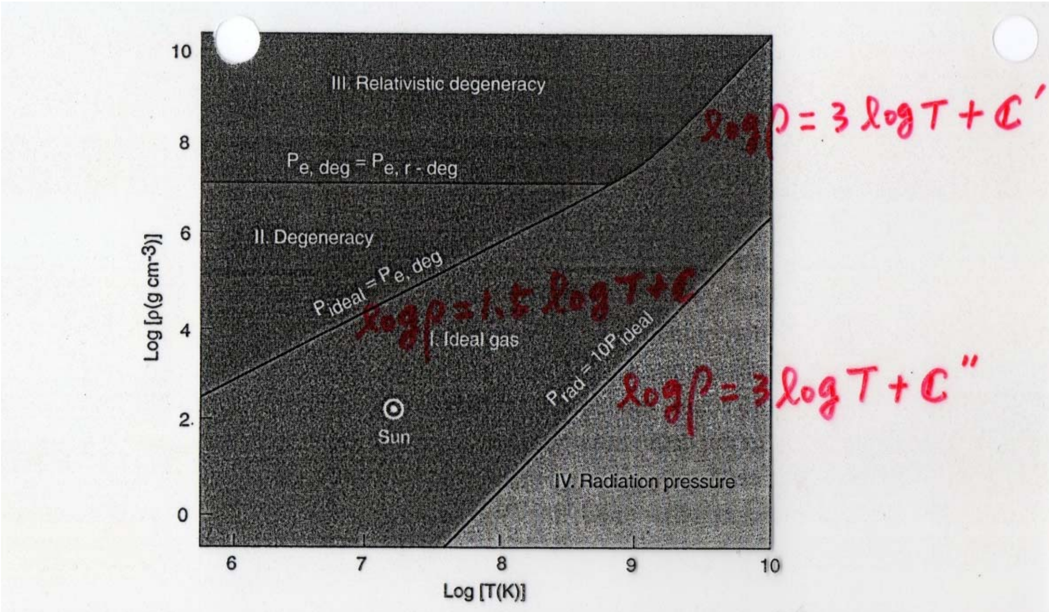

Figure 7.1 Mapping of the temperature-density diagram according to the equation of state.

In general → partial degeneracy

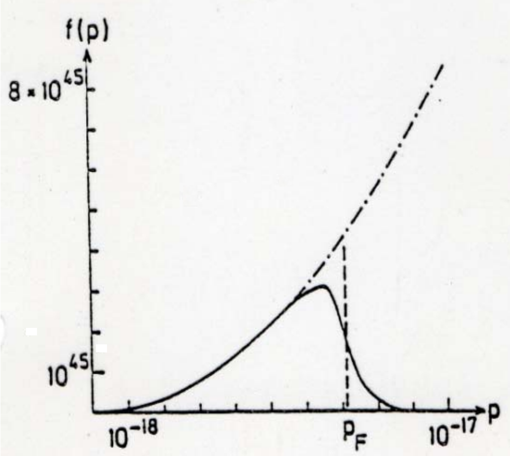

Fig. 15.5. The solid line gives the distribution function ($f(p)$ and p in cgs) for a partially degenerate electron gas with $n_e = 10^{28}$ cm^{-3} and $T = 1.9 \times 10^7$ K, which corresponds to a degeneracy parameter $\psi = 10$ (cf. the case of complete degeneracy of Fig. 15.2). The dot-dashed line shows the further increase of the parabola that defines an upper bound for the distribution function

... need evaluation of each parameter ...

$$n_e = \frac{8\pi}{h^3}\int_0^\infty \frac{p^2\,dp}{1+\exp[E/kT - \psi]}$$

$$P_e = \frac{8\pi}{3h^3}\int_0^\infty p^3 \cdot v(p)\,\frac{dp}{1+\exp\left[\frac{E}{kT}-\psi\right]}$$

$$u_e = \frac{8\pi}{h^3}\int_0^\infty \frac{E\,p^2\,dp}{1+\exp\left[\frac{E}{kT}-\psi\right]}$$

In the non-rel. case $E = p^2/2m_e$

$$n_e = \frac{8\pi}{h^3}\int \frac{p^2\,dp}{1+\exp\left[\frac{p^2}{2m_e kT}-\psi\right]} \equiv \frac{8\pi}{h^3}(2m_e kT)^{3/2}\,a(\psi)$$

where $a(\psi) = \int_0^\infty \frac{\eta^2}{1+\exp[\eta^2-\psi]}\,d\eta$

where $\eta \equiv p/(2m_e kT)^{1/2}$

Note: $n_e \sim T^{3/2}\,a(\psi)$

So, $\psi \equiv \psi(n_e T^{-3/2})$

⋮

(rel. case 略)

Define Fermi-Dirac Integral

$$F_\nu(\psi) = \int_0^\infty \frac{u^\nu}{1 + e^{u-\psi}}\, du$$

$$n_e = \frac{4\pi}{h^3} (2 m_e k T)^{3/2} F_{1/2}(\psi)$$

In general, the condition may be neither highly relativistic, nor completely nonrelativistic.

The pressure can be expressed as

$$P = K f(x)$$

$$f(x) = \cdots \qquad x = p_F / m_e c$$

Tabulation of Fermi integrals

Table 15.1 Numerical values for Fermi–Dirac functions $F_{1/2}$, $F_{3/2}$ (after McDOUGALL, STONER, 1939) F_2, F_3 (after HILLEBRANDT, 1989)

ψ	$\frac{2}{3}F_{3/2}(\psi)$	$F_{1/2}(\psi)$	$F_2(\psi)$	$F_3(\psi)$
−4.0	0.016179	0.016128	0.036551	0.109798
−3.5	0.026620	0.026480	0.060174	0.180893
−3.0	0.043741	0.043366	0.098972	0.297881
−2.5	0.071720	0.070724	0.162540	0.490154
−2.0	0.117200	0.114588	0.266290	0.805534
−1.5	0.190515	0.183802	0.434606	1.321232
−1.0	0.307232	0.290501	0.705194	2.160415
−0.5	0.489773	0.449793	1.134471	3.516135
0.0	0.768536	0.678094	1.803249	5.683710
0.5	1.181862	0.990209	2.821225	9.100943
1.0	1.774455	1.396375	4.328723	14.393188
1.5	2.594650	1.900833	6.494957	22.418411
2.0	3.691502	2.502458	9.513530	34.307416
2.5	5.112536	3.196598	13.596760	51.496218
3.0	6.902476	3.976985	18.970286	75.749976
3.5	9.102801	4.837066	25.868717	109.179565
4.0	11.751801	5.770726	34.532481	154.252522
4.5	14.88489	6.77257	45.20569	213.80007
5.0	18.53496	7.83797	58.13474	291.02151
5.5	22.73279	8.96299	73.56744	389.48695
6.0	27.50733	10.14428	91.75247	513.13900
6.5	32.88598	11.37898	112.93904	666.29376
7.0	38.89481	12.66464	137.37668	853.64147
7.5	45.55875	13.99910	165.31509	1080.24689
8.0	52.90173	15.38048	197.00413	1351.54950
8.5	60.94678	16.80714	232.69369	1673.36371
9.0	69.71616	18.27756	272.63375	2051.87884
9.5	79.23141	19.79041	317.07428	2493.65928
10.0	89.51344	21.34447	366.26528	3005.64445
10.5	100.58256	22.93862	420.45675	3595.14883
11.0	112.45857	24.57184	479.89871	4269.86200
11.5	125.16076	26.24319	544.84118	5037.84863
12.0	138.70797	27.95178	615.53418	5907.54847
12.5	153.11861	29.69679	692.22772	6887.77637
13.0	168.41071	31.47746	775.17183	7987.72229
13.5	184.60190	33.29308	864.61653	9216.95127
14.0	201.70950	35.14297	960.81184	10585.40346
14.5	219.75048	37.02649	1064.00779	12103.39411
15.0	238.74150	38.94304	1174.45439	13781.61356
15.5	258.69893	40.89206	1292.40167	15631.12726
16.0	279.63888	42.87300	1418.09966	17663.37576
16.5	301.57717	44.88535	1551.79837	19890.17470
17.0	324.52939	46.92862	1693.74783	22323.71482
17.5	348.51087	49.00235	1844.19805	24976.56198
18.0	373.53674	51.10608	2003.39907	27861.65710
18.5	399.62188	53.23939	2171.60091	30992.31625
19.0	426.78099	55.40187	2349.05358	34382.23057
19.5	455.02855	57.59313	2536.00711	38045.46629
20.0	484.37885	59.81279	2732.71153	41996.46477

For partial degeneracy : Fermi-Dirac function

See: clayton

Radiation pressure $P_{rad} = \frac{1}{3} a T^4$

$P_{gas} = P_{rad} \Rightarrow T = 3.20 \times 10^7 (\rho/\mu)^{1/3}$

$\boldsymbol{P}_{\text{ideal gas}} \propto \rho\, T/\mu$

$$\boldsymbol{P}^{NR}_{e,deg} = 1.00 \times 10^{13} \left(\frac{\rho}{\mu_e}\right)^{5/3} \text{[cgs]}$$

$$\boldsymbol{P}^{ER}_{e,deg} = 1.24 \times 10^{15} \left(\frac{\rho}{\mu_e}\right)^{4/3} \text{[cgs]}$$

$$\boldsymbol{P}_{\text{rad}} = \frac{1}{3}\, a\, T^4$$

Non-Relativistic, Non-Degenerate (i.e., ideal gas)

Non-Relativistic, Extremely Degenerate

Extremely Relativistic, Extremely Degenerate

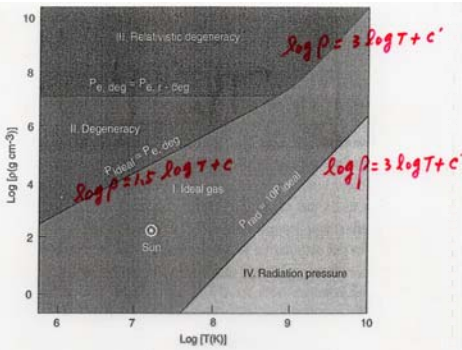

Figure 7.1 Mapping of the temperature-density diagram according to the equation of state.

NR, ND $\quad P \sim \rho T$

NR, ED $\quad P \sim \rho^{5/3}$ $\quad \Big\}\ \log \rho = 1.5 \log T + \text{const.}$

ER, ED $\quad P \sim \rho^{4/3}$ $(\sim \rho T)$ $\quad \Big\}\ \log \rho = 3 \log T + \text{const}$

P_{rad} vs $P_{ideal\ gas}$ $\quad P_{rad} \sim T^4$, $P_{gas} \sim \rho T$ $\quad \Big\}\ \log \rho = 3 \log T + \text{const}$

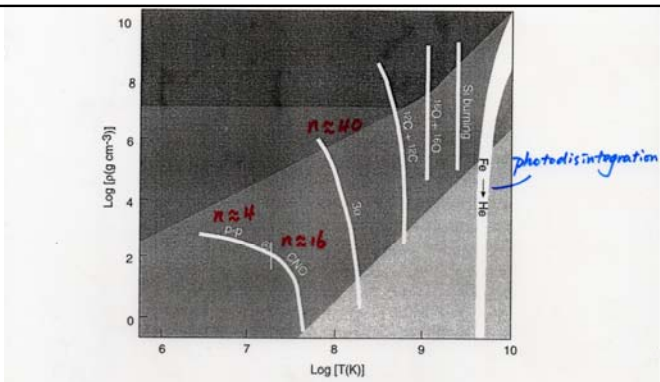

Figure 7.2 Mapping of the temperature-density diagram according to nuclear processes.

$q = q_0 \rho^m T^n$ threshold e.g., $q > q_{min} (\equiv 10^3 \, erg \, s^{-1} g^{-1})$

$\log \frac{q_{min}}{q_0} = m \log \rho + n \log T$ ⇒ important

$\Rightarrow \log \rho = -\frac{n}{m} \log T + \frac{1}{m} \log (q_{min}/q_0)$

slope < 0

For H (p-p, CNO), He (3α), C, O, Si burning, $n \gg m$

⇒ nearly vertical lines

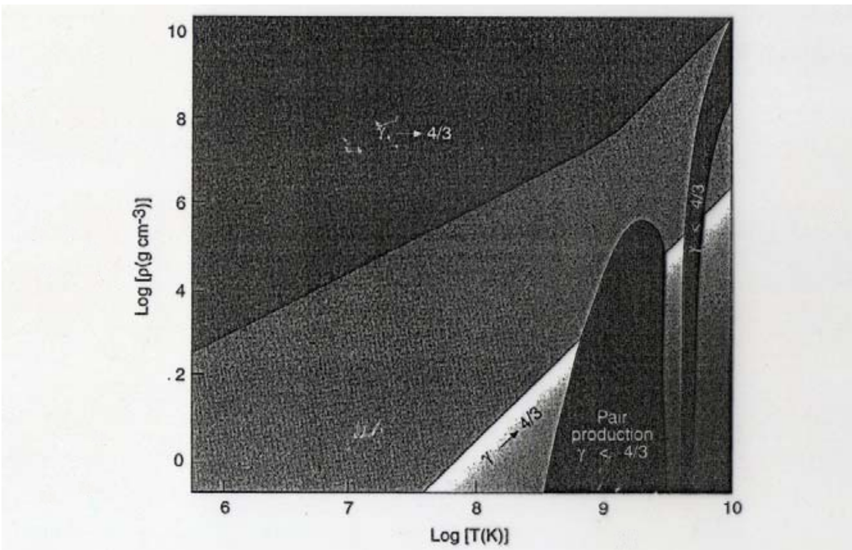

Figure 7.3 Outline of the stable and unstable zones in the temperature-density diagram.

$\gamma > 4/3 \Rightarrow$ stability

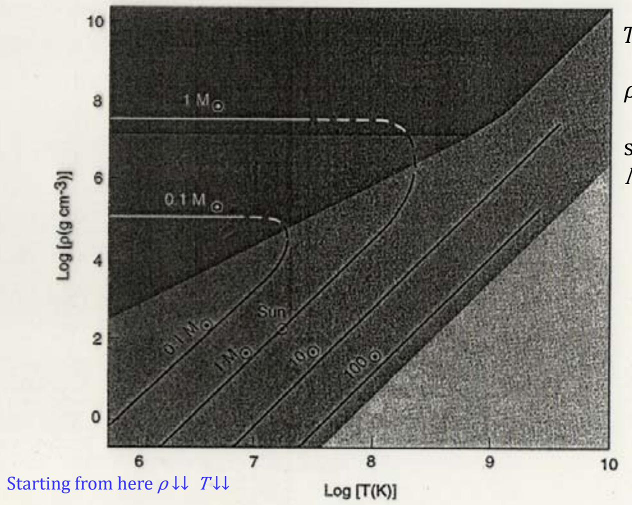

$T_c \propto \mu\, GM/R$

$\rho_c \propto T_c^3 \,/\, M^2$

so for a given M, slope =3

Figure 7.4 Relation of central density to central temperature for stars of different masses within the stable ideal gas and degenerate gas zones.

From Prialnik

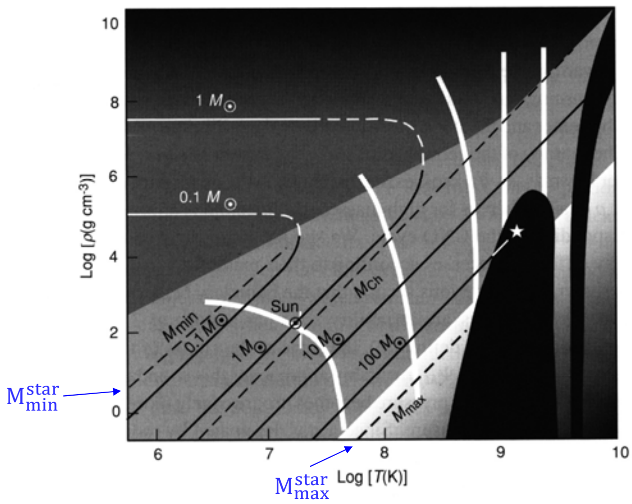

Figure 7.5 Schematic illustration of the evolution of stars according to their central temperature-density tracks.

From nonrelativistic to relativistic degeneracy

In a completely degenerate gas, the equation of state

$$P \sim \rho^{5/3} \quad \text{NR}$$

or

$$P \sim \rho^{4/3} \quad \text{ER}$$

cf. ideal gas $P \sim \rho T$

Hydrostatic equilibrium requires

$$P \sim \frac{M^2}{R^4}$$

In the nonrelativistic case

There is a solution in case of NR.

$$P \sim \frac{M^2}{R^4} \sim \rho^{5/3} \sim \left(\frac{M}{R^3}\right)^{5/3} \sim \frac{M^{5/3}}{R^5}$$

$$\Rightarrow \boxed{R \sim M^{-1/3}}$$

$\therefore$ R ↓ as M ↑ for WDs

The more massive of a WD, the smaller of its size.

Numerically

$$\log\left(\frac{R}{R_\odot}\right) = -\frac{1}{3}\log\left(\frac{M}{M_\odot}\right) - \frac{5}{3}\log(\mu_e) - 1.397$$

(Lang) Vol. 1

For $1\,M_\odot$, $R = 0.0126\,R_\odot$

$\langle \rho \rangle \sim 7 \times 10^5\ \mathrm{g\,cm^{-3}}$

What happens in the ER case?

Total kinetic energy

$$E_K = N_e \frac{p^2}{2m} \quad (NR)$$

$$\left(\begin{array}{l} \text{degeneracy } p \approx \Delta p \\ \text{and } \Delta p \Delta x \sim \hbar \\ n_e = \frac{N_e}{R^3}, \quad \Delta p \sim \frac{\hbar}{\Delta x} \sim \frac{\hbar}{n^{-1/3}} \end{array} \right)$$

$$E_K = \frac{N_e (\Delta p)^2}{2 m_e} = \frac{N_e^{5/3}}{2 m_e} \cdot \frac{\hbar^2}{R^2} \qquad \frac{1}{\mu_e}$$

$$\left(N_e = \frac{MZ}{A m_H} \approx \frac{1}{2} \frac{M}{m_H} \right)$$

Virial theorem (Equipartion)

$$E_p = \left| \frac{GM^2}{R} \right| \simeq 2 E_K \Rightarrow R \approx \frac{\hbar^2}{G m_e m_H^{5/3}} \cdot M^{-1/3}$$

Note $M^{1/3} R \approx$ const

$$\frac{R}{R_\odot} \approx \frac{1}{74} \left(\frac{M_\odot}{M} \right)^{1/3}$$

The luminosity $L = 4\pi R^2 \sigma T_{\rm eff}^4 \approx \frac{1}{74^2} \left(\frac{M_\odot}{M} \right)^{2/3} \left(\frac{T_{\rm eff}}{6000} \right)^4 \quad [L_\odot]$

So a WD with $M = 0.4\ \mathrm{M}_\odot$ and $T_{\rm eff} = 10^4$ K has $L = 3 \times 10^{-3}\ \mathrm{L}_\odot$

Gravity

$$g = \frac{GM}{R^2} \approx 74^2 \left(\frac{M}{M_\odot}\right)^{5/3} \frac{GM_\odot}{R_\odot^2}$$

For a WD with $M = 0.4\ \mathrm{M}_\odot$, $g = 4 \times 10^7 \mathrm{cm\ s}^{-2}$

Gravitational Red shift

$$\frac{\Delta\lambda}{\lambda} = \left(1 - \frac{2GM}{Rc^2}\right)^{-1/2} \approx \frac{GM}{Rc^2} \approx 74 \left(\frac{M}{M_\odot}\right)^{4/3} \frac{GM_\odot}{R_\odot c^2}$$

In case of ER, $\breve{E}_R = N_e\, pc$

There is no solution in case of ER.

$$\breve{E}_R = N_e \frac{\hbar N_e^{1/3}}{R} \cdot c = \frac{M^{4/3}\, \hbar c}{m_H^{4/3} \cdot R}$$

$$\breve{E}_P = \left|\frac{GM^2}{R}\right|$$

$\breve{E}_R \simeq \breve{E}_P$, R cancels out; no solution for $M \equiv M(R)$

$$P = \frac{M^2}{R^4}\ (\text{if}) = \rho^{4/3} = \left(\frac{M}{R^3}\right)^{4/3}$$ ➔ no solution

- For degenerate gas, $M_{\text{WD}} \uparrow$, $R_{\text{WD}} \downarrow$
- For $M_{\text{WD}} = 1\ M_{\odot}$, $R_{\text{WD}} = 0.02\ R_{\odot}$
- There is an upper limit to the mass

$$M_{\text{limit}} \approx \left(\frac{\hbar c}{G M_H^{4/3}}\right)^{3/2} \approx 2\ M_{\odot}$$

$$\mu_e = 1 \text{ (for H)}$$
$$= 2 \text{ (for He)}$$
$$= 56/26 = 2.15$$

Rigorously,

$$M_{\text{limit}} \approx \frac{5.836}{\mu_e^2} M_{\odot}$$

$M_{\text{limit}}\ (\text{Fe}) = 1.26\ \text{M}_{\odot}$

Weinberg (1972) $M_{\text{limit}} \approx 1.2\ M_{\odot}$, Later value $M_{\text{limit}} \approx 1.44\ M_{\odot}$

$M_{ch} = 1.44\ M_{\odot}$ needs corrections

— grav force on nuclei

deg. force on electrons

$\Rightarrow$ separation $\rightarrow \vec{E}$!

— e^- into nuclei $\Rightarrow n_e \downarrow$

TABLE 8.5. Central Densities, Total Mass, and Radius of Different White Dwarf Models, Taking $\mu_e = 2$ (Negligible Hydrogen Concentration).[a]

$\log \rho_c$	$M/M_{\odot}$	$\log R/R_{\odot}$
5.39	0.22	−1.70
6.03	0.40	−1.81
6.29	0.50	−1.86
6.56	0.61	−1.91
6.85	0.74	−1.96
7.20	0.88	−2.03
7.72	1.08	−2.15
8.21	1.22	−2.26
8.83	1.33	−2.41
9.29	1.38	−2.53
∞	1.44	−∞

[a] See text for comments (after M. Schwarzschild (Sc58b)). From *Structure and Evolution of the Stars* ©1958 by Princeton University Press, p. 232.

$$L = \sigma T_e^4 (4\pi R^2)$$

$$\log\left(\frac{L}{L_\odot}\right) = 4 \log\left(\frac{T_e}{T_{e\odot}}\right) + 2 \log\left(\frac{R}{R_\odot}\right)$$

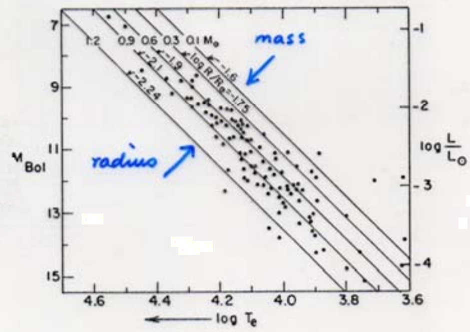

FIGURE 8.14. White dwarf Hertzsprung–Russell diagram. Lines of constant radius are shown. Also shown are the masses based on completely degenerate core models containing elements having $\mu_e = 2$ (after Weidemann (We68)). Reprinted with permission from *Annual Review of Astronomy and Astrophysics*, Vol. 6, ©1968 by Annual Reviews, Inc.).

THE ASTROPHYSICAL JOURNAL, 784:57 (10pp), 2014 March 20

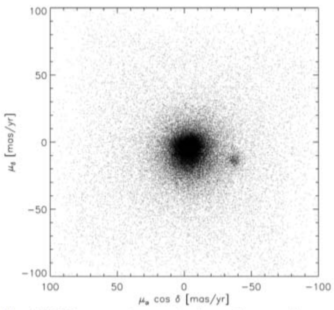

Figure 1. PPMXL proper motion vector point diagram of stars toward Praesepe. Stars within an angular distance of 5° of the cluster center are analyzed. Only stars spatially within the central 2° are displayed here for clarity.

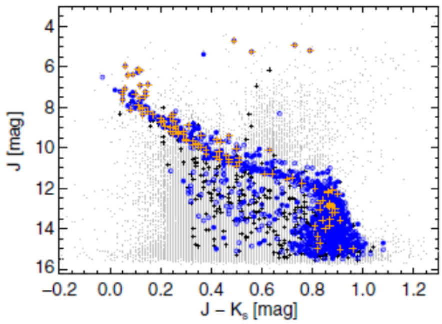

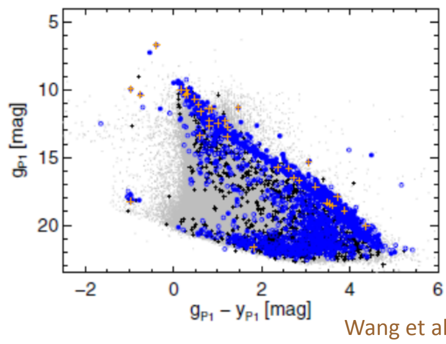

Figure 4. Top: J vs. $J - K_s$ CMD for all the stars (gray dots), those with angular distances greater than 3° from the cluster center but with $\Delta\mu < 9$ mas yr^{-1} (small black crosses), those within 3° from the cluster center and with $\Delta\mu < 9$ mas yr^{-1} (blue open circles), and those within 3° and with $\Delta\mu < 4$ mas yr^{-1} (blue filled circles). The stars at the very center of the cluster, namely within 30′, and with $\Delta\mu < 4$ mas yr^{-1} are highly probable members and are marked as orange crosses. Note the group of blue stragglers beyond the main sequence turn-off point (Andrievsky 1998). Bottom: g_{P1} vs. $g_{P1} - y_{P1}$ CMD, with the same symbols as in the top panel. The group of stars near $g_{P1} = 18$ mag, and $g_{P1} - y_{P1} = -1$ mag include white dwarfs known in the cluster (Dobbie et al. 2004, 2006).

Wang et al. 2014

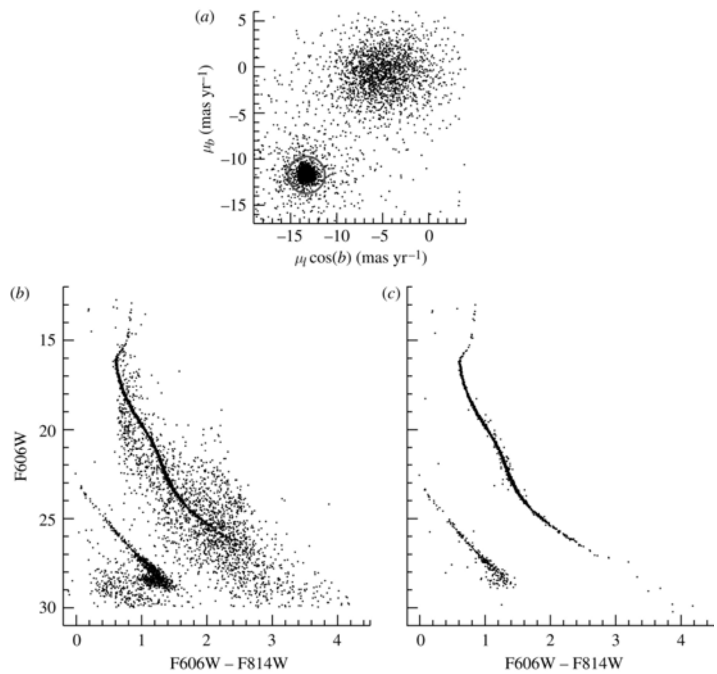

Kalirai 2010

THE ASTRONOMICAL JOURNAL, 143:11 (21pp), 2012 January
doi:10.1088/0004-6256/143/1/11

A DEEP, WIDE-FIELD, AND PANCHROMATIC VIEW OF 47 Tuc AND THE SMC WITH *HST*: OBSERVATIONS AND DATA ANALYSIS METHODS*

JASON S. KALIRAI[1,8], HARVEY B. RICHER[2], JAY ANDERSON[1], AARON DOTTER[1], GREGORY G. FAHLMAN[3], BRAD M. S. HANSEN[4], JARROD HURLEY[5], IVAN R. KING[6], DAVID REITZEL[4], R. M. RICH[4], MICHAEL M. SHARA[7], PETER B. STETSON[3], AND KRISTIN A. WOODLEY[2]
[1] Space Telescope Science Institute, 3700 San Martin Drive, Baltimore, MD 21218, USA; jkalirai@stsci.edu, jayander/dotter@stsci.edu

Figure 1. Wide field ground based image of the Small Magellanic Cloud (SMC) in the southern skies reveals two foreground Milky Way globular clusters, NGC 362 just below the SMC and 47 Tuc to the left of the galaxy. Although the main body of the SMC is separated from 47 Tuc by more than 2°, a diffuse stellar population persists to greater radii and represents a background source of stars in our study (as demonstrated later). This image subtends 6.8 × 4.5 and was taken with a 300 mm lens in 2007 September. The image was made by combining multiple 10 minute exposures in five visible filters (including Hα). Image is courtesy of Stéphane Guisard and reproduced here with permission, http://www.astrosurf.com/sguisard.
(A color version of this figure is available in the online journal.)

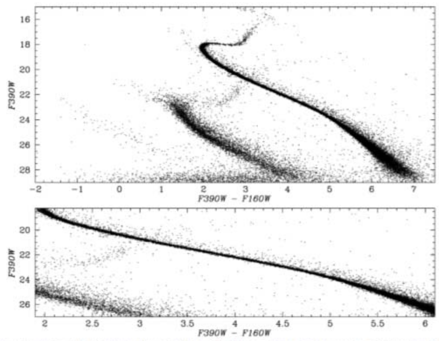

Figure 12. Panchromatic nature of this study is highlighted by constructing a CMD of the stellar populations over the widest baseline of $F390W - F160W$ (i.e., 0.4–1.7 μm). The combined WFC3/UVIS and IR data stretch the stellar populations over a color range of >9 mag (top panel). Despite their faintness in the IR, over 150 white dwarfs form a cooling sequence on this CMD. The bottom panel focuses on the main sequence of 47 Tuc, which is stretched over >4 mag of color.

White Dwarf Cooling

- WDs are supported by electron degeneracy pressure. With no sustaining energy source (such as fusion), they continue to cool and fade ➔ very faint
- The luminosity of the faintest WDs in a star cluster ←→ cooling theory ➔ age
- The age of the oldest globular cluster = lower limit of the age of the universe

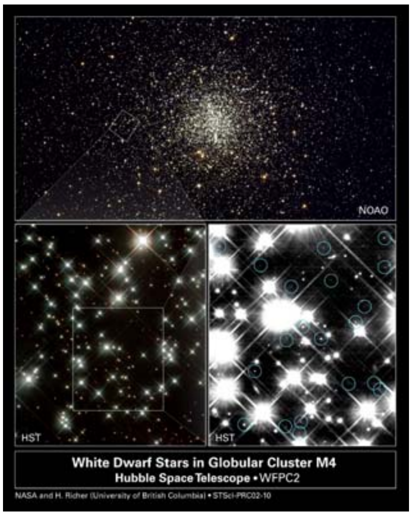

Limiting V=30

White Dwarf Cooling

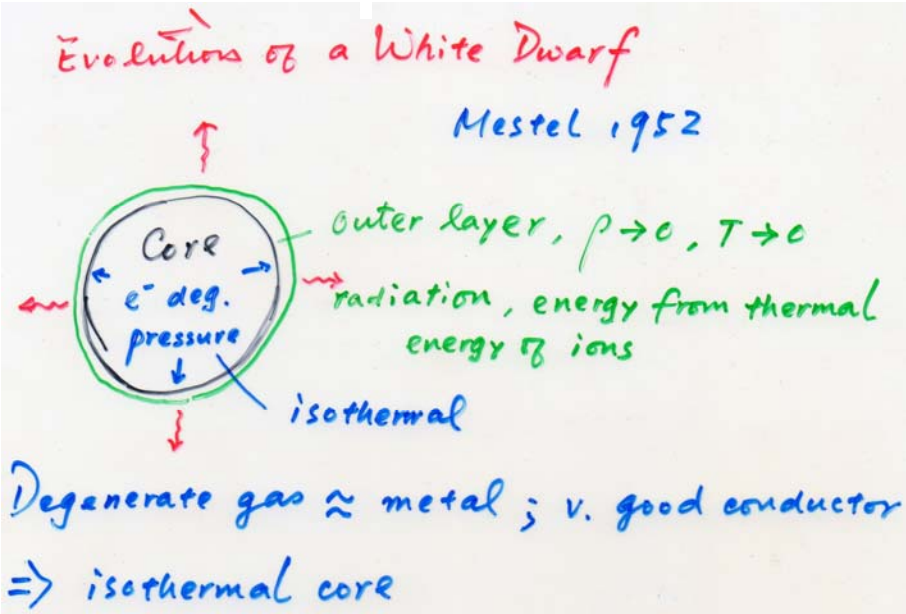

ON THE THEORY OF WHITE DWARF STARS

I. THE ENERGY SOURCES OF WHITE DWARFS

L. Mestel

(Communicated by F. Hoyle)

(Received 1952 May 9)

Summary

Present theories of the origin of white dwarfs are discussed; it is shown that all theories imply that there can be no effective energy sources present in a white dwarf at the time of its birth. The temperature distribution of a white dwarf is then discussed on the assumption that no energy liberation occurs within the star, and that it radiates at the expense of the thermal energy of the heavy particles present. In the resulting picture, a white dwarf consists of a degenerate core containing the bulk of the mass, surrounded by a thin, non-degenerate envelope. The energy flow in the core is due to the large conductivity of the degenerate electrons, while the high opacity of the outer layer keeps down the luminosity to a low level. Estimates of the ages of observed white dwarfs are given and interpreted. Finally, it is shown that white dwarfs may accrete energy sources and yet continue to cool off, provided the temperature at the time of accretion is not too high; this suggests a possible model for Sirius B.

Boundary between the degenerate core & the radiative envelope (r_b)

$r < r_b$, $T = T_c$

$r > r_b$, $L = \text{const}$

$m(r > r_b) \simeq M$

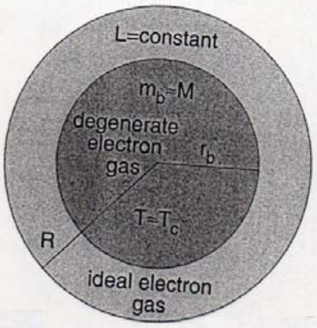

Figure 8.13 Sketch of the configuration of a cooling white dwarf.

In the envelope,

① $$\frac{dP}{dr} = -\rho \frac{GM}{r^2} \quad (\text{i.e. } M(r) \to M)$$

② $$\frac{dT}{dr} = -\frac{3}{4ac} \frac{\kappa \rho}{T^3} \frac{L}{4\pi r^2} \quad (\text{i.e. } F(r) \to L)$$

③ $$\kappa = \kappa_0 \rho T^{-3.5} = \kappa_0 \frac{\mu m_H}{k} P T^{-4.5}$$

Ideal gas

③ into ②, and ① / ②

$\Rightarrow$

$$\frac{dP}{dT} = \frac{GM\,16\pi ac}{3\kappa L} T^3 = \frac{16\pi ac GMT^3}{3\kappa_0 \mu m_H P T^{-4.5}} \cdot \frac{k}{L}$$

$$= \frac{16}{3} K_1 \frac{M}{LP} T^{+7.5}$$

In the envelope,

① $\frac{dP}{dr} = -\rho \frac{GM}{r^2}$ (i.e. $M(r) \to M$)

② $\frac{dT}{dr} = -\frac{3}{4ac} \frac{\kappa\rho}{T^3} \frac{L}{4\pi r^2}$ (i.e. $F(r) \to L$)

③ $\kappa = \kappa_0 \rho T^{-3.5} = \kappa_0 \frac{\mu m_H}{k} P T^{-4.5}$

$$P\,dP = \frac{16}{3} K_1 \frac{M}{L} T^{7.5} dT$$

$$\frac{1}{2} P^2 = \frac{16}{3} K_1 \frac{M}{L} \frac{T^{8.5}}{8.5}$$

← integrate inward, $T \to 0$, $P \to 0$ as surface

$$P = \cdots \left(\frac{M}{L} T^{8.5}\right)^{1/2}$$

$\frac{1}{2} P^2 = \frac{16}{3} K_1 \frac{M}{L} \frac{T^{8.5}}{8.5}$

$$P(T) = \left(\frac{64}{51} K_1\right)^{1/2} \left(\frac{M}{L}\right)^{1/2} T^{17/4}$$

This is the general radiative zero solution to the outer envelope (atmosphere) of stars

or

④ $\rho(T) = K_2 \left(\frac{M}{L}\right)^{1/2} T^{13/4}$

At r_b, e^- ; ideal gas pressure = degenerate gas pressure

$$P_e = \left(\frac{k}{\mu m_H}\rho T\right)_b = P_{deg} = K_1'\left(\frac{\rho}{\mu_e}\right)_b^{5/3}$$

$$\rho T = K_2' \rho^{5/3}$$

$$\rho = K_3' T_b^{3/2}$$ (A)

Here $T_b = T_c$

④ $\therefore \frac{L}{M} \sim \frac{T^{13/2}}{\rho^2} \sim \frac{T^{13/2}}{T^3} \sim T_c^{3.5}$

④ $\rho(T) = K_2 \left(\frac{M}{L}\right)^{1/2} T^{13/4}$

$$\frac{L}{M} = K\, T_c^{3.5}$$

$L \leftrightarrow T_c$

$$\frac{L}{L_\odot} = 6.4\times10^{-3}\frac{\mu}{\mu_e^2}\frac{M}{M_\odot}\frac{1}{\kappa_0}T_c^{3.5}$$ $\leftrightarrow$ chemical composition and opacity

Numerically, with constants (μ, μ_e, K_3') typical for a WD

$$\frac{L/L_\odot}{M/M_\odot} \approx 6.8\times10^{-3}\left(\frac{T_c}{10^7 K}\right)^{3.5}$$

or

$$T_c \approx 4\times10^7\left(\frac{L/L_\odot}{M/M_\odot}\right)^{2/7} [K]$$ (B)

cf $T_F \sim 10^9 K$

The interior of a WD need not be exceedingly hot.

Energy source: $E_{\text{thermal}}^{\text{ions}} = (3/2)\frac{M}{\mu_I m_H}\, kT$

Luminosity $L = -d\, E_{\text{thermal}}^{\text{ions}}/dt$

$$= -(3/2)\frac{M}{\mu_I m_H}\, k\, dT_c/dt$$

$$\frac{L}{M} = K\, T_c^{3.5}$$

$$\frac{dL}{dt} = KM\,\frac{7}{2}\,T_c^{5/2}\frac{dT_c}{dt}$$

(5) $\therefore\ L = -\frac{3}{7}\frac{M}{\mu m_H} k \frac{T_c}{L}\frac{dL}{dt}$

$\Rightarrow\ \frac{dL}{dt} = -M\, T_c^{6}$

$$L = -\frac{M\, T_c}{L}\frac{dL}{dt}$$

$$\frac{dL}{dt} = -\frac{L^2}{MT_c} = \frac{M^2}{MT_c}{T_c}^7$$

Cooling rate ↓↓↓ as T_c ↓

Thermal energy of ions in the isothermal core = energy source of a white dwarf

$$E_{K,ion} = \frac{3}{2}\frac{M}{\mu_I m_H} k T_c$$

Luminosity $L = -\frac{dE_K}{dt} = -\frac{3}{2}\frac{M}{\mu_I m_H} k \frac{dT_c}{dt}$

L ↓ as T_c ↓

but $T_c \sim L^{2/7}$

⇒ lower-mass WD, evolves slowlier

Cooling timescale, from T_c', L' to T_c, L

Integrate (5)

$$\tau_{cool} = 0.6 \frac{k}{\mu_I m_H} M \left(\frac{T_c}{L} - \frac{T_c'}{L'} \right)$$

If $T_c' \gg T_c$ $\left(\frac{T_c'}{L'} \sim T_c'^{\,-2.5} \right) \Rightarrow \frac{T_c}{L} \gg \frac{T_c'}{L'}$

$$\tau_{cool} \approx 2.5 \times 10^6 \left(\frac{M/M_\odot}{L/L_\odot} \right)^{5/7} \quad [\text{yr}]$$

Core Temperature

$M \approx M_\odot$, $L/L_\odot \approx 10^{-4} - 10^{-2}$ (B) → $T_c \approx 10^6$ K

(A) → $\rho_b \approx 10^3$ g cm^{-3}

Envelope

$$\ell \approx \frac{P}{\rho g} \approx \frac{kT}{\mu g}$$

$T \sim 10^6$ K, $l \approx 1 - 10$ km

Envelope mass $< 4\pi R^2 l \, \rho_b \approx 2 \times 10^{-4}\, M_\odot$, is indeed small

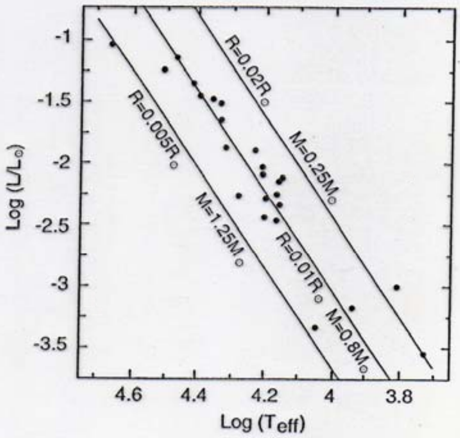

Figure 8.15 White dwarfs in the H–R diagram. Lines of constant radius (mass) are marked [data from M. A. Sweeney (1976), *Astron. & Astrophys.*, 49].

$MR^3 = \text{const}$, and $L \propto R^2\ \mathrm{T_{eff}}$

→ WD evolutionary tracks

$$\log\left(\frac{L}{L_\odot}\right) = 4\log\left(\frac{\mathrm{T_{eff}}}{T_\odot}\right) - \frac{2}{3}\log\left(\frac{M}{M_\odot}\right) + \mathrm{C}$$

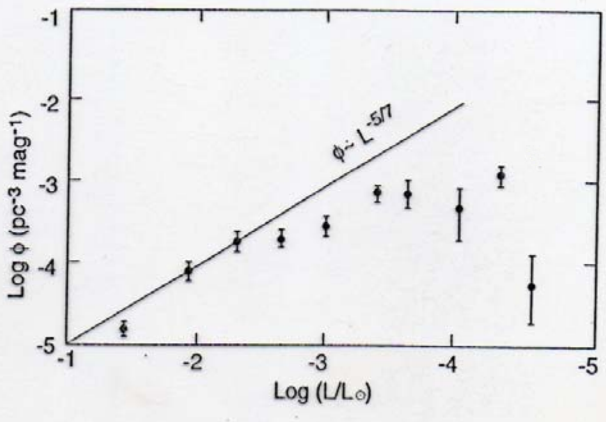

Figure 8.14 White dwarf luminosity function: number density of white dwarfs within a logarithmic luminosity interval corresponding to a factor of $10^{2/5} \approx 2.5$ against luminosity [data from D. E. Winget et al. (1987), *Astrophys. J.*, 315].

The Astrophysical Journal, 574:L155–L158, 2002 August 1

THE WHITE DWARF COOLING SEQUENCE OF THE GLOBULAR CLUSTER MESSIER 4[1]

Brad M. S. Hansen,[2,3] James Brewer,[4] Greg G. Fahlman,[4,5] Brad K. Gibson,[6] Rodrigo Ibata,[7] Marco Limongi,[8] R. Michael Rich,[2] Harvey B. Richer,[4] Michael M. Shara,[9] and Peter B. Stetson[10]
Received 2002 March 5; accepted 2002 June 26; published 2002 July 11

ABSTRACT

We present the white dwarf sequence of the globular cluster M4, based on a 123 orbit *Hubble Space Telescope* exposure, with a limiting magnitude of $V \sim 30$ and $I \sim 28$. The white dwarf luminosity function rises sharply for $I > 25.5$, consistent with the behavior expected for a burst population. The white dwarfs of M4 extend to approximately 2.5 mag fainter than the peak of the local Galactic disk white dwarf luminosity function. This demonstrates a clear and significant age difference between the Galactic disk and the halo globular cluster M4. Using the same standard white dwarf models to fit each luminosity function yields ages of 7.3 ± 1.5 Gyr for the disk and 12.7 ± 0.7 Gyr for M4 (2 σ statistical errors).

White dwarf sequence of M4

Blue – H atmosphere models
Red – He atmosphere models

for a 0.6 M" WD

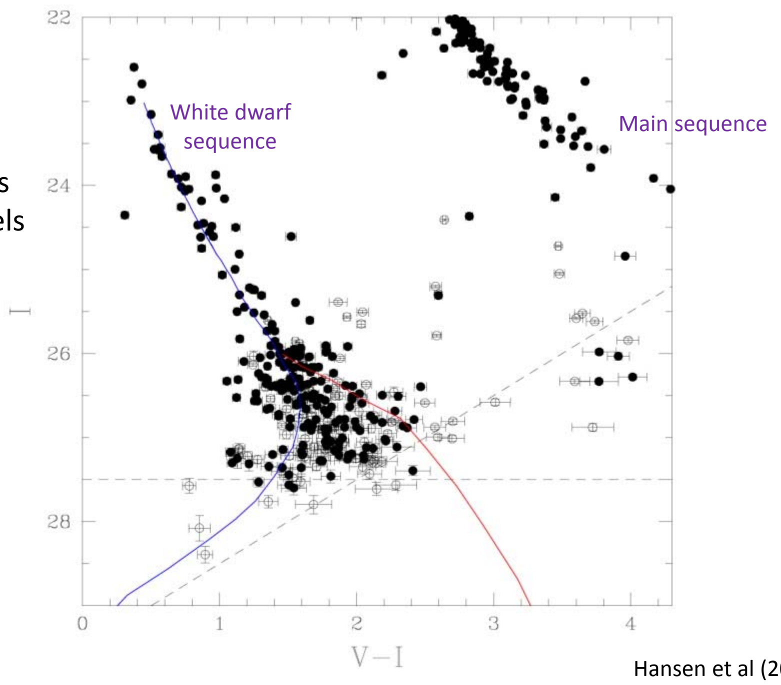

Hansen et al (2002)

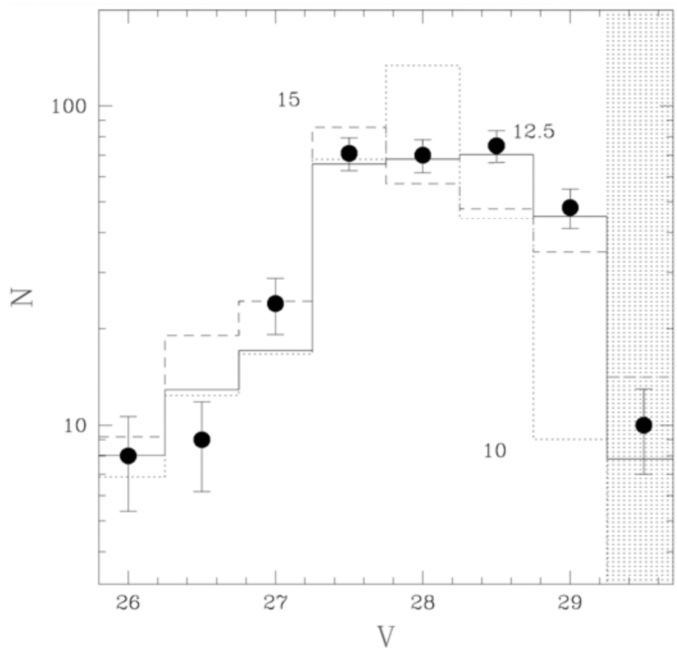

The observed luminosity function of the white dwarfs in M4 (after correction of incompleteness)
versus
model predictions for different ages

Hansen et al (2002)

- The WD envelope is typically thin, ~1% of the total WD radius.
- DA WD: layer of $M_{\rm He} \sim 10^{-2}\ M_{\rm WD}$ outside the CO core, then an outer layer $M_{\rm H} \sim 10^{-4}\ M_{\rm WD}$
- A non-DA WD layer of $M_{\rm He} \sim 10^{-2} - 10^{-3}\ M_{\rm WD}$

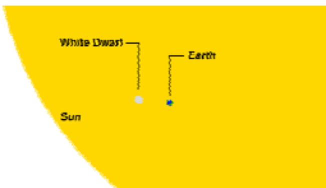

Supernovae and Others

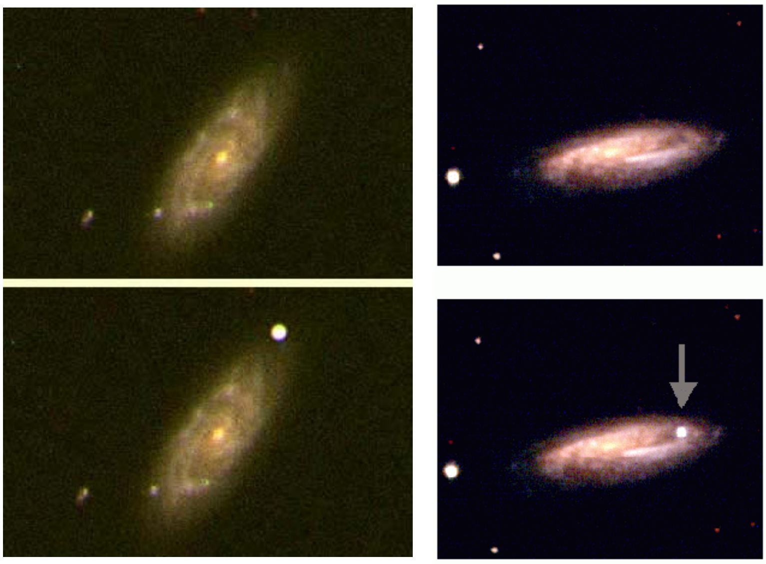

Possible evolutionary paths of a supernova

1. Core collapse
2. Thermonuclear runaway

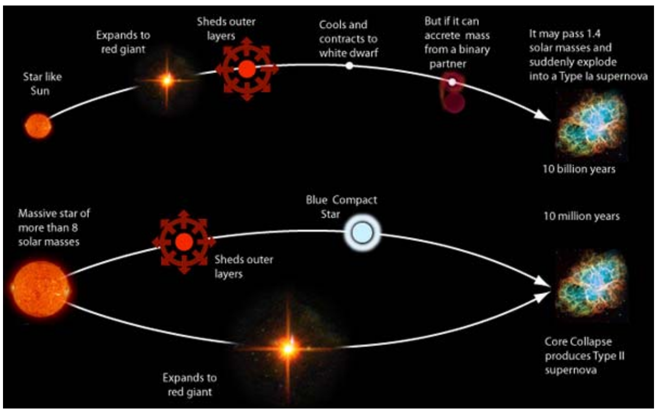

http://hyperphysics.phy-astr.gsu.edu/hbase/astro/snovcn.html

Evolution of an Intermediate-mass (8 to 25 $M_\odot$) or High-mass ($>$25 $M_\odot$) Star

- Core size ~ Earth
- Layers of nuclear reactions (cf an onion)
- Envelope as a supergiant, with the diameter comparable to the Jupiter's orbit

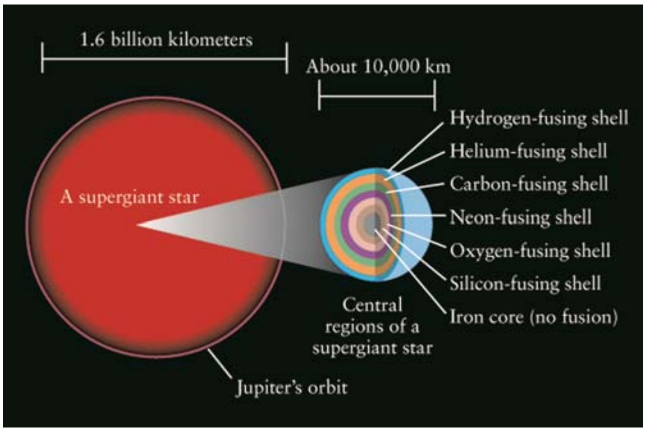

Each subsequent reaction proceeds ever faster; silicon → iron

An iron nucleus is most compact between protons and neutrons
→ further fusion does not release energy
→ iron core collapses (D~3000 km, collapses in ~0.1 s)

Evolutionary Stages of a 25-$M_\odot$ Star

Stage	Central temperature (K)	Central density (kg/m³)	Duration of stage
Hydrogen fusion	4×10^7	5×10^3	7×10^6 yr
Helium fusion	2×10^8	7×10^5	5×10^5 yr
Carbon fusion	6×10^8	2×10^8	600 yr
Neon fusion	1.2×10^9	4×10^9	1 yr
Oxygen fusion	1.5×10^9	1×10^{10}	6 mo
Silicon fusion	2.7×10^9	3×10^{10}	1 d
Core collapse	5.4×10^9	3×10^{12}	0.2 s
Core bounce	2.3×10^{10}	4×10^{17}	milliseconds
Supernova explosion	about 10^9	varies	10 seconds

Iron core collapse → 5 billion K → photodisintegration by energetic gamma rays

The star spends millions of years on the main sequence, synthesizing simple nuclei such as H and He to iron, then takes less than a second to disintegrate back to protons, neutrons and electrons.

Density of the core ↗↗, reaching 4×10^{17} kg/m³ (cf density of a nucleus) in < 1 s → even the electron degenerate pressure cannot support the core → $e^- + p^+ \rightarrow n^o + \nu$

Core supported by neutron degenerate pressure
→ **a neutron star**

Core bounces ➔ **supernova explosion** + **supernova remnant**

Evolution of a Binary System

- Both stars of a few solar masses
- More massive component → RG → transfers and loses mass → a hot WD
- Secondary → RG → fills the Roche lobe → transfers mass to the hot WD via an accreting disk
- Accreted material is compressed and heated, and if $T > 10^7$ K → CNO takes place at the base of the accreted layer (even with a thermonuclear runaway if the material is degenerate)

➔A nova explosion

If accretion onto a C-O WD → core mass > M_{Ch}=1.4 $M_\odot$
→ Catastrophic collapse + C burning ➔ a Type Ia supernova

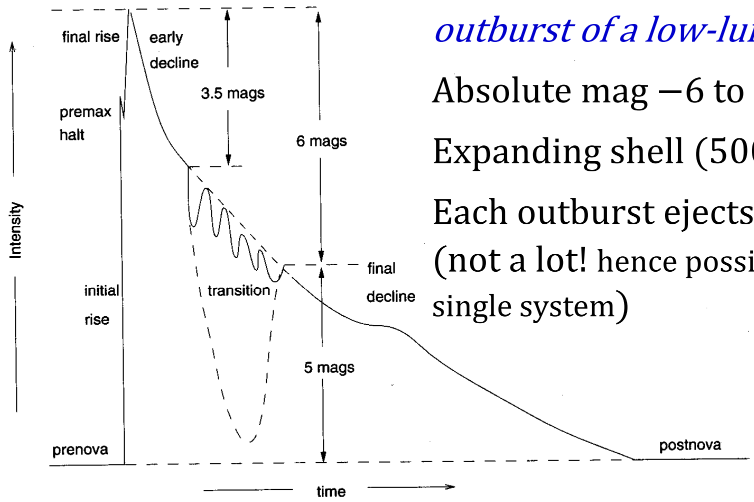

Fig. 7.10. Schematic light curve for a typical nova; the time axis is arbitrary and not to scale.

"A nova is a transient, possibly recurring, outburst of a low-luminosity star."

Absolute mag −6 to −9

Expanding shell (500−2000) km/s

Each outburst ejects $10^{-4} - 10^{-6}$ $M_\odot$ (not a lot! hence possible recurrent events for a single system)

Padmanabhan II

Accreting Binary Systems

A semi-detached binary system with the primary being a WD: (in increasing L)

- ✓ dwarf nova
- ✓ classical nova

  (these may be cataclysmic variables)

- ✓ type Ia supernova

Table 7.4. Taxonomy of binary systems

Name	Description	Remarks
Algols	Two normal stars (main sequence or subgiants): semidetached binary	Provide checks on stellar evolution, information on mass loss
RS Canum Venaticorum	Chromospherically active binaries	Useful for studies of dynamo-based magnetic activity; exhibits starspot chromospheres, corona, and flares similar to the Sun
W Ursae Majoris	Short period (0.2–0.8 days) Contact binaries	High levels of magnetic activity, important for studying stellar dynamo model
Cataclysmic variables and novas	White dwarfs with cool M-type secondaries; short periods	Exhibits accretion phenomena and accretion disks
X-ray binaries	Neutron star or black hole as the compact component; powerful x-ray sources with $L_x > 10^{35}$ ergs s^{-1}	Study of structure and evolution of compact remnants; indirect evidence for black holes
ζ Aurigae/ VV Cephi	Long-period interacting binaries; Late-type super-giant plus a hot companion	Study of supergiant phase, especially atmospheres of supergiants

Padmanabhan II

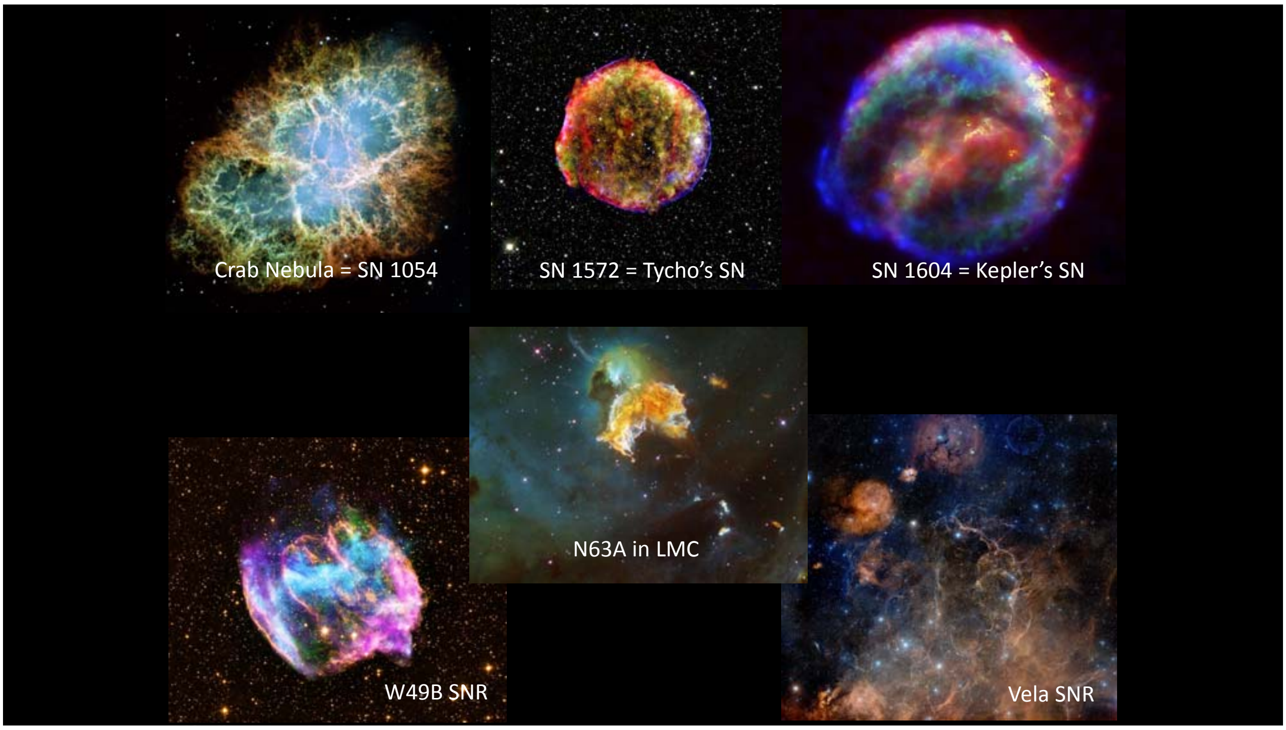

Figure 13-11
Discovering the Universe, Seventh Ed

Gum Nebula is the largest SNR in the sky, originated from a supernova explosion perhaps a Myr ago.

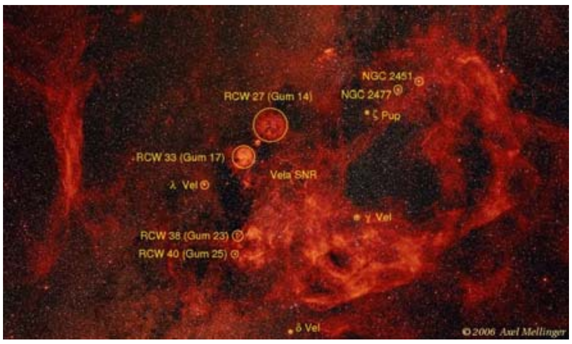

Gum Nebula has a angular extent > 40 deg → linear size more than 2300 ly across → The closest part from Earth ~300 ly

Cassiopeia A SNR is 3.4 kpc from us. The explosion should have been seen 300 years ago, but was not recorded.

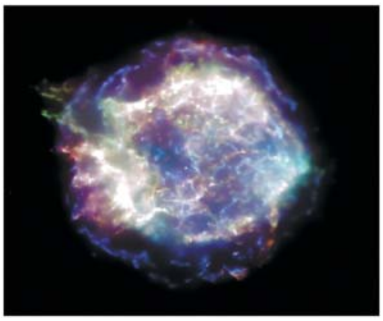

X rays

Visible (HST)

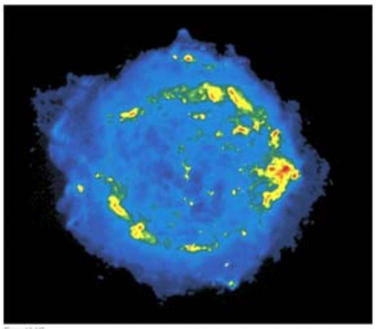

Radio

Supernovae in History

- OB association in Scorpius-Centaurus
  Solar system within 150 ly 2 Myr ago; should have experienced SN explosions

Table 10.1 Historical supernovae

Galaxy: Name	*Year*	*Distance × 3000 ly*
Milky Way:		
Lupus	1006	1.4
Crab	1054	2.4
3C 58	1181(?)	2.6
Tycho	1572	2.5
Kepler	1604	4.2
Cas A	1658±3	2.8
Andromeda	1885	700
LMC: SN1987A	1987	50

Chandra SN1604

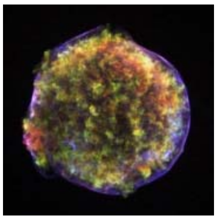

Chandra SN1572

Crab Nebula (in Taurus)

SN clearly recorded in AD1054 by Chinese astronomers
→ "Chinese supernova"

西元1054年七月（宋仁宗至和元年五月）金牛座超新星爆炸，據記載最明亮時相當於太白（金）星的光芒，長達23天在白天可見，直到1056年四月（宋嘉祐元年三月）肉眼才看不見。
天關客星


凡十一日沒三年三月乙巳出東南方大中祥符四
年正月丁丑見南斗魁前天禧五年四月丙辰出軒轅
前星西北大如桃速行經軒轅太星入太微垣掩右執
法犯次將歷屏星西北凡七十五日入濁沒明道元
年六月乙巳出東北方近濁有芒彗至丁巳凡十三
日沒至和元年五月己丑出天關東南可數寸歲餘
稍沒熙寧二年六月丙辰出箕度中至七月丁卯犯
箕乃散三年十一月丁未出天囷元祐六年十一月
辛亥出參度中犯掩側星壬子犯九游星十二月癸
酉入奎至七年三月辛亥乃散紹興八年五月守婁
宋史志卷九

The Expanding Crab Nebula 1973 to 2001

SN 1987A

First observed 24 Feb, 1987

not quite SN II

pre SN progenitor observed and sp. classified

Sanduleak -69 202

Sp: B3 I

$L \sim 1.1 \times 10^5 L_\odot$; $T_{eff} \sim 16{,}000\,K$

($M \sim 16-22\,M_\odot$)

Pop I but metal-poor

Neutrino events (Kamiokande) detected hours before SN visible

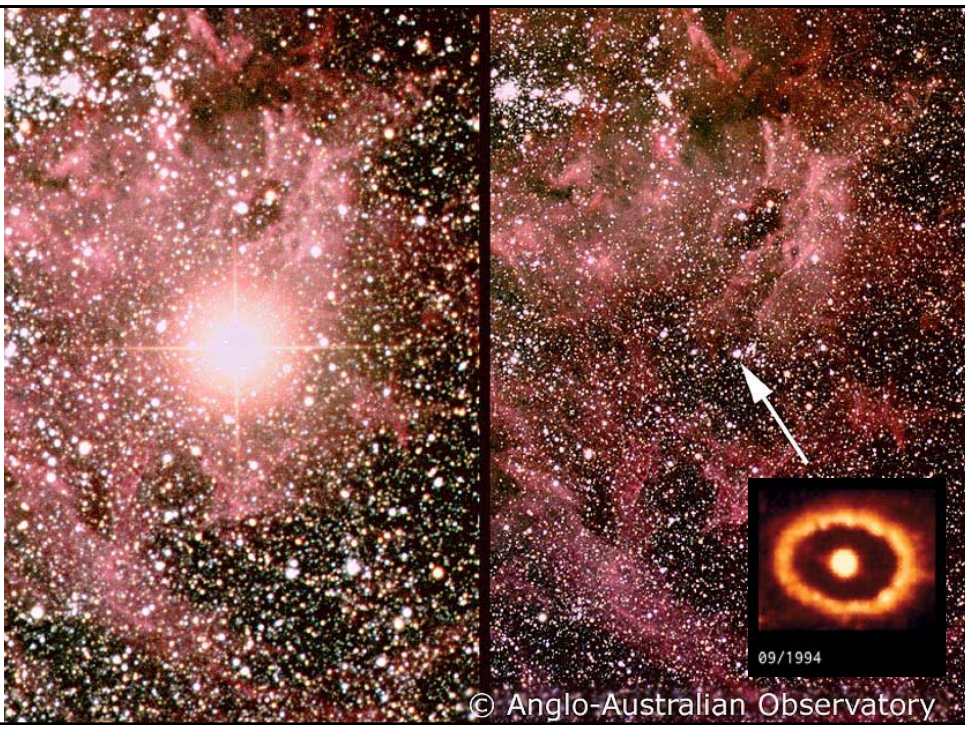
09/1994
© Anglo-Australian Observatory

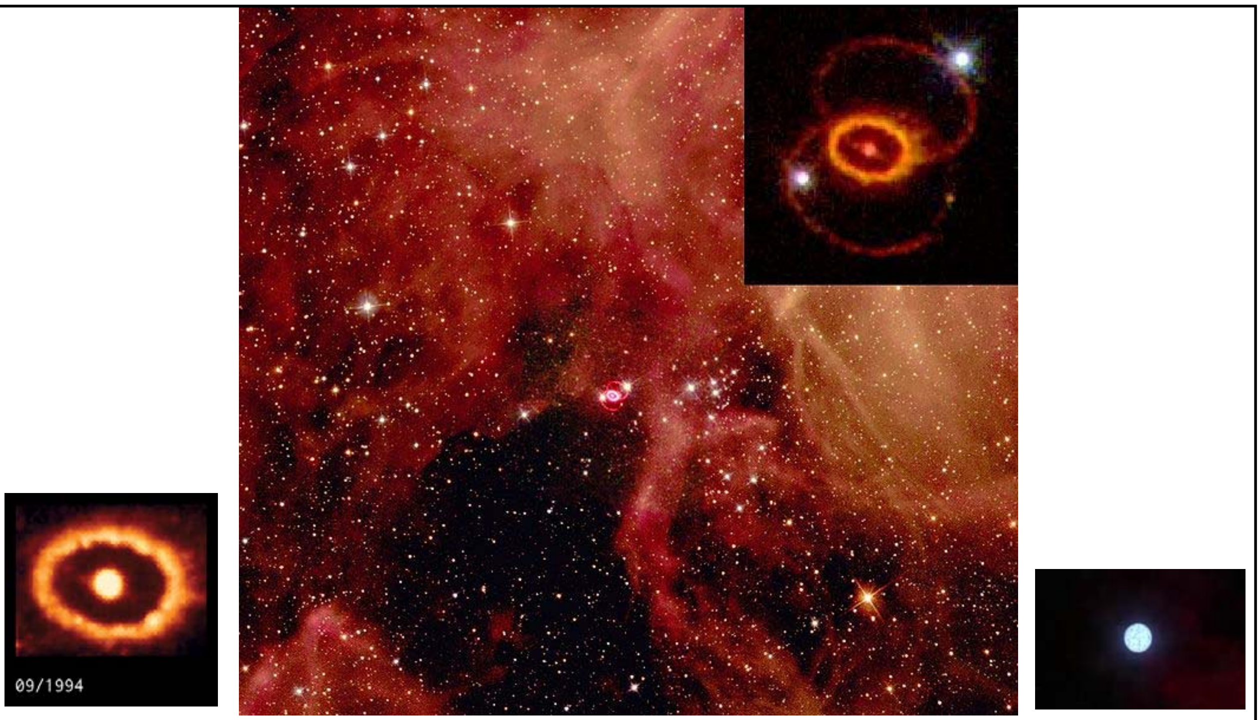
09/1994

Supernova classification

Divided into two types based on spectra

Type I – with no H lines

- Further classification based also on spectra:
  - ✓ Ia – strong Si line
  - ✓ Ib – no H or Si line, but have He lines
  - ✓ Ic – no Si, He or H lines
- Ia found in all types of galaxies

➔ associated with white dwarfs in binary systems

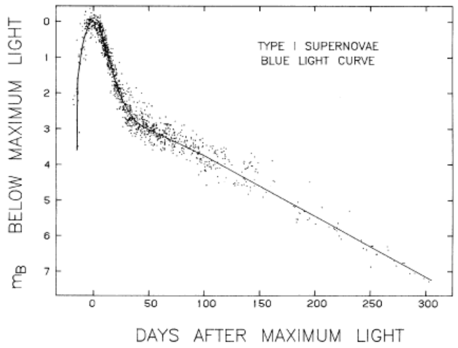

Doggett and Branch (1985)
Astron. J., **90**, 2303

Supernova classification II

Type II – with H lines

Further classification based on light curve

- ✓ II P – flat 'plateau' in LC
- ✓ II L - linear light curve

- Type II, Ib, Ic found only in spiral arms of spiral galaxies (i.e. regions of recent star formation) ➔ massive stars

Core collapse supernovae with mass loss in Ib and Ic

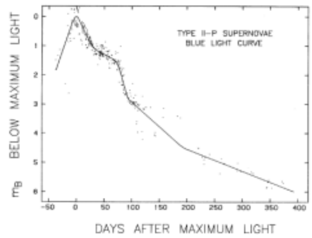

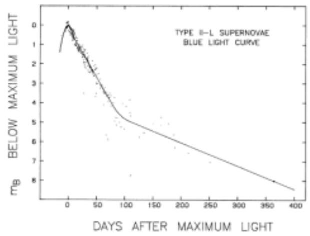

Doggett and Branch (1985)
Astron. J., **90**, 2303

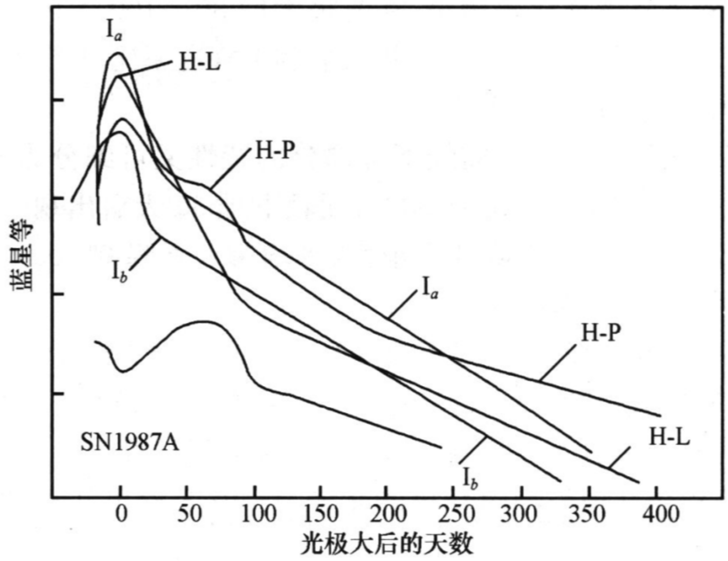

图 10.8　几种类型超新星的光变曲线(Wheeler,Harkness,1992)

Huang

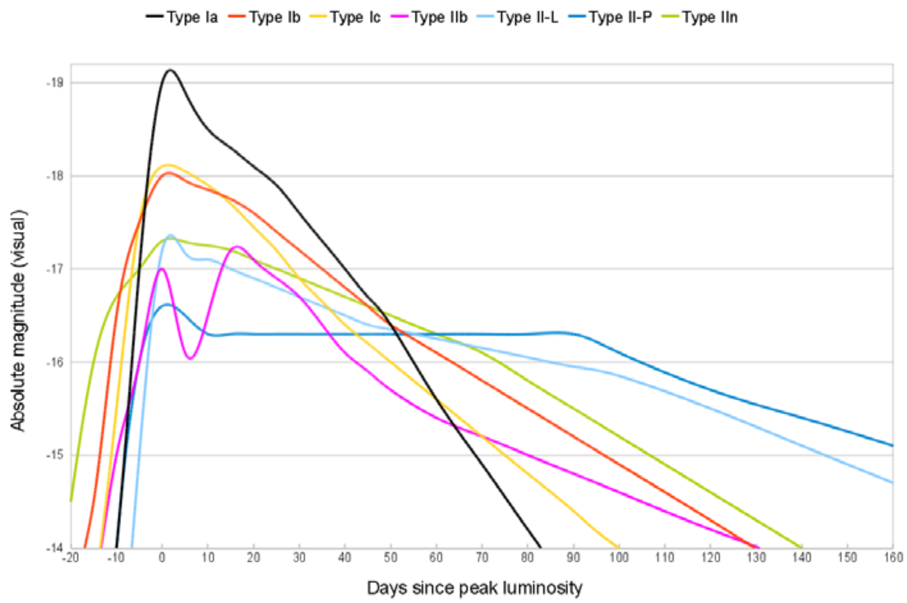

http://upload.wikimedia.org/wikipedia/commons/e/e0/Comparative_supernova_type_light_curves.png

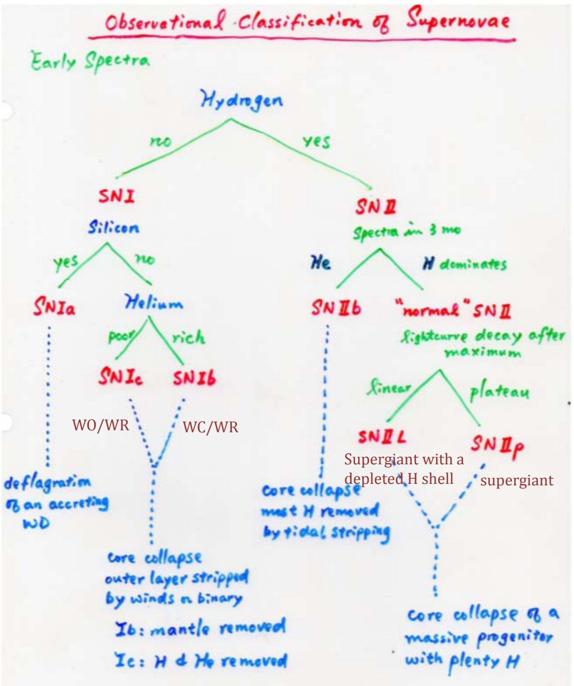

Padmanabhan II

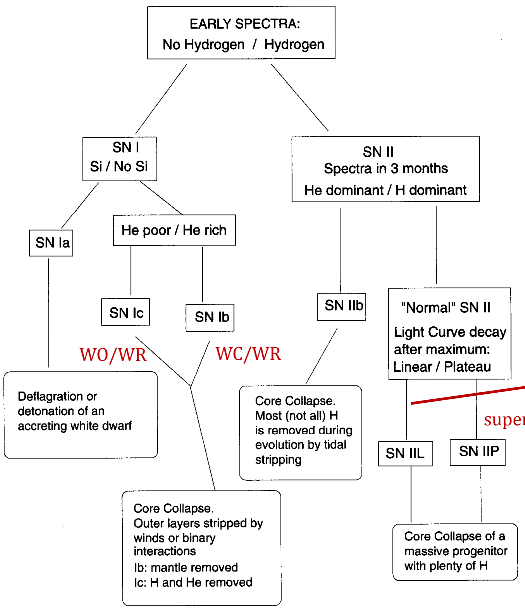

Fig. 7.12. Observational classification of supernovas (SNs).

Padmanabhan II

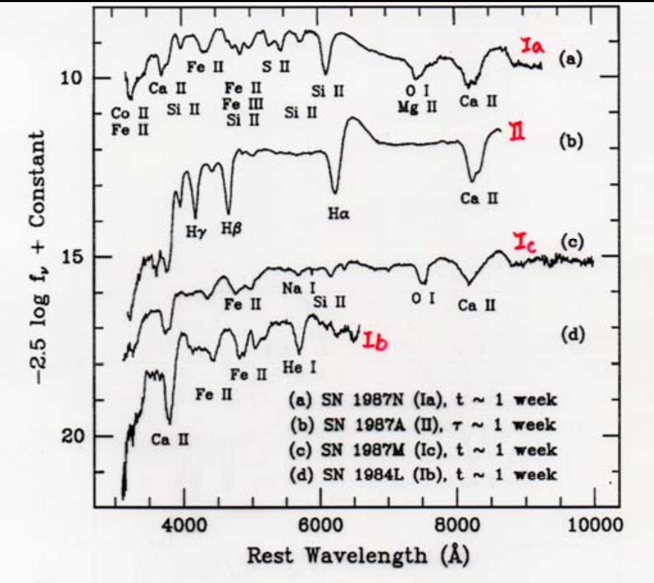

Figure 1 Spectra of SNe, showing early-time distinctions between the four major types and subtypes. The parent galaxies and their redshifts (kilometers per second) are as follows: SN 1987N (NGC 7606; 2171), SN 1987A (LMC; 291), SN 1987M (NGC 2715; 1339), and SN 1984L (NGC 991; 1532). In this review, the variables t and τ represent time after observed B-band maximum and time after core collapse, respectively. The ordinate units are essentially "AB magnitudes" as defined by Oke & Gunn (1983).

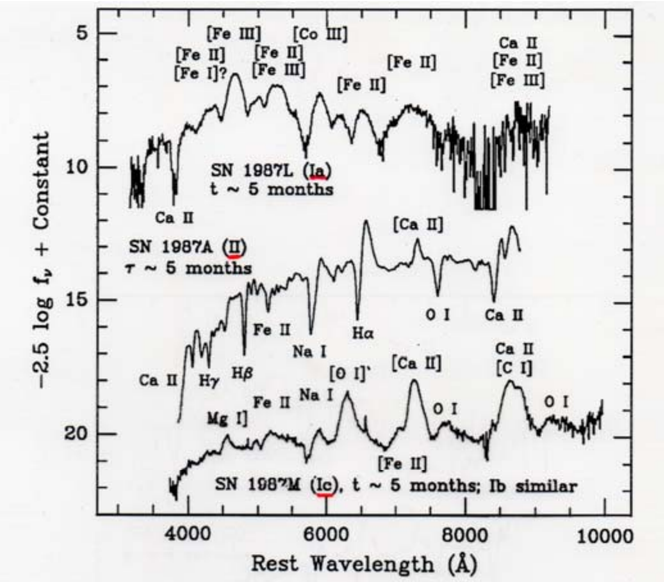

Figure 2 Spectra of SNe, showing late-time distinctions between various types and subtypes. Notation is the same as in Figure 1. The parent galaxy of SN 1987L is NGC 2336 ($cz = 2206$ km s^{-1}); others are listed in the caption of Figure 1. At even later phases, SN 1987A was dominated by strong emission lines of Hα, [O I], [Ca II], and the Ca II near-IR triplet, with only a weak continuum.

Elements observed in SN I spectra

Subclass	~ maximum	~ 6 months
SN Ia	O, Mg, Si, S, Ca, Fe	Fe, Co
SN Ib	O, Ca, Fe	O, Ca, Mg
SN Ic	He, Fe, Ca	O, Mg

Hansen + Kawaler

- The energy source of the type Ia supernovae comes from nuclear fusion. The explosion produces various radioactive isotopes , e.g., nickel becomes cobalt.
- So far, a few thousands SNe have been detected in external galaxies.
- Applying the statistics, the Milky Way should have occurred one type Ia SN every 36 years, and one type II SN every 44 years.
- Each century, therefore, we should have seen about 5 supernovae. So, what happened?
- Which star is most likely the next? In the solar neighborhood?

Supernovae

$M > 8\,M_\odot$ core carbon burning

$\rightarrow {}^{16}_{8}O,\ {}^{20}_{10}N,\ {}^{23}_{11}Na,\ {}^{23}_{12}Mg$ and ${}^{24}_{12}Mg \cdots$

Eventually ${}^{54}_{26}Fe,\ {}^{56}_{26}Fe$, and ${}^{56}_{28}Ni$

Three critical processes

"iron" core

① Neutrino cooling

At this stage, a lot of νs

Ex. during Si burning, a $20\,M_\odot$

$L_{20M_\odot} \sim 4.4 \times 10^{38}\ \mathrm{erg\,s^{-1}}$

$L_\nu \sim 3.1 \times 10^{45}\ \mathrm{erg\,s^{-1}}$

Solar neutrino flux
$= 7 \times 10^{10}\ /\mathrm{cm}^2/\mathrm{s}$

Neutrino mass
< 0.32 eV for the sum of masses of 3 known flavors

② Photodisintegration

Energetic photons disintegrate iron nuclei into α particles and protons

This is an endothermic (吸熱) process; i.e. takes energy away and lowers pressure support at the core

$${}^{56}Fe + \gamma \rightarrow 13\,{}^{4}He + 4n$$

$${}^{4}He + \gamma \rightarrow 2p^{+} + 2n$$

3. Neutronization

possible inverse β decay $p^+ + e^- \rightarrow n^0 + \nu$

$\downarrow$

$n_e \downarrow \Rightarrow P_{deg} \downarrow$

ν escape $\Rightarrow$ cooling

$\Rightarrow$ A rapid collapse of the core

Note: 放熱 exothermic — releasing energy

Outer core/mantle collapses supersonically (free fall) $v \sim 70{,}000\ km\,s^{-1}$

inner core collapse homologously (infall speed ∝ distance to center) subsonically

Inner core collapses until $\rho_c \sim 8 \times 10^{14}\ g\,cm^{-3}$

This is $3 \times \rho_{nucleus}$ → nuclear reactions produce repulsive force (cannot "squeeze" anymore)

This sends an outgoing pressure wave through the infalling material

Two possibilities

when the shock propagates through the inner core → photodisintegration

(i) If the iron core is small, shock emerges energetically → an explosion on the outer material

prompt hydrodynamic explosion

This can explain the explosion of MS stars with 8~12 $M_\odot$, ending with a core < 1.2 $M_\odot$. But the progenitor of SN1987A had 20 $M_\odot$ → need an alternative mechanism to explain more massive SNe

(ii) If the core is massive, inner shock stalls

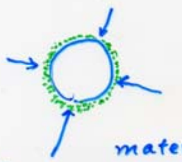

$\rho_{crit} > 1.5 \times 10^{11}\ \mathrm{g\,cm^{-3}}$

accretion shock

cf protostars

material becomes so dense that even νs cannot escape → formation of a neutrino sphere

cf photosphere of a star

when $\rho > \rho_{crit}$ $\quad \tau^{\nu}_{diff} > \tau_{free\,fall}$

Thus deposits some energy to the inner shock → explosion

delayed-explosion mechanism

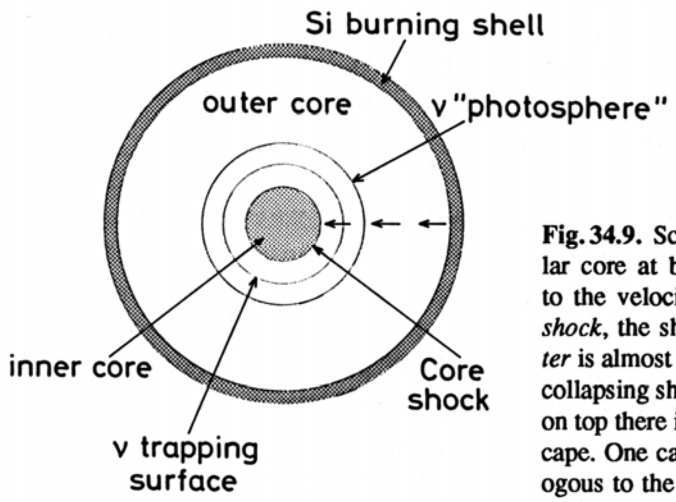

Fig. 34.9. Schematic picture of a collapsing stellar core at bounce. The short arrows correspond to the velocity field. At the sphere labelled *core shock*, the shock is formed inside which the *matter* is almost at rest. Above the shock there is a still collapsing shell in which neutrinos are trapped. But on top there is a shell from which neutrinos can escape. One can define a neutrino photosphere analogous to the photosphere in a stellar atmosphere

Total kinetic energy of outgoing shock

$E_{kin} \sim 10^{51}$ ergs

(This is only 1% of the energy in ~~energy~~ neutrinos)

→ outer material expands & becomes optically thin

⇒ SN explosion, releasing $\sim 10^{49}$ ergs in photons

with $L_{peak} \sim 10^{43}$ ergs s^{-1} $\sim 10^{9} L_{\odot}$

c.f. $L_{Milky Way}$

Roughly if original mass $< 25\ M_\odot$, can be supported neutron pressure; may survive the explosion $\rightarrow$ a neutron star

If $M > 25\ M_\odot$ $\rightarrow$ collapse to a black hole

Neutrino Trapping

Mean free path $\lambda = 1/n\sigma$

cross section $\sigma = \sigma_0 \varepsilon^2$

For neutrinos, $\sigma_0 \sim 2 \times 10^{-44}$ [cm^2]

ε = relative energy in unit of e^- rest mass

In lead $\rho = 11.34\ g\,cm^{-3}$, $A = 208$

A neutrino of 1 MeV, or $\varepsilon = 2$, $\lambda \sim 3.8 \times 10^{20}$ cm

~ 380 ly

In a collapsing stellar core

$$\rho \sim 4 \times 10^{14}\ g\,cm^{-3}$$

Neutrinos have ~ 150 MeV, or $\varepsilon \sim 300$

$$\rightarrow \lambda = 2.2\ cm$$

So if $R \sim 10$ km, the mean free time, or diffusion time $\tau \sim 5\,s$

Supernova Observations

$L_{peak} \sim 10^{9} - 10^{10}\ L_\odot$

Time before peak (rising time) ~ 2 wks

Shell expansion $v \sim 5 - 10 \times 10^{3}\ km\,s^{-1}$

supernova remnant (SNR) lasting $\sim 10^{3}$ yrs

$E_{total} \sim 10^{51} - 10^{53}$ ergs $= E_{photons} + E_{neutrinos} + E_{kinetic}$

($E_{photons}$: usually minor ($\sim 1\%$); $E_{neutrinos}$: predominant)

cooling core $\rightarrow$ a neutron star

$$\rho \sim 10^{14}\ g\,cm^{-3},\ M \sim M_\odot$$

- 1932 Chadwick discovered the neutron.
- Landau thought neutron stars might exist.
- 1934 Baade & Zwicky suggested neutron stars as remnants of supernova explosions.
- 1939 Oppenheimer & Volkoff proposed the first model for neutron stars, with estimates of masses and sizes.
- 1967 Hewish & Bell discovered the pulsar.
- Gold & Pacini proposed pulsars as fast spinning, highly magnetized neutron stars.

Mass limit of neutron degenerate stars uncertain because of uncertain EoS at $\rho > \rho_{nuclear}$, ranging from $0.7\,M_\odot$ for non-interacting neutrons (Tolman-Oppenheimer-Volkoff limit) up to $\sim 2.5\,M_\odot$

$R \sim 10$ km

A pulsar
- $B \sim 10^{13}$ G
- Spin down from periods $\sim$ ms

Some SNRs host no pulsars.

— not enough e^-, not strong enough $\vec{B}$?

— we are not in the 'light house beam' ?

— neutron star destroyed completely

— neutron star 'kicked out'

some NSs (or pulsars) have space motion ~ 1000 $km s^{-1}$

Annu. Rev. Astron. Astrophys. 1992. 30: 359–89

TYPE Ia SUPERNOVAE AS STANDARD CANDLES

David Branch

Department of Physics and Astronomy, University of Oklahoma, Norman, Oklahoma 73019

G. A. Tammann

Astronomisches Institut der Universität Basel, Venusstrasse 7, CH-4102 Binningen, Switzerland, and European Southern Observatory, Karl-Schwarzschild-Str. 2, D-8049 Garching/München, Germany

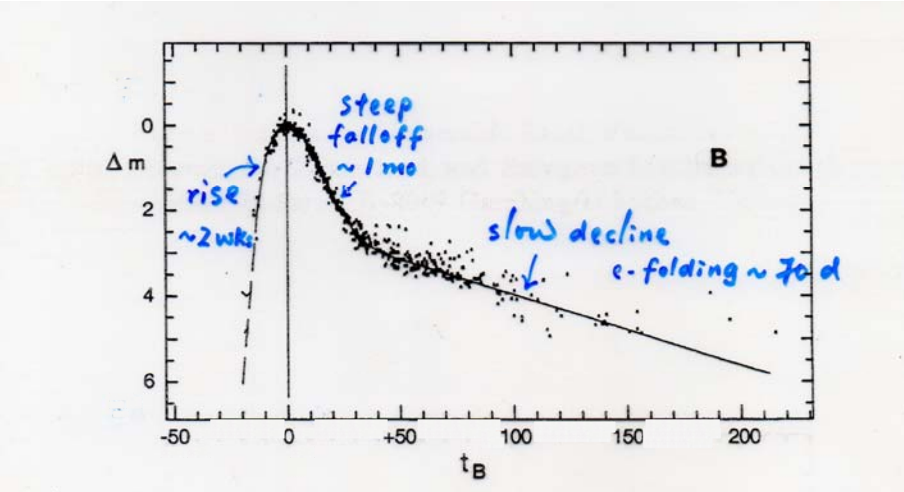

Figure 2 The standard *B* light curve (adapted from Cadonau 1987), based on observations of 22 SNe Ia.

Many sky survey projects, e.g., Pan-STARRS (PS), Palomar Transient Factory (PTF), Sky Mapper, Large Synoptic Survey Telescope (LSST), to catch SNe early on, for pre-SN characterization

Type I

No H in spectra

Located in spirals or ellipticals

If in spirals, usually NOT in arms

but some seen near H II regions or arms → Ib

Ia Standard model

A WD close to Chandrasekhar limit

\+ a mass losing companion

→ accretion onto WD → $R_{WD} \downarrow$

→ $T \uparrow$, If heat not carried away

⇒ ignition of C, O, ...

thermonuclear explosion

Fate of WD depends on accretion rate and M_{WD}

- partial explosion w/ a WD left behind
- disrupt completely ; no stellar remnant
- NS ?

Population II progenitor

SN Ia ~ 80% of Type II

$M_{peak} \sim -17$ mag

All SN Ia lightcurves similar

→ standard candles

Averaged 1 SN I / 100 yrs in a spiral

Type II

$M_{peak} \sim -19$ mag

With hydrogen lines in spectra

Found in spiral arms or Irr.

If formed in the same arm

timescale $< 10^7$ yr $\Rightarrow M > 10 M_\odot$ progenitor

Standard model

End of massive star evolution

gravitational collapse

Population I progenitor

Fate → NS, BH

Type II (core collapse) SN progenitors

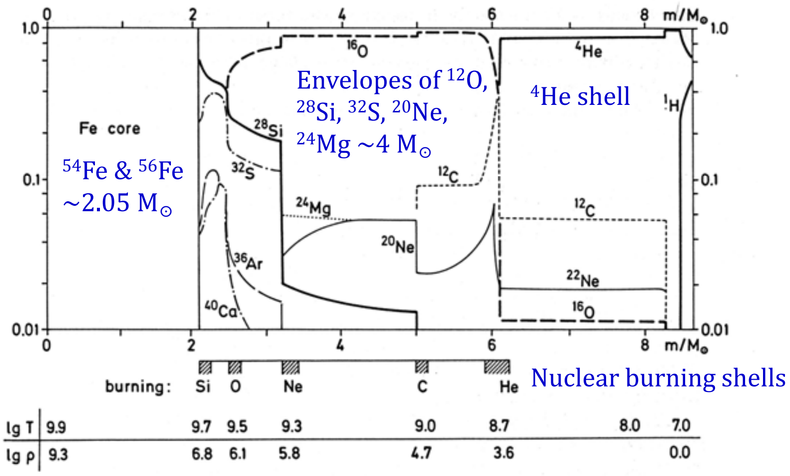

Fig. 34.7. The chemical composition in the interior of a highly evolved model of a $25 M_\odot$ star of population I. The mass concentrations of a few important elements are plotted against the mass variable m. Below the abscissa the location of shell sources and typical values of temperature (in K) and density (in g cm^{-3}) are indicated. (After WOOSLEY, WEAVER, 1986)

Ann. Rev. Astron. Astrophys. 1986. 24 : 205–53

THE PHYSICS OF SUPERNOVA EXPLOSIONS[1]

S. E. Woosley

Board of Studies in Astronomy and Astrophysics, Lick Observatory, University of California, Santa Cruz, California 95064

Thomas A. Weaver

Special Studies Group, Lawrence Livermore National Laboratory, Livermore, California 94550

Table 1 Presupernova models and explosions[a]

Main sequence mass	Helium core mass	Iron core mass	Explosion energy[b] (10^{50} erg)	Residual baryon mass[b]	Neutron star mass[b]	Heavies ejected ($Z \geq 6$)
11	2.4	—[c]	3.0	1.42	1.31	~0
12	3.1	1.31	3.8	1.35	1.26	0.96
15	4.2	1.33	2.0	1.42	1.31	1.24
20	6.2	1.70	—		—	2.53
25	8.5	2.05	4.0	2.44	1.96	4.31
35	14	1.80	—		—	9.88
50	23	2.45	—	—		17.7
75	36	—[d]	—	—	BH?	30?
100	45	~2.3[d]	$\gtrsim 4$	—	BH?	39?

[a] All masses given in units of $M_\odot$.
[b] All except for 100 $M_\odot$ determined by Wilson et al. (1985).
[c] Never developed iron core in hydrostatic equilibrium.
[d] Pulsational pair instability at oxygen ignition.

Woosley & Weaver

210 WOOSLEY & WEAVER

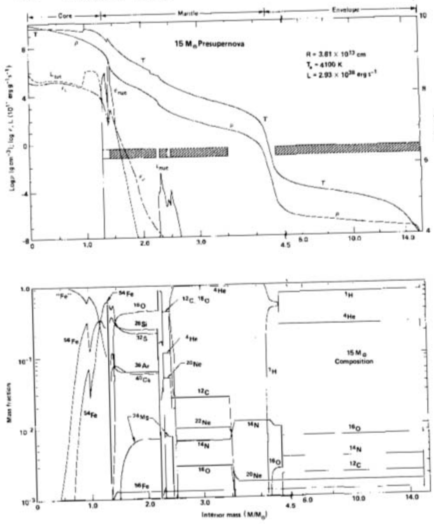

Figure 1 Structure and composition of a 15-$M_\odot$ presupernova star at a time when the edge of its iron core begins collapsing at 1000 km s^{-1}. Neutrino emission from electron capture (ε_ν) dominates photodisintegration in the total energy losses (L_{tot}) throughout most of the iron core. Central temperature here is 7.62×10^9 K and density is 9.95×10^9 g cm^{-3}. Spikes in the nuclear-energy generation rate (ε_{nuc}) show the location of active burning shells, while cross-hatched, blank, and open bars indicate regions that are convective, semiconvective, and radiative respectively. The species "Fe" includes all isotopes from $48 \lesssim A \lesssim 65$ having a neutron excess greater than ^{56}Fe. Note a scale break at 4.5 $M_\odot$. Figure adapted from Woosley & Weaver (1985).

Woosley & Weaver

- Core collapse in free-fall,
  $\tau_{ff} \approx (G\bar{\rho})^{-1/2} \approx 1$ ms, if $\rho = 10^{10}$ g cm^{-3}
- Central density and pressure ↑↑ and becomes subsonic; outer material remains free-fall and supersonic.
- Transition zone = constant speed, force free, relativistic electron degenerate pressure balances gravy
  → Chandrasekhar limit
- Inside $\mathbf{M}_{ch}$, $\rho \approx 2.3 \times 10^{14}$ g cm^{-3} (nuclear),
  strong force; material incompressible; neutron degeneracy
  Outside $\mathbf{M}_{ch}$ → supersonic accretion

➔ Shock wave and bounce

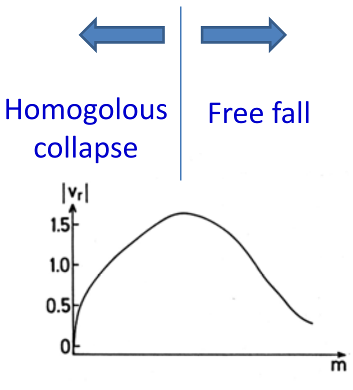

Fig. 34.8. Schematic picture of the velocity distribution in a collapsing stellar core originally of $1.4 M_\odot$ after numerical calculations (VAN RIPER, 1978). Note the two regimes: on the left $|v_r|$ (in units of 10^9 cm s^{-1}) increases in the outward direction. It corresponds to a (roughly) homologously collapsing part, while on the right $|v_r|$ decreases with m. This corresponds to the free-fall regime

Energy released in a core collapse

R: R_{WD} ($0.01\,R_\odot$) $\longrightarrow$ R_{NS} (10 km)

$$\Delta E_{grav} \sim \frac{G M_\odot^2}{R_{NS}} \sim 3 \times 10^{53} \text{ ergs}$$

10% used up by nuclear processes

rest to radiation and ejecting material
↓
(luminosity & neutrinos)

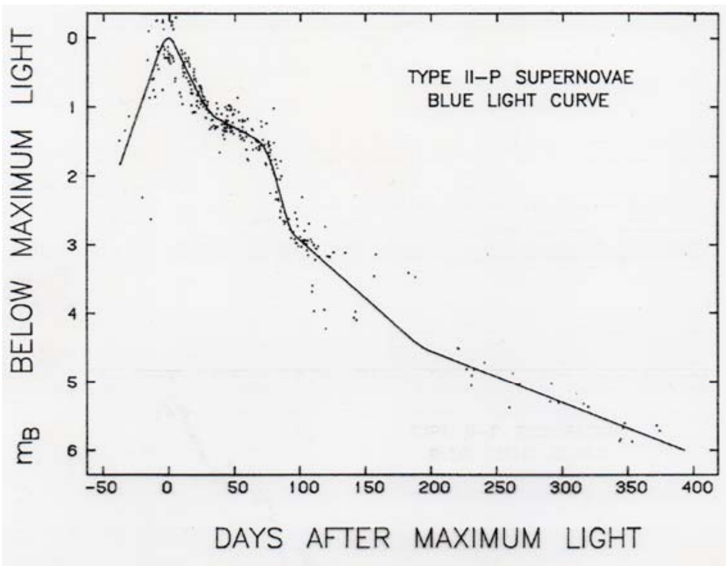

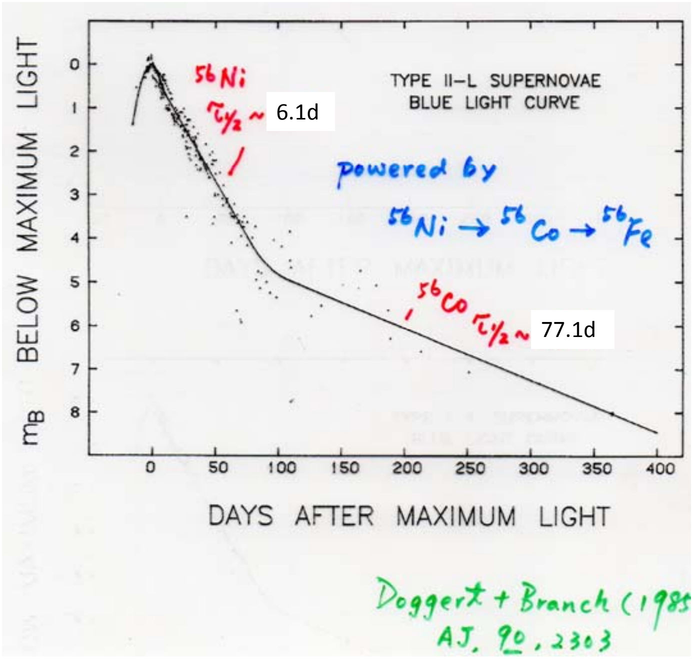

UVOIR light curve

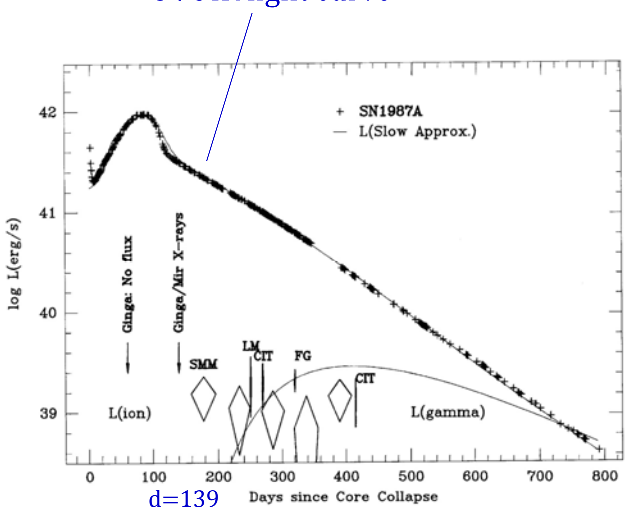

d=139
x-rays

d=178
γ-ray

Arnett

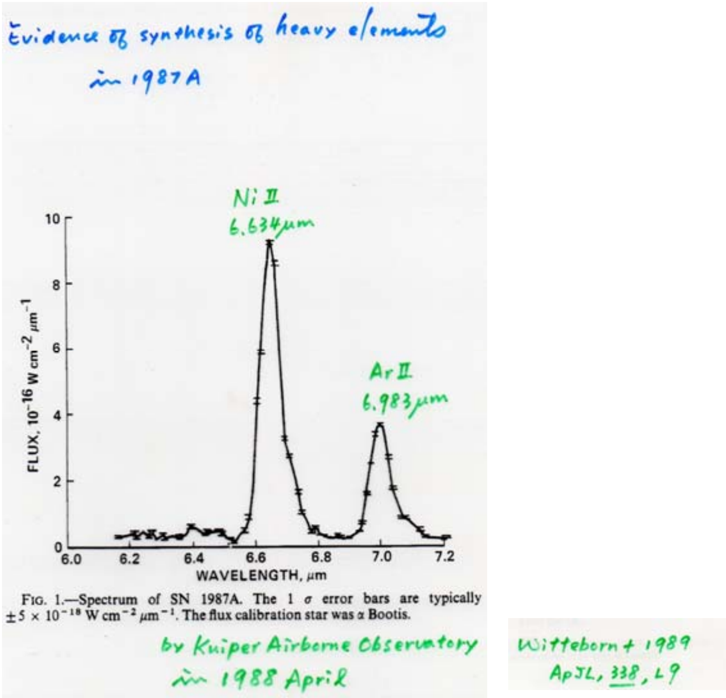

- During a type II SN explosion, the neutron star reaches $T \approx 10^{11} \sim 10^{12}$ K, but cools down quickly by neutrinos, to $T \approx 10^{9}$ K in a day, 10^{8} K in 100 years.
- This is cold, $kT \approx 10$ keV
  cf. Fermi energy ($\rho \approx 10^{14}$ g cm^{-3}), $\varepsilon_F \approx 1000$ MeV,
  so $T_{\text{neutron star}} \to 0$, and all electrons, protons, and neutrons are at the lowest energy states.
- Neutron beta decay process, $n \to p + e^{-} + \overline{\nu_e}$, does not take place, because the resultant electron and neutrino are not energetic enough (energy difference between n and p)
- But inverse beta decay $p + e^{-} \to n + \nu_e$ OK

➔ All neutrons

- So far thousands of SNe have been detected in external galaxies.
- In the Milky Way, a type Ia SN is expected every 36 years, and a type II SN is expected every 44 years. Then each century should see about 5 SNe.

Notable Historical supernovae in the Milky Way			
SN 1006	Lupus	Ia	–7.5 mag, brightest in history
SN 1054	Taurus	II	Chinese SN; Crab Nebula as the SNR
SN 1572	Cassiopeia	Ia	Tycho's Nova
SN 1604	Ophiuchus	Ia	Kepler's Star
SN 1680	Cassiopeia	IIb	Not observed, Cas A as the SNR

Solar System Abundances

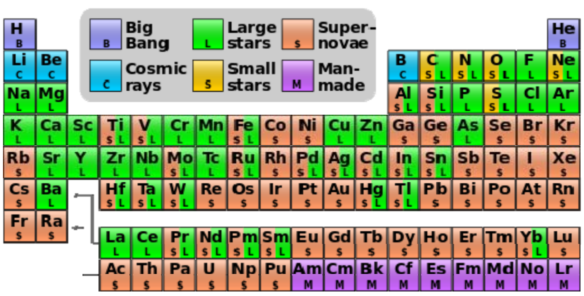

https://en.wikipedia.org/wiki/R-process#/media/File:Nucleosynthesis_periodic_table.svg

The 25 Most Abundant Nuclei

Rank	*Z*	*Symbol*	*A*	*Nucleon Fraction*	*Source (process)*
1	1	H	1	7.057e-01	Big Bang
2	2	He	4	2.752e-01	Big Bang, CNO, pp
3	8	O	16	9.592e-03	Helium
4	6	C	12	3.032e-03	Helium
5	10	Ne	20	1.548e-03	Carbon
6	26	Fe	56	1.169e-03	*e*-process
7	7	N	14	1.105e-03	CNO
8	14	Si	28	6.530e-04	Oxygen
9	12	Mg	24	5.130e-04	Carbon
10	16	S	32	3.958e-04	Oxygen
11	10	Ne	22	2.076e-04	Helium
12	12	Mg	26	7.892e-05	Carbon
13	18	Ar	36	7.740e-05	Silicon, Oxygen
14	26	Fe	54	7.158e-05	*e*-process, Silicon
15	12	Mg	25	6.893e-05	Carbon
16	20	Ca	40	5.990e-05	Silicon, Oxygen
17	13	Al	27	5.798e-05	Carbon
18	28	Ni	58	4.915e-05	Silicon, *e*-process
19	6	C	13	3.683e-05	CNO
20	2	He	3	3.453e-05	Big Bang, pp
21	14	Si	29	3.448e-05	Carbon, Neon
22	11	Na	23	3.339e-05	Carbon
23	26	Fe	57	2.840e-05	*e*-process
24	14	Si	30	2.345e-05	Carbon, Neon
25	1	H	2	2.317e-05	Big Bang

Arnett

Prediction:

✓ [^{4}He/H] ≈ 0.25 → obs OK

✓ [D/H], [^{4}He/H], , [^{3}He/H], [Li/H] density dependent → obs all same densities

WMAP (CMB) obs → consistent result

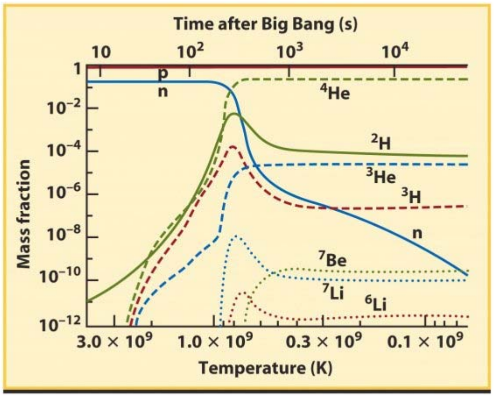

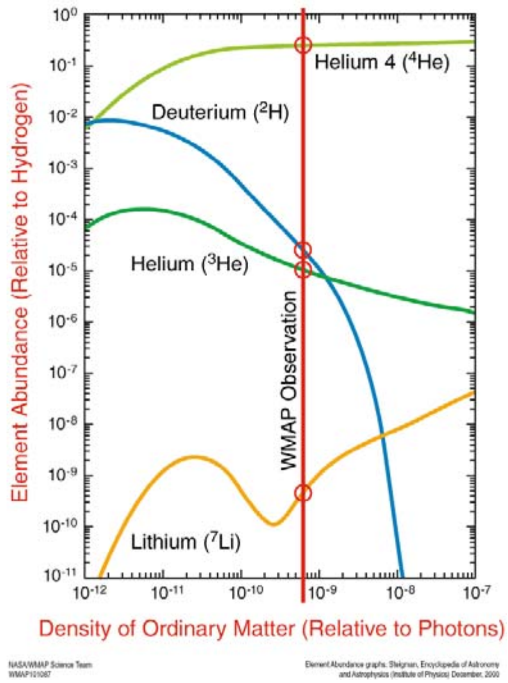

Solar System Abundances

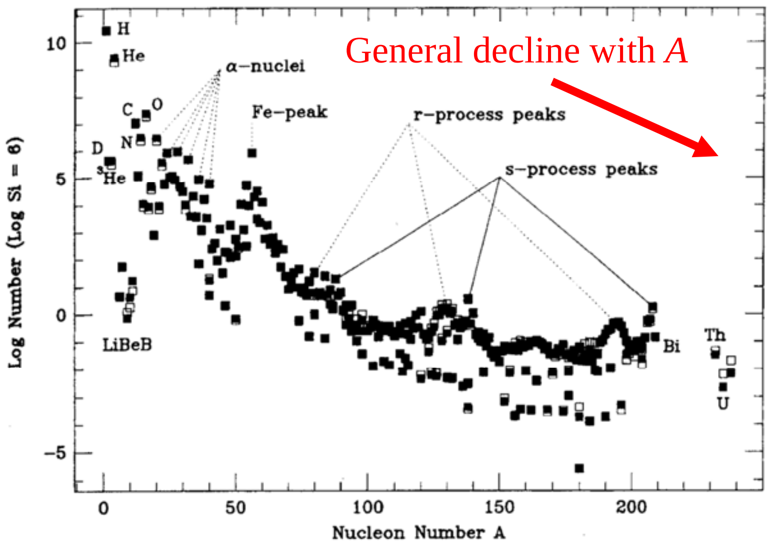

Z ↑, Coulomb barrier ↑ ↑ for charged particle reactions → elements produced by neutron capture

Different symbols from different compilations

Arnett

Cosmic abundance and stellar/galaxy evolution (Burbidge, E. M., Burbidge, G. R., Fowler, W. A., & Hoyle, F. (1957)

Big Bang → H:He=10:1

Stellar Interior

10^7 K → p-p, CNO (fusing proton, in a proton rich or neutron poor gas) **(p process)**

10^8 K → triple-alpha to C → continue to fuse α particles → mass number multiples of 4 by fusing **(α process)**

4×10^9 K → nuclear equilibrium → V, Cr, Mn and elements of the iron group **(e process)**

Explosive events

Neutron capture rapidly (compared to the competing β decays) → neutron-rich isotopes **(r process)**
e, g., the radioactive elements ^{235}U, ^{238}U, at the expense of the iron group

Neutron capture slowly (compared to the competing β decays) → neutron-rich isotopes **(s process)**

Valleys at *A*=5 to 15 (LiBeB) and *A*~ 45 (Sc=scandium)

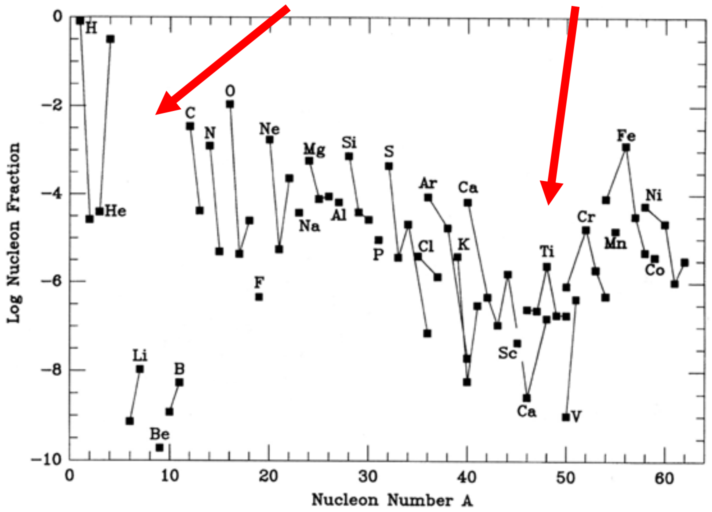

Fig. 2.2. Abundance ($A = 1, 64$)

Isotopes connected by lines.

Arnett

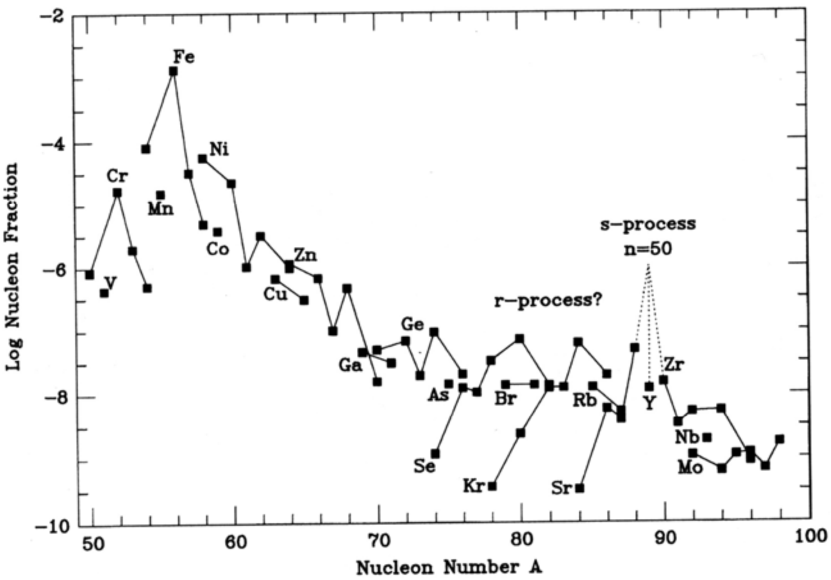

Fig. 2.3. Abundance ($A = 50, 100$)

- Other than H and He, the rest ('metals') is rare

  ∵ penetration prob. between positively charged nuclei has an exponential dependence ($Z_1 Z_2$)
  e.g., O + O → 64 times stronger than in H + H

- Even A nuclei are favored; especially for even-even elements, i.e., even Z and even N.
- $Z=N$ → **α particle nuclei** e.g., ^{12}C, ^{16}O, ^{20}Ne, ^{24}Mg, ^{28}Si, ^{32}S, ^{36}Al, ^{40}Ca
- First odd-A element is ^{25}Mg; placed the 15th
- Among the top, only ^{14}N is not even-even.

- Nuclei, like atoms, have a shell structure;
  "**magic numbers**" of protons are particularly tightly bound, e.g., ^{4}He (Z=N=2), ^{16}O (Z=N=8)

- ^{56}Fe not even-even; most tightly bound is ^{56}Ni.
  SN I and II light curves provide evidence that Ni → Co → Fe for A=56 → Abundance peaks at ^{56}Fe

- For A > 60, via neutron capture
  - ✓ **r-process**: **r**apid relative to beta-decay
  - ✓ **s-process**: **s**low *nuclei already tightly bound → small cross section for neutron capture (slow compare to beta decays)*

  (Burbidge, Burbidge, Fowler, & Hoyle; see Clayton)

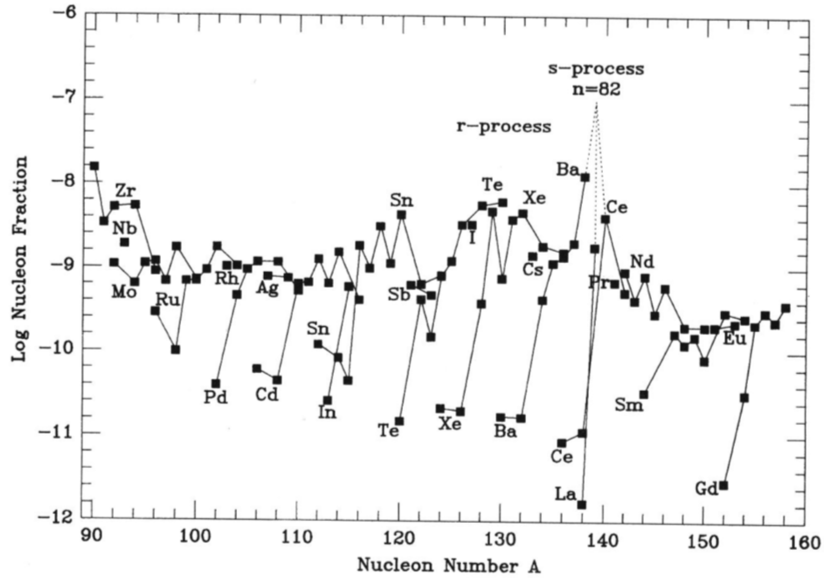

Fig. 2.4. Abundance ($A = 90, 160$)

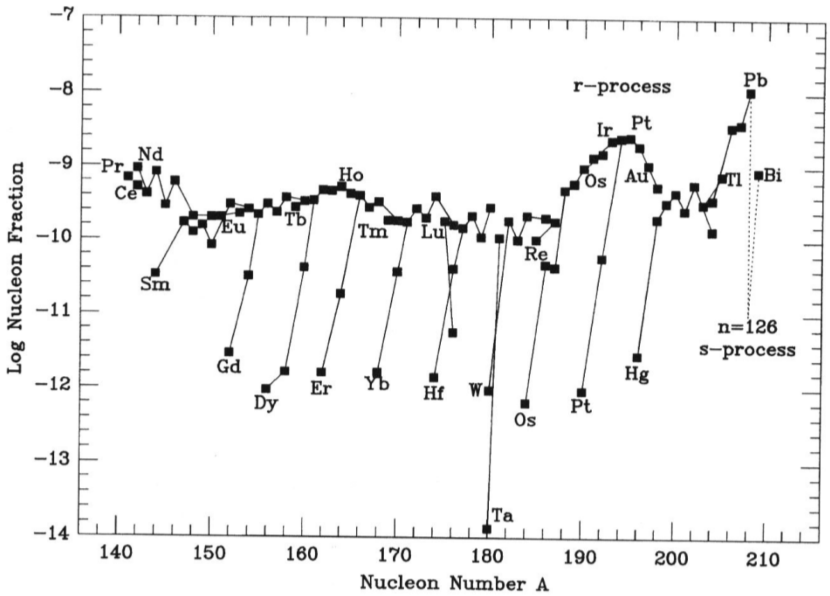

Fig. 2.5. Abundance ($A = 140, 210$)

Stellar Evolutionary Path

Star = (1 .. 8) $\mathcal{M}_\odot$
- Mass loss ↑ → (Stellar wind, PN) white dwarf (0.6 .. 1.4) $\mathcal{M}_\odot$
- Less mass ↓ → Core > 1.4 $\mathcal{M}_\odot$ → (C detonation?) No remnant?

Star > (8 .. 10) $\mathcal{M}_\odot$ → (Core collapse; 20 to 30% mass loss)
- Core < 1.8 $\mathcal{M}_\odot$, neutron star + SNR
- Core > 1.8 $\mathcal{M}_\odot$, black hole (?); a collapsar ↔ gamma-ray bursts

Black Holes predicted by General Relativity

Spacetime near a mass is warped

Total solar eclipse

A full treatment of a BH requires GR. But for an electrically neutral, non-rotating BH, classical derivations give the same results as with the relativisitic approach.

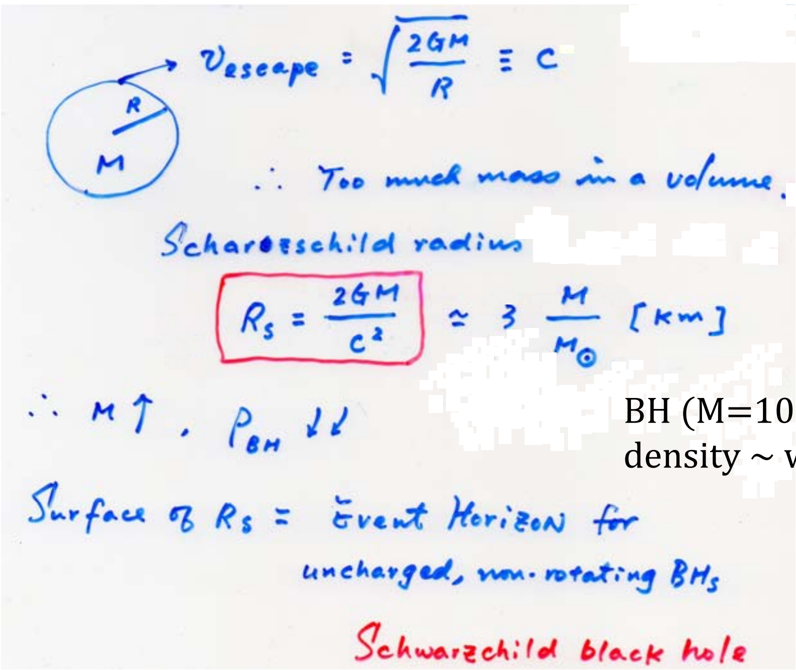

BH ($M=10^8$ sun), average density ~ water

	Nonrotating ($J = 0$)	Rotating ($J > 0$)
Uncharged ($Q = 0$)	Schwarzschild	Kerr
Charged ($Q \neq 0$)	Reissner-Nordström	Kerr-Newman

General BH metric, with M, J and Q = Kerr-Newman metric.

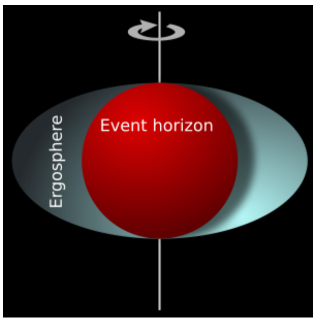

The two physical relevant surfaces of a Kerr black hole.

Table 1.4
Compact Objects in the Solar Neighborhood[a]

Object	Mass Range of Parent Star ($M_\odot$)	Integrated Galactic Birth Rate (yr^{-1})	Number Density (pc^{-3})	$\frac{\rho}{\rho_T}$	$\langle d \rangle$ (pc)
White dwarfs	1–4	0.16	1.5×10^{-2}	0.070	2.5
Neutron stars	4–10	0.021	2.0×10^{-3}	0.020	4.9
Black holes	> 10	0.0085	8.0×10^{-4}	0.22	6.7

[a] These values are obtained from Eqs. (1.3.17)–(1.3.21).
Note: Nearest known white dwarf: Sirius B, 2.7 pc. Nearest known neutron star: PSR 1929 + 10, 50 pc. Nearest known black hole candidate: Cygnus X-1, ~2 kpc.

Size of the Universe

13.7 billion yrs

$R_{observable} \sim 137 \times 10^{8} \times 10^{13}$ km

$\sim 1.4 \times 10^{23}$ km

$M_{obs} \sim 10^{11}\ M_\odot/\text{gal} \cdot 10^{12}\ \text{gal.}$ (+ dark matter + dark energy)

$\sim 10^{23}\ M_\odot$

$\left(R_s \sim 3 \frac{M}{M_\odot} [\text{km}] \right)$

$R_{obs} \sim R_s$

The whole Universe is a BH!

Hypernovae, Kilonovae

- Black-hole mergers
- White dwarf merger → Type I SN
- Neutron-star mergers → gravitational wave radiation → spiral inwards ; merging → a NS or a BH → a short GRB + a kilonovae + r-process elements produced and ejected

  a kilonova: luminosity 100 x of a classical nova
- Hypernova = superluminous supernova

  a hypernova: luminosity > 10 x of a standard

Quark Stars / Strange Stars

hyperthetical type of stars composed of quark matter or strange matter

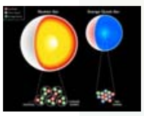

currently 6 "flavors" of quarks
up, down, strange, charm, top, bottom

spin 1/2

when a neutron star is further compressed

neutrons → break down to up and down quarks → break down strange quark

dark matter candidates ?

These highly mathematical & speculative

Some recent observations, e.g. in some SNe
→ existence of quark stars ?

Magnetars

A neutron star w/ an extremely strong $\vec{B}$
(10^{11} teslas or 10^{15} gauss)

Earth/Sun ~ 1 G
Ap/Bp ~ 10^3 G
WDs ~ 10^6 G
NSs ~ 10^{12} G

collapse → energy sources

(i) $E_{grav} \sim 0.2\, Mc^2 \sim 10^{53.8}$ ergs
(ii) $E_{rot} \sim \frac{1}{2} I \Omega^2 \sim 10^{52.7}$ ergs $I_{45}\, \Omega_4^2$

$\vec{B}$ links the fast spinning core to the outlying envelopes
magnetic breaking

D ~ 20km ; spin : several times/s

Time spans short, $\lesssim 10^4$ yr
$\vec{B}$ decays

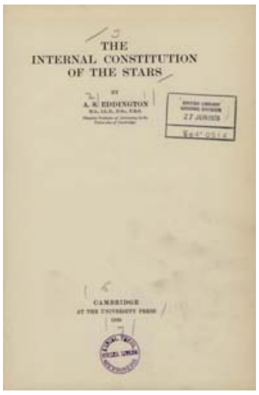

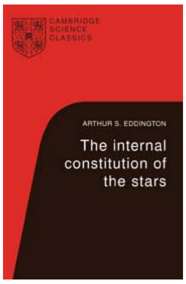

To recall Kelvin's classic phrase, there are two clouds obscuring the theory of the structure and mechanism of the stars. One is the persistent discrepancy in absolute amount between the astronomical opacity and the results of calculations based either on theoretical or experimental physics. The other is the failure of our efforts to reduce the behaviour of subatomic energy to anything approaching a consistent scheme. Whether these clouds will be dissipated without a fundamental revision of some of the beliefs and conclusions which we have here regarded as securely established, cannot be foreseen. The history of scientific progress teaches us to keep an open mind. I do not think we need feel greatly concerned as to whether these rude attempts to explore the interior of a star have brought us to anything like the final truth. We have learned something of the varied interests involved. We have seen how closely the manifestations of the greatest bodies in the universe are linked to those of the smallest. The partial results already obtained encourage us to think that we are not far from the right track. Especially do we realise that the transcendently high temperature in the interior of a star is not an obstacle to investigation but rather tends to smooth away difficulties. At terrestrial temperatures matter has complex properties which are likely to prove most difficult to unravel; but it is reasonable to hope that in a not too distant future we shall be competent to understand so simple a thing as a star.

https://archive.org/details/TheInternalConstitutionOfTheStars